Characterization of atmospheric ice nucleating at remote sites

Yannick Bras

THÈSE DE DOCTORAT
DE L'UNIVERSITÉ CLERMONT AUVERGNE

ÉCOLE DOCTORALE N° 178

Sciences Fondamentale – Sciences Atmosphériques

Spécialité du doctorat : Physique-Chimie de l'atmosphère et du climat

Thèse présentée et soutenue à Aubière, le 08/07/2022

Par

M. Yannick Bras

Characterization of atmospheric ice nucleating particles at remote sites

Thèse encadrée par :

Mme Karine Sellegri	CNRS - Université Clermont Auvergne	Directrice de thèse
Mme Evelyn Freney	CNRS - Université Clermont Auvergne	Co-directrice de thèse

Composition du Jury :

M. Luis Ladino Moreno	Universidad Nacional Autónoma de México	Rapporteur
M. Jonathan Duplissy	University of Helsinki	Rapporteur
Mme Barbara Ervens	CNRS - Université Clermont Auvergne	Examinatrice
Mme Claire Pirim	Université de Lille	Invitée

Characterization of atmospheric ice nucleating particles at remote sites

Abstract

Understanding how aerosol particles interact with atmospheric water is critical to understanding their impact on climate and precipitations. Ice Nuclei Particles (INPs) trigger the formation of atmospheric ice crystals. They are challenging to characterize because of their scarceness in the atmosphere and their variability. This variability depends partly on the different INP sources but also on the temperature at which they are activated. Considerably more variability being observed at warm temperatures (T>-20 °C), where biogenic particles have been identified as a key contributor. This is especially the case in marine regions, where the impact of ocean activity on the atmosphere is still largely unknown. The influence of atmospheric transport and aging on the IN properties of the ambient aerosols is another uncertainty in ice nucleation research. This thesis focused on the measurement and characterization of INPs in mountainous and oceanic regions, at T>-20 °C in the immersion freezing mode. Additional treatment of the samples allowed the retrieval of the concentration of biological INPs.

The first half of this thesis focused on characterizing INP populations in the Southern Hemisphere waters sampled during two cruise campaigns: One in tropical waters near the Tonga volcanic arc, and the other in poor oligotrophic waters south of New Zealand. The concentrations of sea spray (SSA) INPs and seawater (SW) INPs measured in both campaigns were lower than in other marine environments, but similar to other studies in the Southern Oceans. The best correlations were observed between INPs and organic matter, bacteria and photosynthetic pigments, highlighting the strong link between biological activity and INP concentrations. Parameterizations for predicting SW and SSA INPs were developed, showing that the transfer from SW INP to SSA INPs can be calculated based on the relationship between SW INPs and a SW organic carbon.

In order to understand the effect of atmospheric transport and aging on the IN properties of the aerosols, we measured INP concentrations at a continental site that is influenced by different air masses types. Two consecutive field campaigns took place at the Puy de Dôme station in Central France: the intensive, one-month long PICNIC campaign, and the long term WINS campaign. We measured concentrations between 0.001 and 0.1 INP/L_{air}, depending on the temperature. We also observed a majority of heat labile, potentially biogenic INPs at T>-12 °C. INP concentrations were at a minimum in winter and at a maximum in autumn and spring. Lower ratios of biogenic INPs were observed in the winter, explained by a decrease in vegetation cover and biogenic aerosols emissions. A parameterization for predicting warm INPs using the total aerosol concentrations as a predictor was successfully developed and tested.

In summary, this thesis provides new information of ice nuclei particles properties in various remote sites. We were also able to develop empirical parameterizations for predicting INPs for each of these environments.

Keywords: ice nucleating particles, nucleation, clouds, aerosols, remote sites

Laboratoire de Météorologie Physique (LaMP)
– Aubière – France – – –

Résumé

Il est essentiel de comprendre comment les aérosols interagissent avec l'eau atmosphérique pour comprendre leur impact sur le climat et les précipitations. Les noyaux glaciogènes (Ice Nuclei Particles, INPs) déclenchent la formation de cristaux de glace atmosphérique. Ils sont difficiles à caractériser en raison de leur rareté dans l'atmosphère et de leur variabilité. Cette variabilité dépend en partie des différentes sources d'INPs, mais aussi de la température à laquelle ils sont activés. Une variabilité beaucoup plus importante est observée aux températures chaudes (T>-20 °C), où les INPs biogéniques ont été identifiés comme un contributeur clé. C'est notamment le cas dans les régions marines, où l'impact de l'activité océanique sur l'atmosphère est encore largement inconnu. L'influence du transport atmosphérique et du vieillissement sur les propriétés glaciogènes des aérosols ambiants est une autre incertitude dans la recherche sur la nucléation de la glace. Cette thèse s'est concentrée sur la mesure et la caractérisation des INPs dans les régions montagneuses et océaniques, à T>-20 °C en mode de gel par immersion. Un traitement supplémentaire des échantillons a permis de retrouver la concentration des INPs biologiques.

La première moitié de cette thèse s'est concentrée sur la caractérisation des populations d'INPs dans les eaux de l'hémisphère sud échantillonnées lors de deux campagnes par bateau : l'une dans les eaux tropicales près de l'arc volcanique de Tonga, et l'autre dans les eaux oligotrophes pauvres au sud de la Nouvelle-Zélande. Les concentrations en INPs des embruns marins et de l'eau de mer mesurées lors des deux campagnes étaient plus faibles que dans d'autres environnements marins, mais similaires à d'autres études menées dans l'Océan Austral. Les meilleures corrélations ont été observées entre les INPs et la matière organique, les bactéries et les pigments photosynthétiques, mettant en évidence le lien étroit entre l'activité biologique et les concentrations d'INPs. Des paramétrisations pour prédire les INP dans l'eau de mer et les embruns ont été développées, montrant que le transfert des INP dans l'eau de mer aux INPs dans les embruns peut être calculé sur la base de la relation entre les INPs et le carbone organique dans l'eau de mer.

Afin de comprendre l'effet du transport atmosphérique et du vieillissement sur les propriétés INs des aérosols, nous avons mesuré les concentrations d'INP sur un site continental influencé par différents types de masses d'air. Deux campagnes consécutives ont eu lieu à la station du Puy de Dôme : la campagne PICNIC, intensive et d'une durée d'un mois, et la campagne WINS, de longue durée. Nous avons mesuré des concentrations comprises entre 0,001 et 0,1 INP/L_{air}, en fonction de la température. Nous avons également observé une majorité d'INPs biogéniques à T>-12 °C. Les concentrations d'INP étaient minimales en hiver et maximale en automne et au printemps. Des ratios plus faibles d'INPs biogéniques ont été observés en hiver. Une paramétrisation pour prédire les INP à T>-20 °C en utilisant la concentration d'aérosols comme prédicteur a été développée et testée avec succès.

En résumé, cette thèse fournit de nouvelles informations sur les propriétés des particules de noyaux de glace dans divers sites éloignés. Nous avons également été en mesure de développer des paramétrisations empiriques pour prédire les INP pour chacun de ces environnements.

Mots clés : noyaux glaciogènes, nucléation, nuages, aérosols, sites distants

Remerciements

Not all who wander are lost.

J.R.R. Tolkien

Cette citation de Tolkien, auteur si cher à mon cœur, on peut finalement facilement l'appliquer à la thèse, car, qu'est-ce qu'une thèse sinon qu'un long voyage aux fins fonds de la connaissance dans lesquels chacun vagabonde à son rythme ? Je pense qu'il est important de reconnaître ce côté errant de la thèse. En effet, le but n'est pas évident, et le chemin à parcourir l'est encore moins. L'objet de cette partie est donc de remercier tous ces gens qui m'ont guidé ou accompagné mes pas sur ce chemin qui m'a pris presque quatre ans.

Donc, en premier lieu, je souhaite remercier les membres de mon jury de thèse, Luis Ladino, Jonathan Duplissy, Claire Pirim et Barbara Ervens, pour avoir lu mes 140 et quelques pages de bêtises dans la langue de Shakespeare, et dont les commentaires et suggestions ont été fort appréciés. Je remercie aussi, en tant qu'entités, l'UCA, l'OPGC et le LaMP.

Comme je le disais plus haut, la thèse est un long chemin, et il me faut donc remercier mes guides, Karine Sellegri et Evelyn Freney. Elles ont su, par leur esprit scientifique et leur rigueur, m'aider à mener à bien ce projet ainsi qu'à gagner en autonomie. Pour retomber dans la métaphore, elles ont guidé mon chemin, mais m'ont aussi appris à lire une carte et à utiliser une boussole.

Il me faut aussi remercier tout le monde au LaMP et à l'OPGC, car l'ambiance y est très agréable pour y faire sa thèse, des cafés le matin aux routines au Puy de Dôme (un très bon endroit pour faire des raclettes aussi). Un merci tout particulier à Aurélie, Laëtitia, Clémence, Angelica, Jean-Marc, David, Pierre, Mickaël, Laurent, Céline, Agnès, Jean-Luc, Marlène, Régis, Marie, Géraldine, Louis, Guillaume, Miao, Maija, Charlotte, Clément, Etienne, Laurence et Lucas, pour leur bonne humeur de manière générale, et leurs contributions (scientifiques ou non) à ma thèse et à mon séjour au LaMP.

Voici venu le tour de ma famille et des amis ! Merci à mon père et à ma mère pour leur soutien, même s'ils ne se rendaient pas compte de ce que représentait

une thèse (est-ce un travail ou des études ?). C'est grâce à leur éducation que j'en suis là. Évidemment, tout cela n'aurait pas été possible sans Erwan (Youpi !), qui a été là, du travail aux loisirs. Et enfin, même si elle là depuis moins longtemps, à Dr. Julie, dont les pas ont partagé les miens sur cette fin de thèse.

La suite va représenter une grosse liste de noms, pas forcément pas ordre d'importance. Il y a d'abord les fiers camarades de Lyon : Grégoire et Aurélien, pour les parties de coinche endiablées et les discussions de physique à 1h du matin, Guilliam pour les randonnées et ses fesses blanches, Léa pour la bonne humeur permanente et qui permet à tout ce beau monde de se voir, Guillaume pour la guitare tout au long de la soirée, et enfin Grégory, pour la règle numéro 1, les proverbes nains, la stratégie de l'échec dont on n'a pas réussi à suivre les enseignements, et bien d'autres choses dont il faudrait parler autour d'une bonne bière. Merci aussi à Robin pour les mille photos (même si on n'en a vu que 10). Je remercie aussi les camarades de la promo du master SOAC, notamment Danaël, Clément, Amélie, Adrien, Lucas et Antoine.

Ensuite, viennent les camarades de Clermont (les Auvergnats qui sans façon...), avec qui j'ai partagé le quotidien de la thèse pendant ces quatre années. Florian pour les expéditions au marché et les cafés (et le fauteuil !), Mélissa pour la bonne humeur, Cédric pour les parties de Terraforming Mars, Guillaume pour les découvertes métalliques et l'anarchie, Boris pour l'escalade, les randos et les binouzes, et Manon pour la collocation bureautique et les pétages de câble à 18h. Gros bisous aussi à l'asso Doct'Auvergne pour le rapprochement des doctorants et les événements, tant de travail que de détente. Merci en passant à JB, Loélia, Magali, Alix, Pauline, Jeanne et tous les autres doctorants que j'ai pu croiser à ces événements.

J'arrive ensuite à une belle communauté, unie par le sel récolté sur les internets mondiaux et les shitposts de qualité. Merci dans le désordre à Kyo, Héra, Khromer, Hayu, Lutcha, Adrien, Tcherki, Tsuba, Ima, Cookiz, Cypher, Moumix, Sush et Skith. Merci aussi à Jeanne d'être elle-même, à Mith pour raconter des conneries (ou philosopher, les deux sont interchangeables), à Pawn pour le nuke, à Ysendrin pour fanfaronner (non sans forfanterie quelque fieffés forfaits farfelus effrontés), à HMS pour m'avoir appelé Grogro.

Et pour finir, je veux remercier la belle communauté du discord PhD francophone qui a été d'une importance incommensurable à bien des égards pendant ma thèse. D'abord, merci à Mathilde d'avoir créé ce merveilleux espace. Merci ensuite à Victor et Elizabeth pour les discussions historiques intéressantes, à Marie pour le fromage et les jeux de mots, à Pierre pour le metal et les discussions sur le Seigneur des Anneaux, à Chloé pour les haricots, à Solène pour me gronder quand je me blesse, à Jim pour éclairer tout le monde, à Misa pour les chansons en soirée, à Nico pour critiquer mes skills sur Paint, à Elise pour l'escalade et la spéléo, à Victoria pour ses engagements, à Antoine pour les jeux, à Lise pour compter des mes MP, à la Capitaine Lulu pour le rhum et la piraterie. Merci aussi à Marie, Louis, Mathieu, Val, Galaad, Floriane, Ronan, Eva et Laurène. Merci à tous les autres que j'ai oubliés, et qui (j'espère) ne m'en tiendront pas rigueur.

Acronyms

A | B | C | D | E | F | G | H | I | L | M | N | O | P | S | T | U | W | Z

A

AA Amino acids.
ACTRIS Aerosol, Clouds and Trace Gases Research Infrastructure.
AIDA Aerosol Interaction and Dynamics.

B

Bact. Bacterial abundance.
BC Black Carbon.

C

CCN Cloud Condensation Nuclei.
CFDC Continuous Flow Diffusion Chamber.
CHN Carbon, hydrogen and nitrogen (analyser).
CHO Carbohydrates.
CNT Classical Nucleation Theory.
CSU-CFDC Colorado State University CFDC.
CTD Continuity Temperature Depth (rosette).

D

D10 DeMott et al. (2010b) parameterization for INPs.
D15 DeMott et al. (2015) parameterization for INPs.
Dia Diatoms.
Difl Dinoflagellates.
DMA Differential Mobility Analyser.
DOC Dissolved Organic Carbon.
DOM Dissolved Organic Matter.

E

EF Enrichment factor from the SW to the SML.

F

FCM Flow Cytometry.
Fl Flagellates.
FRIDGE Frankfurt Ice Deposition Freezing Experiment.
FT Free Troposphere.
FW Frontal Waters.

G

GAW Global Atmosphere Watch [programme].

H

HL Heat labile [INPs].
HPLC High-Performance Liquid Chromatography.
HS Heat stable [INPs].

I

IC Ion Chromatography.
INA Ice Nucleation Activity.
INP INPs Particle.
INSEKT Ice Nucleation Spectrometer of the Karlsruhe Institute of Technology.
IPCC Intergovernmental Panel on Climate Change.

L

LACIS Leipzig Aerosol and Cloud Interaction Simulator.
LINDA Led-Based Ice Nucleation Detection Apparatus.
LOD Limit of detection.

M

M18 McCluskey et al. (2018c) fit for pristine SSA INPs.
M92 Meyers (1992) parameterization for INPs.
MOUDI-DFT Micro-Orifice Uniform Deposit Impactor-Droplet Freezing Technique.
MPC Mixed Phased Cloud.
MSA Montsec d'Ares station.
MW Mixed Waters.

N

N12 Niemand et al. (2012) parameterization for INPs.
Nano Nanophytoplanktons.

O

OPC Optical Particle Counter.

P

PCF Pore Condensation and Freezing.
PCR Polymerase Chain Reaction.
PICNIC Puy de Dôme Ice Nucleation Intercomparison Campaign.
Pico Picophytoplanktons.
PINC Portable Ice Nucleation Chamber.
POC Particulate Organic Carbon.
PUY Puy de Dôme station.

S

S2C Sea2Cloud cruise.
SAW Subantarctic Waters.
SML Surface microlayer.
SMPS Scanning Mobility Particle Sizer.
SO Southern Ocean.
SOA Secondary Organic Aerosol.
SPIN Spectrometer for INPs.
SSA Sea Spray Aerosols.
STW Subtropical Waters.
SW Sea Water.
Syn *Synechococcus*.

T

TNG TONGA cruise.
TOC Total Organic Carbon.
TSG Thermo-salinometer.

U

UWAY Underway system of the ship.

W

W15 Wex et al. (2015) parameterization for INPs.
WAI Whole Air Inlet.
WBF Wegener-Bergeron-Findeisen [process].
WBOAT Pneumatic work boat.
WIBS Wideband Integrated Bioaerosol Sensor.
WINS Weekly INPs Samples.

Z

ZINC Zurich Ice Nucleation Chamber.

Table of contents

List of Tables

List of Figures

I

General introduction and state of the art on ice nucleation research

Outline of the current chapter

Even though water represents only a small fraction of the total mass of the atmosphere (about 0.25%, Trenberth et al. 2005), it has tremendous effects on the Earth's climate and biosphere. One of the effects of water in the atmosphere is through the formation of clouds. Clouds are crucial components of the Earth water cycle. They cover about 70% of the Earth's surface (Stubenrauch et al. 2013), and interact with a number of effects that in turn affect the water cycle, precipitation and global energy budget (Timofeyev et al. 2008).

Clouds can be composed of varied hydrometeors: liquid droplets, ice crystals or a combination of the two. The size and shape of these hydrometeors determines how they interact with incoming radiations and initiate precipitation. As shown on Figure I.1, clouds composed of liquid droplets will mostly interact with visible or near infrared light, whereas clouds composed of ice crystals will mostly interact with thermal infrared light. The variable morphology of hydrometeors makes deriving their interaction with light a complex challenge and as a result, the clouds contribution to the Earth's global energy balance is difficult to estimate.

There are still large uncertainties related to clouds, as a result of their variability, their formation mechanisms and the influence of atmospheric dynamics. Despite considerable progress in the recent years, Masson-Delmotte et al. (2021)(IPCC, Intergovernmental Panel on Climate Change) reports that clouds remain the greatest source of uncertainty in our understanding of climate and in our ability to predict it.

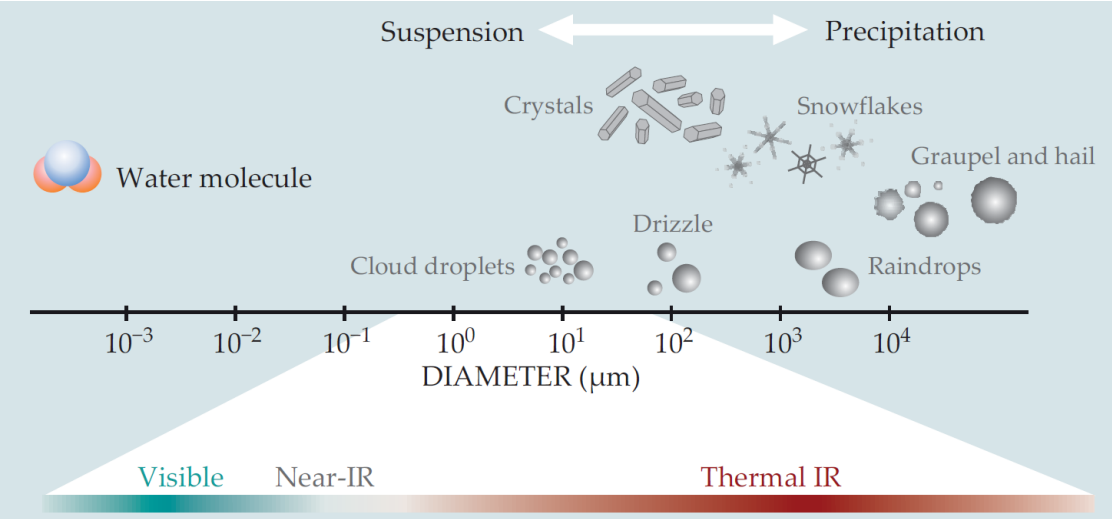

Figure I.1 – Summary of the size and interactions of the different types of hydrometeors with radiation wavelength. Figure adapted from Stevens et al. (2013).

I.1 Cloud formation

The formation of clouds and precipitations depends mainly on three parameters: the availability of water vapor (humidity), atmospheric conditions (temperature and pressure) and the presence of aerosol particles. The general mechanism of formation of a cloud is when an air parcel rises and cools down in the atmosphere, where the water vapor condenses to form either liquid droplets or ice crystals. Depending on the atmospheric conditions, three types of clouds may exist in the atmosphere: liquid clouds that are composed exclusively of liquid droplets (such as cumulus clouds), ice clouds (such as cirri) that are composed exclusively of ice crystals, and mixed-phase clouds (MPC) that are composed of both liquid droplets and ice crystals.

Liquid clouds are the most well known type of clouds, and their formation conditions have been studied for decades. Their formation is described by the Köhler theory (Köhler 1936): for liquid droplets to start condensing in the atmosphere, the temperature has to be sufficiently low and the humidity sufficiently high to pass the energy barrier of condensation. Furthermore, there needs to be aerosol particles that allow the water molecules to accumulate on their surface, which lowers the energy barrier for condensation. Such aerosol particles are called Cloud Condensation Nuclei (CCN) and they represent typically about 10 to 50% of the total number of aerosols in the atmosphere, and up to 80% (Lohmann et al. 2016). The rate at which cloud droplets may form is studied through the Classical Nucleation Theory (CNT, Pruppacher et al. 2012), which is the most common model used for calculating the kinetics of nucleation. As a result, the formation of liquid clouds is nowadays generally well understood (Charlson 2001; Dusek et al. 2006; McFiggans et al. 2006).

The formation of ice crystals in the atmosphere is much less well understood than that of liquid droplets, despite the first studies on the subject date back several decades (Bigg 1966; Vali 1971). This is partly because the microphysics involved is much more complex than in liquid clouds, due to the presence of two phase transitions (from water vapor to liquid droplet, and from liquid droplet to ice crystal, or from vapor to ice crystals), and the diversity of pathways for this transition.

The formation of ice occurs either homogeneously, when the temperature and humidity are respectively sufficiently low and high for metastable liquid droplets to freeze with nothing else to induce freezing ; or heterogeneously, when the phase change is induced by the presence of an *Ice Nucleating Particle* (INP). Heterogeneous freezing may occur at much warmer temperature than homogeneous freezing because the presence of an INP lowers the energy barrier required for the phase transition. Both homogeneous and heterogeneous freezing are described in the following sections.

I.1.1 Homogeneous freezing

In the atmosphere, the conditions for homogeneous freezing are very rarely met, and thus it is generally considered relevant only at temperatures colder than -37 °C and humidity above 145% (DeMott 2002; Murray et al. 2010), typically at altitudes >10 km, in high altitude clouds such as cirrus. It only requires sufficient water availability and low temperatures to allows the formation of ice crystals without the help of any aerosol particle to lower the energy barrier for phase change. As such, a molecular cluster of ice, also called *ice embryo*, serves as the nucleus for the phase transition (Pruppacher et al. 2012). By the definition proposed by Vali et al. (2015a), an ice embryo is a "thermodynamically unstable aggregate of water molecules in a structure that favors further development into stable ice". In homogeneous freezing, an ice embryo might form through fluctuations in density and temperature, which leads to collisions and clustering of water molecules. The formation of such clusters can be described by the CNT.

The change in Gibbs free energy for homogeneous nucleation ΔG_{hom} can be expressed as the sum of a volume term and a surface term (Nishinaga 2015):

$$\Delta G_{hom} = \underbrace{-n_i \Delta\mu(T)}_{\text{Volume term}} + \underbrace{4\pi r^2 \sigma_{iw}(T)}_{\text{Surface term}}, \tag{I.1}$$

where $\Delta\mu(T)$ is the change in the chemical potential between the ice and the liquid phase, r is the radius of the ice embryo, $\sigma_{iw}(T)$ is the interfacial tension between the water and the ice phase, and $n_i = \frac{4\pi r^3}{3}\frac{1}{V_i(T)}$ is the number of molecules in the ice cluster, with V_i the volume of water molecules in the ice. The volume term in the equation represents the energy gained by the volume of the ice cluster through the movement of n_i molecules, and thus is a positive energy (gain). The surface term represents the energy required for the formation of an interface, and is a negative energy (loss).

The term $\Delta\mu$ is the driving force of the ice nucleation and allows to overcome the energy barrier of forming a new interface. The minimum size required for the formation of a stable ice crystal is called the critical size r_c: when a cluster reaches this size, the volume term becomes larger than the surface term, and thus the energy barrier for phase transition is overcome and a stable ice crystal may grow. It has been observed that pure water droplets smaller than 5 µm (thus r_c = 5 µm) will freeze spontaneously at temperatures <-38 °C (Pruppacher 2010).

The probability of creating a stable ice crystal increases as the temperature decreases and also with the supersaturation with respect to ice. Supersaturation happens when the relative humidity is over 100%: in the atmosphere, both supersaturation with respect to ice (SS_i) and with respect to liquid water (SS_w) may happen depending on the temperature, pressure and humidity conditions (Gierens et al. 2012).

I.1.2 Heterogeneous freezing

I.1.2.1 Theoretical description

At temperatures >-37 °C, heterogeneous freezing is the most likely pathway for ice crystals formation in the atmosphere. Heterogeneous freezing requires the presence of an INP, which lowers the energy barrier ΔG^* for the phase transition and facilitates the formation and growth of an ice embryo (the initial molecular cluster). The interaction between the INP and the ice embryo is described using a contact angle θ, which represents the angle between the INP and the spherical ice embryo. The contact angle θ is thus defined as follows:

$$\cos\theta = \frac{\sigma_{sw} - \sigma_{si}}{\sigma_{iw}}, \tag{I.2}$$

with σ_{sw}, σ_{si} and σ_{iw} the surface tensions of respectively the substrate-water interface, the substrate-water interface and the ice-water interface (Pruppacher et al. 2012).

The value of θ thus represents the compatibility between the INP and the ice embryo, with lower values of θ representing greater compatibility. Thus, homogeneous freezing can be represented as $\theta = 180°$, while a perfect planar interaction can be represented as $\theta = 0°$.

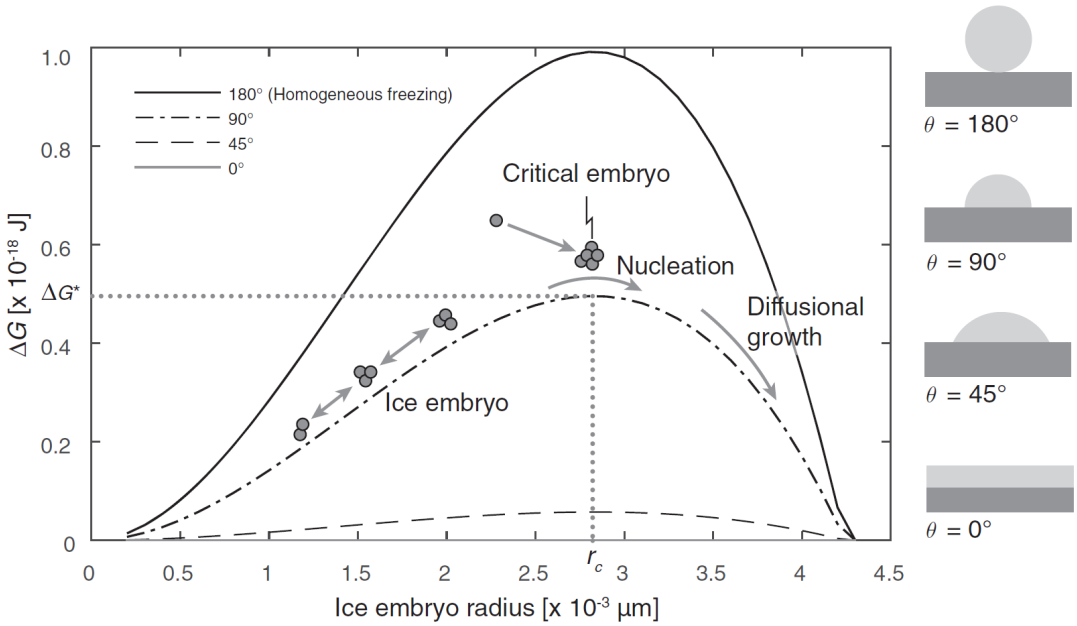

Figure I.2 – Gibbs free energy ΔG at 273 K as a function of the ice embryo radius r, for homogeneous freezing ($\theta = 180°$) and heterogeneous freezing ($\theta = 0°$, 45° and 90°). The dotted lines represent the Gibbs free energy barrier (ΔG^*) and the corresponding critical embryo radius r_c. The different contact angles are illustrated on the right side schematics. The dark gray area represent the INP surface and the light gray area the ice embryo. Picture adapted from Lohmann et al. (2016).

This is illustrated in Figure I.2 at $T = 253$ K using different contact angles θ:

the Gibbs free energy barrier ΔG decreases with the value of θ. The presence of an INP with $\theta = 90°$ (dash-dotted line) decreases ΔG by about half compared to the homogeneous freezing value ($\theta = 180°$, solid line). The reduction in ΔG is even more important for $\theta = 45°$ (dashed line), thus the bigger the INP, the higher the probability a freezing event occurs. The value of ΔG is also dependent on the radius of the ice embryo, and the critical radius r_c is the value at which ΔG is maximum at a given temperature: in Fig. I.2, at $T = 253$ K, the critical size is $r_c \approx 2.6$ nm. r_c is constant for all contact angles, and thus does not change between homogeneous and heterogeneous freezing.

Formally, the change in Gibbs free energy ΔG_{het} for heterogeneous freezing is dependant on ΔG_{hom} (homogeneous freezing) and a geometric factor $f(\theta)$, such as:

$$\Delta G_{het} = f(\theta) \cdot \Delta G_{hom}, \tag{I.3}$$

with $f(\theta)$ describing the contact angle θ between the INP surface and the ice embryo. In the case of a planar INP surface, which is justified in the case of INPs bigger than 0.1 µm, $f(\theta)$ is defined as:

$$f(\theta) = \frac{1}{4}(2 + \cos\theta)(1 - \cos\theta^2). \tag{I.4}$$

When θ decreases, $f(\theta)$ also decreases and so does the energy barrier. In particular, when the size of the INP decreases, the curvature of the surface increases and thus plays a bigger role. We can see that $f(\theta = 0) = 0$, meaning that a contact angle $\theta = 0°$ represents an energy barrier required for heterogeneous freezing $\Delta G_{het} = 0$ J. On the contrary, the maximum value of $f(\theta)$ is reached for $\theta = 180$°C and is 1: in this case $\Delta G_{het} = \Delta G_{hom}$.

It has been suggested that $f(\theta)$ decreases rapidly for particles below 0.1 µm, thus the hypothesis of a planar INP becomes less justified (Fletcher et al. 1962; Pruppacher et al. 2012). However, it has also been showed by Jamieson et al. (2005) that the size of the INP only becomes significant when it is close to the critical size r_c of the ice cluster. There is still no consensus on what makes a particular class of aerosols good INPs, and as such this is still a heavily discussed topic (see Sections I.2 and I.3.1).

I.1.2.2 Activation modes

When discussing heterogeneous freezing, one may also consider the different pathways by which an ice crystal may form, called *activation modes*. They are summarized in Figure I.3, and explained hereafter based on the work of Kanji et al. (2017) and of Vali et al. (2015b):

- *Deposition ice nucleation* takes place when ice directly nucleates from supersaturated water vapor with respect to ice ($RH_i > 100\%$) at the surface of an INP. This process supposedly does not involve liquid water, and is relevant at low temperatures (lower than -30 °C) under cirrus clouds formation conditions (Cziczo et al. 2013), but not in MPCs (Ansmann et al.

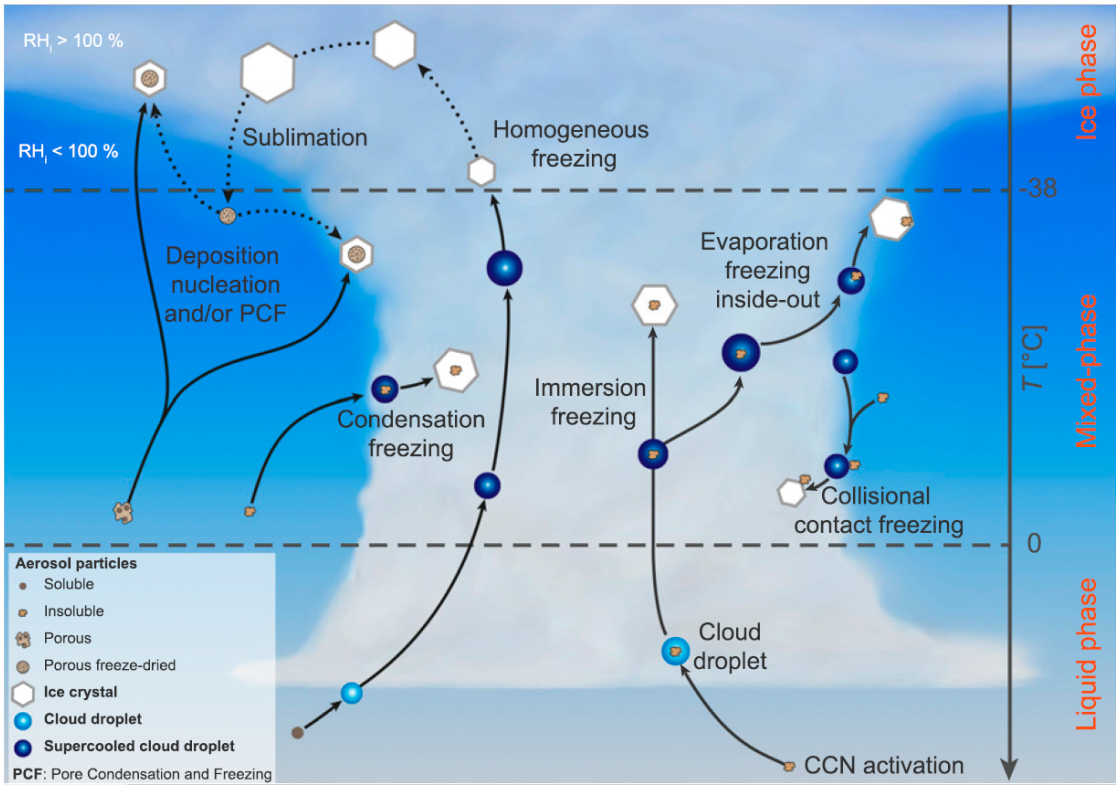

Figure I.3 – Ice nucleation pathways in the atmosphere as described by Kanji et al. (2017).

2008).

- *Contact freezing* is initiated when an INP comes directly into contact with the air-water interface on the outside of the droplet, for example following a collision. Inside-out contact freezing has also been observed (Durant 2005; Fornea et al. 2009), when an INP touches the surface of the droplet from within. It has been suggested that the evaporation of a droplet could lead to inside-out contact freezing, due to the immersed INP reaching the surface of the droplet. This process is still poorly understood, but could be relevant in mixed-phased clouds.

- *Immersion freezing* takes place when an INP that is immersed in a droplet becomes active. Such INPs could have been immersed through activation via a CCN during liquid cloud formation, thus suggesting that a number of CCNs could also be effective INPs. Immersion freezing is thought to be the most important ice nucleation pathway in mixed phase clouds (e.g. Ansmann et al. 2008; Boer et al. 2011; Murray et al. 2012), and is also the most studied mode as it is the easiest to reproduce experimentally (see Section I.2.3). In this thesis, immersion freezing is the only mode we will study.

- *Condensation freezing* is a heavily discussed fourth mode for nucleation. It is thought to happen when water vapor condenses on the INP surface, and

then, consecutively, the liquid film freezes. It is still not clear if condensation freezing should be considered as its own nucleation mode, or if it is only a special case of deposition nucleation or immersion freezing (Vali et al. 2015a).

I.1.2.3 The time independent approach versus stochastic approach

One of the questions regarding heterogeneous freezing, but not related to the activation mode, is whether this is a deterministic (time-independent) or a stochastic (time-dependent) process.

The *time independent* approach, or *singular hypothesis*, assumes the presence of impurities at the surface of the INPs, called ice-active sites (Vali et al. 1966; Vali et al. 2015a, Pruppacher et al. 2012). Active sites are surface features such as cracks, steps or functional groups (Fletcher 1969) that favor the formation of ice crystals on them. The hypothesis behind this approach is that each active site induces freezing at a constant temperature, and thus that no time dependence is involved in the ice nucleation. It also implies that the probability of an INP to contain an ice-active site directly scales with the surface area of the aerosol.

This property has been suggested as early as 1971 by Vali (1971), and has since been the basis for a number of studies of the Ice Nucleating Ability (INA) of different types of aerosols (DeMott 1995; Connolly et al. 2009; Atkinson et al. 2013) and has been used as a basis for developing empirical parameterizations in order to predict INP concentrations (DeMott et al. 2010a; Niemand et al. 2012; Schneider et al. 2021). In the case where there are several ice active sites available, the most active one will induce nucleation. This can occur with a droplet containing several INPs, or with an INP with several ice active sites on its surface.

On the other hand, the *stochastic* approach assumes that heterogeneous freezing is dependant on time, and is thus described by a nucleation rate J (in $\mathrm{cm}^{-3}\,\mathrm{s}^{-1}$), such as:

$$J = K \exp\left(-\frac{\Delta G}{k_B T}\right), \tag{I.5}$$

where K is the kinetic prefactor in $\mathrm{cm}^{-3}\,\mathrm{s}^{-1}$, ΔG is the energy barrier for the phase change k_B the Boltzmann constant and T the temperature. The nucleation rate J represents the number of nucleation events per unit volume and unit time in the liquid phase. The stochastic approach assumes that identical INPs have the same probability that an ice embryo at their surface will reach its critical size. It is impossible to determine if and when a nucleation event will occur for an individual INP. At constant temperature and supersaturation, the proportion of frozen droplets in a population of supercooled cloud droplets grows with time, according to the stochastic hypothesis. Furthermore, the order in which supercooled droplets freeze is totally random in a freezing experiment with a given set of supercooled droplets kept at constant temperature or supersaturation.

In conclusion, heterogeneous freezing regroups a large number of parameters and mechanisms under the same concept, and as such is a complex topic. The open questions regarding the relevance of the different nucleation modes highlight that the formation of ice in the atmosphere is still a very poorly understood process, and even though a lot of progress has been made recently, more studies are needed to grasp it completely.

I.1.3 The Wegener-Bergeron-Findeisen effect

Hypotheses of the growth of ice crystals at the expense of liquid droplets have been coined by three scientists in the first half of the 20th century: Alfred Wegener, Tor Bergeron and Walter Findeisen. Wegener first showed in 1911 that the co-existence of a liquid and an ice phase in clouds is a thermodynamically unstable state (Wegener 1911). Bergeron, after some observations in a forest in winter in 1928, developed a theoretical explanation that ice crystals could scavenge water vapor from the surrounding supercooled cloud droplets at negative temperatures, therefore growing at the expense of the droplets (Bergeron 1935). Finally, Findeisen was able to contribute to Bergeron's work through additional theoretical and experimental work in a cloud chamber (Findeisen 1938).

The Wegener-Bergeron-Findeisen (WBF) process, or Bergeron-Findeisen process, is a phenomenon that takes place in mixed-phase clouds. This is the process by which ice crystals may grow rapidly at the expense of the nearby liquid droplets, which affects the radiative properties of the MPC, as well as precipitations (Pruppacher et al. 2012). A review of the WBF process is available in Storelvmo et al. (2015).

The scavenging of water vapor by ice crystals occurs when the water vapor pressure in the cloud e is between the saturation water vapor pressure over liquid and ice surface (respectively e_l and e_i) at temperature below 0 °C, such as $e_l > e > e_i$ (Storelvmo et al. 2015). An environment that is saturated with water will be heavily supersaturated with ice, and such difference will increase as the temperature decreases. Thus, when those conditions are met, ice crystals are able to scavenge the water vapor that evaporates from the liquid droplets, which allows them to gain mass at the expense of the cloud droplet. After reaching a critical mass, the ice crystals can fall as snow and continue growing by accretion as they travel through the cloud. Depending on the atmospheric conditions, those crystals could also melt and reach the ground as rain.

The WBF process has a significant impact on the lifetime of clouds and precipitations, and is especially important to consider because it only requires a small initial number of ice crystals with respect to supercooled droplets (which means it is worth studying the INA of particles present in low concentrations in the atmosphere), and also because it is a very rapid process (in the order of minutes). Recently, efforts have been made to include the WBF process in precipitation and climate models (Storelvmo et al. 2008; Lohmann et al. 2009), however this is a difficult task because of the time scale of the process.

I.2 Ice Nucleating Particles measurements and identification

INPs are a subclass of aerosols that are very rare in the atmosphere, with concentrations ranging between 0.1 to 10 per liter of air, which means that about 1 out of 10^5 to 10^6 aerosols could act as an INP (Rogers et al. 1998; Boose et al. 2016a). In addition to the uncertainties related to the nucleation modes presented previously, there is still no consensus on what feature(s) of an INP are responsible for its ability to nucleate ice.

I.2.1 Aerosols variability

Aerosol particles are suspended particulate matter in liquid or solid form, that have highly variable chemical composition (mineral dusts, soots, bacteria...), morphology and size distribution.

With sizes generally between 0.01 to 20 µm (Putaud et al. 2010), aerosols sizes span several orders of magnitude, which is why it is useful to segregate them in different classes of sizes (Fig. I.4).

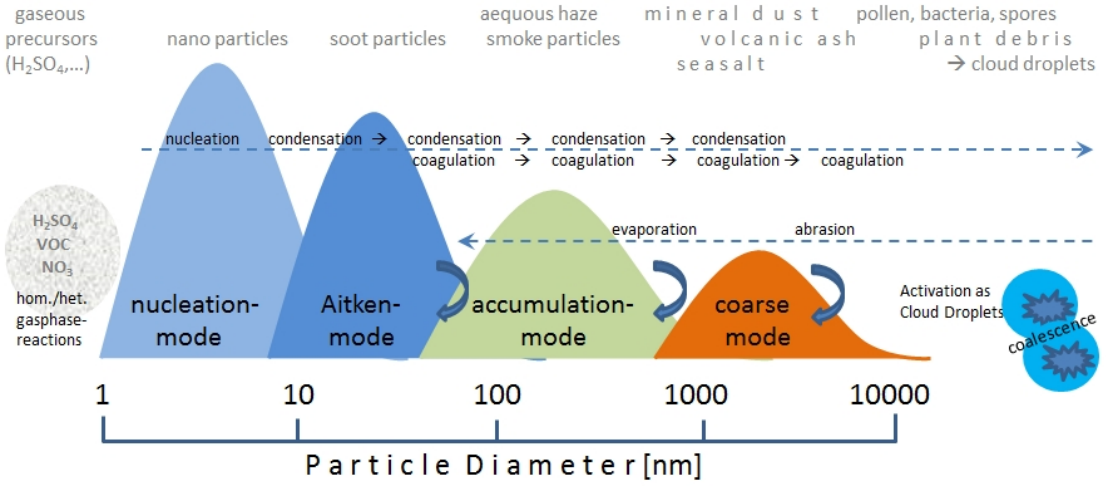

Figure I.4 – Multi modal particle size distribution and the typical transformations they can undergo in their life cycle - Source: Deutscher Wetterdienst

Nucleation mode corresponds to the newly formed particles, with sizes inferior to 10 nm. Nucleation mode particles also grow by condensation and coagulation to the Aitken mode. Particles in the Aitken mode have sizes between 10 to 100 nm and grow generally through coagulation and coalescence. They are generally depleted by coagulation with other particles. The accumulation mode corresponds to medium-sized particles, from about 100 to 1000 nm. They represent the majority of the total surface area of aerosols, as well as the majority of the aerosol mass (Seinfeld et al. 2006). Contrary to the particles in the nucleation or Aitken mode, particles in this mode have longer residence time in the atmosphere, and are thus more susceptible to long range transport by

airmasses. Finally, the coarse mode corresponds to bigger particles that exceed 1 µm in diameter. In general, because they are more sensible to atmospheric removal mechanisms like fragmentation, evaporation or sedimentation, they are present in lower numbers than particles in the accumulation mode.

Furthermore, aerosols can be classified using their chemical properties or their sources. Aerosols can either be emitted directly in the atmosphere (primary aerosols) or can be the results of chemical reactions in the atmosphere (secondary aerosols). Aerosols can be emitted through natural processes or by human activities.

In additions to these variations inherited from their formation, aerosols can undergo various size or composition changes as they travel in the atmosphere, a process defined as atmospheric aging. Finally, an other source of variability for aerosols concentrations are the seasonal variations due to atmospheric dynamics and hence dilution processes. Figure I.5 provides a summary of aerosols sources and sinks in the atmosphere.

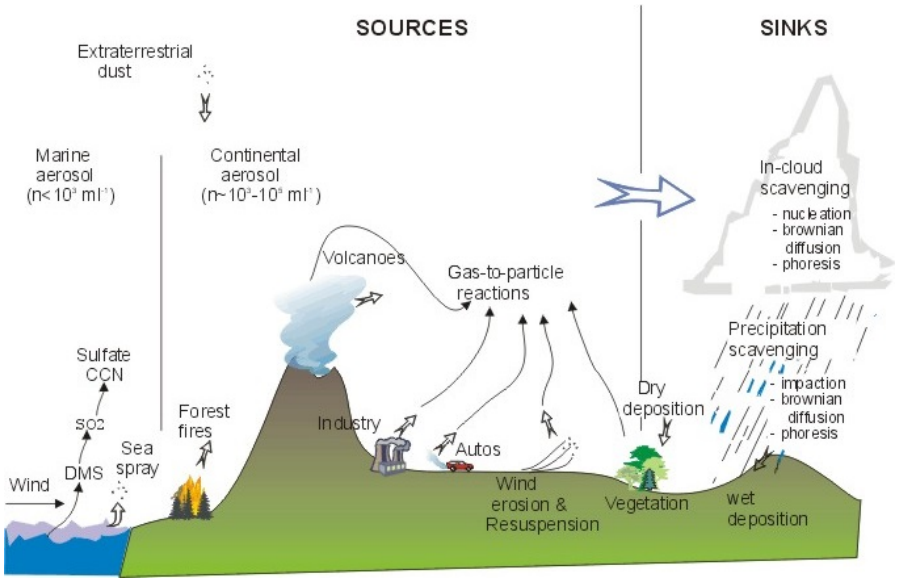

Figure I.5 – Summary of aerosols sources and sinks in the atmosphere - Source: https://personal.ems.psu.edu/~lno/Meteo437/Aerosol.jpg

INPs exhibit the same diversity than general ambient aerosols, which makes their identification a challenging task. A few characteristics have previously been established as necessary for a particle to be an effective INP: the aerosol should be highly water insoluble, larger than about 0.1 µm and have a crystallographic structure that can fit an ice lattice (Vali 1985; Pruppacher et al. 2012). However, a lot of observations challenge those views, and such requirements are not considered mandatory anymore, as described in Kanji et al. (2017).

I.2.2 Identification and properties of Ice Nucleating Particles

Figure I.6, taken from the overview on INP by Kanji et al. (2017) shows the results of a number of studies from field measurements all over the globe. This

figure illustrates perfectly how the INP concentrations from one site to an other can vary, as well as the variability in composition. From the lower end of the spectrum at -5 °C to the higher end at -40 °C, the INP concentrations span 5 to 10 orders of magnitude. Furthermore, at a given temperature, the concentrations span about 3 to 4 orders of magnitude, with greater differences at temperatures >-20 °C than at temperatures <-20 °C. Nevertheless, INP concentrations roughly exhibit an exponential trend as temperature decreases, which has been observed since the beginning of INP related studies (Vali 1971). In the following, we will give a broad overview of the current knowledge of atmospheric INPs.

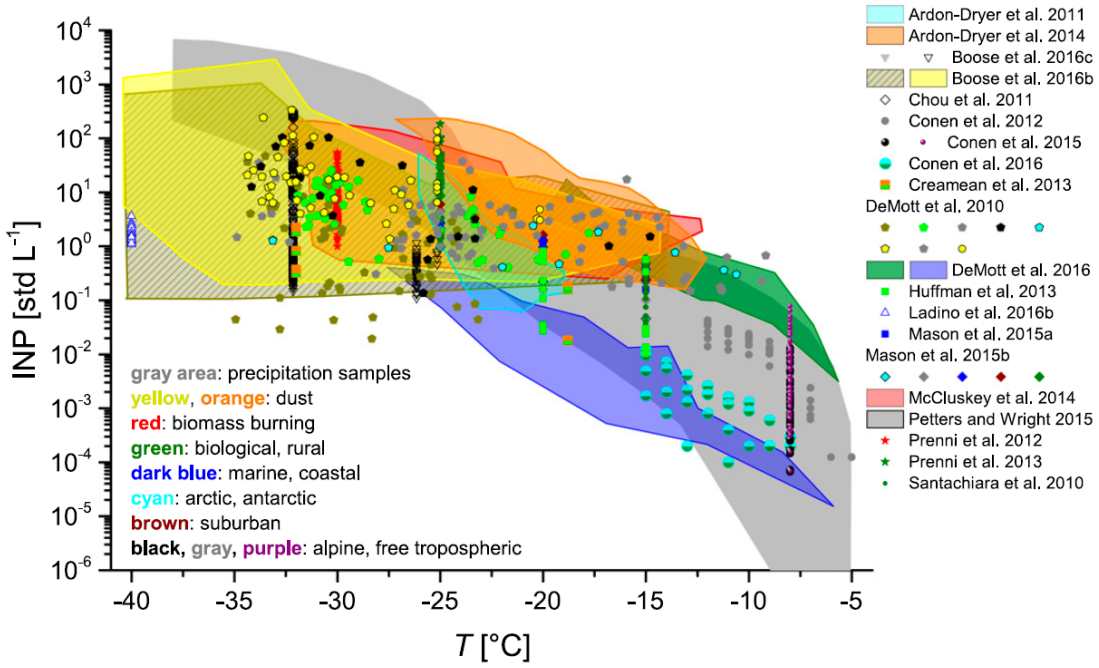

Figure I.6 – Summary of INP concentrations from field measurements conducted globally (taken from Kanji et al. 2017). The symbol color and font color give indication on the sampled air mass type, aerosol type or sampling location, and dual-colored symbols indicate the two different air mass or aerosol types that were sampled. Hashed areas and open symbols present measurements conducted below water saturation, while all other measurements were taken above water saturation. Masking of data was avoided by using different symbol sizes or shading of the relevant areas. INP concentrations are given at standard conditions (1013 hPa and 273.15 K), except the Antarctic INP measurements from Ardon-Dryer et al. (2011).
List of references mentioned:

Ardon-Dryer et al. (2011);
Ardon-Dryer et al. (2014);
Boose et al. (2016a);
Boose et al. (2016b);
Chou et al. (2011);
Conen et al. (2012);
Conen et al. (2015);
Conen et al. (2016);
Creamean et al. (2013);
DeMott et al. (2010a);
DeMott et al. (2016);
Huffman et al. (2013);
Ladino et al. (2016);
Mason et al. (2015a);
Mason et al. (2015b);
McCluskey et al. (2014);
Petters et al. (2015);
Prenni et al. (2012);
Prenni et al. (2013);
Santachiara et al. (2010);

I.2.2.1 Mineral dusts

Mineral dusts, of desert, volcanic or agriculture origin, are considered to be one of the most important types of INP (Hoose et al. 2012; Murray et al. 2012; Tang et al. 2016). As a result of their large mass emission rates (Engelstaedter et al. 2006), which makes them well distributed worldwide (Prospero 1999; Prospero 2002; Knippertz et al. 2014). Hoose et al. (2012) showed that dust particles act as ice crystals at T <-15 °C (see Fig. I.6), however dust-based INPs have been observed to be active at higher temperatures, depending on the particle size, amount of K-feldspar fraction and particle concentration per droplet. Indeed, K-feldspar has been identified as the most important component of dust INP (Kumai 1976; Atkinson et al. 2013), and it is active at warmer temperatures than the other typical components of mineral dusts (Augustin-Bauditz et al. 2014; Peckhaus et al. 2016). Despite its relatively low abundance, K-feldspar may be a significant contributor to ice nucleation in MPCs, especially at temperatures warmer than -20 °C, i.e. warmer than the onset temperature of other mineral dusts.

Desert dust particles are both important at a regional scale and at a global scale, because they are susceptible to be transported over long distances, and therefore influence ice formation up to thousands of kilometers away from the source. For example, studies have shown that dust has a large influence on the formation of orographic wave clouds and cirrus clouds in the upper troposphere (Pratt 2009; Creamean et al. 2013; Cziczo et al. 2013). Kumai (1976) found that 60% of ice crystals residuals were clay minerals, and, in Europe, Chou et al. (2011) observed that Saharan dust events coincided with increased INP concentrations at -31 °C. DeMott et al. (2003b) observed increased INP numbers in air masses containing Saharan dust over Florida, and Creamean et al. (2013) also observed Saharan and Asian dust in precipitations in California. It is still unclear why mineral dust, and in particular K-feldspar, is a particularly efficient INP. The main hypotheses are that it either caused by a strong hydrogen bonding at the surface of the INP, or by ionic interaction between the water molecules and the INP surface. These hypotheses were made both from deposition mode (Yakobi-Hancock et al. 2013) and immersion mode observations (Atkinson et al. 2013; Zolles et al. 2015).

Soil dust particles are emitted from pastures and agricultural crops and are thought to contribute to about 20% of the global dust emissions (Forster et al. 2007). O'Sullivan et al. (2014) showed that they are efficient INPs, comparable to some bioaerosols or feldspar dusts. Onset temperatures as high as -6 °C have been observed corresponding to INP concentrations of about 0.01 L^{-1} (Garcia et al. 2012; Conen et al. 2011; O'Sullivan et al. 2014; Hill et al. 2016), whereas such concentrations for natural dusts or clay have only been observed at temperatures between -12 °C and -25 °C (Murray et al. 2012). O'Sullivan et al. (2014) and Tobo et al. (2014) suggested that the high INA of soil dusts can be explained by internal mixing with biogenic matter, which in general exhibit high INA at warmer temperatures (Huang et al. 2021). Experiments that aimed to remove biological material either through heating or hydrogen per-

oxide showed a high reduction of their INA at T > -35 °C (Garcia et al. 2012; O'Sullivan et al. 2014; Hill et al. 2016). Still, it remains necessary to determine whether the organic material or the host soil dust particle is the INP, especially considering how widespread agricultural activities are.

Volcanic dust and ash particles are emitted at irregular intervals, but with potentially high emission rates (Dentener et al. 2006). The INA of volcanic particles varies significantly depending on the ice nucleation mode considered. It has been shown that in immersion or deposition freezing mode, volcanic particles could act as INP at temperatures colder than -30 °C (Zolles et al. 2015, Hoyle et al. 2011; Steinke et al. 2011; Schill et al. 2015), but it was observed that they could be active in contact freezing mode at higher temperatures (Fornea et al. 2009). Field studies have shown that INP concentrations significantly increased when a volcanic plume was sampled (Prenni et al. 2009; Bingemer et al. 2012). Overall, INP studies on volcanic particles suggest that they could be important INPs at colder temperatures, especially in the absence of more effective INPs.

I.2.2.2 Metals compounds

Metallic particles in the atmosphere mostly originate from anthropogenic activities, such as smelting, urban dust and aircraft engine ablation. They have been observed frequently inside ice residuals from cirrus clouds (Cziczo et al. 2009; Cziczo et al. 2013). Their INA has been shown to vary a lot depending on their chemical composition. Both pure metal or metal oxides have been found to nucleate ice at temperatures lower than -45 °C (Archuleta et al. 2005; Yakobi-Hancock et al. 2013). Lead seems to be one of the most efficient metal INPs (Cziczo et al. 2009), and has been found in multiple locations over the globe (Kamphus et al. 2010).

I.2.2.3 Combustion particles

Combustion particles are mainly emitted by the burning of either biomass, in events like wildfires or agricultural fires, or of fossil fuels with, transportation or industrial activities (Penner et al. 1992). As a result of the diversity of potential sources, they are in general very chemically complex particles. Combustion particles are separated in black carbon (BC) particles, or soots, and organic material. Given their high emission rates, their ubiquity and their high atmospheric concentrations (Schwarz et al. 2010), they can play an important role in the interactions between particles and clouds, and therefore in atmospheric ice formation. However, there is still no consensus whether these particle act as INPs in the atmosphere, as contradictory observations raise both from laboratory and field experiments. For example, a number of laboratory studies reported that BC particles were efficient INPs at cirrus-relevant temperatures in the deposition mode (DeMott et al. 1999, Möhler et al. 2005; Abbatt 2006; Koehler et al. 2009; Chou et al. 2013). However, other studies (e.g.Friedman et al. 2011; Schill et al. 2016) showed that BC particles did not act as INP in the

immersion mode. Additionally, a recent laboratory study in cirrus conditions showed that soot particles coated with H_2SO_4 exhibited reduced ice nucleating abilities (Gao et al. 2022).

Field campaigns also yield divergent results: DeMott et al. (2003b) found ash particles in ice crystals residuals at cirrus temperatures, but in similar conditions biomass particles were depleted in ice crystals residuals (Cziczo et al. 2013). McCluskey et al. (2014) found that particles originating from biomass burning could nucleate ice between -12 and -32 °C. Prenni et al. (2009) showed that a large amount of INP were carbonaceous particles and that they could play an important role at a regional scale.

I.2.2.4 Biological aerosols

Bioaerosols (or biological aerosol particles) refer to particles that are emitted by biogenic sources such as forests, oceans, soils and living organisms (Després et al. 2012; Fröhlich-Nowoisky et al. 2016). Bioaerosol include a wide range of particles, which are extremely varied in size (from a few nanometers to hundreds of micrometers) and in nature. Biological materials include pollen, fungal spores, algae, lichens, bacteria, viruses, biological molecules (e.g. proteins, lipids, polysaccharides) and biological fragments (e.g. insects, plant fragments). These biological materials have been shown to be active as INPs at various temperatures, and are ubiquitous in the atmosphere (DeMott et al. 2010a; Zhai et al. 2018; Felgitsch et al. 2018; Huang et al. 2021).

The INA of bioaerosols strongly depends on the nature of particle and on their atmospheric relevance at tropospheric concentrations. Even though they have been detected in ice samples in clouds (Creamean et al. 2013, Pratt 2009), it remains unclear whether their impact is limited to a regional scale or if they also have a global influence. Some studies found that only a small proportion of biological materials could accelerate ice nucleation (Joly et al. 2014; Akila et al. 2018; Hu et al. 2020), and that the INA of those particles is strongly linked to a few species of bacteria, fungi, algae, plants and insects (Christner 2010; Kunert et al. 2019; Karimi et al. 2020). In particular, it has been shown that the bacteria *Pseudomonas Syringae* is an efficient INP at temperatures as warm as -2 °C (Maki et al. 1974, Joly et al. 2013, Araujo et al. 2019). This bacteria is used in an artificial form with Snomax©. Pandey et al. (2016) showed that the INA from *P. syringae* comes from the active sites of the nucleation protein (inaZ) found on the outer cell membrane of the bacteria, which exhibit hydrophilic-hydrophobic patterns that promote the ordering of the water molecules, thus allowing ice nucleation on the surface.

Bioaerosols in precipitation samples have been shown to be efficient INPs (Christner et al. 2008a, Pouzet et al. 2017), and are, by their nature, strongly affected by climatic and land-use types, and thus exhibit strong temporal and spatial variations (Christner et al. 2008a, Christner et al. 2008b). Biological materials can be single aerosols, or be attached to other particles (such as soil dusts, see I.2.2.1), and are able to be transported over long distances, thus af-

fecting cloud formation and precipitations far away from the source (Joyce et al. 2019).

Biological INPs have been gaining traction as a subject recently (Huang et al. 2021), and have been the focus of several field campaigns (Wolf et al. 2020a; Steinke et al. 2020; Schneider et al. 2021). Despite this recent interest, observational data is still lacking due to the limitation of the current measurement methods (Huang et al. 2021). This leads to inaccurate assessment of their influence over the climate system (Hoose et al. 2010; Burrows et al. 2013; Spracklen et al. 2014), and thus more data is needed in order to better constrain the parameters and hypothesis for our understanding of regional and climate processes.

I.2.2.5 Marine aerosols

An important uncertainty on the sources of INP in the atmosphere comes from marine aerosols, especially given that oceans cover 70% of the Earth's surface. A number of field campaigns both on coastal/island sites (Mason et al. 2015a; Irish et al. 2017; Ladino et al. 2019; Gong et al. 2020) and in the open oceans and seas (McCluskey et al. 2018b; Trueblood et al. 2021), have highlighted the importance of marine INPs (Wilson et al. 2015; DeMott et al. 2016).

Marine aerosols exhibit roughly the same nucleating ability than soil dusts (DeMott et al. 2016), however their concentrations are much lower than ground-based aerosols (Fig. I.6). This suggests that marine aerosols could be atmospherically relevant only at the regional scale, where dust aerosols are absent (Burrows et al. 2013; Gong et al. 2020). Some marine aerosols exhibit organic and biological material that promote ice nucleation, such as cell fragments, vesicles, carbohydrates, amino acids and proteins (Wolf et al. 2019).

In general, marine INPs have been linked to biological activities such as plankton bloom in remote marine and coastal sites (McCluskey et al. 2017; McCluskey et al. 2018a; McCluskey et al. 2018c). Biological INPs were found to be predominant in both the surface microlayer (SML) and bulk seawater in the Canadian Arctic, were several studies showed that most of the measured INPs were heat-sensitive materials measuring between 0.02 and 0.22 µm (Wilson et al. 2015; Irish et al. 2017; Irish et al. 2019a; Irish et al. 2019b). In the Mediterreanean Sea, Trueblood et al. (2021) was able to divide the INPs in the sea spray in two classes, and found that warm INPs (T > -22 °C) were correlated with water soluble organic carbon and surface sea water parameters (e.g. particulate organic carbon, INPs in the bulk sea water), while cold INPs (T < -22 °C) were correlated with water insoluble organic carbon and dissolved carbon concentrations in the SML.

In conclusion, there are still tremendous uncertainties on the observational data and thus in model simulations for biological INPs in the ocean. These points will be further developed in the introduction of Chapter III.

I.2.3 Measurement techniques

> *"Historically, the measurement of ice nucleating activity has been found to be stubbornly difficult. Ice nucleation is sensitive to a large number of complex variables, so that the requirement that measurements reflect the reaction of the nuclei to the state of those variables in natural clouds is indeed a demanding one."*

This quote by Gabor Vali in 1976 (Vali 1976) perfectly encapsulates the issues with measuring ice nucleation with precision in the atmosphere: INPs are very scarce, have varied chemical and physical properties and can exhibit significant variability over small time periods and have ambient concentrations ranging over several orders of magnitude. Furthermore, no single instrument is suited for measuring the whole INP spectrum, due to the wide the range of the temperature spectrum at which heterogeneous freezing occurs.

INP measurement methods were first developed in the 1940s, using cloud chambers which contained air with controlled humidity and temperature reproducing cloud conditions (e.g. Schaefer 1946; Vonnegut 1947; Palmer 1949; Aufm Kampe et al. 1951; Mason 1962; Bigg 1966). Aerosols were then injected into the chamber where they were able to nucleate ice crystals, which could then be counted. Vonnegut (1947), for example, used this technique to test a variety of aerosol particles and determined that silver iodide was an efficient INP. The first expansion chamber suited for aircraft sampling of INPs was developed by Palmer (1949), who measured INP concentrations between 1 and 50 per liter of air between -15 °C and -31 °C, which is well within concentrations measured nowadays. Despite these encouraging results, measurements from this period all came with extreme variability, caused either by the methods used, experimental artifacts or the type of particles sampled.

Since then, considerable improvement has been made in INP measurement techniques, but even today there is still no instrument that is capable of measuring the full range of temperatures relevant for ice nucleation. In the following section, we will discuss the different types of methods that have since been developed within the IN community.

Because of the variability of the instruments and techniques involved, comparing instruments in laboratory workshops is of great interest. Consequently, international workshops have been organised as early as 1967 in Lannemezam, France, in order to study any difference between the instruments developed by the community. Since then, international workshops on ice-nucleation have taken place in various locations (Grant 1971; Vali 1976; DeMott et al. 2008; DeMott et al. 2011; DeMott et al. 2018; Brasseur et al. 2022).

I.2.3.1 On-line measurements

On-line instruments are able to measure INPs with a very high temporal resolution (of the order of minutes), thus making them powerful tools to evaluate the influence of rapidly changing conditions, such as various airmasses at a

given site. However, because of their low sampling volumes (a few liters of air), they are not suited to measure lower INP concentrations, which is a liability at temperatures warmer than -20 °C (see previous section and Figure I.6). One solution for measuring low INP concentrations with on-line chamber is to pair them with particle concentrators (Gute et al. 2019), which can increase the aerosol concentrations by factors of 10 to 20. Nonetheless, on-line instruments typically operate at temperatures <-20 °C.

Following the initial expansion chambers described at the beginning of this section, portable expansion chambers were developed for aircraft measurements (Bigg 1957; Warner 1957), where high time resolutions are needed. Following this development, the Continuous Flow Diffusion Chambers (CFDC) were developed and have since become the most used on-line sampling technique. The first designs of CFDCs included diverse orientations and geometries (Hussain et al. 1984; Rogers 1988), however the design that was retained was the vertical cylindrical version developed by Rogers et al. (2001), the Colorado State University CFDC (CSU-CFDC). Other CFDCs were later developed and used in various field campaigns, including the Zurich Ice Nucleation Chamber (ZINC, Stetzer et al. 2008), the Portable Ice Nucleation Chamber (PINC, Chou et al. 2011) or the Spectrometer for ice nucleating particles (SPIN, Garimella et al. 2016).

The principle of operation of CFDCs is to flow air containing particles between two ice-coated plates at different temperatures, creating a temperature and saturation gradient by which the aerosol stream passes with typical residence times of about 10 seconds. This allows the INPs to nucleate ice crystals, which are then counted by an optical counter on the exit of the chamber (Rogers 1988; Nicolet et al. 2010). The conditions recreated in CFDCs are most of time those from MPCs, and are in the immersion freezing mode, although they can sometime sample in the deposition or condensation mode (Welti et al. 2014; Boose et al. 2019). The ability of CFDCs to have high time-resolved INP measurements is also a drawback, as the sampling volume is rather small. This is a problem for sampling the rarer INPs, typically at temperatures warmer than -20 °C, and restricts the application of CFDCs to lower temperatures. In the following section I.2.3.2 we will present techniques that have been developed for temperatures warmer than -20 °C.

Other on-line methods also exist at present, like flow tubes, where aerosol particles are activated into droplets at supercooled temperatures, before freezing. This design is used to investigate immersion freezing with the Leipzig Aerosol and Cloud Interaction Simulator (LACIS, Hartmann et al. 2011).

Finally, more modern simulation chambers have been designed since the 1960s, that allow large scale experiments in laboratory studies, such as the Aerosol Interaction and Dynamics (AIDA, Mohler et al. 2006). This chamber reproduces atmospheric conditions and mimics the process by which an air mass is cooled as it rises and expands in the atmosphere. Its huge size (84.5 m^3[1] allows several studies on ice nucleation to be conducted by different instruments

[1] https://www.imk-aaf.kit.edu/73.php

simultaneously, under controlled conditions (DeMott et al. 2018), however it is not portable and can only allow the study of artificial aerosols.

I.2.3.2 Offline measurements

Offline methods have first been developed in the 1960s by Bigg et al. (1963) and consist of first collecting atmospheric aerosols onto filters or other substrate surfaces using sampling time of several hours to several days, and then analysing those filters for INPs in a laboratory, which allows to work under controlled temperature and relative humidity (RH) conditions.

Different approaches exist today for the filter analysis. The first approach is to place substrates containing INPs (e.g. filter cut-outs or glass substrates) on a cold stage with humid air, while controlling freezing optically. Examples of this method are the Micro-Orifice Uniform Deposit Impactor-Droplet Freezing Technique (MOUDI-DFT ; Mason et al. 2015b; Ladino et al. 2019) or the Frankfurt Ice Deposition Freezing Experiment (FRIDGE ; Bundke et al. 2008; Schrod et al. 2016). The second approach consists in extracting the aerosol impacted onto the filter into pure water and then freezing droplets of the resulting solution, while also counting freezing droplets optically. Examples of this approach include the LED-Based Ice Nucleation Detection Apparatus (LINDA; Stopelli et al. 2014; Pouzet et al. 2017) or the Ice Nucleation Spectrometer of the Karlsruhe Institute of Technology (INSEKT; Schiebel 2017; Schneider et al. 2021).

Because offline techniques rely on longer integrated sampling times and volumes, they are well suited to analyze the lower INP concentrations at warmer temperatures, particularly biological INPs (Huang et al. 2021). In return, they have a very coarse time resolution which makes them unable to distinguish differentiate INP in rapidly changing atmospheric conditions.

I.2.4 Prediction and modeling of INPs

Representating and predicting cloud microphysical processes in general, and ice nucleation in particular, is still a challenge because the microphysics involved are still poorly understood (see previous sections I.1.1 and I.1.2.1 on ice nucleation processes). One of the ways to improve climate models is to predict INP concentrations with empirical parameterizations.

Similarly to what was exposed in section I.1.1 and I.1.2.1, two approaches are used to describe INP parameterizations: a time-dependent approach that is based on the CNT or other models (i.e. Vali et al. 2015b), and a time-independent (or stochastic) approach which uses active surface sites as a function of temperature only,

I.2.4.1 Time-dependant approach

The time-dependant approach uses the set of equations described briefly in I.1.2.1, from Pruppacher et al. (2012) and recalled by Kanji et al. (2017):

$$F_{ice}(T) = 1 - \exp\left(J_{het} A_i \Delta t\right), \tag{I.6}$$

$$J_{het}(T, S_i, \theta) = \kappa \exp\left[\frac{\Delta G(T, S_i) f_{het}(\theta)}{kT}\right], \tag{I.7}$$

$$f_{het}(\theta) = \frac{(2 + \cos\theta)(1 - \cos\theta)^2}{4}, \tag{I.8}$$

with F_{ice} the fraction of INPs with a surface area A_i at a given temperature T and S_i saturation with respect to ice, Δt the change in time, k the Boltzmann constant, ΔG the change in Gibbs free energy, J_{het} the heterogeneous nucleation rate, f_{het} the scaling factor and θ the contact angle. Finally, κ is the kinetic parameter which defines the speed of conversion to the fraction of ice phase, but the exact value and composition of this term is still debated (Thomson et al. 2015; Welti et al. 2014). Different studies have given estimates of the value of κ, with a wide range of values, including about 10^{24} $m^{-2}s^{-1}$ given by Fletcher (1969) or ranging from 10^{9} to 10^{19} $m^{-2}s^{-1}$ by Welti et al. (2014) between -20 °C and -55 °C.

Another studied parameter is the contact angle θ, with models using a single contact angle for the whole population of INPs, or models that consider a distribution of contact angles (multicomponent stochastic models, Marcolli et al. 2007). Multicomponent models have seen a lot of development, and now include both the CNT framework and the deterministic approach, as they consider active sites with a given nucleation coefficient (Broadley et al. 2012; Niedermeier et al. 2011). Examples of such models include Lüönd et al. (2010), Murray et al. (2011) or Murray et al. (2012).

I.2.4.2 Stochastic approaches

Because the stochastic approach is based on the idea that the ice-nucleating ability of an INP is only defined by the ice-active sites at its surface, a variable that is often used is the surface density of sites active on a particle at a given temperature $n_s(T)$. As an approximation, it is defined as the INP concentration n_{INP} divided by the total surface of aerosols S_{aer}:

$$n_s(T) = \frac{n_{INP}}{S_{aer}}. \tag{I.9}$$

n_s is expressed in INPs per unit surface (i.e. INP.m^{-2}, or simply in m^{-2}). It is a useful tool to evaluate the INA of aerosols while taking their size into account.

Vali (1971) defines the fraction of particles that result in freezing at a given

temperature $F_{ice}(T)$ as:

$$F_{ice}(T) = \frac{N_{ice}(T)}{N_{tot}} = 1 - \exp(-n_s(T)S_{aer}), \tag{I.10}$$

with $N_{ice}(T)$ the number of frozen particles or ice crystals at a given temperature T. N_{tot} is the total number of particles, defined as the sum of the number of liquid droplets N_D and N_{ice}, such as $N_{tot} = N_D + N_{ice}$, in the case all particles are immersed within droplets or ice crystals during the experiment.

Since n_s can be determined empirically for a given INP, Eq. I.10 can be used to predict F_{ice} for a given aerosol type, requiring only the measurement of S_{aer}. Many studies have thus developed parameterizations from laboratory data using n_s for only one type of INP. Examples include Niemand et al. (2012) for desert dusts, Atkinson et al. (2013) for feldspar, Niedermeier et al. (2010) for Arizona Test Dust or Welti et al. (2012) for illite. For example, Niemand et al. (2012) suggest the following exponential fit for desert dust:

$$n_s(T) = \exp\Big[-0.517 \cdot (T_K - 273.15) + 8.934\Big], \tag{I.11}$$

with n_s in m^{-2} and T_K the cloud temperature in Kelvin.

Other stochastic parameterizations use atmospheric INP measurements in order to not be constrained to a single type of particle. For example, DeMott et al. (2010a) used the number of aerosols larger than 500 μm and INP data from several studies worldwide in order to develop a parameterization in the form:

$$n_{INP}(T) = a(273.16 - T_K)^b \cdot n_{aer,>500\mu m}^{c(273.16-T_K)+d}, \tag{I.12}$$

with n_{INP} the number concentration of INP in stdL^{-1}, T_k the cloud temperature in Kelvin and $n_{aer,>500\mu m}$ the number of aerosols larger than 500 μm in cm^{-3} ; and $a = 5.94 \times 10^{-5}$, $b = 3.33$, $c = 2.64 \times 10^{-2}$, $d = 3.30 \times 10^{-3}$. The aim of this parameterization was to predict INPs globally, and was used in both lidar (Peng et al. 2015) and global modeling studies (Tan et al. 2016). This parameterization was improved by Tobo et al. (2013), and modified by DeMott et al. (2015) with a final form of:

$$n_{INP}(T_K) = (\mathrm{cf}) n_{aer,>500\mu m}^{\alpha(273.16-T_K+\beta)} \cdot \exp\Big[\gamma(273.16 - T_K) + \delta\Big], \tag{I.13}$$

where cf = 1, $\alpha = 0$, $\beta = 1.25$, $\gamma = 0.46$ and $\delta = -11.6$. This parameterization is robust as it is based on a large number of INP datasets representing several regions of the globe. It also has the advantage of being easily integrated into other studies with only requiring information on particle size. Other stochastic parameterizations for INPs in particular environments exist, for example in forest areas (Schneider et al. 2021) or in the oceans (Wilson et al. 2015; Trueblood et al. 2021).

The drawback from stochastic parameterizations is that they are unreliable when used outside the temperature range they have been developed in (Hoose

et al. 2012). Furthermore, it is challenging to unify the whole heterogeneous freezing spectrum (≈-5 to -38 °C) under one parameterization, as it requires combining results from off-line and on-line measurements. An other limitation is the assumption of a uniform type of INP under the temperature spectrum studied. For example, Niemand et al. 2012 assumes that all INPs used for prediction are of the dust type, and McCluskey et al. (2018c) assumes that all INPs were of the "pristine" marine SSA type.

As an argument in favor of stochastic parameterizations, Vali (2014) suggested that time-dependent effects could be negligible over the time-independent effects because of the importance of ice active surface sites for nucleation. This hypothesis should work well in cases where the cooling rates are high because the ice nucleation is extremely sensible to temperature: Ervens et al. (2013) suggest that an uncertainty of 0.2 °C has the same effect than differences in time of a factor of 100.

Thus, the multicomponent stochastic models offer a way to predict INP populations in cases where time is of significance or in cases with a high variability in the behavior of the particles, and they are probably the most accurately way to represent the formation of ice in clouds (Kanji et al. 2017). However, CNT-based parameterizations also have drawbacks. They have been shown to misrepresent the temperature dependence in various cases, and in some cases have overpredicted the number of ice crystals (Kanji et al. 2017).

This overview shows that INP parameterizations is a critical topic for our understanding of the formation of ice and for our ability to implement these processes in global models.

I.3 Open questions and aim of this thesis

I.3.1 Open questions in ice nucleation studies

As discussed previously, there are still large uncertainties associated with the formation and lifetime of ice crystals in the atmosphere, despite a considerable increase in dedicated studies. A non exhaustive list of the questions that still remain to be answered is given and discussed below, as a summary from the recommendations from Kanji et al. (2017) and Coluzza et al. (2017).

I.3.1.1 Question 1: What is the origin of the INA of an INP?

What gives a particular INP its INA is still largely unknown. A number of hypothesis on the nature of the surface sites exist in the literature, including the morphology of the site mimicking the ice lattice, surface chemistry, the bulk composition or the ions released from the INP. Multiple studies have used computer simulations to investigate active sites, and have showed that INA is influenced by several molecular properties, such as surface hydrophobicity, surface

morphology and local electric fields (e.g. Matsumoto et al. 2002; Cox et al. 2012; Sanz et al. 2013; Lupi et al. 2014; Yan et al. 2011).

Fitzner et al. (2020) recently used a data-driven approach to suggest that four microscopic properties may control the INA of an INP: the "lattice match" of the substrate (i.e. the shape of the surface site mimicking the shape of the ice lattice), the local ordering of the molecules induced in the liquid water, the density reduction of liquid water near the surface and the corrugation of the adsorption energy landscape felt by water (i.e. the diversity of the possible adsorption energy vales).

Several observations and calculations (Pedevilla et al. 2016; Bi et al. 2016; Kiselev et al. 2017) have shown that amorphous surfaces could also be good INPs, challenging the most widespread hypothesis that the surface of INPs are similar to the crystallographic structure of ice. Thus, there is still need for studies to answer these fundamental questions, which could also help determine what type of parameterization is the best.

I.3.1.2 Question 2: What are the actual nucleation modes?

Differentiating the heterogeneous nucleation modes is still under controversy. As presented in section I.1.2.1, four freezing mechanisms are currently considered (Vali et al. 2015a): deposition ice nucleation, contact freezing, immersion freezing and condensation freezing. However, this perception was different in the past, as immersion and condensation freezing were considered the same process (Fukuta et al. 1982), and this is likely to change again in the future as more observations are done. Indeed, Vali et al. (2015a) question the hypothesis that condensation freezing is a distinct mode from immersion freezing and deposition nucleation. For example, both Wex et al. (2014) and Hiranuma et al. (2015) have observed similar results between immersion and condensation freezing.

A process called pore-condensation could also take place in cavities and lead to trapped water and freezing at low supersaturations (Marcolli 2014). This PCF (Pore Condensation and Freezing) could be distinct but mistaken for deposition freezing in some cases, making it an additional nucleation mode.

Controversies surrounding the condensation mode also exist, where it is suggested that an inside-out process exists where the INP touches the droplet surface from the inside of the droplet. This could be caused by evaporation of the droplet. It is still unclear what the frequency of these two processes is, but it could be of importance in MPC processes (Kanitz et al. 2011; Coluzza et al. 2017).

I.3.1.3 Question 3: What is the contribution of biological or organic INPs?

Finally, quantifying the effect of the biological or organic INPs, especially in natural environments like forests, mountains or oceans, is of importance. In the recent years, this particular topic has received more and more attention from the INP community (Huang et al. 2021), and a lot of studies have been

conducted to answer this question, as discussed previously in sections I.2.2.4 and I.2.2.5.

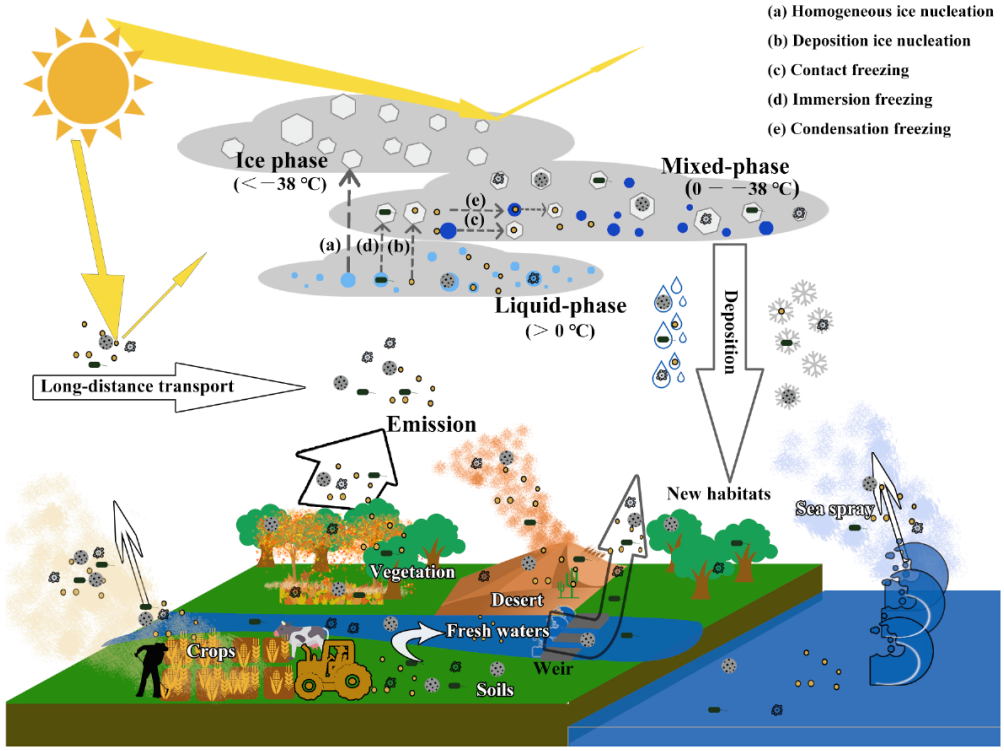

Figure I.7 – Schematic of the life cycle of biological INPs in the Earth system - Figure adapted from Huang et al. (2021)

It is more and more clear that biogenic INPs have a high contribution on ice formation in the atmosphere. Figure I.7 summarizes the influence and diversity of biological INPs on the atmosphere, land and earth processes. For example, Amato et al. (2015) showed that the INA of airborne bacteria could remain unchanged after several hours of residence in the atmosphere. Additionally, multiple studies suggested that different biological INPs develop efficient ice nucleation mechanisms in order to trigger precipitations, allowing them to be transported and deposited over long distances (Constantinidou et al. 1990; Morris et al. 2008; Möhler et al. 2008; Morris et al. 2014). Joly et al. (2013) and Pouzet et al. (2017) found that ice nucleating bacteria in precipitation and cloud water are very efficient INPs.

Biological marine aerosols also saw more focus recently, with very recent studies that tried to link the INP concentrations or the INA of particles with the biogeochemistry of seawater, along with new parameterizations (e.g. O'Sullivan et al. 2018; Irish et al. 2019a; Wolf et al. 2020b; Gong et al. 2020; Trueblood et al. 2021). The most common link found between INP activity and seawater properties is some form of organic carbon, like particulate (Wilson et al. 2015) or dissolved carbon (Trueblood et al. 2021). An increase in biological activity in the seawater is generally linked with an increase in INPs in the form of sea spray aerosols (Wolf et al. 2020b). Lacher et al. (2021) also found that sea spray

is transported over long distances and influences the INP concentrations in free troposphere (FT) conditions.

The issue is that very few instruments are able to differentiate the biological INPs, especially in dynamic or monitoring conditions. The classical methods for differentiating biological/organic INPs from other types (e.g. heat or hydrogen peroxide treatments) often lead to important uncertainties (Huang et al. 2021). The link between meteorological conditions and biological activity should also be studied, as the link between rainfall and biological concentrations is still unclear: some studies showing an increase in INPs with rainfall (Tobo et al. 2013; Joly et al. 2014; Iwata et al. 2019), and other studies show poor correlation with rainfall (O'Sullivan et al. 2018).

Furthermore, mechanisms by which biological INPs are able to promote ice nucleation are also poorly understood, and are also dependant on the type of bioaerosol considered. Understanding such mechanisms could help develop more parameterizations for specific biological material. Today, very few parameterizations focus on biological INPs (e.g. Wilson et al. 2015; Schneider et al. 2021).

I.3.1.4 Question 4: What is the effect of atmospheric processing and aging on INPs?

A better understanding of atmospheric processing and transport is also needed. Indeed, because the morphology and chemistry of the surface of an aerosol impacts its ability to nucleate ice, it is important to evaluate the influence of cloud processing, like preactivation or chemical aging. Aging occurs during the particle's lifetime and transport in the atmosphere, and includes chemical modification from reactions and physical modifications caused by collisions or by changes in atmospheric conditions. A number of studies have worked on the effect of aging on the INA of INPs, resulting in either a decrease or an increase in the INA of the particles. As a result it is still unknown how aged particles interact with ice formation in clouds.

In the free troposphere (), DeMott et al. (2003a) observed some INPs that were internally mixed, and thus subject to aging. Richardson et al. (2007) did not confirm these findings in their study at the same site, but they found that INP concentrations were lowered when the site was influenced by airmasses containing biomass burning particles coated with soluble substances. Zhang et al. (2020) studied the effect of coating on the INA of BC particles near cirrus regime, and observed that Secondary Organic Aerosol (SOA) coating generating from oxidation with O_3 did not have an effect on the INA. They however found that SOA coating from oxidation with OH showed a strong deactivation effect on the INA of the particles considered. Pouzet et al. (2017) found that biological INPs subjected to acidification in clouds had lower INA, which suggested an effect of anthropogenic activities on the efficiency of biological INPs.

On the other hand, Boose et al. (2016b) observed that dust particles internally mixed with ammonium sulfate lead to an increased INA. Kumar et al.

(2018) showed that immersion in NH_3 and NH_4 solutions could lead to an increase in INA, and Kumar et al. (2020) suggested that aged particles after monsoon events could lead to increased number of INPs in a high-altitude station in India. An other study in FT conditions showed that INPs were coated with organic material, and that the freezing onset did not exhibit much variability, which indicates that the aging process could overall equalize the INA of the INPs at the site (Knopf et al. 2010). This is especially relevant for particles exposed to long range transport.

In order to investigate long-range transport, more FT measurements are needed. Indeed, FT measurements provide access to ambient air that is not affected by local sources, but rather by long range transported air masses, thus giving insights on the processes aerosols undergo during their transport in the atmosphere. However, due to the nature of the sample sites and their accessibility, FT measurements are frequently limited: most FT measurements are done (1) in research flights, which are very limited in time due to practical reasons and cost; and (2) at ground-based stations at mountain summits, which are often hard to access and are only in FT conditions seasonally. Only relatively few FT stations have seen INP measurements take place. Examples include: the High Altitude Station Jaungfraujoch (3580 m a.s.l., Switzerland; Chou et al. 2011; Boose et al. 2016a; Lacher et al. 2017; Lacher et al. 2018; Lacher et al. 2021), the Storm Peak Laboratory (3220 m a.s.l., Colorado, USA; DeMott et al. 2003a; Richardson et al. 2007; Garimella et al. 2017) or the Whistler Mountain air chemistry laboratory (2182 m a.s.l., British Columbia, Canada; Mason et al. 2016). Measurements in these station often span only a few weeks, and thus are not able to retrieve information on seasonal variations of INPs in the FT, which is a critical information for climatology and meteorology.

I.3.2 Scope of this thesis

We showed that ice nucleation in the atmosphere is a complicated and poorly understood process, with intertwined microphysical, chemical, and biological factors. INPs are very scarce in the atmosphere, and are active over a wide range of temperatures. The aim of this thesis is for the most part in the scope of Question 3 (Section I.3.1.3), that is to understand the emission rates and processes of biological INPs in various environments. Since we focus on the biological component, we incorporate offline techniques that allow the upper end of the temperature spectrum (>-20 °C) to be investigated. To do so, we will be using the data from two marine and a mountainous sites. Indeed, biological aerosols (and hence, INPs) have been identified as a key influence on atmospheric processes and cloud formation in remote oceans, and we discussed previously (Sec. I.2.2.5) a lack of data availability in such sites due to technical limitations.

Similarly, mountainous free-troposphere sites are background sites that are interesting for studying low-concentrations INPs, and that are a great asset in understanding the transport and aging of these aerosols. Thus, ambient INPs will be studied at a high altitude remote observatory over a six months long

period.

INP concentrations in those sites will be in relation with other meteorological or co-localised data such as aerosols properties or the ocean's biogeochemical state. Such data should help us understood the nature and sources of low concentration INPs at those sites.

In Chapter II, we will present the experimental methods used throughout in this study. In particular, the offline INP analysis instrument LINDA will be thoroughly presented. In Chapter III, we present the results of the ship-based measurement campaigns TONGA and Sea2Cloud, that took place within the frame of the Sea2Cloud project[2]. We will be investigating the ice nucleating properties of seawater and sea spray in remote oceans of the Southern Hemisphere, and link them with the biochemical properties of the ocean. In Chapter IV, results from the two consecutive measurement campaigns at the Puy de Dôme station will be discussed, where the ice nucleating properties of ambient aerosols were investigated over the course of six months. These results will be submitted as a research paper in *Atmospheric Chemistry and Physics*. Conclusions and future work on the subject are presented in Chapter V.

[2] https://sea2cloud.wordpress.com/

II

Experimental methods and instruments

Outline of the current chapter

With the main goal of this thesis being to measure and characterize INPs in different environments, various instruments were setup in order to measure the physical, chemical or biological properties of the aerosols and INPs.

The instruments and parameters measured were mostly specific to each measurement campaign and sampling site, so the focus here is on the measurement methods common to the different chapters. The instruments and measurements specific to each of the measurement campaigns are presented in the corresponding chapters for better readability. Thus, we introduce here the INP analysis method using the LED-based Ice Nucleation Detection Apparatus (LINDA), as well as the methods used for aerosol analysis and characterization.

II.1 INP sampling in air and seawater

INPs in this study were measured from two distinct sources: the atmosphere and the ocean. The different methods used for sampling the INPs will be described in this section.

II.1.1 Atmospheric filter-based measurements

For atmospheric sampling a Dekati© four stage cascade impactor (Fig. II.1) was used to collect size segregated quartz filters. This impactor allows to determine the particle gravimetric mass size distribution through inertial size classification. The airflow passes through the different stages of the impactor, with diameter cutoff points of the different stages are 0.1-1 µm, 1-2.5 µm, 2.5-10 µm and >10 µm, thus allowing a wide representation of the aerosol size distribution. The Dekati© impactor was operated using an airflow of 10 L/min.

Figure II.1 – Four stage Dekati© cascade impactor used in this study. The stages correspond to, from top to bottom: >10 µm, 2.5-10 µm, 1-2.5 µm and 0.1-1 µm.

Additionally, high volume filter based measurements were also performed during the Puy de Dôme Ice Nucleation Intercomparison Campaign (PICNIC) campaign (see Chapter IV): 15 cm ⌀ quartz filters were used with an airflow

of 500 L/min. These high volume measurements allowed for the sampling of higher concentration of INPs, but are not as portable as the size-segregated low volume measurements from the Dekati© impactor.

Both types of filters were used as part of the INP analysis (see II.2), and were also used to derive the chemical properties of the sampled aerosols (see II.3.2).

The samples were stored frozen at -20 °C immediately after being collected until the INP analysis.

II.1.2 Seawater measurements

Chapter III involves the sampling and measurements of seawater INPs in addition to air filter-based measurements, in order to study the link between the ocean and the atmosphere.

The seawater samples were constituted of bulk seawater and surface microlayer (SML) samples. Bulk seawater was sampled at a 5 meter depth using water pumped into the ships, while SML samples were sampled from a pneumatic boat away from the ship, to avoid possible contamination and pollution.

The samples were stored frozen at -20 °C in 25 mL Falcon© tubes immediately after being collected and until the INP analysis a few months later.

II.2 INP analysis: the immersion freezing technique LINDA

Ice nucleation in this thesis was only measured in the immersion freezing mode (Sec. I.1.2.2). The immersion freezing technique used in this thesis is the LED-Based Ice Nucleation Detection Apparatus (LINDA). This droplet freezing assay was developed by Lukas Zimmermann and Franz Conen at the University of Basel in 2012 and is fully Open Source, along with the software used for analysis, on the Website `https://azug.minpet.unibas.ch//~lukas/FNA/index.html`.

Thanks to its simple design and operation, LINDA has been used in multiple studies and research teams to study immersion freezing and biological INPs (Amato et al. 2015, Joly et al. 2014, Pouzet et al. 2017, Pummer et al. 2015, Stopelli et al. 2014), for example on rain, snow, seawater or seawater samples. The operating principle is described extensively in Stopelli et al. (2014).

II.2.1 Operating principle of LINDA

LINDA consists of a camera taking pictures of a plate containing 52 Eppendorf tubes, which is placed in a cooling bath with a JULABO FP40 thermostat. Pictures of the experimental set-up are shown in Fig. II.2, and the detection principle is illustrated in Fig. II.3.

The Eppendorf© sample tubes containing the sample are placed on a plate (total: 52 tubes, (Fig. II.2b)) that is immersed in a cooling liquid. The tem-

perature is measured using four Pt_{1000} sensors in each corner of the plate (Fig. II.2c), with a precision of 0.1 °C. The temperature is decreased from 0°C down to -18°C as a rate of -0.33°C per minute (Fig. II.2c).

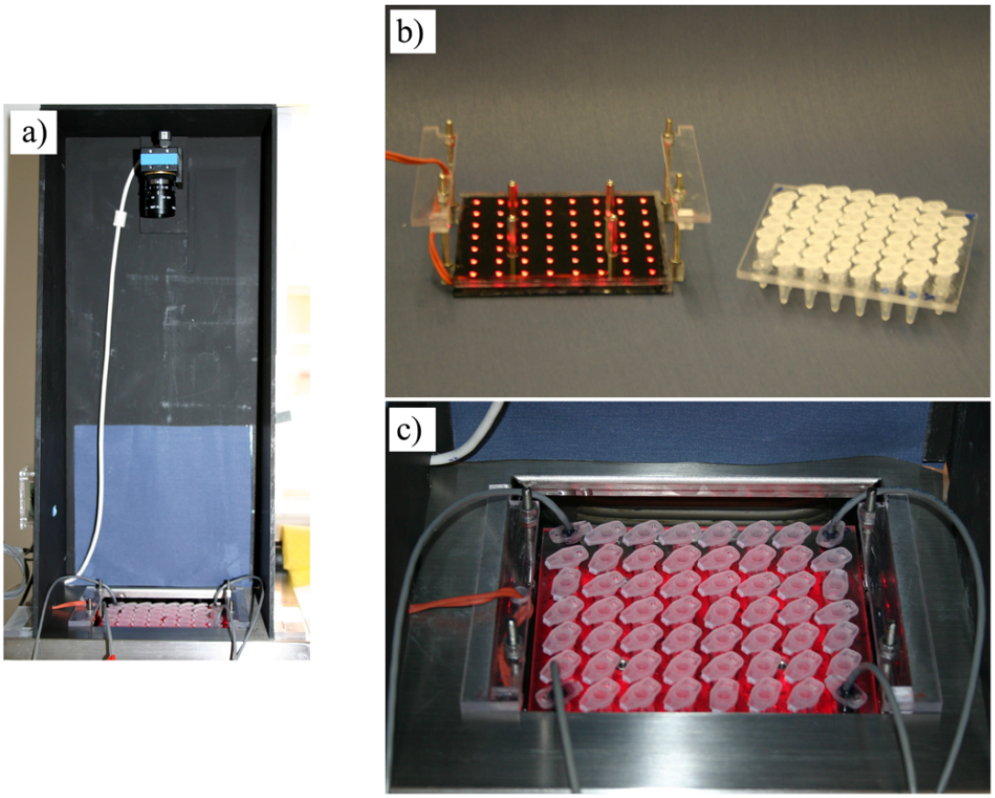

Figure II.2 – Experimental setup of LINDA. a) Cold bath set-up with camera recording from above; b) LED array and plate holding 52 Eppendorf© tubes; c) Tubes and Pt_{1000} sensors in the corners inside the cooling bath. Pictures taken from Stopelli et al. (2014).

The detection of freezing is based on the principle that the transfer of light changes when it passes through either water or ice, with light being scattered more by impurities in ice, such as crystals facets or air bubbles (Perovich 2003). The sample plate is placed over a LED array, with each LED corresponding to one sample tube. An USB CMOS Monochrome Camera is placed over the plate (Fig. II.2a), that allows the recording of light intensity passing through each tube, and the detection the exact moment and temperature at which a tube freezes.

Because the aforementioned impurities do not appear when pure water freezes, and also to avoid osmotic stress on the living cells, the sampling solution contains a small amount of sodium chloride. Thus, the mass fraction of NaCl used for preparing the samples is 0.9% NaCl. Stopelli et al. (2014) has shown that such concentrations have no impact on the freezing temperatures. Through this method, the sudden change of light intensity when a sample freezes is clearly noticeable in Fig. II.3, where we show a full LINDA plate, both with unfrozen tubes (represented by white dots) and with frozen tubes (gray dots). This sys-

tem enables the detection of freezing events with more precision than visual inspection of the tubes.

The 0.9% NaCl solution was prepared using ultrapure water with sterilized sodium chloride. This blank solution was then analysed for INP content using LINDA to check for its purity.

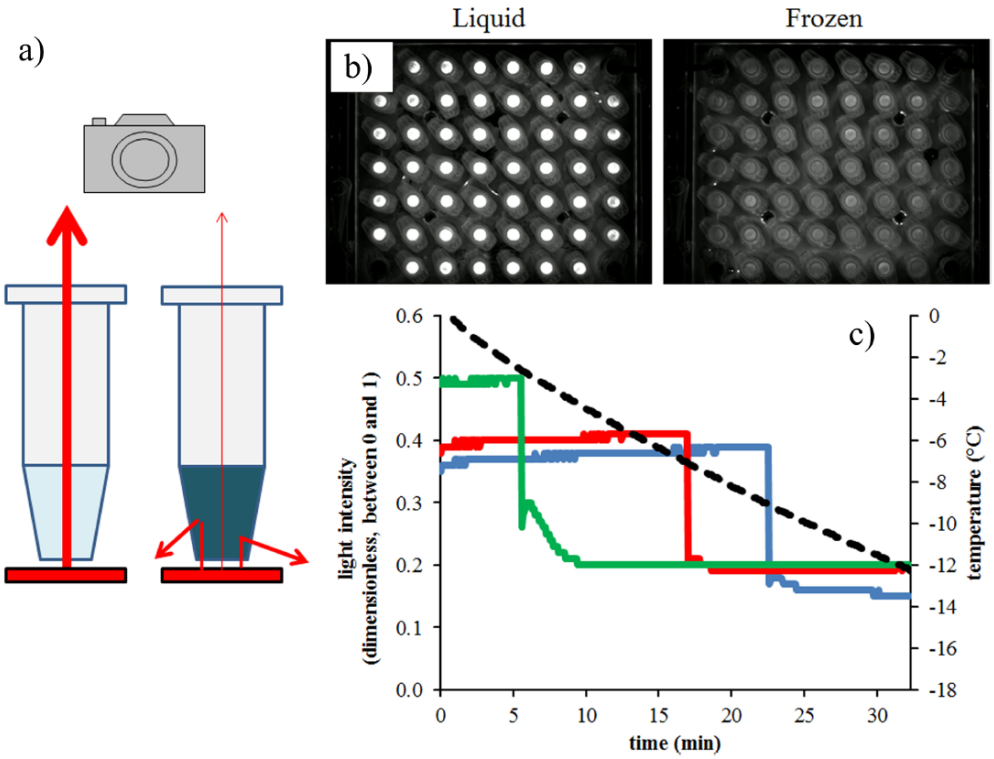

Figure II.3 – Schematic of the detection principle of LINDA - Taken from Stopelli et al. 2014. a) Schematic representation of the change in light transmission between liquid and freezing samples. b) Images taken by the camera of a full unfrozen plate (left) and full frozen plate (right). c) Time series of the temperature (black dotted line) and light intensity of three different tubes (colored full lines).

II.2.2 Sample preparation for analysis

Because LINDA only allows the analysis of liquid samples, a necessary step of the analysis of filter-based samples is to extract the aerosols from the filters. Punches of the filters were used for the analysis: the surfaces used for each different filter in all campaigns are given in Table II.1. The filter punches were then washed in 25 mL of 0.9% NaCl solution for 20 minutes while being agitated, then the filter was removed from the tube. Half of the Ependorf© tubes (26 tubes) of those samples were filled using the resulting solution. The volume of liquid poured in each Ependorf tube is indicated in Table II.1 for each campaign and sample type.

The remaining solution was then heated for 30 minutes at 100 °C in boiling water, before being used to fill the remaining 26 tubes. This heat treatment

Table II.1 – Variables used for INP analysis with LINDA for all types of samples of this study. The campaign, name and type of each sample is shown. The volume in each Ependorf© tube is stat and extraction filter surfaces are indicated.

Campaign	PICNIC	WINS	TONGA			Sea2Cloud				
Name	High volume	Size segregated (impactor)	Bulk SW	<1 µm	>1 µm	Bulk SW	SML SW	<1 µm	>1 µm	Ambiant
Type	Filter	Filter	Seawater	Filter	Filter	Seawater	Seawater	Filter	Filter	Filter
Surface used for analysis (cm²)	4.5	4.3	N/A	4.3	4.9	N/A	N/A	4.3	4.9	4.3
Volume in each Ependorf© tubes (mL)	0.4	0.4	0.2	0.4	0.4	0.2	0.2	0.2	0.2	0.2

eliminates biological INPs (Christner et al. 2008a; Wilson et al. 2015; O'Sullivan et al. 2018), allowing the number of biological INPs to be determined by comparing unheated and heated samples. This procedure is shown in Figure II.4.

The seawater samples were thawed at 20 °C. Half of the Ependorf© tubes were then filled with the untreated sample. The seawater samples were then subjected to the same heat treatment than filter samples, and the second half of the Ependorf© tubes was filled using the heated samples.

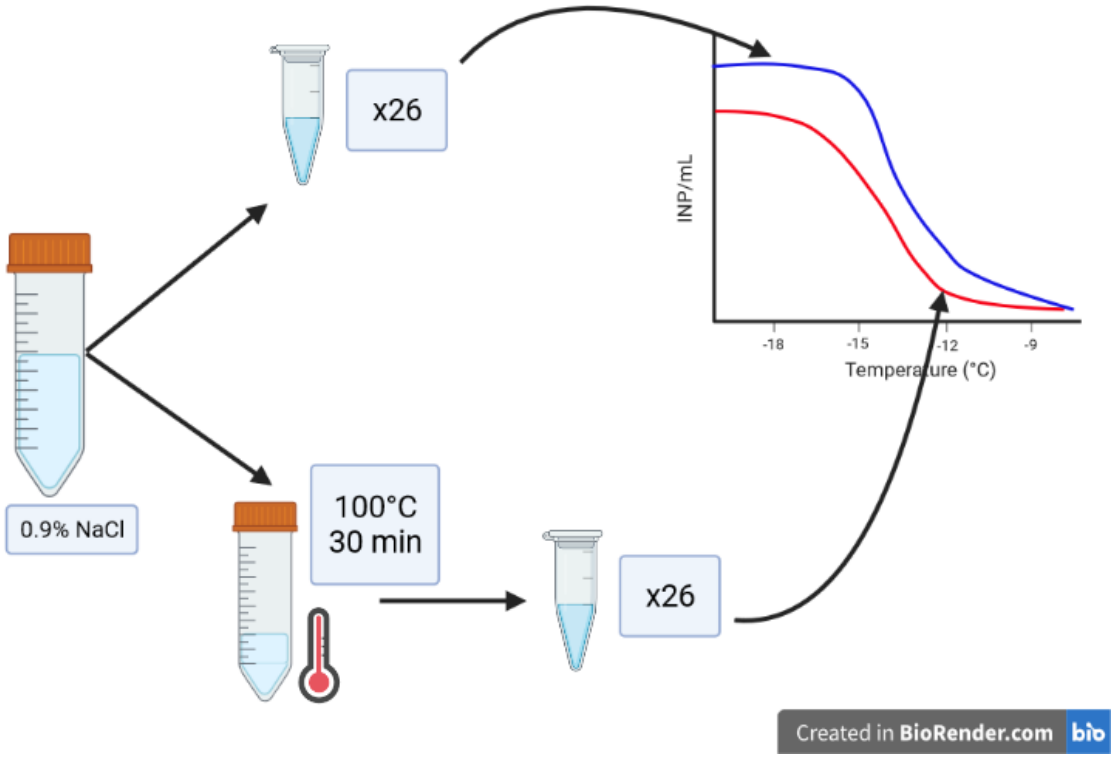

Figure II.4 – Schematics of the LINDA analysis of the samples. The blue and red curves on the top right are the cumulative INP concentrations per mL of solution used for analysis, corresponding respectively to the unheated and heated samples. These INP concentrations are calculated using the Eq. II.1. The derivation of INP concentrations is presented in Sec. II.2.3.

II.2.3 Derivation of the concentration of INP

For the analysis, the concentration of INP n_{INP}^{mL} at a given temperature is calculated through the Vali (1971) formula (Eq. II.1):

$$n_{INP}^{mL}(T) = \frac{\ln N_{tot} - \ln N_{UF}(T)}{V_d}, \tag{II.1}$$

where N_{tot} is the total number of Ependorf© tubes, $N_{UF}(T)$ is the number of tubes still unfrozen at the temperature T, and V_d is the volume of solution in a tube in mL (or droplet volume). n_{INP}^{mL} is given as a concentration of INP per milliliter of liquid analysed.

The limit of detection (LOD) is determined by the total number of tubes analysed N_{tot} and the volume V_d used for the analysis. A droplet volume of 200 µL with 26 tubes is associated to a LOD of 16.29 INP mL^{-1}, while a droplet volume of 400 µL is associated to a LOD of 8.15 INP mL^{-1}.

For filter samples, we must convert the number of INP per mL of liquid analysed to the number of INP per volume of air, using Eq. II.2:

$$n_{INP}^{L_{air}} = \frac{n_{INP}^{mL}}{V_{air}} \cdot \frac{S_F V_{dil}}{S_P}, \tag{II.2}$$

where $n_{INP}^{L_{air}}$ and n_{INP}^{mL} are INP concentrations per liter of air and per mL of solution, respectively. V_{air} is the volume of air sampled for each filter in L, S_F the total surface of the sampling filter in cm^2, V_{dil} = 25mL the volume used for washing the filter, S_P the surface of punches of filter used for the analysis in cm^2.

II.2.4 Blank samples and background treatment

Blank filters were analysed using the same procedure in order to estimate background errors. We show an example of blank filters INP analysis in Figure II.5, using two different blank filters samples from the TONGA campaign (Chapter IV). On average, blank samples started freezing at around -10 °C, and they were below the filter samples until about -18 °C.

However, heated blank samples showed increased IN activity at all temperatures compared to unheated blanks, which hints that the heat treatment results in some contaminated the samples, which is not surprising considering the added manipulation steps. However, the effect of this pollution is rather small, and appears only at temperatures <-17 °C.

For filter measurements, the values from blank filters were substracted from the values from sample filters that were above two standard deviations of the blank samples ($2\sigma_{BL}$). Values of the samples that were below this threshold were considered lower than the LOD. This threshold of $2\sigma_{BL}$ was chosen to make sure the measured INP concentration were above the statistical uncertainty of the background data. Thus, the INP concentration corrected for background

$n_{INP,corr}(T)$ is:

$$n_{INP,corr}(T) = n_{INP,raw}(T) - n_{INP,BL}(T), \tag{II.3}$$

with $n_{INP,raw}(T)$ the raw INP concentration given by the LINDA analysis and $n_{INP,BL}(T)$ the INP concentrations from blank filters.

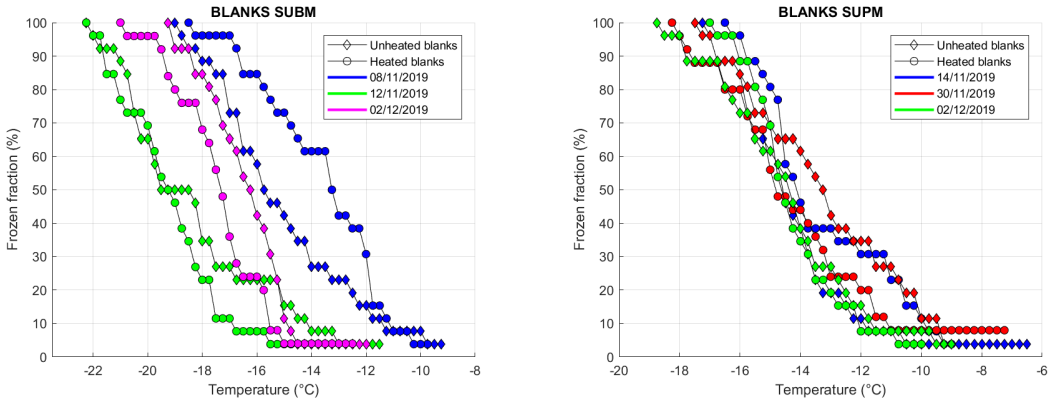

(a) Blank samples for <1µm filters during the TONGA campaign.

(b) Blank samples for >1µm filters during the TONGA campaign.

Figure II.5 – Summary of blank samples analysis with LINDA for a) Submicron samples and b) Supermicron samples during the TONGA campaign. Results are shown as frozen fractions of unheated (diamonds) and heated samples (circles).

The data from seawater samples was shifted by 2 °C to take into account the effect of salinity on the freezing temperature (Doherty et al. 1974). Contrary to filter samples, the seawater samples were not corrected for background. This choice was made because it is not possible to define a background error for seawater samples. Therefore there are no blank samples associated, and using a laboratory made solution induces further error and hypothesis.

II.2.5 Definition of INP classes used in this study

We define here the different classes of INP data used in the analysis of this study. The data are all used after the background treatment (for filter samples) or after the salinity shift (for seawater samples). INP from untreated samples will be referred to as total INP (INP_{tot}), and those from heated samples, will be referred to as heat stable INPs (INP_{HS}). We define the number concentration of heat-labile INP (INP_{HL}) as the difference between the total number concentrations of INP from untreated samples (INP_{tot}) and the number concentrations of non heat labile INP from heated samples (INP_{HS}), such as :

$$INP_{HL} = INP_{tot} - INP_{HS}. \tag{II.4}$$

II.3 Aerosol analysis

Several instruments were used to investigate the physical and chemical properties of the aerosols at the different sites in order to link these properties to their ice nucleating abilities.

II.3.1 Particle size distributions

As explained previously in Section I.2, aerosols in the atmosphere have sizes spreading several orders of magnitude (Fig. I.4), and it is not possible to explore the full particle spectrum using only one method. Therefore, in this study, particle size distributions were measured using two types of instruments:

- A Scanning Mobility Particle Sizer (SMPS) was used to measure the aerosols number concentration and size distributions from 10 to 650 nm. This instrument is based on the mobility of charged particles in an electric field. The sampled particles are first neutralized to obtain a known aerosol charged distribution, and then enter a Differential Mobility analyser (DMA) where they are classified using their electrical mobility. As they exit the DMA, the size of the particles is determined using their charge and mobility distribution.

- An Optical Particle Counter (OPC-GRIMM) was used to measure the size distribution of particles of sizes between 0.2 and 20 µm. The principle of operation of an OPC is based on the light scattering by particles. The sampled particles are contained in a focused laminar flow and irradiated by a laser diode. The scattered signal is then processed using the Mie theory, assuming the particles are spherical and homogeneous.

Combining the size distribution data from these two methods allows to have access to the aerosol size distribution from 10 nm to 20 µm. These data were used in the following to correlate the INP concentrations to the aerosol numbers and sizes. Furthermore, having access to the aerosol numbers and size distribution allows to derive the total aerosol surface area, which is an important variable to normalise INP concentrations, such as :

$$n_{IN/aer} = \frac{n_{INP}}{N_{aer}}, \tag{II.5}$$

with $n_{IN/aer}$ the number of INP per aerosol, n_{INP} the number concentration of INP per unit volume of air and N_{aer} the total number concentration of aerosols per unit volume of air. The number of INP per surface area of aerosol n_S, also called *surface site density* (see Chapter I), can also be used:

$$n_S = \frac{n_{INP}}{S_{aer}}, \tag{II.6}$$

with n_{INP} the number concentration of INP per unit volume of air and S_{aer} the total surface area of aerosols per unit volume of air.

The two variables $n_{IN/aer}$ and n_S are used to take into account the role of the number or surface of aerosols and to compare our observations with those of other studies.

II.3.2 Aerosol chemistry

An other aspect of the understanding of the IN activity in the atmosphere is the link with the aerosol chemistry. As explained in Chapter I, INPs across the -5 to -38 °C temperature spectrum have variable origins (Fig. I.6), and have very variable chemical properties.

The same filters used for the INP analysis were analysed using Ion Chromatography (IC), using the technique described in Sandrini et al. (2016): The extraction consists in putting punches of the filters (2.0 cm^2 for high-volume filters, 3.4 cm^2 for PM1 impactor filters, 8.6 cm^2 for PM>1 impactor filters) with Milli-Q water (32 mL for high-volume filters, 10 mL for PM1 impactor filters, 20 mL for PM>1 impactor filters) in a 32 mL Schott© bottle, then sonicated for 30 min. The extracted solution was analyzed by ion chromatography (ThermoFisher©) for the quantification of the main inorganic ions (Cl^-, NO_3^-, SO_4^{2-}, oxalates, Na^+, NH_4^+, K^+, Mg^{2+} and Ca^2+).

III

Ice Nucleating properties of sea spray in the Southern Hemisphere: Case study with the TONGA and Sea2Cloud cruise campaigns

Outline of the current chapter

III.1 Introduction

The oceans cover 70% of the surface of the planet, and thus they have a huge influence on the Earth's climate and water cycle. Given the lack of contribution from land sources, it is essential to understand the role of marine aerosols on cloud formation over the remote oceans. However, due to instrumental limitations and the scarcity of data sets (measurements in these remote regions are difficult due to the need for expensive field campaigns), the contribution of marine aerosols to cloud formation is not yet well characterized.

Marine aerosols, or sea spray aerosols (SSA) are generated from the breaking of bubbles at the air-water interface. The process for their formation is shown in Fig. III.1. As they rise through the column of water, those bubbles scavenge organic matter at their interface. This process creates the surface micro-layer (SML). This micrometer-wide layer at the ocean surface is thus enriched in organic material by the rising bubbles (Cunliffe et al. 2013). When a bubble bursts, the organic material is ejected, resulting in submicrometer film-drops that are richer in organic content and biological material than larger jet drops (Aller et al. 2005; Russell et al. 2010; Schmitt-Kopplin et al. 2012). These organic-enriched film drops are then ejected in the atmosphere and transported by the wind currents. They can act as cloud condensation nuclei (CCN) or INPs and thus can impact the cloud phase (liquid, mixed or ice).

Previous observations have shown that the ice nucleating ability of marine particles is lower than those of terrestrial particles (DeMott et al. 2016), however, due to the lower aerosol concentrations in remote oceanic regions, these marine aerosols are likely of primary importance (Burrows et al. 2013; Vergara-Temprado et al. 2017; Wilson et al. 2015, Gong et al. 2020). The importance of marine aerosol would be especially true at mixed-phase clouds temperatures (> -20 °C), as SSA can contain biogenic material that is active at warmer temperatures.

A small number of studies have attempted to link the biogeochemical state of the ocean to the properties of marine INPs (Table III.1). For example, particles derived from the phytoplankton *Prochlorococcus* (Wolf et al. 2019) or from the marine diatom *Thalassiosira Pseudonana* (Knopf et al. 2011a; Wilson et al. 2015) were identified as being able to promote ice nucleation under mixed-phase conditions. In the ambient environment, McCluskey et al. (2018c) linked an increase in INP concentrations with plankton blooms in remote and coastal sites, and heat labile material was found to be the dominant type of INP in the Arctic SML by Irish et al. (2017). Furthermore, Trueblood et al. (2021) was able to quantitatively link both dissolved and particulate organic matter in the seawater and in the SSA to its IN activity.

In a mesocosm study, McCluskey et al. (2018b) proposed that the marine INPs could be classified in two distinct populations. The first population are the *Dissolved Organic Carbon-type INPs* (DOC-type INPs). These particles are able to pass through a 0.2 μm filter and are generally not heat labile. McCluskey

Table III.1 – Overview of recent cruise and laboratory works on marine INPs. For the campaign acronyms, please refer to the cited articles.

Study	Location	Sampling medium	INP analysis	Temperature range	Parameterization (INP data, parameter used)
Wilson et al. (2015)	Arctic (ACCACIA) Atlantic (WACS II) Northeast Pacific (NETCARE)	SML[1], surface SW[2]	Droplet freezing CFDC[3] Heat treatment	-5 to -30 °C	INP per gram TOC[4]
DeMott et al. (2016)	Laboratory expriments Northeast Pacific (NETCARE) Caribbean sea (ICE-T) Diverse (MAGIC) Bering Sea (SHIPPO)	SSA[5], SW	CFDC Droplet freezing	-5 to -35 °C	None
McCluskey et al. (2017) McCluskey et al. (2018a)	Mesocosm experiments	SSA, SW, SML	Ice Spectrometer CFDC Heat treatment H2O2 treatment	-8 to -30 °C	None
Irish et al. (2017) Irish et al. (2019b)	Canadian Arctic (NETCARE)	SML, bulk SW	Droplet freezing Heat treatment	-10 to -35 °C	Conservation of n_{INP}[6] per gram NaCl in SW and SSA
McCluskey et al. (2018b)	Southern Ocean (CAPRICORN)	SSA, SW	Ice Spectrometer CFDC Heat treatment H2O2 treatment	-8 to -30 °C	None
McCluskey et al. (2018c)	North Atlantic Ocean (Mace Head Obs.)	Ambiant SSA	Ice Spectrometer, CFDC, DFPC[7] Heat treatment H2O2 treatment	-10 to -30 °C	n_S[8] for pristine SSA
Gong et al. (2020)	Cabo Verde (ocean and land)	SW, SML Ambiant aerosols	Droplet freezing	-5 to -30 °C	Conservation of n_{INP} per gram NaCl in SW and SSA
Welti et al. (2020)	Arctic Southern Ocean Atlantic Pacific Antarctic	Ambiant aerosols	Droplet freezing CFDCs	0 to -38 °C	None
Wolf et al. (2020b)	Florida Straits Eastern Tropical North Pacific	SW, SML SSA (artificial)	CFDC	-20 to -35 °C	None
Trueblood et al. (2021)	Mediterranean Sea (PEACETIME)	SW, SML SSA (artificial)	Droplet freezing DFPC	-8 to -30 °C	Dual component: Warm INPs (OC_{SSA})[9] Cold INPs ($WIOC_{SSA}$)[10]

[1] Surface microlayer
[2] Seawater
[3] Continuous Flow Diffusion Chamber
[4] Total organic carbon
[5] Sea spray aerosol
[6] INP concentration
[7] Dynamic Filter Processing Chamber
[8] Surface site density
[9] Organic carbon in the SSA
[10] Water insoluble organic carbon in the SSA

Table III.2 – Summary of INP parameterization works in marine environments.

Study	Medium	INP data	Parameter(s)	Equation	Temp. range
Wilson et al. (2015)	SML	INP_{gTOC}[1]	TOC_{SML}[2], T	$INP_{gTOC} = \exp\left[11.2186 - (0.4458 \times T)\right]$	-5 to -30 °C
McCluskey et al. (2018c)	SSA	n_S	T	$n_S = \exp\left[1.0125 - (0.545 \times T)\right]$	-10 to -30 °C
Irish et al. (2019a) Gong et al. (2020)	SSA	INP_{air}[3]	$NaCl_{air}$[4], $NaCl_{SW}$[5]	$INP_{air} = INP_{SW} \cdot NaCl_{air}/NaCl_{SW}$	-5 to -30 °C
Trueblood et al. (2021) (single component)	SSA	INP_{SSA}[6]	POC_{SW}[7], T	$INP_{SSA} = \exp\left[-28.6963 - (0.2729 \times T) + (0.0366 \times POC_{SW})\right]$	-8 to -30 °C
Trueblood et al. (2021) (two-component)	SSA	INP_{air}	OC_{SSA}[8], T	$INP_{air} = \exp\left[-7.9857 - (0.3178 \times T) + (0.4643 \times OC_{SSA})\right]$	>-22°C
			$WIOC_{SSA}$[9], T	$INP_{air} = \exp\left[-6.6606 - (0.2712 \times T) + (0.5755 \times WIOC_{SSA})\right]$	<-22°C

[1] INP concentration per gram TOC in the SML
[2] Total organic carbon in the SML
[3] INP concentration per volume of air
[4] NaCl concentration in the SSA
[5] NaCl concentration in the SW (salinity)
[6] INP concentration per aerosols in the SSA
[7] Particulate organic carbon in the SW
[8] Organic carbon in the SSA
[9] Water insoluble organic carbon in the SSA

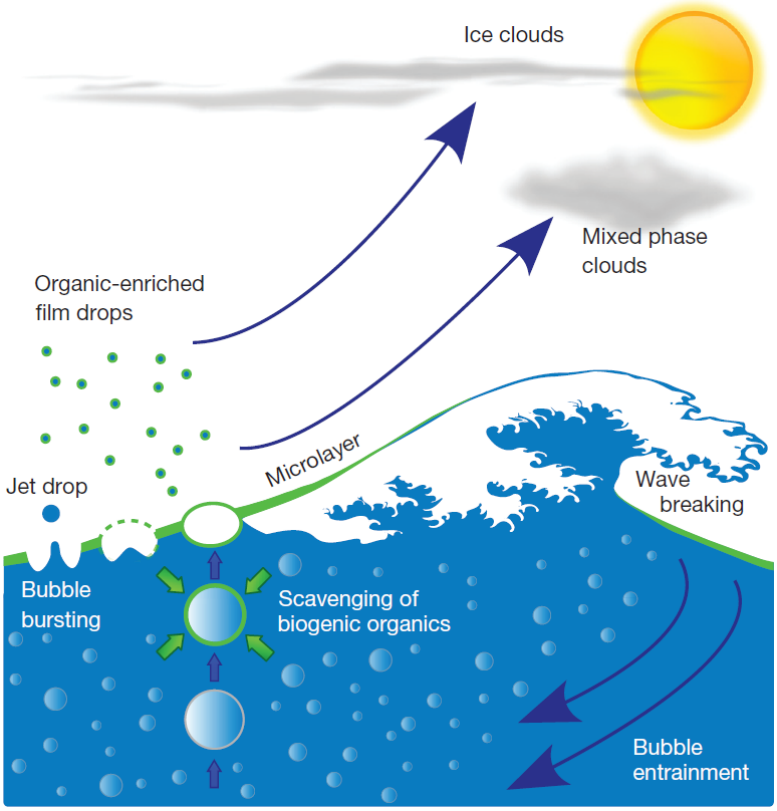

Figure III.1 – Schematic of the generation of sea-spray aerosols by bubble bursting in the oceans. Rising bubbles scavenge biogenic organics and burst at the surface. This enriches and creates the SML (green layers), and generated organic-enriched film drops that are transported in the atmosphere. Figure adapted from Wilson et al. (2015).

et al. (2018b) suggested that DOC-type INPS could be important in situations of dense phytoplanktons blooms. The second population is the *Particulate Organic Carbon-type INPs* (POC-type INPs), which are ice active micro-organisms in the form of whole cells or cells fragments. These POC-type INPs are larger than the DOC INPs and are heat labile, and their contribution depends on the microbial abundances in the seawater.

The Southern Ocean (SO) in particular is a poorly understood region in terms of ocean-atmosphere interactions, and even more so in terms of aerosol cloud interactions. There have been a small number of cruise campaigns that focused on measuring INPs that took place in this region, and Burrows et al. (2013) noted that the lack of modern knowledge INP concentrations in the SO is a major limitation for understanding their role in clouds in the SO. Past studies on INPs in the SO (Bigg 1973, Bigg 1990) revealed lower INP concentrations in the SO region than in other marine regions. More recently, McCluskey et al. (2018a) also noted lower INP concentrations in this region, and additionally illustrated that the INP populations were commonly organic and heat-stable. Modeling studies have suggested that more supercooled clouds exist in the Southern Ocean due to the very low INP concentrations in this region (Burrows

et al. 2013; Tan et al. 2016; Vergara-Temprado et al. 2018).

As already discussed in Chapter I, the ability of models to predict INP numbers and the development of new empirical parameterizations is one of the key areas of research of INP studies, and marine INPs are no exception to this need, with the added difficulty of taking into account the differences in oceanic regions, particularly with variable biological specificities. McCluskey et al. (2017) noted that finding predictors for marine INPs was of a primary importance.

We provide a summary of previous parameterization work in marine environments in Table III.2. Some studies focused on parameterizing the link between seawater INP and SSA INP, using the concentration of sodium chloride in both mediums (e.g. Irish et al. 2019a; Gong et al. 2020). However, these two parameterizations have the disadvantage of relying on the knowledge of the INP concentration in the seawater, which is not parameterized as a function of the seawater biogeochemistry. The two existing parameterizations of marine INPs that take into account ocean biogeochemistry use organic matter as a variable, such as Particulate Organic Carbon (POC) or Total Organic Carbon (TOC) (e.g. Wilson et al. 2015, Trueblood et al. 2021).

Trueblood et al. (2021) was able to separate the INPs properties of sea spray from the Mediterranean Sea into two classes based on their organic matter content, with warm INPs ($T > -22$ °C) associated with Water-Soluble Organic Carbon, and cold INPs ($T < -22$ °C) associated with Water-Insoluble Organic Carbon. Trueblood et al. (2021) also proposed a parameterization of INP per SSA number as a function of the POC concentration in the seawater. This parameterization could be used in atmospheric models provided that take into account seawater POC values as an input. However, it might be very specific of oligotrophic seawaters such as the Mediterranean Sea.

It is in this context that two cruise campaigns were organised in 2019-2020 in the Southern Ocean, with the general objectives of linking the biological state of the ocean to aerosol formation, emissions and properties in the marine atmosphere. The first cruise, TONGA (TNG) took place in the region of the Tonga volcanic arc in the Western Tropical South Pacific Ocean in November 2019; the second cruise, Sea2Cloud (S2C) took place south of New Zealand in March 2020.

More specific to this thesis, the objective in both cruises was to evaluate the INP concentration in both the ocean and in sea spray, and quantitatively link them to the the ocean biogeochemistry in order to identify potential proxies for parameterizing the INP concentrations in the marine environment. To achieve these goals, INP abundances were measured both in the seawater and in the SSA during both cruises, and also in the SML for the S2C cruise. The biogeochemical properties of the seawater was also measured continuously in parallel.

In the following sections, we will first present and discuss the results from the 2019 TNG cruise, then the results from the 2020 S2C cruise and finally propose parameterizations performed using the data from both campaigns, and discuss the differences in IN properties between the two regions.

III.2 IN properties of sea spray in a volcanic area of the South Pacific Ocean

The TONGA project[1] (shallow hydroThermal sOurces of trace elemenNts: potential impacts on biological productivity and bioloGicAl carbon pump), is a a three-year interdisciplinary research examining the role of micronutrients from hydrothermal sources on ocean productivity and carbon sequestration. The TONGA campaign was also the opportunity to achieve some of the objectives of the wider Sea2Cloud project. In this context, numerous ocean biogeochemical parameters (nutrients, microorganisms and planktonic abundances, organic matter markers) were measured during the cruise under contrasted conditions.

We first present in more details the TONGA cruise and its instrumentation and experimental approach, then we discuss the IN properties of the SW and of the SSA.

III.2.1 Experimental approach

III.2.1.1 Track of the TONGA cruise and sampling stations

The TONGA cruise campaign took place on board the French Research Vessel *L'Atalante* in the region of the Tonga volcanic arc in the Western Tropical South Pacific Ocean. The ship departed from New Caledonia (22° 21'S, 166°59'E) on 01 November 2019, and traveled in a eastward direction until it reached its most eastern point (20°19'S, 166°33'W) on 19 November 2019. It then returned to New Caledonia, arriving on the 3rd of December 2019 (Fig III.2).

The red encircled area corresponds to a section of the Tonga-Kermadec Ridge, an oceanic ridge that stretches for 3000 km, from south of the American Samoa to New Zealand's Northern Island. This area (henceforth Volcanic Zone or VZ) is defined as the zone encompassed between 183.1°E and 185.5°E in Fig. III.2. Outside of this area, we define the Oligotrophic Zone (or OZ), which corresponds to an oceanic area of poor nutrient abundance.

More precisely, using the previous definitions, the cruise was in the OZ from 01/11/2019 to 07/11/2019, then in the VZ from 08/11/2019 to 15/11/2019, then again in the OZ from 16/11/2019 to 23/11/2019, then back in the VZ from 24/11/2019 to 29/11/2019.

The measurements used in this study came from two different mediums: the bulk seawater (SW) and the generated (SSA). The bulk SW was pumped from about 5 m depth into the underway system (UWAY) of the ship. This water was then sampled by a variety of instruments. In particular, it was used to generate artificial SSA using the technique used by Sellegri et al. (2005), Schwier et al. (2015) and Trueblood et al. (2021). This method allows to simulate sea spray emissions that occur during high winds events and the breaking of waves.

[1] http://tonga-project.org

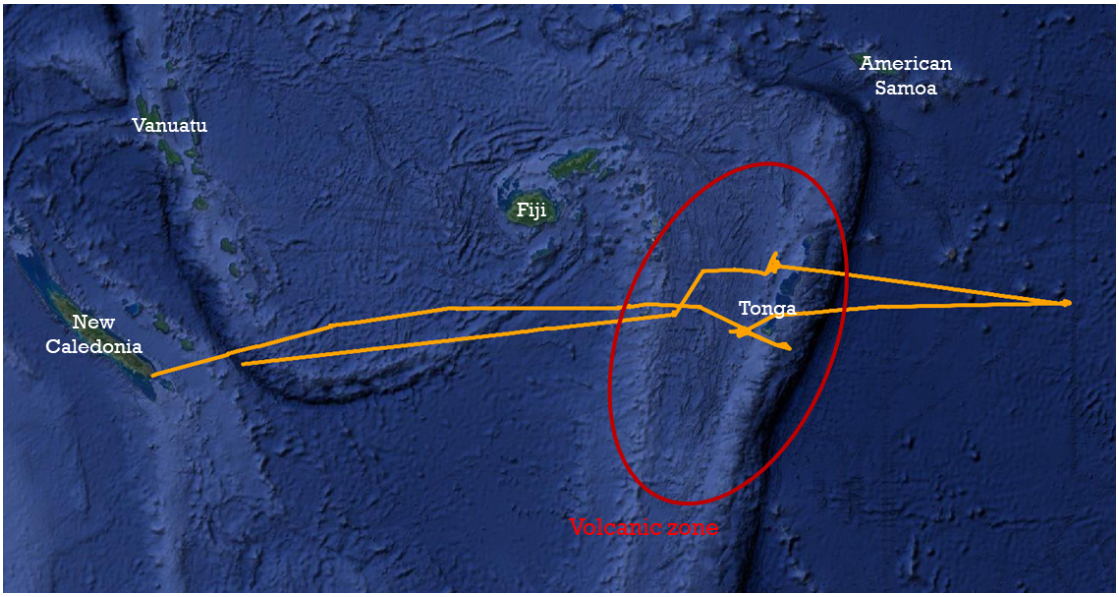

Figure III.2 – Track of the TONGA cruise from 01/11/2019 to 01/12/2019. The red encircled area represents the Tonga volcanic arc. - Satellite data from Google Earth.

A continuously circulating seawater jet system produces wave-breaking SSA, which is exposed to air in a closed unit. The generated sea spray is then sampled by various instruments in order to characterize its properties (size distribution, chemical composition, etc). The experimental setup for the underway system and the generation and sampling of SSA is presented in Figure III.3.

III.2.1.2 INP sampling

INPs were analyzed in both SW and SSA. Bulk SW was sampled with a time resolution of about 4 hours during daytime, using 50 mL Falcon tubes and immediately stored at -20 °C for later analysis at the laboratory.

Seawater samples were thawed at ambient temperature (≈20 °C) prior to analysis. They were then split into 26 Ependorf tubes (200 µL in each tube) without any future treatment, and 26 other Ependorf tubes that were subjected to a heat treatment (see Chapter II). The temperature shift induced by salinity was then taken into account for correcting the samples. This induced a correction of -2 °C, with salinity values of about 35 g/L (Doherty et al. 1974).

SSA were sampled using a 4 stages Dekati impactor with a resolution of about 23h from the Sea Spray generation device described in Fig. III.3. Briefly, the underway seawater is injected in a 10 L tank through 1 mm jets, creating bubbles in the half way filled seawater part of the tank, in a similar way than the breaking wave process. Sea spray generated via bubble bursting are emitted into the upper part of the tank which is flushed with particle filtrered air. The tank's headspace, filled with sea spray particles, is continuously sampled for analysis of the sea spray size distribution, chemical composition and CCN

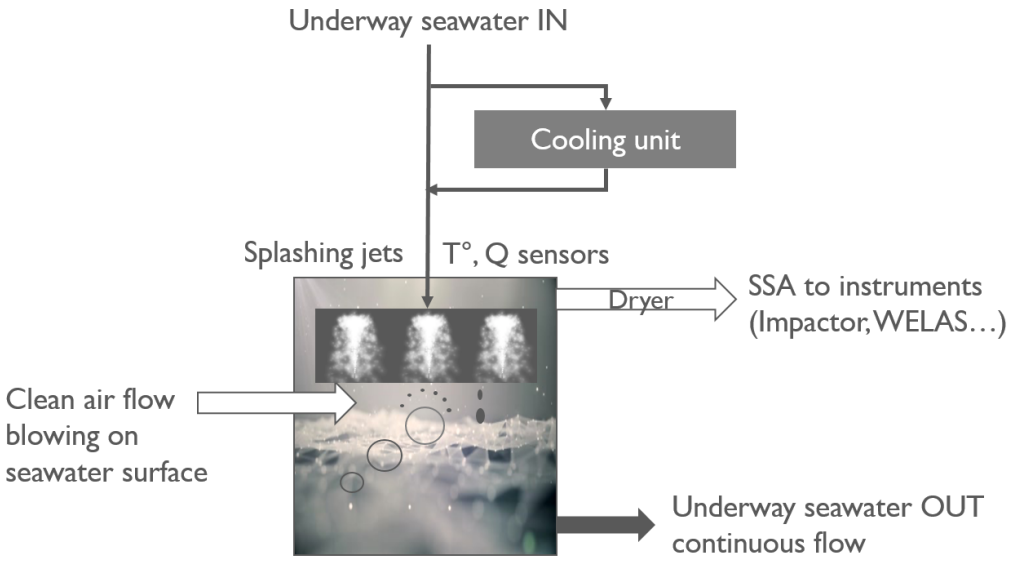

Figure III.3 – Experimental setup for underway and SSA measurements during the TONGA campaign. Seawater was continuously sampled with the underway system. Sea sprays were generated by blowing clean air on the seawater surface. After passingthrough a drier, the generated SSA were measured by the aerosol instruments (cascade impactor, WELAS, etc). The seawater in the water tank was continuously replaced.

properties (additionnal to the INP analysis). Filter samples from the Impactor were immediately stored at -20 °C for further offline analysis of INPs and chemistry.

As INPs were not very concentrated on the filters, we combined several impactor stage filters for each analysis. Filter samples were therefore separated into submicronic (<1 µm) and supermicronic (> 1 µm) samples, by using the size segregated filters from the Dekati impactor. For submicronic INPs, half of a 47mm filter was used for the analysis; while for supermicronic INPs, half of the 1-2.5 µm (total surface: 8.7 cm^2) stage filter and half of the 2.5-10 µm stage filter (total surface: 4.9 cm^2) were used.

INP were analyzed using the LINDA technique described in Section II.2. After the LINDA analysis, blank filters were used for calculating the background correction of filter samples. We show the results of the blanks analysis in Figure III.4. Blanks from < 1 µm filters show a high variability in temperature spectra. The onset temperatures of < 1 µm filters is about -10 °C, and a 100% frozen fraction is reached between -18 °C and -22 °C. Heated blank < 1 µm samples froze at temperatures 0.5 to 1 °C warmer than untreated blank < 1 µm samples. This is probably explained by the added experimental steps and possible contamination from the heat treatment. On the other hand, > 1µm blanks had lower variability and consistently started to freeze around -6 °C and reached 100% frozen fraction between -16 °C and -18 °C. The difference between untreated and heated samples is also lower than for < 1µm blanks.

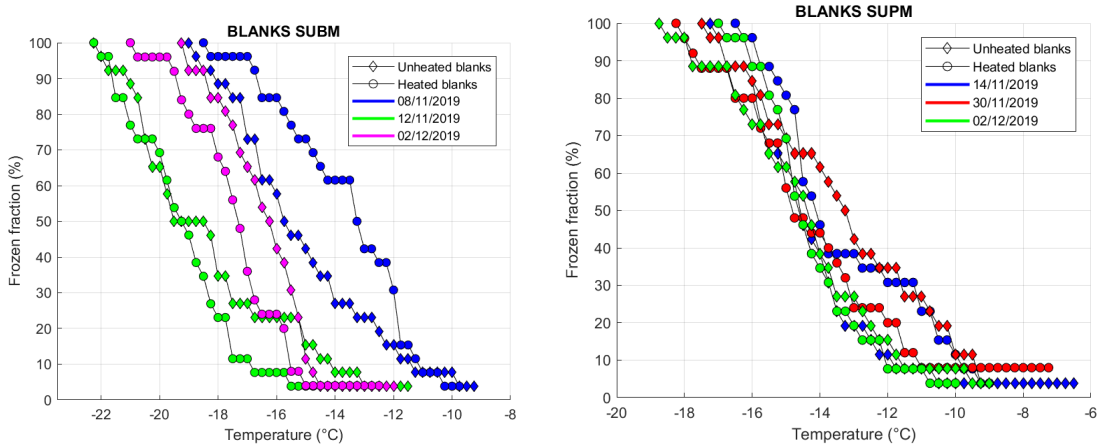

(a) Blank samples for <1 µm filters.

(b) Blank samples for >1 µm filters.

Figure III.4 – Summary of blank samples analysis with LINDA for a) Submicron samples, b) Supermicron samples. Results are shown as frozen fractions of unheated (diamonds) and heated samples (circles).

As sea spray aerosols were generated artificially, the INP concentrations from filters are normalized either by the total number of aerosols (INP/SSA) or by the total aerosol surface (surface site density n_S or INP/m^2) of the sea spray generated.

III.2.1.3 Other instruments and data

A wide array of instruments were used for sampling during the cruise, however only a few of them were used in conjunction with INP data. They can be divided into seawater and atmospheric sampling. We will describe those instruments and associated data here. They are summarized in Table III.3.

III.2.1.3.a Seawater sampling

We summarise here the instruments and methods used for retrieving the seawater properties, such as temperature, salinity, microorganisms abundances and organic matter concentration.

- Seawater properties (salinity, temperature) were measured continuously using Thermo-salinometers (TSG). Seawater surface tension was measured on seawater samples taken from the ship's underway seawater system using a dynotester instrument with the same resolution as the INP and discrete samples for flow cytometry. Once the samples were taken, they were stored for a few hours at -20 °C, then brought back to ambiant temperature with a surface tension measurement performed for each temperature with a resolution of about 1 °C.

- A 0.45 µm polyethersulfone filter (Supor©) was used to filter samples for Dissolved Organic Matter (DOM) on-line. Within 24 hours of collection, all samples were acidified with ultrapure hydrochloric acid (HCl,

Table III.3 – Summary of parameters used for biogeochemistry analysis with INPs. Continuity Temperature Depth rosettes CTD sampling were used for most the of off-line analysis. They allow to sample seawater at different depths using an array of Niskin bottles. CTD measurements can only be made when the ship is stationary, and were therefore only performed at specific predefined locations and stations.

Name	Instrument	Sampling info.	Symbol	Unit
Surface tension at 21 °C	TSG[2]	Same as INP[1]	σ_{21}	$N.m^{-1}$
Water temperature	TSG[2]	Continuous	T_{SW}	°C
Water salinity	TSG	Continuous	S	$g.kg^{-1}$
Bacteriochlorophyl-a	HPLC[3]	CTD[4]	BChl-a	$mg.m^{-3}$
Total Chlorophyll-a	HPLC	CTD	Chl-a	$mg.m^{-3}$
Peridin	HPLC	CTD	Per	$mg.m^{-3}$
Total carotenes	HPLC	CTD	Car	$mg.m^{-3}$
Picophytoplanktons	FCM[5]	UWAY (same as IN)	PicoPhyto	mL^{-1}
Nanophytoplanktons	FCM	Same as INP	NanoPhyto	mL^{-1}
Total Eukaryotes	FCM	Same as INP	TotEuk	mL^{-1}
Total heterotrophic Bacteria	FCM	Same as INP	Bact	mL^{-1}
Prochlorococcus	FCM	Same as INP	Proc	mL^{-1}
Synechococcus	FCM	Same as INP	Syn	mL^{-1}
Cyanobacterium UCYN-A	qPCR[6]	CTD	UCYN-A	cells/mL
Cyanobacterium UCYN-B	qPCR	CTD	UCYN-B	cells/mL
Cyanobacterium UCYN-C	qPCR	CTD	UCYN-C	cells/mL
Dissolved oxygen	SEC[7]	TMC[8]	O_2	µmol.kg
Biopolymers	SEC	TMC	BP	µMC
Degraded biopolymers	SEC	TMC	dBP	µMC
Humic substances	SEC	TMC	HuS	µMC
Low Molecular Weights acids	SEC	TMC	LMW acids	µMC
Low Molecular Weights neutrals	SEC	TMC	LMW neutrals	µMC
Dissolved organic carbon	SEC	TMC	DOC	µMC or $\mu g.L_{SW}^{-1}$
Particulate organic carbon	CHN[9]	CTD	POC	$\mu g.L_{SW}^{-1}$

[1] Discrete samples from continous UWAY sampling, same timesteps as INP samples
[2] Thermo-salinometer
[3] High-Performance Liquid Chromatography
[4] Continuity Temperature Depth rosette
[5] Flow Cytometry
[6] Quantitative Polymerase Chain Reaction
[7] Size-Exclusion Chromatography
[8] Trace Metal Clean rosette
[9] Carbon-Hydrogen-Nitrogen

Merck, 0.1 percent, final pH 2.3) and immediately frozen at -20 °C. The filters were than analysed at LEMAR laboratory (Brest, France) with size-exclusion chromatography (SEC, Huber et al. 2011). DOM includes dissolved oxygen, biopolymers, humic substances and low molecular weight acids and neutrals. DOM data is only available at the fixed observation stations.

- On CTD-rosette devices, an optical package (Eco FLBBCD (fChl, bbp, fC-DOM, and C-Rover) ; Eco 3X1M sensor) was placed to capture optical data concurrently with discrete biogeochemical and diversity measurements (Phytofloat protocole). These measurements were accompanied by discrete sampling (3 depths) of seawater from the Niskin bottles for POC, flow cytometry and polarized microscopy.

Pigment concentrations in the seawater were also measured using High-Performance Liquid Chromatography (HPLC), performed by the oceanography laboratory of Villefranche-sur-Mer). Seawater samples were taken with CTDs at 12 different depths, from 4.5m to 400.9m. Seawater samples were then filtered on Whatman GF/F glass fiber filters, and then analysed with HPLC on the same day. The procedure is fully described in Ras et al. (2008). HPLC allows the retrieval of several chlorophylls and carotenoids pigments. POC from CTD samples was analysed using a CHN (Carbon, Hydrogen and Nitrogen) analyser from the LOV (Villefranche).

Flow Cytometry (FCM) analysis was performed on seawater samples taken from the underway seawater system with the same time resolution as the samples taken for INP analysis. This allows the measurement of microorganisms such as cyanobacteria (prochlorococcus, synochoccus) and viruses, and were performed by the Station Biologique de Roscoff team (from Roscoff, France).

- Details on plankton abundances measurements are given in Benavides et al. (2021). Briefly, plankton biomass was collected on filters using an automated filtration system. Quantitative Polymerase Chain Reaction (PCR) targeting the *nifH* gene was then used on the DNA extracted from the filters. This allowed diazotrophs abundances to be collected (UCYN-A, UCYN-B and UCYN-C) so that we could follow there evolution.

We give a brief explanation in Sec. A.1.1 for differentiating the different types of organisms measured during the cruise.

III.2.1.3.b Atmospheric measurements

As shown in Figure III.3, SSA were generated from the seawater sampled in the underway system of the ship. After passing through a drier, the aerosols were sampled by an SMPS and a WELAS providing physical characterisation of aerosol size and number concentration from 10 nm up to >10 µm (see section II.3). A Dekati 4-stage cascade impactor was used to collect the primarily generated aerosols onto filters (section II.1.1). Ion chromatography was performed on the filters by the Laboratoire d'Aérologie (Toulouse, France) for chemical analysis of the SSA (Sec. II.3.2).

III.2.2 Overview of the variability of the biogeochemical parameters measured during TNG

As mentioned above, a series of collocated seawater measurements were made in parallel to the INP measurements (Table III.3). The goal of this section is to provide an overview of the variability of those parameters during the cruise.

We show in Figures III.5 and III.6 the comparison between the VZ and the OZ for all parameters discussed here. We also provide the full time series in Figures A.1 to A.3.

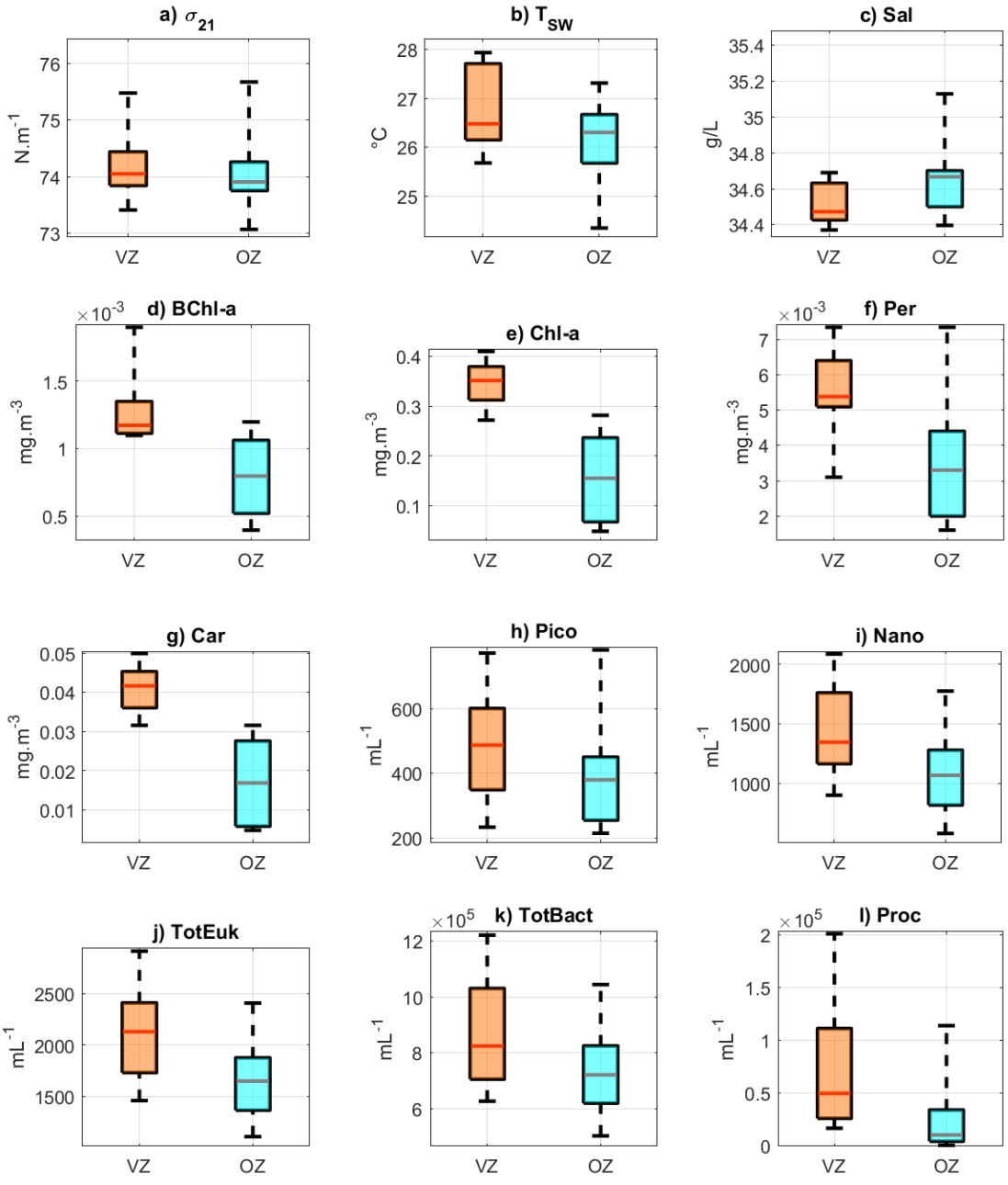

Figure III.5 – Boxplots of SW parameters in the VZ and in the OZ - Part 1.

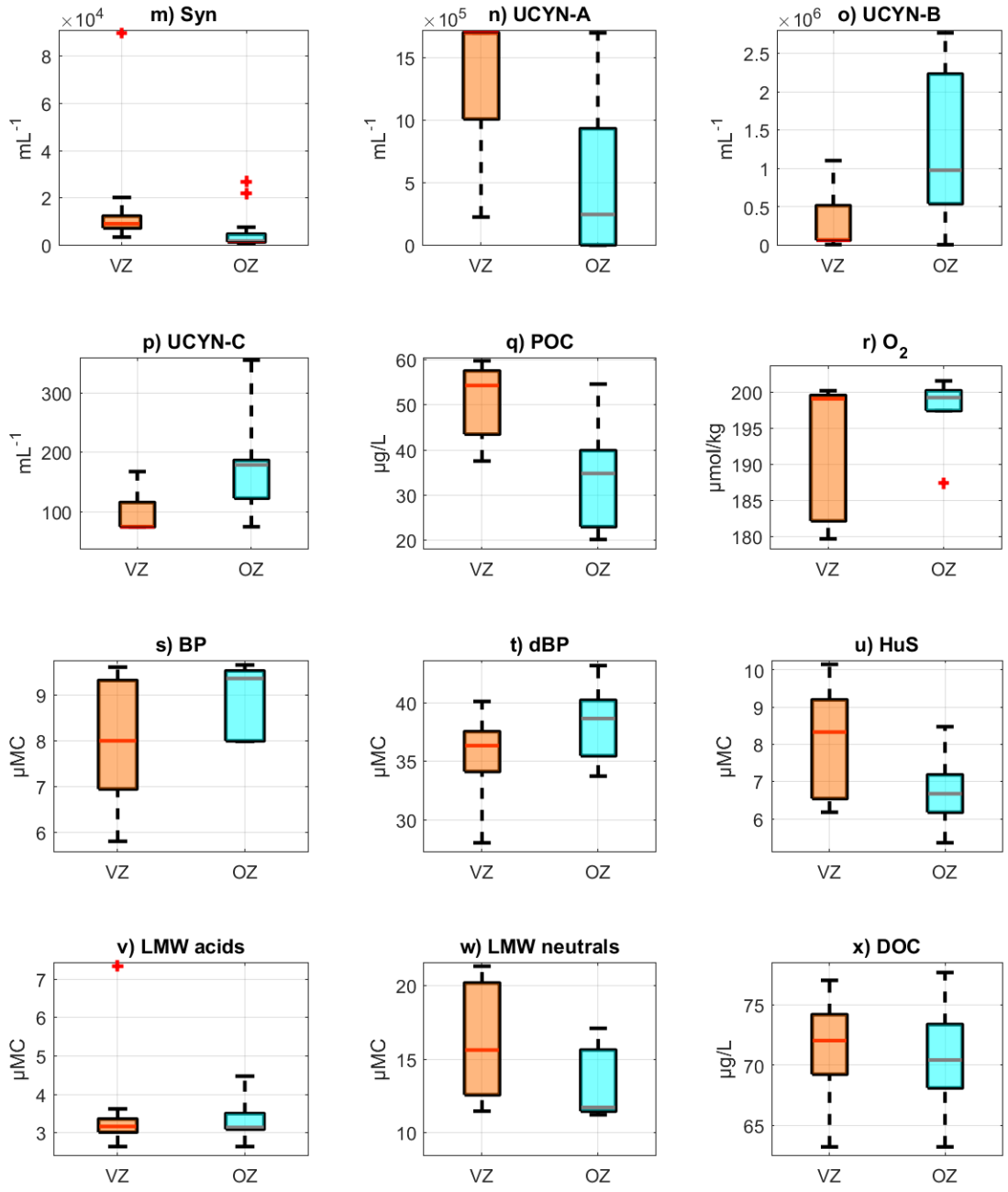

Figure III.6 – Boxplots of SW parameters in the VZ and in the OZ - Part 2.

Higher abundances of microorganisms were consistently observed in the VZ than in the OZ. *Prochlorococcus* and *Synechoccocus* are more than an order of magnitude higher in the VZ compared to the OZ. The total bacterial abundance also exhibits highs in the VZ and lows in the OZ, but with lower magnitude than *Prochlorococcus* and *Synechoccocus*. Both picophytoplanktons and the total eukaryotes concentrations almost double in the VZ compared to the OZ. Nanoplanktons were slightly more abundant in the VZ than in the OZ. Diazotrophs have a slightly different behavior with some of them being enriched in the VZ, as other microorganisms (UCYN-A) while others are depleted in the VZ compared to the OZ (UCYN-B and UCYN-C).

POC, HUS and LMW neutrals exhibits strong peaks in the VZ, while DOC and LMW acids, are relatively unchanged between the two regions. The variability is however in general higher in the VZ than in the OZ. The water temperature is higher in the western OZ and during the second passing of the VZ (22/11 to 28/11). This is also the case for salinity. The concentrations in O_2 are higher by an order of magnitude in the first half of the campaign, until 20/11, regardless of the presence of volcanoes.

Additional details on the differences between the VZ and the OZ, are presented in Table A.1 the statistics of the different parameters presented here. Those statistics include the mean, the standard deviation, the minimum and maximum values of each parameter during the whole cruise and separated between the VZ and the OZ.

In the following section, we will explore the relationship between the INP spectra and biogeochemical parameters in more detail. This will allow us to gain a better understanding of the composition of the INPs during the campaign.

III.2.3 Observations of INPs in the seawater

III.2.3.1 General features

Average frozen fractions measured for unheated and heated samples in the SW during the campaign are reported in Fig. III.7b. In order to characterize the INP temperature spectra, we define T_{10}, T_{50} and T_{90} as the temperatures at which respectively 10%, 50% and 90% of the tubes have frozen for a given sample. For unheated samples, the average $T_{10,UH}$ is -13.0 ± 1.9 °C, the average $T_{50,UH} = -15.5 \pm 0.9$ °C, and the average $T_{90,UH}$ was -17.0 ± 1.2 °C.

The concentrations vary between 10^2 and 10^3 INP/L_{SW} at T>-14 °C, and between 5×10^3 and 2×10^4 INP/L_{SW} at T<-16 °C (Fig. III.7a). Similar INP concentrations have been observed in other studies in oligotrophic waters (McCluskey et al. 2018a; Gong et al. 2020 and Trueblood et al. 2021).

Heated samples exhibit similar T_{10}, T_{50} and T_{90} than unheated samples with values of $T_{10,H}$, $T_{50,H}$ and $T_{90,H}$ being respectively -12.7 ± 2.2 °C, -15.8 ± 1.9 °C

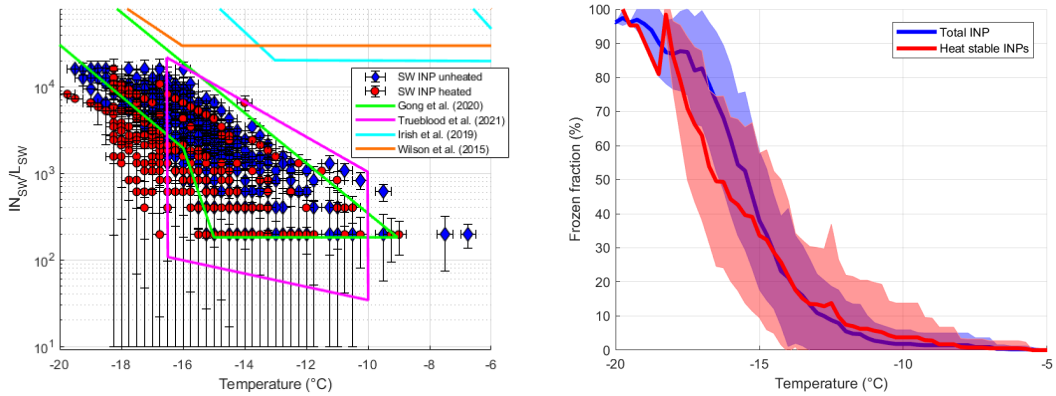

(a) Cumulative INP concentrations.

(b) Frozen fractions of INPs.

Figure III.7 – Mean a) cumulative INP concentrations and b) frozen fractions of INP in the seawater for INP_{tot} (blue), INP_{HS} (red) and INP_{HL} (green). The shaded areas and error bars correspond to the 68% confidence interval ($\pm 1\sigma$). Data from previous studies includes Gong et al. (2020) at Cabo Verde; Trueblood et al. (2021) in the Mediterranean Sea; Irish et al. (2019b) in the Canadian Arctic; Wilson et al. (2015) in the Arctic, Pacific and Atlantic.

and -17.0 ± 1.5. Similarly to other studies in marine environments (eg. Wilson et al. 2015; Irish et al. 2017; McCluskey et al. 2018a), heating the samples results in a visible decrease in INP concentrations, especially at temperatures warmer than -17 °C, as a result of the loss of heat labile material. At any given temperature, the fraction of heat-labile INP concentrations represents 63% to 100% (average: 81 ± 11%) of the total INP concentrations. The highest fractions of HL INPs are at temperatures higher than -14 °C, whereas the lowest fractions are at temperatures between -14 °C and -18 °C. This hints at the presence of heat labile proteinaceous material, which are known to be potential INPs in the SW.

We observe concentrations of $(2.5 \pm 3.7) \times 10^2$ INP/L_{SW}, $(2.0 \pm 1.5) \times 10^3$ INP/L_{SW} and $(7.2 \pm 4.9) \times 10^3$ INP/L_{SW} for INP_{tot} at -12 °C, -15 °C and -17 °C respectively. For INP_{HS}, those values are $(1.9 \pm 2.9) \times 10^2$ INP/L_{SW}, $(1.1 \pm 1.5) \times 10^3$ INP/L_{SW} and $(2.3 \pm 2.3) \times 10^3$ INP/L_{SW}; and they are $(4.8 \pm 4.2) \times 10^2$ INP/L_{SW}, $(1.6 \pm 1.3) \times 10^3$ INP/L_{SW} and $(5.4 \pm 4.1) \times 10^3$ INP/L_{SW} for INP_{HL}.

However, our samples exhibit a much lesser shift in activation temperature than Irish et al. (2017) and Irish et al. (2019b). Their samples activity was shifted by 2 to 10 °C with heat treatment, whereas our samples are shifted by only 2 °C. The difference in trophic regimes between the two campaigns could explain this variation: the Arctic region where their samples come from is an eutrophic region, whereas the Southern Pacific is generally oligotrophic, which is illustrated by the difference in INP concentrations (in the order of 10^2 to 10^4 INP/L_{SW} for our observations, 10^4 to 10^7 INP/L_{SW} for theirs). An other explanation for this difference could be the INP sampling method, as LINDA is not able to analyse INP below -20 °C, while the methods used by Irish et al. (2017) were able to sample at -30 °C.

In the following sections, the INP data will be split in three different categories: the total INP data from untreated samples (INP_{tot}), the INP data from heated samples (Heat Stable INPs, or INP_{HS}) and the heat labile INP (INP_{HL}). In order to cover evenly the whole temperature spectrum and according to the previous discussion, these INP classes are then studied at three fixed temperatures, at -12 °C, -15 °C and -17 °C, corresponding roughly to the average T_{10}, T_{50} and T_{90} of the samples.

III.2.3.2 Daily variations and effect of volcanoes

Time series of INP concentrations and parameters presented in Table III.3 were studied to gain insight into the daily variations and impact of volcanoes on INP activity, and whether this impact can be explained by the variation in seawater biogeochemical parameters. As previously described in the Methods Section (III.2.1.1), the cruise passed through the different zones, OZ and VZ, throughout the course of the cruise. The limits of the VZ are marked by orange dotted lines on Fig. III.8.

In figure III.8, we show the daily variations of INP samples in the seawater as cumulative bars corresponding to HS and HL INPs, at the three temperatures of interest. The higher values at all temperatures are observed between 08/11/2019 and 15/11/2019, and between 24/11/2019 and 29/11/2019, clearly corresponding to the passage of the ship in the VZ. Early days of the campaign (02/11 to 08/11) exhibit the lower INP concentrations at all temperatures, while the later days show more medium INP concentrations. Another representation of INP concentrations over the course of the cruise is shown in Figures A.5, with the total INP concentrations shown as points on the map corresponding to the cruise. One can separate this map in three areas: the highest concentrations of INPs correspond to the VZ, the lower concentrations to the eastern OZ, and the low-medium concentrations correspond to the western OZ. Noticeably higher concentrations are observed near the volcanic arc in comparison to the OZ. The concentration of INP in the VZ $n_{INP,VZ}$ is on average 3 ± 1.8 times higher than the concentration of INP in the OZ $n_{INP,OZ}$, at all temperatures (Fig. A.6). For example, at -12 °C, -15 °C and -17 °C, $n_{INP,VZ}$ was respectively 2.3 times larger, 1.6 times larger and 2.2 times larger than $n_{INP,OZ}$.

This is consistent with the general increase in biological activity observed in Section III.2.2, which is in line with previous studies in marine environments that linked increased biomass with increased INP concentrations in the SW (e.g. Irish et al. 2017; McCluskey et al. 2018b; Wolf et al. 2020a). This increase could also be directly due to volcanic ashes dissolved in the seawater. Durant et al. (2008) assumed that volcanic ash particles could have a similar ice nucleating effect than mineral dust in the immersion freezing mode at temperatures below -20 °C, however Schill et al. (2015) noted that the INA of volcanic ashes was dependent on its mineral composition. Furthermore, Fahy et al. (2022) recently observed that volcanic ash INA was greatly reduced (by two order of magnitude) when it was dissolved in water for several days. Overall, previous

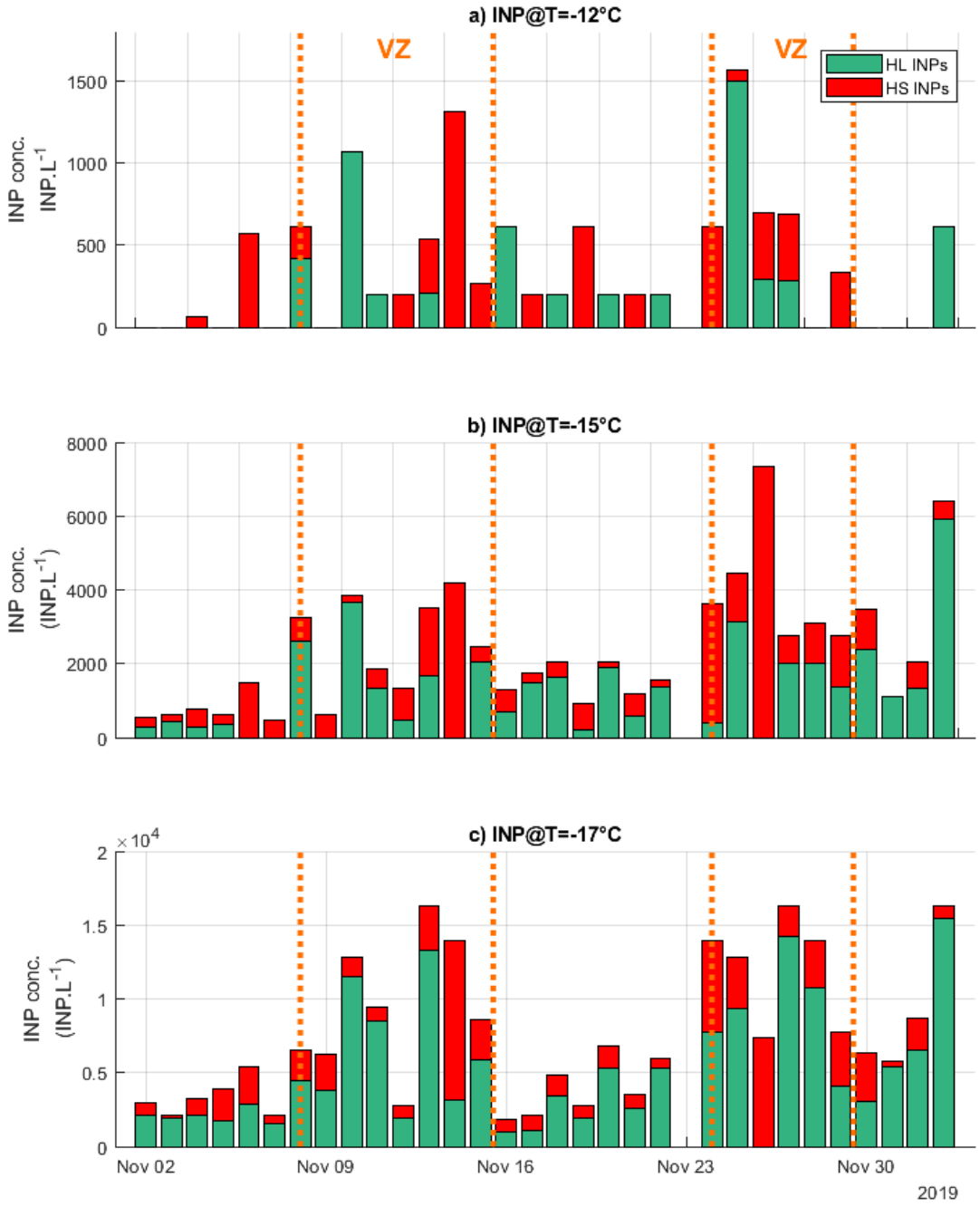

Figure III.8 – Time series of HS (red) and HL (green) INPs in the SW at -12 °C, -15 °C and -17 °C. Orange dotted lines and VZ labels mark the limits of the Volcanic Zone.

observations suggest that volcanic ashes would be active at temperatures colder than relevant for our study, and we speculate that the increased INP abundance near the Volcanic Arc is instead a result of increased biological activity.

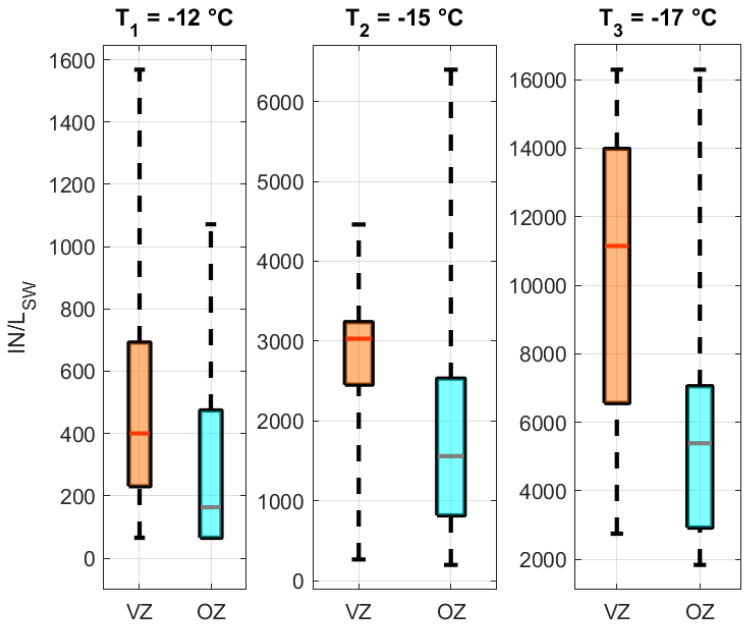

Figure III.9 – Boxplots of INP concentrations in the volcanic zone (orange) and oligotrophic zone (cyan) at -12 °C, -15 °C and -17 °C. The edges of the boxes represent the 25th and 75th percentile, the red lines represent the median, the whiskers represent the points lower than 3 times the interquartile interval and the red crosses represent the outliers.

We show in Figure III.9 and III.10 the boxplots of INP concentrations at -12 °C, -15 °C and -17 °C in the VZ and in the OZ. While all three datasets (total, HL and HS) exhibit higher values in the VZ than in the OZ, the increase in total INPs in the VZ is mostly explained by the increase in HL INPs. HS INPs show however the highest relative increase (Fig. III.10b), with $n_{INP,VZ}$ is on average 3.2 ± 0.9 times larger than $n_{INP,OZ}$ at all temperatures : values of $n_{INP,VZ}$ at T_1, T_2 and T_3 were respectively 3.5, 3.8 and 2.8 times larger than $n_{INP,OZ}$.

This larger contribution of HS INPs indicates that the INPs in the VZ contain less proteinaceous biogenic than the INPs in the OZ. On the other hand, HL INPs had smaller differences between the OZ and the VZ (Fig. III.10a), with $n_{INP,VZ}$ on average 1.6 ± 0.5 times larger than $n_{INP,OZ}$. At T_1, $n_{INP,VZ}$ and $n_{INP,OZ}$ were almost equal, and at T_2 and T_3 $n_{INP,VZ}$ was 1.2 and 2 times larger than $n_{INP,OZ}$.

In summary, INPs were in general more abundant at all temperatures in the VZ than in the OZ, with larger differences at the lower temperatures, which is line with a general increase in several biomass markers in the VZ, such as pigments, phytoplanktons and POC. These observations are also true for both the heat stable and heat labile INP populations, with overall a bigger increase

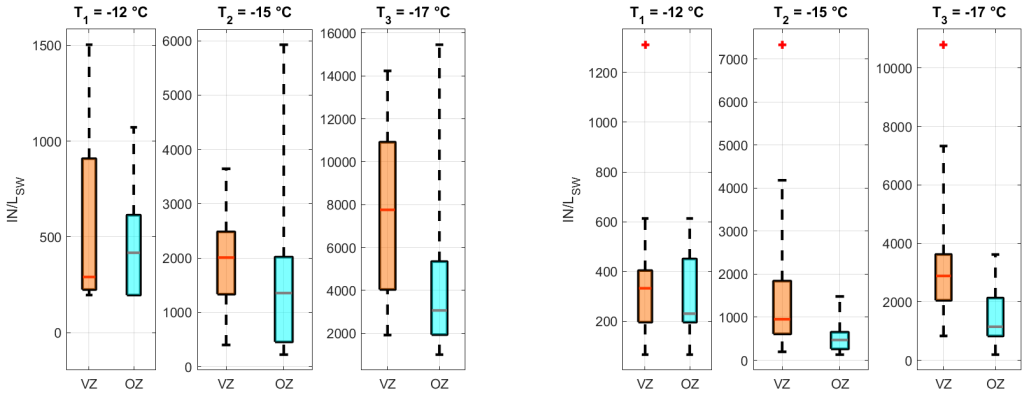

(a) HL INPs.

(b) HS INPs.

Figure III.10 – Boxplots of SW INP concentrations separated between the volcano (orange) and the oligotrophic (cyan) zones at -12 °C, -15 °C and -17 °C, for a) Heat Labile INPs and b) Heat Stable INPs. The edges of the boxes represent the 25th and 75th percentile, the red lines represent the median, the whiskers represent the points lower than 3 times the interquartile interval and the red crosses represent the outliers.

for HS INPs in the VZ than for HL INPs. Heat-labile INPs dominate consistently throughout the sampling, even in the VZ.

III.2.3.3 Correlations with the seawater biogeochemistry

The objectives of this section is to quantify what links exist between the variability and abundance of INP and the biogeochemical properties of the SW. Correlations between the biogeochemical parameters from the SW presented in Table III.3 and the INP data in the SW were determined. The INP data used in this section are the ones described in Section III.2.3.1 : total INP (INP_{tot}), heat stable INP (INP_{HS}) and heat labile INP (INP_{HL}) at -12 °C, -15 °C and -17 °C.

The summary of the correlations are shown in Table III.4. We divided the discussion between the correlations with biological species (heterotrophic bacteria, cyanobacteria, diazotrophs), biogeochemistry (T_{SW}, salinity, pigments) and organic matter (POC, DOC, etc).

III.2.3.3.a Biological species

Among all biological species, bacteria show the best correlations for all INP data sets and temperatures, with $R \approx 0.5$. After the heat treatment we observe a decrease to $R = 0.38$ in the case of HS INP and an increase to $R = 0.74$ for HL INP with bacteria concentrations. This suggests that a large part of the INP activity at the warmer temperatures can be explained by the concentration of bacteria, which are heat sensitive.

The concentrations of eukaryotes (PicoPhyto, NanoPhyto and TotEuk) exhibit a few moderate relationships with HS INPs at -15 °C and -17 °C ($R \approx 0.4 - 0.5$ and $R = 0.4 - 0.6$ respectively). Total bacteria abundances correlate

Table III.4 – Correlations between SW INP concentrations (total INPs, heat stable INPs and heat labile INPs) at -12 °C, -15 °C and -17 °C and ocean parameters. Only significant ($p < 0.05$) correlation coefficients ($-1 < R < 1$) are shown. Non significant coefficients are shown as "—". Bold values indicate the significant correlations with $P < 0.005$.

		T_{SW}	Sal.	BChl-a	Chl-a	Per.	Car.	Pico	Nano
IN_{-12}	R(P)	0.37(0.04)	—	0,61(0,02)	—	—	—	—	—
IN_{-12} HS	R(P)	—	—	—	—	—	—	—	—
IN_{-12} HL	R(P)	—	—	—	—	—	—	—	—
IN_{-15}	R(P)	—	-0,39(0,03)	**0,76(<0,005)**	0,61(0,02)	0,68(0,01)	0,62(0,02)	—	—
IN_{-15} HS	R(P)	0,41(0,02)	-0.35(0.05)	—	—	—	—	0,48(0,01)	
IN_{-15} HL	R(P)	—	—	**0,81(<0,005)**	—	—	0,64(0,05)	—	—
IN_{-17}	R(P)	—	0,35(0,05)	**0,74(<0,005)**	**0,71(<0,005)**	0,59(0,03)	**0,73(<0,005)**	—	—
IN_{-17} HS	R(P)	0.38(0.04)	0,41(0,02)	—	—	0,68(0,01)	—	0,44(0,02)	0,40(0,3)
IN_{-17} HL	R(P)	—	0,40(0,03)	0,72(0,01)	0,71(0,01)	0,56(0,05)	**0,74(<0,005)**	—	—

		Euks	Bact	Proc	Syn	UCYN-A	UCYN-B	UCYN-C
IN_{-12}	R(P)	—	**0,54(<0,005)**	—	—	—	—	—
IN_{-12} HS	R(P)	—	0,38(0,03)	—	—	—	—	—
IN_{-12} HL	R(P)	—	0,74(0,01)	—	—	—	—	—
IN_{-15}	R(P)	—	**0,51(<0,005)**	—	—	—	—	—
IN_{-15} HS	R(P)	**0,54(<0,005)**	0,47(0,01)	—	—	—	—	-0,40(0,05)
IN_{-15} HL	R(P)	—	0,39(0,05)	—	—	—	—	—
IN_{-17}	R(P)	—	—	0,41(0,03)	—	0,48(0,01)	-0,47(0,02)	—
IN_{-17} HS	R(P)	**0,58(<0,005)**	**0,59(<0,005)**	—	—	—	—	—
IN_{-17} HL	R(P)	—	—	0,40(0,03)		0,42(0,04)	-0,41(0,04)	—

		POC	DOC	O_2	BP	HuS	dBP	LMW acids	LMW neutrals
IN_{-12}	R(P)	—	—	—	—	—	—	—	—
IN_{-12} HS	R(P)	—	—	—	—	—	—	—	—
IN_{-12} HL	R(P)	—	—	—	—	—	—	—	—
IN_{-15}	R(P)	0,64(0,02)	—	0,56(0,05)	—	—	—	—	—
IN_{-15} HS	R(P)	—	**0,75(<0,005)**	—	0,71(0,01)		0,71(0,01)	0,60(0,01)	—
IN_{-15} HL	R(P)	—	—	—	—	—	—	—	-0,71(0,02)
IN_{-17}	R(P)	**0,79(<0,005)**	—	0,56(0,05)	—	—	—	—	—
IN_{-17} HS	R(P)	0,62(0,03)	0,70(0,01)	—	0,61(0,04)	—	—	—	—
IN_{-17} HL	R(P)	**0,77(<0,005)**	—	—	—	—	—	—	—

with almost all of the INP data, with values that vary between $R = 0.38$ and $R = 0.74$. The best correlation is observed at -12 °C with HL INPs ($R = 0.74$, $p = 0.01$), and HS INPs at this temperature show the lower correlation ($R = 0.38$, $p = 0.03$). However, this difference is not observed at -15 °C, where the correlation is stronger with HS INPs than with HL INPs ($R = 0.47$ and $R = 0.39$ respectively). Previous studies on the link between marine INP concentrations and bacterial abundances have yielded mixed results, with Irish et al. (2017) finding no significant relationship between INP and bacteria in the Arctic Ocean, but McCluskey et al. (2017) observed that aerosol INPs were positively correlated with aerosolized bacteria.

Correlations with specific types of cyanobacteria yield very mixed results. *Prochlorococcus* (Proc) and *Synechococcus* (Syn), yield few significant values, with the only relationships found at -17 °C for total INP and heat labile INP with Proc ($R \approx 0.4$, $p = 0.03$). *Prochlorococcus* is known to contain no Chl-a but is the only procaryote with α-carotenes (Ralf et al. 1992). Similarly to Proc, UCYN-A

correlates positively with IN_{T_3} (total and heat labile), with $R \approx 0.4$. However, both UCYN-B and UCYN-C are negatively correlated with INP data: $R \approx -0.4$ with IN_{T_3} (UCYN-B), and $R = -0.40$ with HS IN_{T_2} for UCYN-C.

III.2.3.3.b Biogeochemistry

We observe negative correlations between IN_{-15}, IN_{-17} and salinity, with $R \approx -0.4$ and $p \approx 0.04$, similar to Irish et al. (2017), who observed negative correlations as low as $R = -0.7$. They associated this correlation to increased INPs from melting sea ice (associated with lower salinity). However, in our case no sea ice is observed, suggesting other processes are important. Furthermore, they observed values of salinity varying between 28 and 34 g/L, whereas we observe finer variations (34-35 g/L). We additionally observed that salinity was negatively correlated with the seawater temperature ($R = -0.75$, $p < 0.005$) and with the total chlorophyll-a concentrations ($R = -0.61$, $p = 0.02$) and carotenes ($R = -0.60$, $p = 0.02$). Hence the anticorrelation between INP and salinity is likely a result of the covariation of biological tracers with seawater salinity.

They also suggest that a non-colligative effect is not accounted for when correcting for salinity in the seawater samples. However, non-colligative effects have not been previously observed in INP experiments with seawater (Wilson et al. 2015) or sodium chloride solutions (eg. Zobrist et al. 2008; Knopf et al. 2011b).

Bacteriochlorophyll-a actually exhibits the strongest correlations with INP concentrations over the whole INP spectrum, with R ranging from 0.61 to 0.81. The weakest correlation ($R = 0.61$) is reported for IN_{-12}, while the strongest correlation ($R = 0.81$) is with HL IN_{-15}. Bacteriocholorophyll-a is a photosynthetic pigment that is linked to light harvesting activity from various phototrophic bacteria (Senge et al. 1995, Frigaard et al. 2006). The strong link between this pigment and the HL INP activity suggests that such bacteria have good INP properties or emit ice active materials.

IN_{-15}, IN_{-17} and HL IN_{-17} also correlate strongly ($R = 0.6 - 0.7$, $p < 0.02$) with chlorophyll-a (Chl-a) concentrations. The correlations are stronger and more significant at -17 °C than at -15 °C. Chlorophyll-a is a classic tracer for phytoplanktonic biomass, as it is used for photosynthesis by algae, phytoplanktons and cyanobacteria (Bryant et al. 2006, Sinha et al. 2008, Foster et al. 2019), suggesting that such species could be INPs at colder temperatures. Similar observations were observed in a mesocosm study on INPs in the SSA, (McCluskey et al. (2018b)), where INPs were generally heat-stable and comprised of organic material.

Strong correlations are also observed from carotene pigments (Peridinin - Per.) and the total carotene abundance (Car.). Car. correlates only with total and HL INPs at T_2 and T_3, with best correlations at T_3. Per. also correlates with INP at T_2 and T_3, but the best correlations are found for IN_{T_2} and HS IN_{T_3}. Carotenes, and peridinin in particular, are pigments associated with chlorophyll-a as proteins used by dinoflagellates to harvest light (Schulte et al.

2010). This hints at the potential contribution of dinoflagellates on ice nucleation in the SW.

III.2.3.3.c Organic matter

Concentrations of organic matter have been linked in previous studies with INP concentrations and have been used in various parameterizations (e.g. Wilson et al. 2015; Trueblood et al. 2021). Here, we show that both POC and DOC correlate well with INP concentrations at both -15 °C and -17 °C, with $R \approx 0.7$ and p-values below 0.1, but not at -12 °C. That might show again variability that are more uncertain due to their low concentrations. While POC seems to be better correlated to the total and HL INPs, DOC correlates best with the heat stable fraction of INP, which can be explained by the fact that DOC is often processes by biological and chemical degradation, and is thus a more aged and degraded organic matter than POC. Like DOC, other organic compounds (biopolymers, low molecular weight acids) correlate well ($R > 0.6$) with HS INPs. This is in line with the classification proposed by McCluskey et al. (2018b), where DOC-type INPs are more heat stable and POC-type INPs are more heat labile.

In summary, INPs in the seawater during TONGA exhibit strong links with both biological and organic data. In general, Heat labile INP are best correlated to bacteriochlorophyll-a and bacterial cell abundances, hinting that the bacteria themselves are responsible for the ice nucleation activity observed, which is also consistent with POC-type INPs (McCluskey et al. 2018b) and at the coldest freezing temperatures with cyanobacteria, among them *prochloroccocus*.

In a future section (Sec. III.4), we will use these results to derive parameterizations that use the biogeochemical properties of the SW as a predictor for INP concentrations.

III.2.4 Observations of INP in the SSA

In the following sections, we will discuss the INP concentrations measured in the generated SSA. They were measured at two size ranges, submicron (<1 µm) and supermicron (>1 µm) (see Sec. III.2.1.2).

III.2.4.1 General features

SSA INPs measured in this study were in general quite rare: Figure A.8 shows the comparison between INP concentrations from blank filters and raw INP concentrations from sampled filters. More than half of the samples are below the INPs concentrations on blanks, thus severally limiting the amount of exploitable samples. In the following, only the values that were superior to 2 times the standard deviation of blank concentrations were used, and values that were below that threshold were set to zero. For submicronic INPs (Fig. III.11a and III.11c), all the heated samples were below the limit of detection (LOD) defined by the blanks, and 13 samples out of 30 were above the LOD for unheated samples. For supermicronic INPs (Fig. III.11b and III.11d), respectively

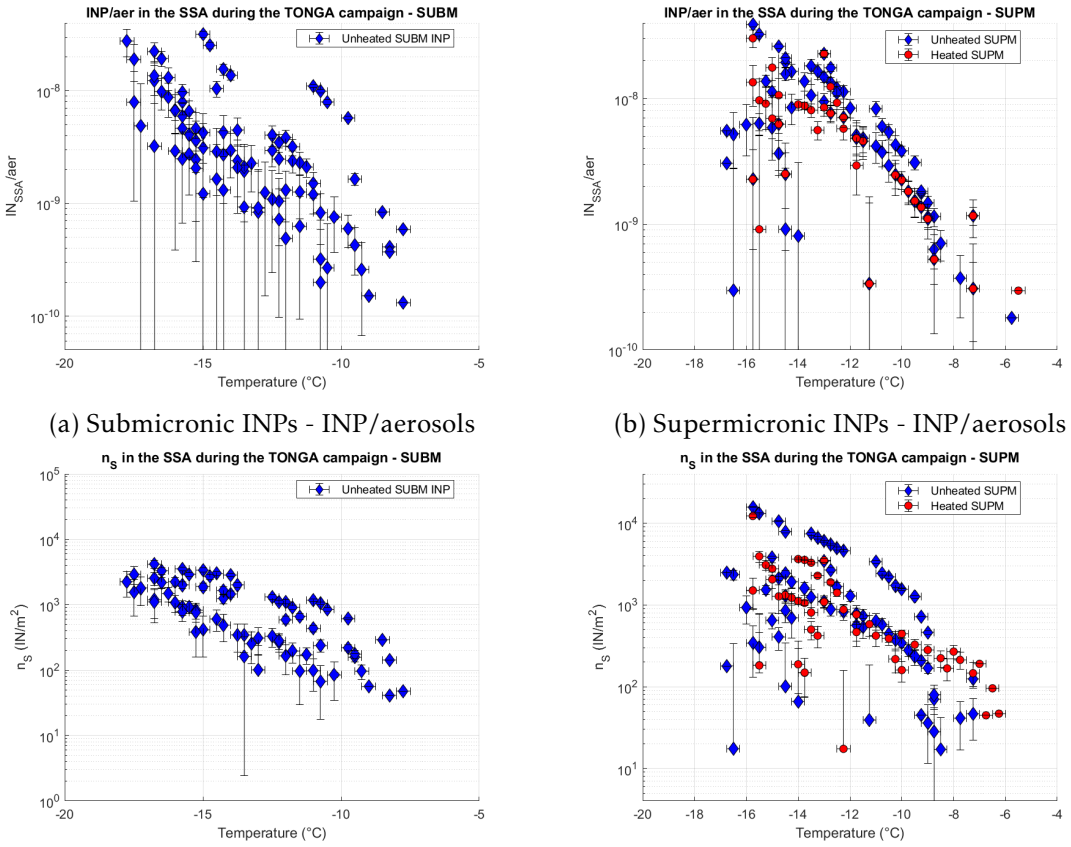

(a) Submicronic INPs - INP/aerosols

(b) Supermicronic INPs - INP/aerosols

(c) Submicronic INPs - INP/cm^2

(d) Supermicronic INPs - INP/cm^2

Figure III.11 – Cumulative INP concentrations in the SSA for a) Submicronic INP/SSA; b) Supermicronic INP/SSA; c) Submicronic INP/cm^2; d) Supermicronic INP/cm^2. Unheated INPs are shown in blue, heated INPs are shown in red. Error bars are defined by a standard deviation of blank samples.

15 and 12 samples were available after background corrections for unheated and heated samples.

The concentrations of INPs in the submicron mode were on average close to the concentrations of supermicron INPs, with fractions of respectively 56%, 44% and 46% at -12 °C, -15 °C and -17 °C (Fig. III.13, gray bars). However, supermicronic INPs exhibit more variability at the lower temperatures than the submicronic INPs.

As all heated submicron mode samples were below the LOD, heat labile INP concentrations in this mode were 100%. In comparison, HS INPs contributed 56%, 49% and 50% at -12 °C, -15 °C and -17 °C, respectively for supermicron INPs (Fig. III.13, green bars). Supermicron SSA are made of biological heat stable material such as $CaCO_3$ (calcium carbonate from shells), which could explain these observations.

Total INP concentrations normalized by the number of aerosols and by the total surface of aerosols are shown in Figure III.12. Trueblood et al. (2021)

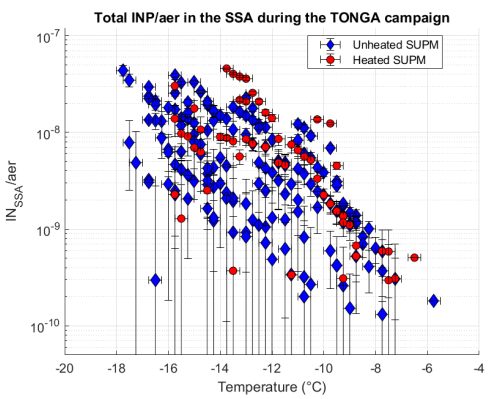

(a) INP/SSA

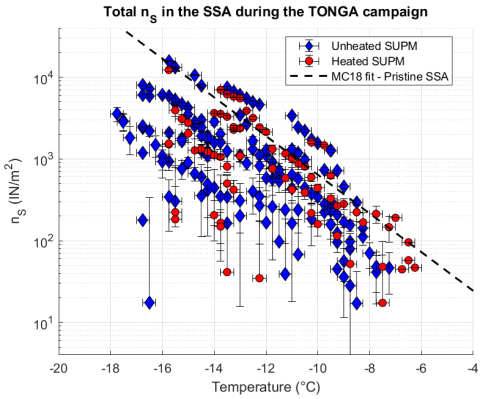

(b) n_S and McCluskey et al. (2018c) fit for pristine marine SSA (dashed line).

Figure III.12 – Total cumulative INP concentrations in the SSA. Only the dates where both the submicronic and supermicronic are above the LOD are shown.

observed lower concentrations of INP/aer during the PEACETIME campaign in the Mediterranean than our study, with observed values in the range of 10^{-9}INP/aer. However, the only point of comparison is at -18 °C, as the instrument used is a Dynamic Filter Processing Chamber (DFPC, DeMott et al. 2018) that measures INP in the condensation freezing mode.

As done in previous aerosol samples, the INP concentrations normalized by the aerosol surface (surface site density, n_S) are in line with previous observations, but generally in the lower range of measured concentrations (DeMott et al. 2016; McCluskey et al. 2018c). In Fig. III.12b, we also plot the equation of a fit for SSA INPs proposed by McCluskey et al. (2018c). This fit is based on measurements of SSA INPs over Mace Head Research Station in the North Atlantic Ocean. It aims to predict n_S values in the SSA as a function of the freezing temperature T_K, with the assumption that all particles are representative of the marine organic INP type, such as:

$$n_S = \exp -0.545(T_K - 273.15) + 1.0125. \tag{III.1}$$

Our measurements are also generally 1 to 2 orders of magnitude lower than this fit. This is consistent with the observations by McCluskey et al. (2018a) that INP concentrations in the Southern Ocean boundary layer were generally lower than in other marine regions.

III.2.4.2 Variations and relationship to seawater data

We plot in Fig. III.14 the boxplots of INP concentrations in the VZ and in the OZ at -12 °C, -15 °C and -17 °C for the total SSA INP, submicron SSA INP and supermicron SSA INP (both unheated and heat stable INPs). The total SSA INPs have roughly the same values between the VZ and the OZ, however the values in the VZ are much more variable (Fig. III.14a). Heat Stable total INPs are higher in the VZ than in the OZ (Fig. III.14b). Submicron INPs also exhibit roughly

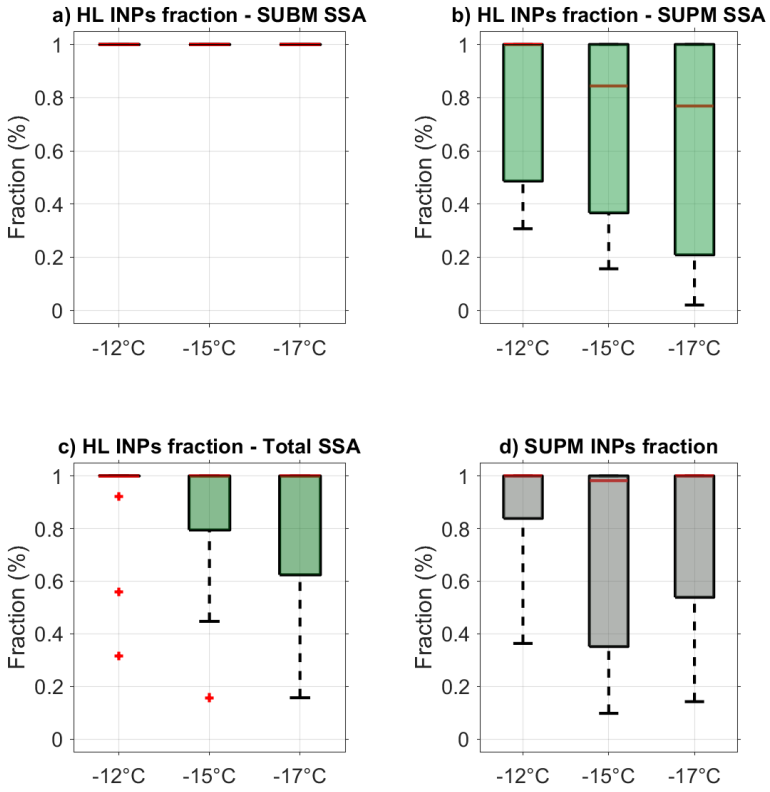

Figure III.13 – Different fractions in the SSA: Heat Labile INPs in the submicron mode (light green), in the supermicron mode (medium green) and in the total INPs (dark green); and fraction of supermicron INPs (grey).

the same values in the VZ and in the OZ, although with a 10% decrease at -17 °C (Fig. III.14c).

The supermicron INP in the VZ are much more abundant than in the OZ at temperatures warmer than -14 °C, with an increase up to five-fold at -12 °C (Fig. III.14d). They are however less abundant in the VZ at the coldest temperatures. HS supermicron INPs are generally more abundance in the VZ than in the OZ at temperatures colder than -14°C, but they are roughly equal at the warmer temperatures (Fig. III.14e). Because SW INP were predominantly heat labile and enriched in the VZ compared to the OZ, these results would indicate that seawater INP of volcanic origin are preferentially transfered to the sea spray in the form of supermicron particles (hence likely via the ejection of jet drops rather than film drops). One caveat of this observation is that we have a limited amount of data above the LOD in the VZ, which makes it harder to interpret, with a much higher variability exhibited by the remaining samples.

The correlations between INP concentrations in the SW and n_S in the SSA were computed at each temperature along the temperature spectrum, for each of the three SSA INP datasets (submicron, supermicron, total). We report no

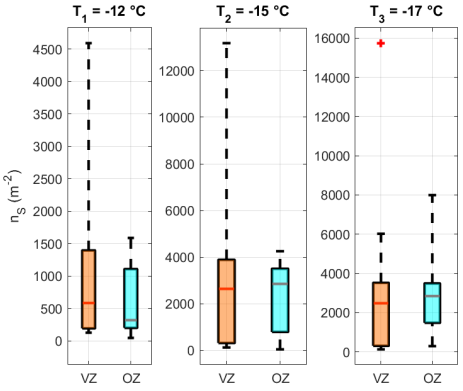

(a) Total SSA INPs.

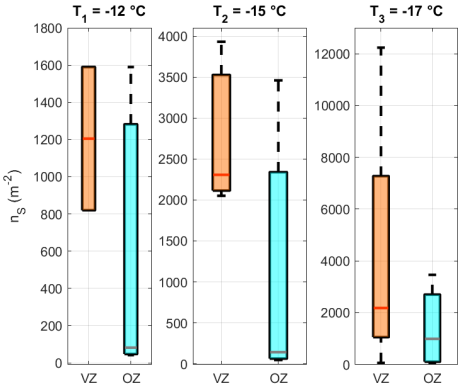

(b) Total SSA INPs - Heat stable.

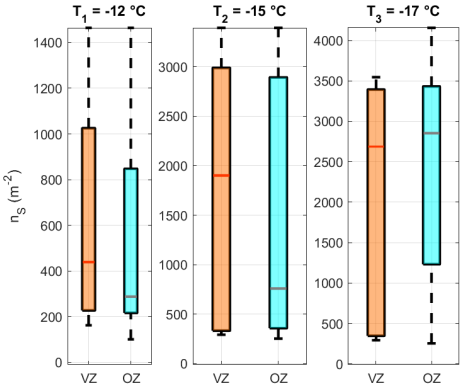

(c) Submicron SSA INPs.

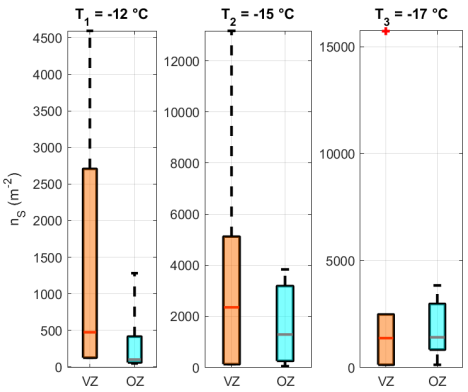

(d) Supermicron SSA INPs.

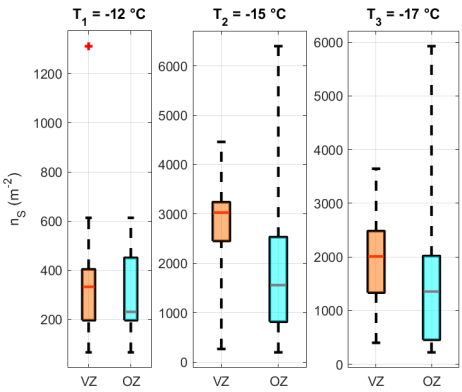

(e) Supermicron SSA INPs - Heat stable.

Figure III.14 – Box plots comparing SSA INP concentrations in the OZ (blue) and in the VZ (orange) at $T_1 = -12$ °C, $T_2 = -15$ °C and $T_3 = -17$ °C. The edges of the boxes represent the 25th and 75th percentile, the red lines represent the median, the whiskers represent the points lower than 3 times the interquartile interval and the red crosses represent the outliers. No figure for submicron HS INPs is shown because all of the samples were below the LOD.

significant correlation at any temperature, for any of the three SSA INP datasets, presumably because the INP in SSA data is too scarse for reliable statistical relationships, given the uncertainty on INP concentrations in SSA at these low levels n_S.

In Section III.4, we will use the SSA data of TNG as a comparison to the S2C data and for discussing a parameterization for SSA INPs.

III.2.5 Conclusions on the TNG cruise

INP abundances in the seawater collected in the region of the Tonga Volcanic arc and in the generated SSA were measured daily. A variety of other biogeochemical parameters were also measured throughout the campaign, allowing the characterize the state of the ocean during the cruise. Two areas of different water types were identified: the volcanic zone (VZ), which was overall richer in nutrients and biomass, and the oligotrophic zone (OZ), a nutrient-poor area.

Results show that INPs in the bulk seawater were generally active at temperatures <-10 °C. The INP abundances were overall lower than in previous works in richer waters (Wilson et al. 2015, Irish et al. 2017), but were comparable to other oligotrophic waters (McCluskey et al. 2018a; Trueblood et al. 2021). The majority of the INP in the SW were heat labile. Increased INP abundances were observed in the VZ compared to the OZ, with higher differences near -15°C. This increase was consistent with a general increase in biological markers such as microorganisms, planktons, pigments and POC. Medium to strong correlations were found with pigment data, bacterial abundances and POC ($0.6 < R < 0.8$), suggesting that the INP population was most related to the POC-type INPs as assumed by McCluskey et al. (2018b), highlighting the strong influence of microorganisms and planktons on the IN activity in the SW. Heat stable INPs exhibited correlations with the dissolved organic matter data, suggesting that DOC-type INPs were also present. POC, bacterial abundance and the pigment bacteriochlorophyll-a were found to be the best predictors for INP concentrations in the SW.

SSA INPs were artificially generated using seawater through a bubbler system, and were available as size segregated data (<1 µm and >1 µm). Results show that SSA INPs exhibited generally low concentrations compared to other marine regions, which is consistent with other observations in the Southern Ocean (McCluskey et al. 2018a). About half the untreated samples were below the limit of detection for the INP analysis, as well as all of the heated submicron samples. The abundances of submicron and supermicron INPs were generally equal, but heat labile INPs were more abundant in the submicron mode. Heat labile INPs represented about 70% of the total. Because of the missing samples, the conclusions on the influence of the VZ on SSA INPs were less clear. Supermicron INPs were generally more abundant in the VZ, while submicron INPs did not exhibit much variability both water types. Heat stable INPs were generally more abundant in the VZ. No significant correlation was found between

SSA INPs and SW INPs, or between SSA INPs and the SW parameters, which can be explained by the missing data and by the fact that SSA INPs could be more influenced by the INPs in the SML, which were not available in this study.

For studying the transfer of INP from the SW to the SSA via the SML, and for evaluating if the conclusions found during the Tonga cruise can be applied to other water types, we now turn to the Sea2Cloud Tangaroa ship campaign.

III.3 Ice Nucleating properties of sea spray in various seawater types of the Western Southern Pacific Ocean

The Sea2Cloud project[2] (S2C) is a multidisciplinary project with the general objective of better understanding the link between the oceans and the atmosphere. The S2C cruise took place in the framework of this project, with the objectives to sample varied water types having different plankton communities and thus attempt to generalize the role of ocean biology on marine aerosol emission and formation (Sellegri et al, submitted to BAMS, 2022).

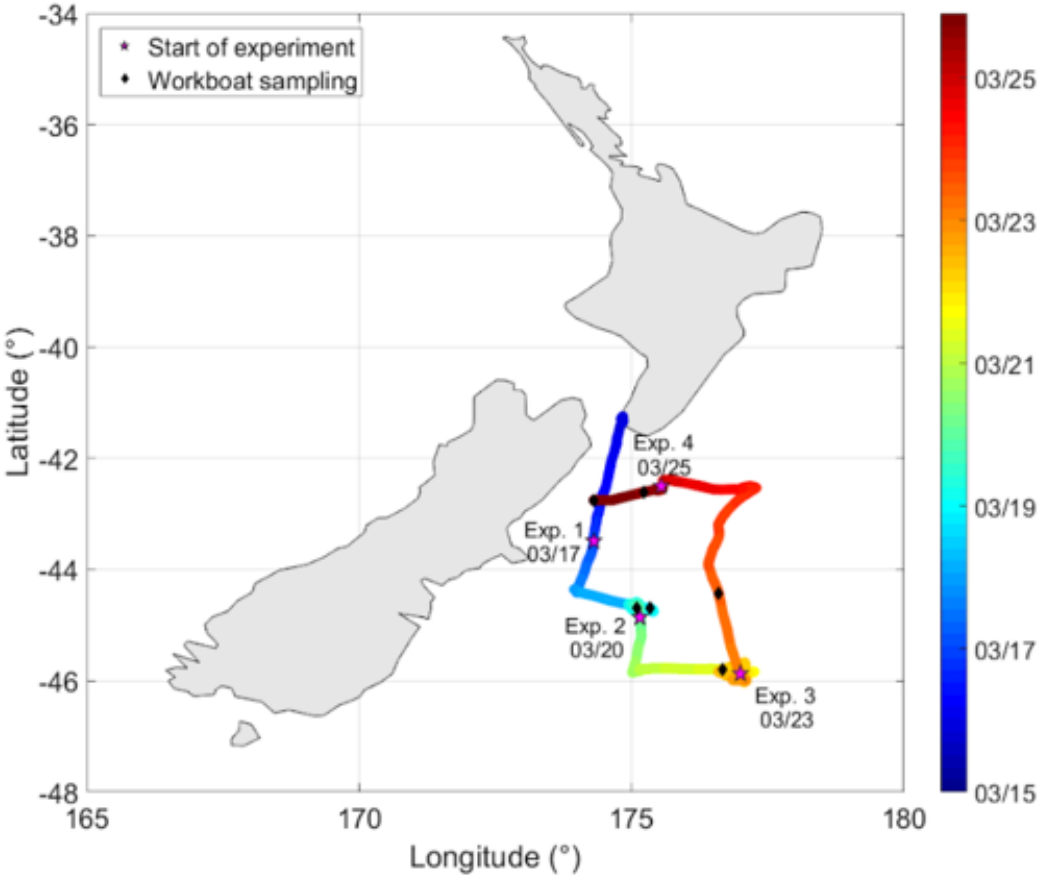

Figure III.15 – Track of the RV *Tangaroa* during the Sea2Cloud campaign

In this chapter, we use the same methodology than in the previous chapter to relate the various seawater properties throughout the cruise to the INP concentrations sampled in the seawater (both in the bulk seawater and in the surface micro-layer) and in the generated sea spray aerosols. As in previous chapters, we first present the experimental approach and instrumentation of

[2] https://sea2cloud.data-terra.org/en/home/

the cruise, and then discuss and characterize the measured INP concentrations in the different environments (SW, SML, SSA).

III.3.1 Experimental approach

The 2020 ship campaign Sea2Cloud took place from 15 to 27 March 2020, on board of the research vessel (RV) *Tangaroa* from Wellington, New Zealand. The track of the *Tangaroa* is indicated in Figure III.15: the ship travelled between -42° and -46° latitudes, and 172° and 177° longitudes in the Northern Southern Ocean. The ship was at it farthest point from the land on 23/03. The sampled area was chosen because it is at the cross where subantarctical seawaters traveling up North meet subtropical seawaters travelling down South, in the upper levels of the ocean with the help of a underwater topography that has a plateau East of NZ (the Chatham Rise). The Chatham Rise is visibly enriched in Chl-a on satelite ocean colour images. The details of the methodical approach used in the campaign are described in Sellegri at al. (submitted to BAMS, 2022).

As *L'Atalante* during the TONGA campaign (Chap. III), the *Tangaroa* was equipped with a wide array of instruments for measuring various biogeochemical parameters during the campaign. A schematic of the instrumental setup on board of the ship is shown in Fig. III.16. In particular, the data for the INP analysis in this study were sampled from the three encircled areas shown in Fig. III.16: the main aerosol inlet (1) for ambient aerosol measurements, the sea-spray generator for primary sea spray emissions (2), and the seawater biological analysis (3).

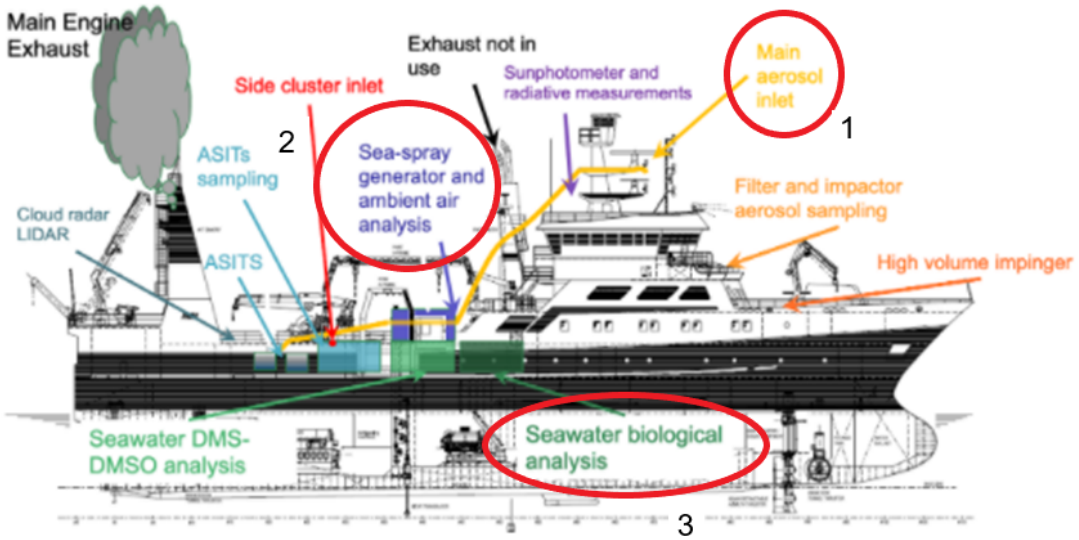

Figure III.16 – Schematics of the instrumental facilities of the RV *Tangaroa* during the Sea2Cloud campaign. The relevant instruments for this study are circled in red. Figure courtesy of Sellegri et al. (submitted to BAMS, 2022).

III.3.1.1 Bulk seawater and surface microlayer

The seawater salinity was used to distinguish the different water types during the sampling campaign according to the criteria defined by Chiswell et al. (2015): Subantarctic waters (SAW) are defined by salinity lower than 34.5 g/L, Frontal waters (FW) by salinity between 34.5 and 34.8 g/L and Subtropical water (STW) by salinity greater than 34.8 g/L. Given the variability of salinity at the end of the campaign, we also define a fourth water type as Mixed waters (MW), corresponding to the mixture of subtropical and frontal waters.

Each type of seawater is described more thoroughly in Sellegri et al, (submitted to BAMS, 2022). Briefly, frontal waters were sampled from 17/03 11:00 to 20/03 17:00 (NZ time), Subantarctic waters from 20/03 17:00 to 24/03 04:00, and Subtropical waters from 24/03 04:00 to 25/03 8:00. Mixed waters were encountered from 25/03 8:00 to the end of the voyage on 27/03 00:00 (Figure III.17). Elevated biomass was sampled in frontal waters from 18/03 onwards, while the lowest biomass was observed in subantartic waters between 20/03 and 23/03. Low biomass was also observed in subtropical waters on 24-25/03. SAW and MW were high in nitrate concentrations, while STW were low.

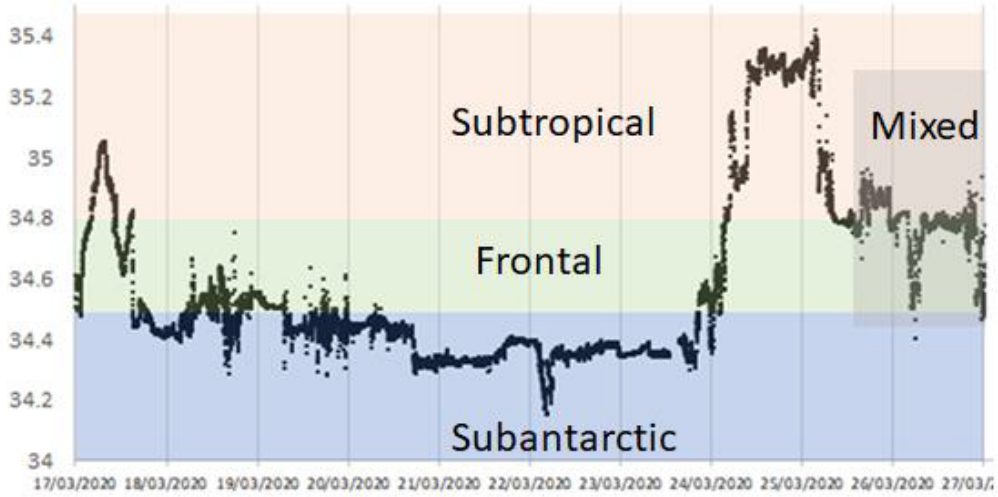

Figure III.17 – Water salinity used to define the different types of waters during the cruise. Figure courtesy of Sellegri at al. (submitted to BAMS, 2022).

The same setup used in the TONGA campaign (Fig. III.3) was used to sample 5 m depth bulk seawater using the underway system of the ship (henceforth UWAY) and for generating artificial SSA. Bulk seawater sampling was also analyzed for various biogeochemical parameters (Table III.5). The concentrations of phytoplankton cells (prokaryotic, picophytoplankton, nanophytoplankton, Table III.5) were measured using FCM over 4 hours intervals.

Sampling of the SML took place from a pneumatic workboat (henceforth WBOAT) approximately 1 km away from the *Tangaroa*. A total of 7 samples (5 in the morning, 2 in the afternoon) were taken in the SML during the campaign. In order to deploy the WBOAT, the wind speed had to be lower than 10 m/s

and the wave height had to be lower than 2 m. Sampling was done using the glass plate method (Cunliffe et al. 2015): a glass plate is drawn perpendicular through the sea-air interface and SML water attaches to the surface of the plate. The sampled water is then collected into a sample bottle. This method allows the sampling of 20 to 150 µm of the sea surface microlayer.

Table III.5 – Summary of the data used in this study.

Name	Symbol	Medium	Unit
Salinity	S	SW	g/L
Temperature	T_{SW}	SW	°C
Chlorophyll-a	Chl-a	SW	$mg.m^{-3}$
Synechococcus	Syn.	SW	cells/mL
Nanophytoplanktons	NanoPhyto	SW	cells/mL
Picophytoplanktons	PicoPhyto	SW	cells/mL
Bacteria	Bact.	SW	cells/mL
Dinoflagellates	DiFl.	SW	$mgC\cdot m^{-3}$
Diatoms	DiA.	SW	$mgC\cdot m^{-3}$
Flagellates	Fl.	SW	$mgC\cdot m^{-3}$
Total Organic Carbon	TOC	SW/SML	µg/L or µM
Total Nitrogen	TN	SW/SML	µg/L or µM
Dissolved Amino Acids	DAA	SW	nmol/L
Total Amino Acids	TAA	SW	nmol/L
Dissolved Carbohydrates	DCHO	SW	nmol/L
Total Carbohydrates	TCHO	SW	nmol/L
Aerosol concentration	N_{aer}	SSA	cm^{-3}
Aerosol surface	S_{aer}	SSA	$m^2\cdot cm^{-3}$
NaCl in the SSA	$NaCl_{SSA}$	SSA	µg/aer
TOC in the SSA	TOC_{SSA}	SSA	µg/aer

III.3.1.2 Sea spray aerosols

Aerosols were measured from two sources during the cruise: aerosols from the ambient air were sampled through the main aerosol inlet (area 1 in Fig. III.16), and aerosols from the artificially generated SSA that were produced continuously using the same method as during the TONGA campaign using seawater from the Underway system (Fig. III.3).

After passing through a drier, the generated SSA flux was analyzed using a DMPS and WIBS for the aerosol concentrations and size distribution. As in Section III.2, a 4-stage cascade impactor was used to sample size-segregated INPs. The stages correspond to sizes 0.1-1 µm, 1-2.5 µm, 2.5-10 µm and > 10 µm. A 13 stages Cascade impactor was used to sample SSA over 23 hours for chemical analysis (inorganic and organic content) using Ion Chromatography (Sec. II.3.2). For our analysis, we used the TOC and NaCl concentrations normalised

per aerosol in the SSA, in order to account for the variation of the sampled volume.

III.3.1.3 INP analysis and treatment

Following the same methods as Chapter III, the INP were analysed using LINDA for SSW, SML, SSA and ambient aerosol. The samples were submitted to a heat treatment in order to remove the heat labile fraction. For seawater INP (bulk SW and SML INP), the samples were directly poured into Ependorf tubes for the analysis. For filter samples, punches of the filters were washed in a 0.9% NaCl solution for 20 minutes, and then analysed with LINDA.

In order to take into account the shift in temperature caused by the high salinity of the water samples, the SSW and SML data sets were corrected by 2 °C (Doherty et al. 1974). A number of blank filters were acquired to correct for background error on the filter samples.

III.3.2 Overview of the variability of the biogeochemical parameters during S2C

The variability of the biogeochemical parameters described in Table III.5 is presented in Figures III.20 (biological parameters) and III.19 (chemical parameters). The variability of each parameter between the different water masses is illustrated in Figure. III.18.

T_{SW} exhibits similar variability to the salinity, with a peak in the STW and intermediate values in the MW; however, there is no difference in T_{SW} between the FW and the SAW (Fig. III.19a).

Total organic carbon in the SW (TOC_{SW}) is consistently higher in the FW than in the other water types, with an average value of 1097 ± 51 µg/L in the FW, and 890 ± 31 µg/L in the SAW/STW/MW (Fig. III.19b). Similarly to TOC_{SW}, the normalised total organic carbon in the SSA (TOC_{SSA}, in µg TOC per SSA aerosol) is about 50% higher on average in the FW than in the SAW (Fig. III.19c). Normalised $NaCl_{SSA}$ exhibit very low variability, with two peaks at the beginning of the campaign in the FW (17/03 and 18/03), and constant values from 18/03 to 24/03. Total nitrogen (TN) exhibits a lot of variability in the FW, and is consistently higher in the SAW, contrarily to the other parameters measured (Fig. III.19b). TN is lowest in the STW and in the MW.

Amino acids (AA) and carbohydrates (CHO) are consistently higher in the FW than during the rest of the cruise, except for the dissolved AA which exhibit similar values in the MW than in the FW, and very variable values in the SAW (Fig. III.19d) and III.18i)B.1). Dissolved CHO also exhibits a slightly higher values on the 24/03.

As briefly described in Section III.3.1.1, chlorophyll-a (Chl-a) abundances are highest in the FW with values of about 2 $mg.m^{-3}$ (Fig. III.20a). The peak

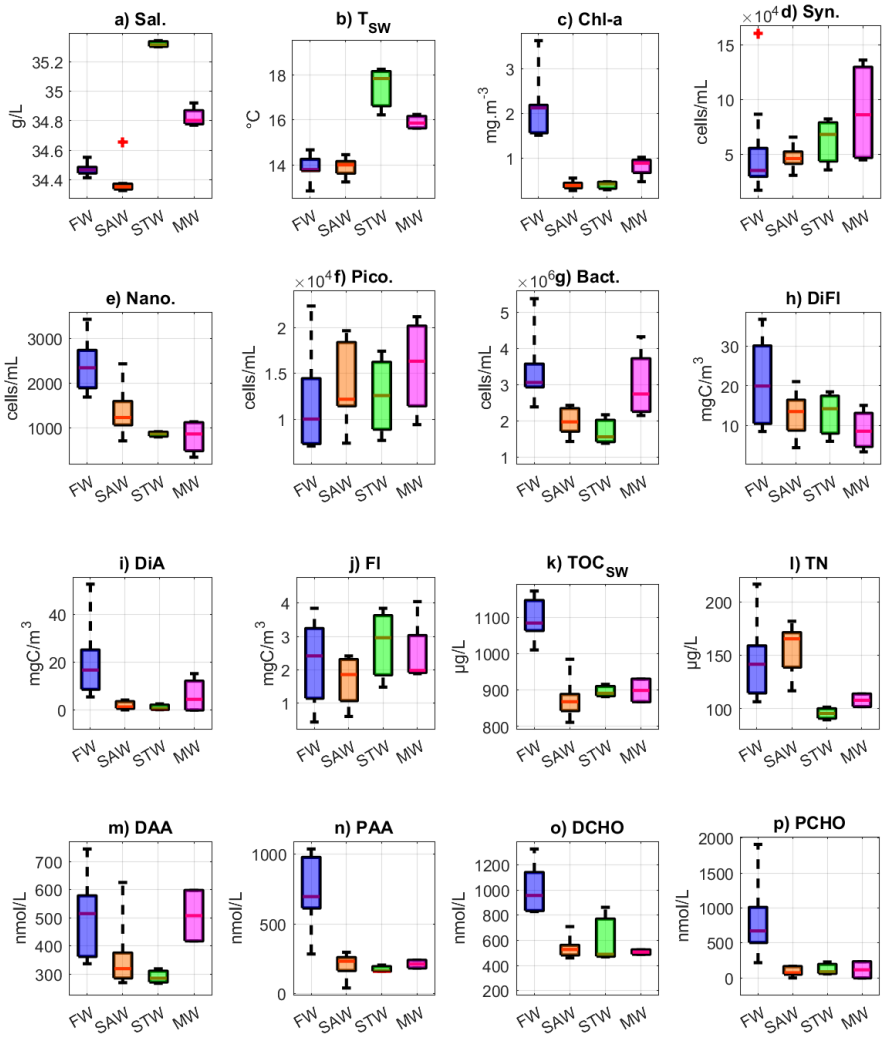

Figure III.18 – Boxplots of the parameters measured in the SW for the different watertypes.

value of about 4 mg.m^{-3} corresponds to a phytoplankton bloom observed on 19/03. Chl-a is lowest in the SAW and in the STW with values of about 0.2-0.5 mg.m^{-3}, and only increases in the MW to about 1 mg.m^{-3}.

The different types of organisms measured in this study are briefly explicited in Sec. A.1.1. The total heterotrophic bacterial abundance (Bact., Fig. III.20b) is higher in the FW and in the MW , but short term high concentration are visible on the 19/03 (FW), 23/03 (SAW) and 26/03 (MW). However, specific species such as Nanophytoplanktons (Nano, Fig. III.20c) show highest in the FW, and are the lowest in the MW, with intermediate values in the SAW . On the other hand, *Synechococcus* (Syn, Fig. III.20b) and picophytoplanktons (Pico, Fig. III.20c) are at their lowest in the FW, although they exhibit a high variability, with a peak observed on 18/03 for both populations. They are on average higher in the MW than during the rest of the campaign.

Bigger single-cells algae species (Fig. III.20d), such as dinoflagellates (DiFl), diatoms (DiA) and flagellates (Fl) are highly variable throughout the cruise, and

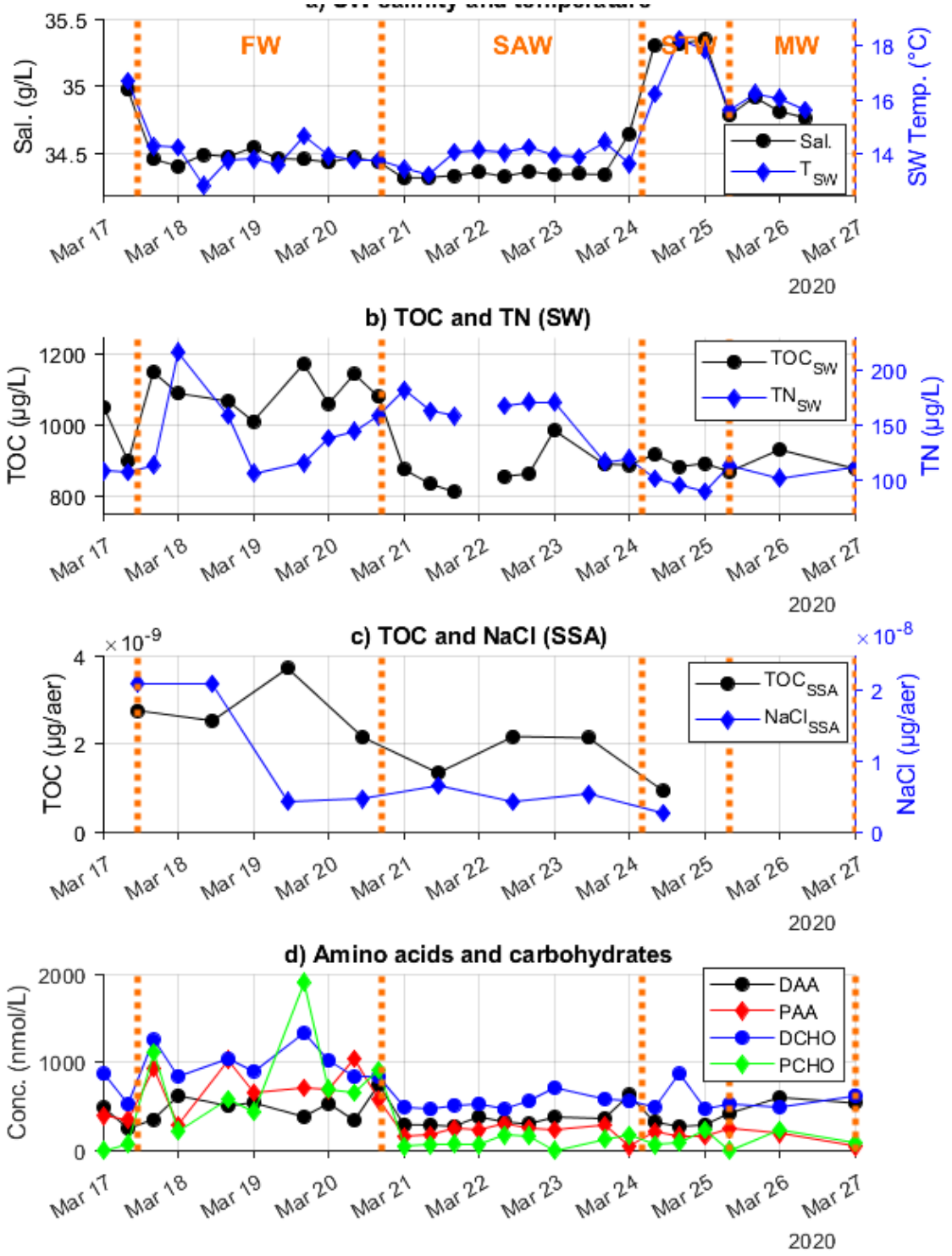

Figure III.19 – Time series of chemical parameters of the SW and of the SSA: a) Seawater salinity and temperature, b) seawater TOC and TN, c) generated SSA TOC and NaCl, d) Dissolved and particulate amino acids and carbohydrates. Salinity and T_{SW} are both averaged over the INP sampling times.

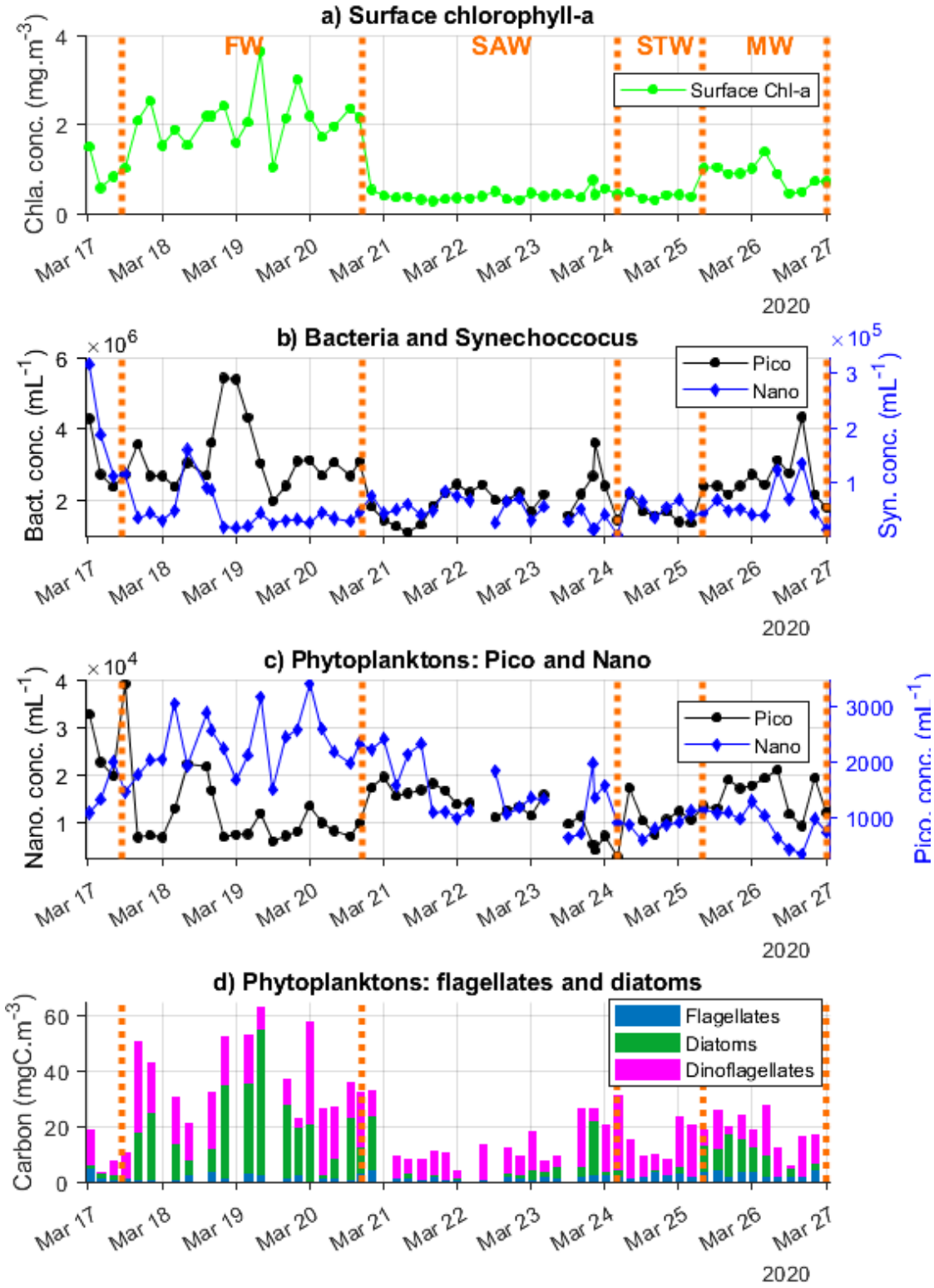

Figure III.20 – Time series of biological parameters of the SW: a) Surface chlorophyll-a concentrations, b) Bacteria and *Synechococcus*, c) Nanophytoplanktons and picophytoplanktons, d) Flagellates, diatoms and dinoflagellates.

their concentrations are mainly driven by DiFl and DiA. DiA in particular exhibit peak concentrations in the FW, with concentrations tenfold that of in the SAW and in the STW. DiFl are highest in the FW, average in the SAW/STW and lowest in the MW, while Fl are highest in the STW/MW and lowest in the SAW.

To summarize, the FW and STW were the regions with highest and second highest biological activity and biomass, especially for larger phytoplankton groups and chlorophyll-a. The smaller phytoplanktons (Pico, Syn) showed the opposite, with higher activity in the subantarctic waters. More details on the variability of the different nutrients and biological markers measured during the voyage are available in Sellegri et al. (submitted to BAMS, 2022).

III.3.3 General observations on the IN activity in the SW and SSA

III.3.3.1 INP in the seawater

In this section, we investigate the IN activity from the seawater, from two sources: the bulk seawater (SW) from the underway system and the surface microlayer (SML) from the workboat. The variability between the water masses is also explored, and we discuss the enrichment from the bulk SW to the SML.

III.3.3.1.a Bulk seawater

The frozen fractions and INP concentrations spectra in the bulk seawater from the underway system are shown in Figures. III.21 and III.22.

Similarly to Sec. III, we define T_{10} and T_{50} as the temperatures at which respectively 10% and 50% of the tubes have frozen for a given sample. For unheated samples from the UWAY, the average $T_{10,UH}$ and $T_{50,UH}$ were respectively -13.8 ± 1.0 °C and -14.9 ± 0.5 °C (Fig. III.21). This is within the range

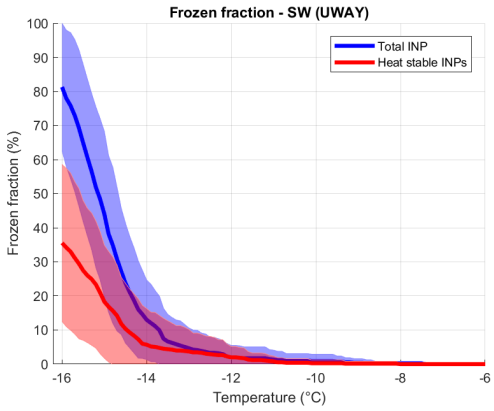

Figure III.21 – Frozen fractions in the SW.

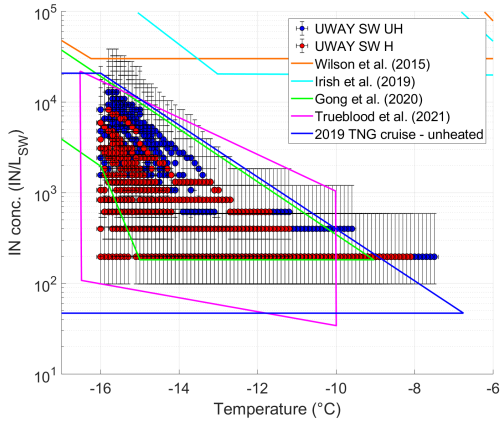

Figure III.22 – INP concentrations in the SW and comparison to other studies.

from the observations during TNG (Sec. III.2.3.1), where $T_{10,UH}$ and $T_{50,UH}$ were respectively -13.8 ± 1.9 °C and -14.9 ± 0.9 °C.

The SW INP concentrations observed during the S2C are within the same order of magnitude than observations from the TONGA campaign and from Trueblood et al. (2021) in the Mediterranean Sea and Gong et al. (2020) at Cabo Verde, all of which are lower than Wilson et al. (2015) and Irish et al. (2019a) (Fig. III.22) performed in biologically richer seawater of the northern hemisphere.

Heating the samples reduces their freezing temperatures: for heated samples, the average values of $T_{10,H}$ was -14.3 ± 1.8 °C. Both types of samples did not reach 100% freezing fraction at the end of the analysis at -16 °C, however the difference in activation fraction is about 40% between untreated and heated samples (Fig. III.22). Thus, heating the samples has a visible effect on the average freezing temperatures and activated fraction of droplets. Additionally, untreated samples exhibited a steeper activation slope than heated samples, with the majority of the freezing spectrum spread over only 3 to 4 °C. At the warmest temperatures, the INP concentrations for unheated samples are about 2×10^2 IN/L_{SW}, and they vary between 2×10^3 and 1.5×10^4 IN/L_{SW} at the coldest temperatures. The effect of heat treatment is illustrated by a drop of concentrations: at the coldest temperatures, the concentrations from heated samples is between 2×10^2 and 8×10^4 IN/L_{SW}. The fraction of heat labile INP varies between 60% to 100% from the coldest to the warmest temperatures, with values of 87.6±19.8% at -14 °C and 74.9±17.9% at -16 °C. These values are also similar to what we observed during the TONGA campaign, and show a very important contribution of heat labile, potentially biogenic material in the INP population in the SW.

III.3.3.1.b Surface microlayer

As mentioned in Section III.3.1.1, the SML samples were taken every 2 to 3 days. A total of 7 samples were collected over the cruise period with 2 samples being collected in the FW, 2 in the SAW, 0 in the STW and 3 in the MW. The INP concentrations and frozen fractions temperature spectra are presented in Fig. III.23.

For the unheated samples, the measured $T_{10,UH}$ and $T_{50,UH}$ are respectively -13.9 ± 0.5 °C and -15.1 ± 0.2 °C; for the heated samples, $T_{10,H}$ is -14.5 ± 0.6 and $T_{50,H}$ could not be defined as no samples reached 50% activated fraction at the end of the analysis (Fig. III.23a). This is is line with the previous observation that heating the samples results in a shift of the freezing temperatures and activated fractions towards the colder temperatures by about 1 °C.

The INP concentrations in the SML are also of the same order of magnitude as those in the bulk seawater, with values between 2×10^3 and 2×10^4 INP/L_{SW}. However, there is a much larger difference in the concentrations of heat stable INP. As illustrated in Fig. III.23b, the heat stable INP concentrations are between 2×10^2 and 10^3 from -12 to -16 °C. Although highly variable due to the

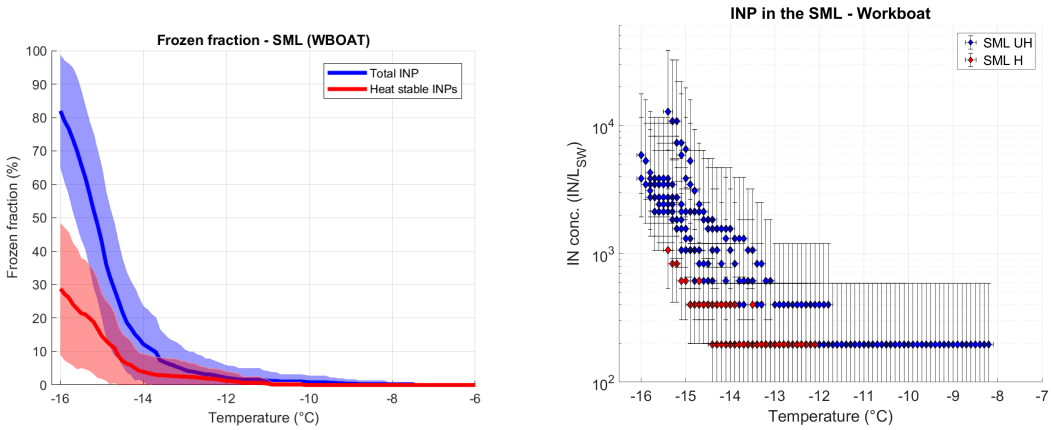

(a) Frozen fractions of INPs in the SML.

(b) Concentrations of INPs in the SML.

Figure III.23 – INP concentrations and frozen fractions in the SML. The unheated INPs are shown in blue and the heat stable INPs are shown in red. The shaded area and error bars correspond to one standard deviation ($\pm 1\sigma$, 68% confidence).

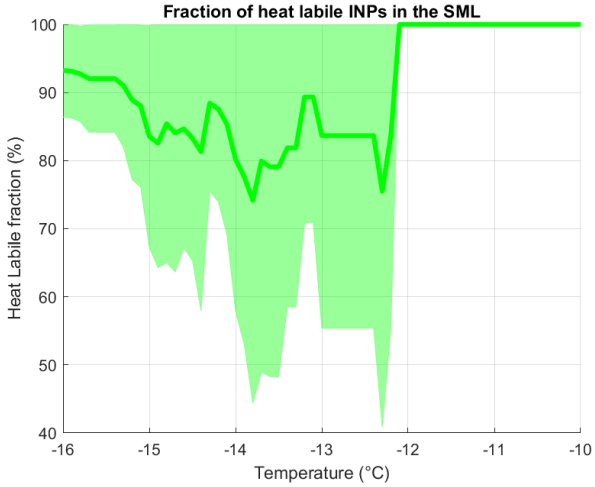

Figure III.24 – Fraction of heat labile INPs in the SML.

smaller number of samples in the SML, the fraction of heat labile INP averages between 75 and 100%, with values of $80.2 \pm 22.3\%$ at -14 °C and $93.2 \pm 6.9\%$ at -16 °C (Figure III.24), showing that INP from the SML contain more heat sensitive material than INP in the SW.

III.3.3.1.c Variability of SW and SML INPs and influence of water types

III.3.3.1.c.i General observations and tendencies

Like in the previous studies, the time series of INPs concentrations were studied at fixed temperatures: in order to have the best possible representation of the data set an following the discussion and T_{10} and T_{50}, the temperatures chosen are -14 °C and -16 °C. The impact of the types of water defined in Section

III.3.1.1 is also studied in this section, with the different water types (FW, SAW, STW and MW) delimited on figure III.25.

At -14 °C for SW INPs (Fig. III.25a), clear peaks are observed on the 24-25/03 with values over 1000 INP/L. These samples correspond to the subtropical waters, which thus seem to exhibit larger INP concentrations. At -16 °C in the SW (Fig. III.25b), the lowest values are observed in the SAW, while the highest values are observed in the FW from 19/03 to 21/03. The STW exhibits medium INP concentrations. The highest Heat Labile INPs ratio is observed in the SAW, while a decrease in this ratio is observed in the STW and in the SW. This hints that the biologically richer waters have more Heat Stable INPs than the poorer subantarctic waters. The contribution of biological and heat liable material is greater in the SAW and Frontal waters than STW.

In general, due to a low number of samples, the variability of SML INPs (both HS and HL) is harder to interpret than that of the SW INPs. Unfortunately, SML samples were not available for comparison in the STW. Highest concentrations are observed for SML samples at -14 °C on the 18/03 and the 26/03 (Fig. III.25c), with values of respectively 800 and 1500 IN/L (compared to about 200 IN/L on the other days), a period during which low concentrations were observed in the SW. The heat labile SML concentrations were also extremely variable at -14 °C, which can be explained by the inherent variability of the INP concentration at warmer temperatures (Fig. III.23).

The variability of T_{10}^{UH} is similar to that of the total INPs at -14 °C, while the variability of T_{10}^{H} is closer to that of the total INPs observed at -16 °C (III.25e and f). Higher variability and values of T_{10}^{UH} are observed in the STW and FW, and higher values of T_{10}^{H} are measured in the FW and SAW. With only 7 points in the SML, the variability is less apparent, however it can be noted that the absolute INP values for the SW and the SML are similar, suggesting that both water layers have a similar behaviour at temperatures >-14 °C.

The variability in the T_{50}^{UH} is similar to that of the variability in INP concentrations, for both data sets. In the SML, T_{50}^{H} could not be calculated, which means none of the samples were above 50% freezing at the end of the analysis. However, for SW samples, about half the samples were below 50% freezing at -16 °C, and the dates where T_{50}^{U} could not be defined in the SW do not systematically correspond to the SML dates. This suggests that INPs in the SML were more heat labile than the SW samples, which is confirmed by the high fraction (80%) of HL INPs at -16 °C for SML.

III.3.3.1.c.ii Differences between the water types

The variability within each water type is high (Figure III.26), but the observable tendency is that both the Frontal and Subtropical waters exhibit the highest concentrations, which is especially visible at -16 °C. The MW and SAW have similar concentrations, with MW being slightly higher. The same tendencies are observed for heat stable INPs, especially at -16 °C with an even greater difference between the FW/STW and SAW/MW (Fig. B.8). These similarities could be explained by the fact that frontal waters are at the frontier between

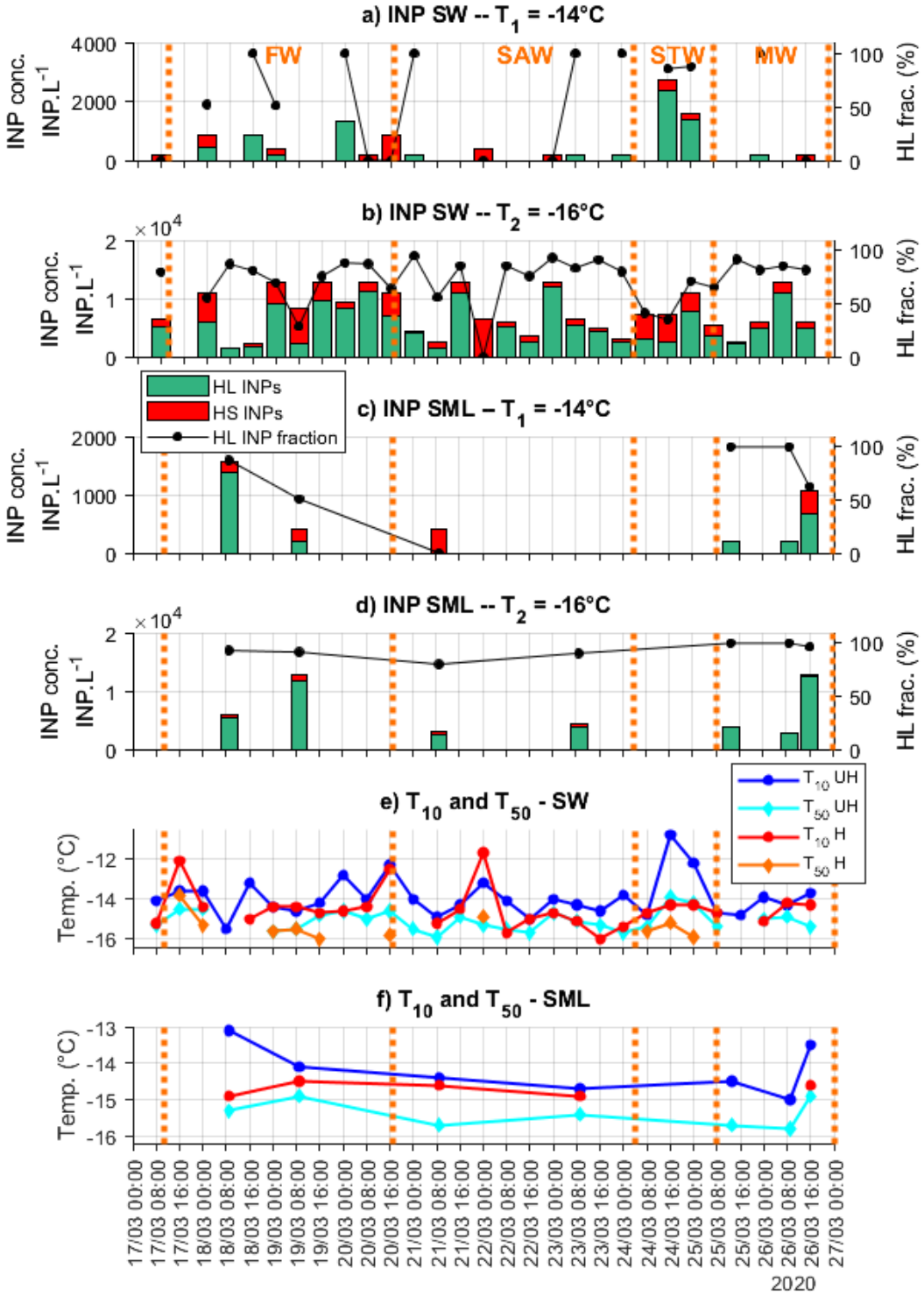

Figure III.25 – Time series of a) INP concentrations in the bulk SW at -14 °C, b) INP concentrations in the SW at -16 °C, c) INP concentrations in the SML at -14 °C, d) INP concentrations in the SML at -16 °C, e) T_{10} for unheated and heated samples in the bulk SW, f) T_{10} for unheated and heated samples in the SML. The Heat Labile INP fraction is indicated as a black line in figures a) to d).

SAW and STW, and it is thus possible that the signature of STW (high in INP and in biomass) is also observed in the FW.

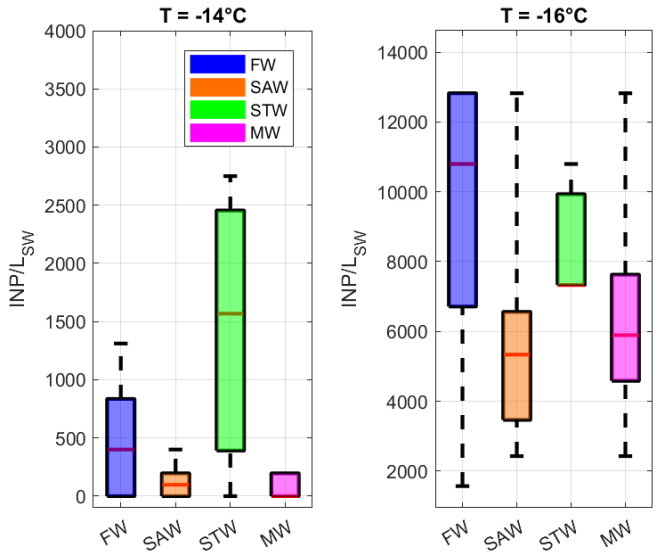

Figure III.26 – Boxplots of INP concentrations for UH INPs in the SW at -14 °C and -16 °C for the different water types. Blue boxes represent the SW, orange boxes the SAW, green boxes the STW and pink boxes the MW. The edges of the boxes represent the 25th and 75th percentile, the red lines represent the median, the whiskers represent the points lower than 3 times the interquartile interval and the red crosses represent the outliers. The number of non-zero points for each water type is respectively 6, 4, 3 and 2 at -14°C; and 9, 10, 3 and 5 at -16°C (respectively for the FW, SAW, STW and MW).

III.3.3.1.c.iii Enrichment and comparison between the SML and the bulk SW

To complete these observations, we present in Figure III.27 a comparison of T_{10} and T_{50} for SW and SML samples. The T_{10} for UH samples is widely spread around the 1:1 line, which is in contrast to what was observed by Wilson et al. (2015) in North Atlantic waters, and Irish et al. (2019b) in Canadian Arctic waters, who observed consistently warmer temperatures for T_{10} in the SML, while Irish et al. (2017) (Canadian Arctic) had similar freezing temperatures between the SW and SML. However, the T_{50} from the SML samples is consistently colder than that of the SW samples. For the heated samples, the points are more closely centered around the 1:1 line, suggesting that HS material has similar INP properties independent of the seawater layer.

All three studies sampled INPs in the Arctic. In addition, the methods for sampling the SML in our study and in Wilson et al. (2015), Irish et al. (2017) or Irish et al. (2019b) also differed. It has been shown by Aller et al. (2017) that different sampling techniques lead to different SML/SW enrichments. In our study, the SML was sampled using a glass plate, a sipper and a permeable tube (Sellegri et al., submitted to BAMS, 2022). Irish et al. (2017) and Irish et al. (2019b) used a glass plate technique, while Wilson et al. (2015) collected the

SML samples using a revolving drum with a hydrophilic Teflon coating attached to a remote-controlled sampling catamaran. We also observe no enrichment for bacteria (Fig. B.6), which is similar to Wilson et al. (2015), where no enrichment was observed for bacteria sampled with the glass plate technique. Thus, the differences between those study and our observations could be explained by differing sampling method and/or differing environments. Also, for a given environment, enrichment in the SML may be varying on a day to day basis, according to biological processes.

To get insight into the variability, the enrichment factor (EF) from the bulk SW to the SML was computed. It is defined as:

$$EF = \frac{n_{INP}^{SW}}{n_{INP}^{SML}}, \tag{III.2}$$

where n_{INP}^{SW} and n_{INP}^{SML} are the INP concentrations in the SW and the SML, respectively. This EF is shown as a function of temperature for each day of the field campaign in Figure III.28 for unheated INPs. We also show the EF for the other data measured in the SML (TOC, Syn, Nano, Pico, Bact) in Fig. B.6.

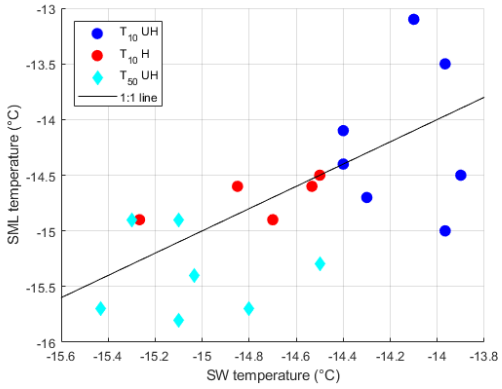

Figure III.27 – Comparison of T_{10} (unheated and heated) and T_{50} for the SW and and SML.

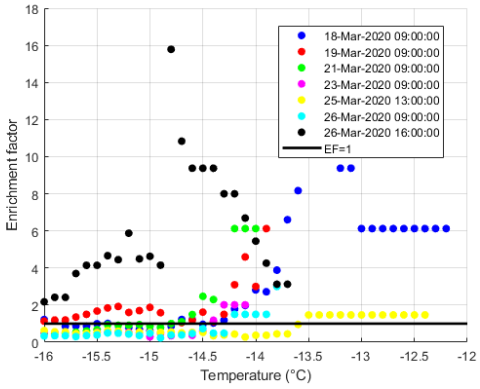

Figure III.28 – Enrichment factor between the SML and the SW at all temperatures for unheated samples.

With the exception of the 25th of March the EF is always greater than 1 at warmer temperatures (i.e INP activity is greater at warmer temperatures in the SW than in the SML). However for colder temperatures, the opposite is true: for 5/7 samples analysed the INP activity in the SML was greater than that in the SW. This observation is also valid for HL INPs (Fig. B.3. These observations show that the SML is on average enriched in INPs (total and heat labile) near the coastlines (corresponding to the 18/03, 19/03 and 26/03) and less enriched further from land. We also observe generally lower TOC and higher Nano in the SML (Fig. B.6), but the variations EFs of those parameters do not correspond to the variations of EF of INPs. Thus, INPs start freezing at the same temperature in the SML and in the bulk SW, but they are present in higher concentrations

and the freezing ramp is steeper in the SML.

It is however difficult to conclude in a quantitative way on the influence of water types on the EF because of the limited amount of data points in the SML. Our observations suggests that the INP in the SML are on average more heat sensitive and contain more biogenic material than the INP in the bulk seawater. No enrichment was observed for heat stable INPs (Fig. B.2), which also suggests that the INPs in the SML were only enriched in biological heat sensitive material, and not in thermally stable material, as was observed by Wilson et al. (2015).

III.3.3.2 INP in the aerosol phase

In this section, we investigate the general IN properties and variability of the SSA during the S2C campaign. These measurements were acquired from the generated SSA using the bubbler, and the data from ambient air sampling. Like in the previous section, we also investigate the variability of the INP concentrations over the campaign and in relation to the different water masses. Aerosol particles were collected onto filters which were later extracted and analysed using LINDA, using the methods described in Section II.2.

III.3.3.2.a SSA generated from the underway system

The INP in the generated SSA are split into submicron and supermicron INPs. The frozen fractions are considerably lower those observed in the SW and SML. At -18 °C, the frozen fractions for unheated samples were on average 29.6 ± 29.4% and 14.8 ± 7.7% for submicron and supermicron INPs; while for heated samples they were 15.4 ± 29.1% and 15.0 ± 9.9% (Fig. III.29). Deriving a T_{50} and T_{90} is thus impossible for most samples.

For unheated and heated submicron INPs, the average T_{10} was −16.0 ± 2.3 °C and −16.5 ± 1.3 °C, respectively. While for supermicron INP they were frozen at slightly colder temperatures of −17.4 ± 0.3 °C and −17.2 ± 0.5 °C, respectively .

The measured n_S for submicron and supermicron INPs are shown in Figure III.30. The equivalent INP per aerosol (IN/aer) are given in Figure B.4. In the submicron phase, the concentrations vary from 10^2 and 10^4 IN/m^2 for temperatures colder than -15 °C, and the heat treatment decreases these values to 10^2 to 10^3 IN/m^2. The supermicron concentrations are lower, with values between 10^2 and 10^3 IN/m^2 for unheated samples, however the heated samples concentrations are on the same order of magnitude.

Between -16 °C and -18 °C, where the majority of the INP activity is measured, the submicron INP exhibit a higher fraction of heat labile material than the supermicron INPs. At -16 °C and -18 °C, the HL INP fraction is 56.1 ± 48.5% and 74.5 ± 40.8%, respectively for the submicron INPs, and it is 60.0 ± 54.8% and 31.6 ± 37.8% in the supermicron phase. This is illustrated in Figure III.32. Thus, supermicron INPs are rarer than submicron INPs, and are on average less heat sensitive than their submicron counterparts. This observation was also true during the TONGA campaign.

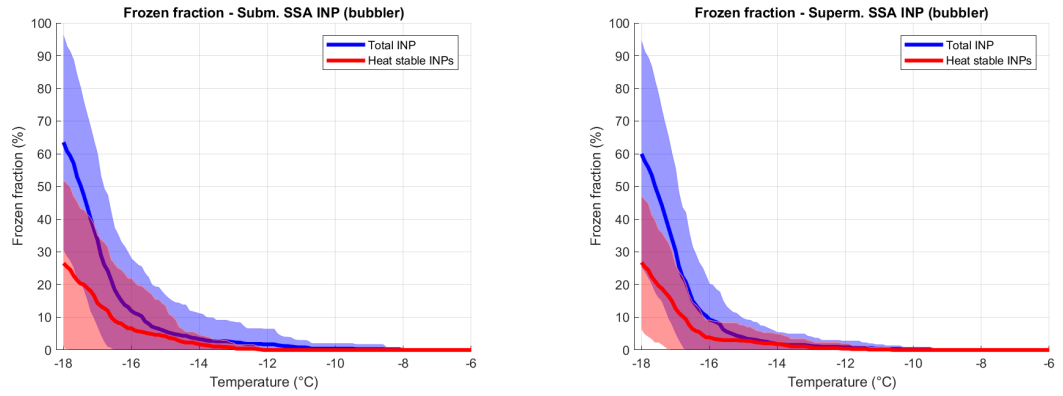

(a) Submicron INP. (b) Supermicron INP.

Figure III.29 – Frozen fractions in the generated SSA (bubbler) for a) the submicron INPs, b) the supermicron INPs. The unheated and heated samples are represented in blue and red respectively. The plain lines corresponds to the average and the shaded area to the standard deviation of the data set.

The total n_S measured in the generated SSA are shown in Fig. III.31, with the fit for pristine marine SSA in the Northern Atlantic proposed by McCluskey et al. (2018c), which is calculated on the assumption that all particles are representative of the marine organic INP type, with following equation:

$$n_S = \exp -0.545(T_K - 273.15) + 1.0125. \quad \text{(III.3)}$$

The values we measure in this study are more than one order of magnitude lower than the fit, and also lower than our observations during the TONGA campaign by a factor 2 to 10 (Fig. III.31, blue line). Given that INP concentration in SSW during TONGA were of the same order of magnitude than the INP concentrations in the SSW during S2C, this result would indicate that the transfer of INP from SSW to SSA is less efficient during S2C than TONGA. This will be discussed further in Section III.3.4.2.

As shown in Fig. III.32, the heat labile INPs represented $57.9 \pm 47.9\%$ and $43.0 \pm 40.2\%$ of the measured INPs at -16 °C and -18 °C. Submicron INPs represented about two thirds of the measured INPs, which is also consistent with our previous observations during the TONGA campaign.

III.3.3.2.b Ambient SSA

Following the same methodology as in the previous sections, the frozen fractions and n_S temperature spectra for the total ambient INPs are presented in Figure III.33. Similarly to the generated SSA, most samples did not reach 100% frozen fraction at -18 °C, and less than 40% of the tubes were frozen on average for heated samples. The average T_{10} and T_{50} were -12.8 ± 2.3 °C and -15.3 ± 1.7 °C for unheated samples; and they were -14.1 ± 0.8 °C and -16.3 ± 1.7 °C for heated samples. Ambient INPs were thus activated at warmer temperature on average than the size segregated INPs in SSA.

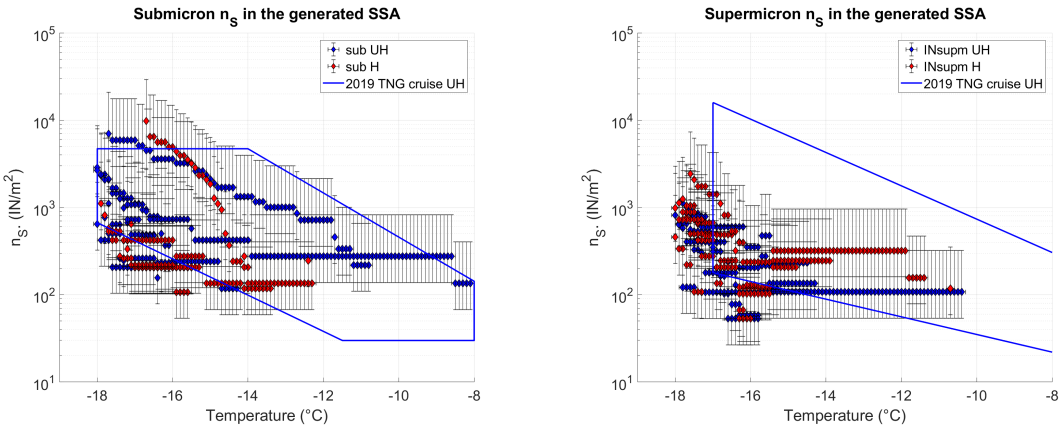

(a) Submicron INPs. (b) Supermicron INPs.

Figure III.30 – n_S temperature spectra for the generated SSA (bubbler): a) Submicron INPs, b) Supermicron INPs. The unheated and heated samples are represented as blue and red respectively. The solid blue line corresponds to the observations in the SSA from TNG cruise (Sec. III.2.4).

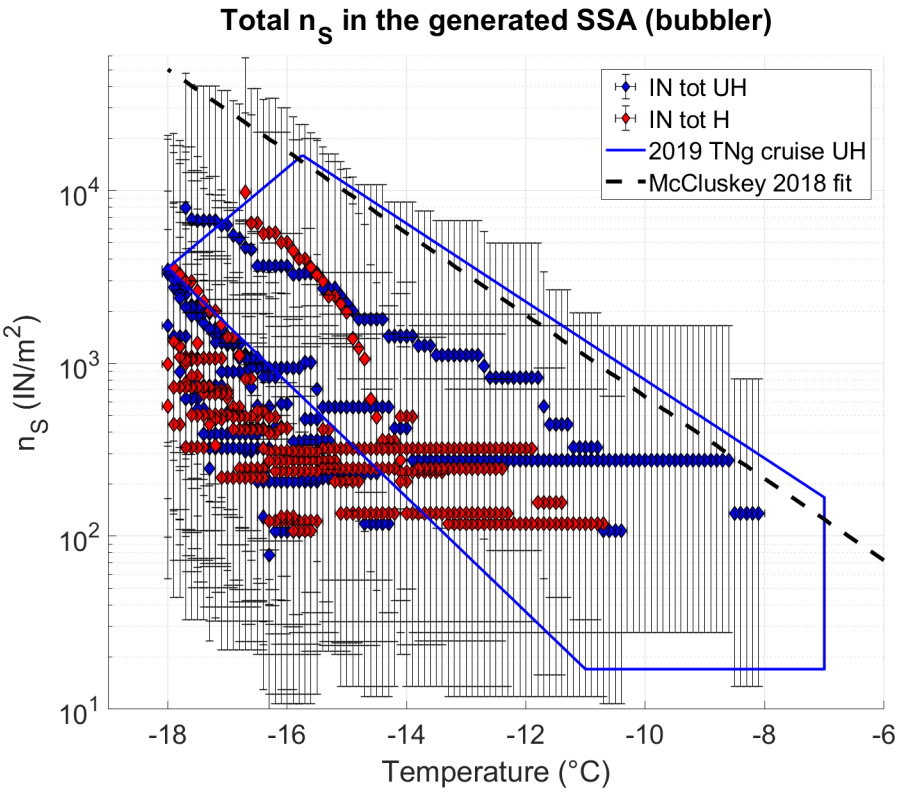

Figure III.31 – Concentrations of total (submicron+supermicron) INPs in the generated SSA from the bubbler. Unheated values are shown as blue markers, heated values are shown as red markers. The solid blue line corresponds to the observations in the SSA from TNG cruise (Sec. III.2.4).

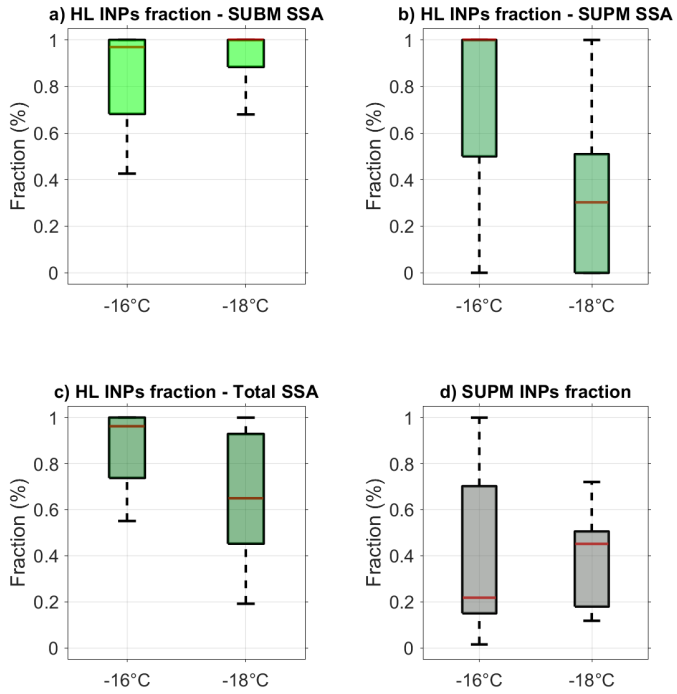

Figure III.32 – Fractions of Heat Labile INPs in the submicron (light green), and supermicron (medium green) and total (dark green) generated SSA; and fraction of supermicron INP in the total SSA at -16 °C and -18 °C.

However, the concentrations of ambient INPs were lower than the concentrations in the generated SSA, with values of n_S comprised between 2×10^1 and 3×10^3 m^{-2} between -14 °C and -18 °C. The reason for this difference could be explained either by the fact that generated SSA are more active than ambient air because primary SSA becomes quickly diluted in ambient air that contains other less INP active aerosols, or that SSA quickly lose their IN properties are they are transported in the atmosphere. No heat stable INPs were measured at temperatures warmer than -13 °C, and heat labile INPs represented between 40 to 65% of the total INPs between -14 and -18 °C (Figure B.11), which is similar to the fractions in the SSA (Fig. III.32). Similar to the SSA, ambient INPs are also consistently lower by an order of magnitude than the McCluskey et al. (2018c) fit.

To summarize, both the generated SSA and the ambient SSA were lower than previous observations in other regions of the globe (e.g. Wilson et al. 2015; DeMott et al. 2016; McCluskey et al. 2018c). This is consistent with the observations by McCluskey et al. (2018a) which were the first observations in the Southern Ocean boundary layer since several decades (Bigg 1973). They were also lower, although in the same order of magnitude, than the SSA INPs observed during the TNG cruise (Sec. III.2.4). Furthermore, the heat labile INPs

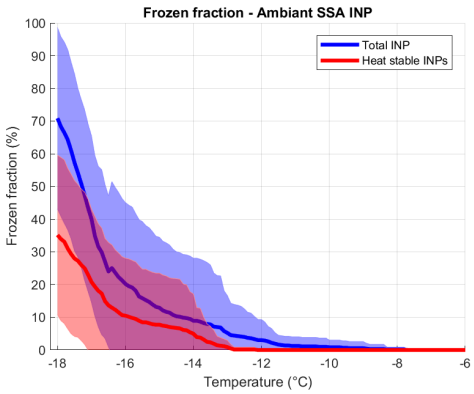

(a) Frozen fractions in the ambient SSA INP. The plain lines corresponds to the average and the shaded area to the standard deviation of the data set.

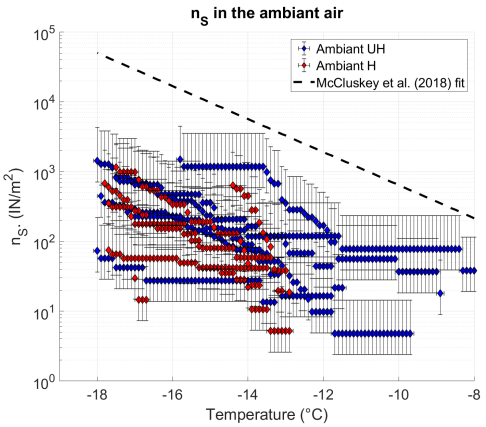

(b) n_S temperature spectra for ambient SSA INP and the line fit from McCluskey et al. 2018c

Figure III.33 – Frozen fractions and n_S temperature spectra for ambient SSA INP: a) Frozen fractions, b) n_S. The unheated and heated samples are represented as blue and red respectively.

represented about half of the observed INPs in all classes (submicron, supermicron, total, ambient), with lower ratios at lower temperatures except for the submicron INPs. This is also consistent with McCluskey et al. (2018a). The HL ratios observed during S2C were also similar, although generally lower than during the TNG cruise, especially in the submicron sizes.

III.3.3.2.c Variability of SSA INPs

III.3.3.2.c.i General observations and tendencies

Following the previous discussion, the variability of the INP concentrations in the SSA were studied at two fixed temperatures, -16 °C and -18°C, corresponding roughly to the average T_{10} and T_{50} of the three data sets. Those results are presented in Figures III.34 (generated SSA INPs) and III.35 (ambient air INPs).

The submicron INPs (Fig. III.34a-b) are marked by a peak in the STW on 24/03 at both temperatures, which coincides to the peak observed for SW INPs (Fig. III.25). The submicron concentrations at both temperatures are mostly composed of HL INPs, with fractions above 90% on most days at -18 °C, except in the FW where it is about 75%. This is illustrated by the cold T_{10} for heated samples, and by the very low activation fraction at -18 °C (only 5 heated submicron samples had a frozen fraction above 10% at the end of the analysis). At -18 °C, only two days (18/03 and 26/03) have fractions of HL INPS lower than 50%. Both these days have HL fraction of about 0%.

The supermicron INPs (Fig. III.34c-d) do not exhibit a peak as high as the submicron INPs, but had comparable values on the non-peak days. The heat labile fraction at -18 °C is lower for supermicron INPs than for submicron INPs: 3 days have HL fractions above 50% (18/03, 24/03 and 25/03), and 5 days have

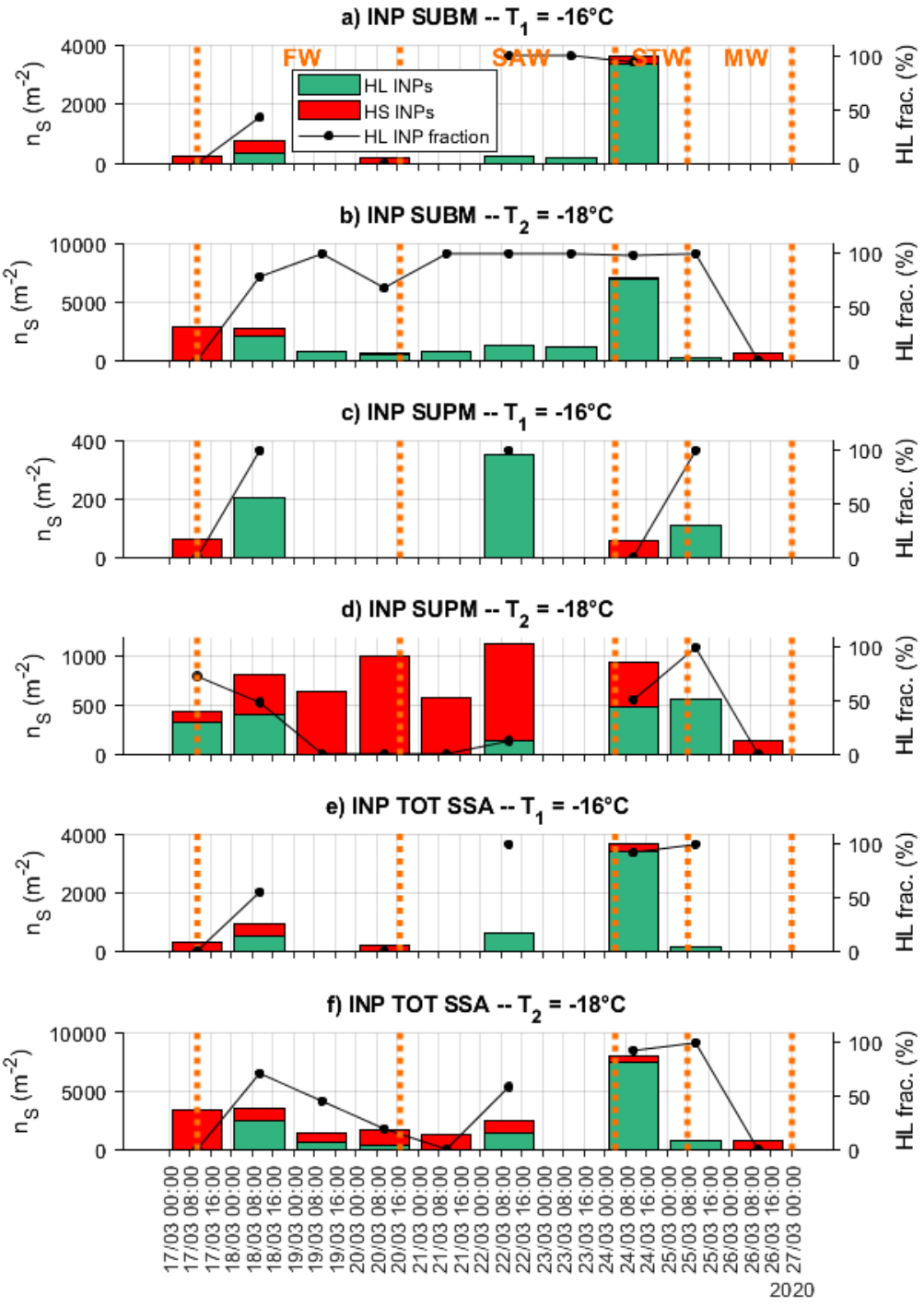

Figure III.34 – Time series of n_S in the generated SSA: a) Submicron INPs at T_1 = −16 °C, b) Submicron INPs at T_1 = −16 °C, c) Supermicron INPs at T_2 = −18 °C, d) Supermicron INPs at T_2 = −18 °C, e) Total SSA INPs at -16 °C f) Total SSA INPs at -18 °C . The Heat Labile INP fraction is indicated as a black line in figures.

HL fractions below 50% (20-23/03, 26/03).

The total INP from the bubbler (Fig. III.34e-f) are dominated by the submicron INPs on the 24/03 at -16 and -18 °C. However, at -18 °C the concentrations are dominated by the Heat Stable INPs, and thus by the supermicron INPs that exhibited lower heat labile fractions. Apart from the peak on the 24/03, the highest values were in the FW, which also corresponds to the regions of elevated biomass.

Thus, at the start of the FW sampling period and again in the STW, we observe high HL fractions for supermicron and total SSA INPs. During the later parts of the FW sampling period and the SAW and MW these fractions are much lower. This is consistent with the increase in biomass in these regions.

Ambient n_S exhibit higher values near the coastline in richer waters (Fig. III.35), on the 25/03 (MW) at -16 °C and on the 18/03 (FW), which is also what was observed in the SW and in the SSA from the bubbler. The HL concentrations were very variable, but generally lower than 50% at both temperatures.

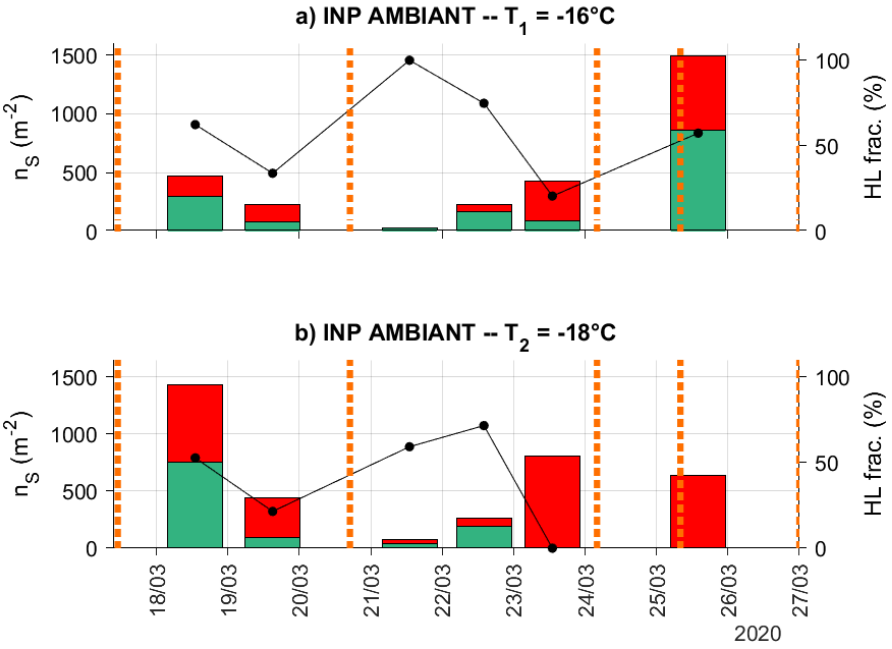

Figure III.35 – Time series of ambient SSA n_S: a) at T_1 = −16 °C, b) at T_1 = −16 °C. The Heat Labile INP fraction is indicated as a black line.

III.3.3.2.c.ii Influence of the water types on the IN activity in the SSA

Boxplots of INP concentrations in the SSA comparing the influence of the types of waters during the cruise are presented in Figure III.36.

The highest concentrations are observed in the STW, both for total (Fig. III.36a) and submicron SSA (Fig. III.36b). This follows the previous observations in the SW and SML of a noticeable peak on the 24/03 and 25/03 (Fig. III.34). Due to the limited amount of data points during this time interval, it is

hard to say whether this peak is a results of a real increase in INP concentrations, or is an outlier.

The unheated supermicron INPs (Fig. III.36c) also exhibit a slightly higher INP concentration in the STW than in the FW and SAW, and the concentration in the MW is the lowest of all water masses. In the submicron and total SSA, the INP concentrations in the MW are also lower than in the FW and SAW, and the difference is larger than in the supermicron INP. Furthermore, supermicron INP exhibit far less variable INP concentrations in the FW and SAW than the submicron and total SSA. These observations are somewhat different from those in the SW, where the water types could be split into two pairs (FW/STW and SAW/MW). HS SSA INPs also have a different behaviour than UH SSA INPs(Fig. B.10, where the concentrations are higher and more variable in the FW/MW, and lower in the SAW/STW.

The generated SSA INPs were mostly smaller than 1 µm and heat stable at temperatures less than -16 °C. According to the classification proposed by McCluskey et al. (2018b), this means the SSA INPs during S2C are probably related to the presence of the DOC INP type, which is characterized by sizes smaller than 0.2 µm and a resistance to heating. McCluskey et al. (2018b) assumes that such INPs may be important contributors in case of phytoplankton blooms, which is consistent with our observations, with blooms appearing notably in the FW. It is important to note that we do not have access to sizes other than > or < 1 µm for INPs, so we can not assess the contribution of INPs smaller than 0.2 µm in the SW.
To answer the question of whether the INPs during S2C were more of the DOC or POC type (McCluskey et al. 2018b), we investigate the correlations with the biogeochemical composition of the seawater.

III.3.4 Characterization and origin of INPs during the campaign

The objective of this section is to characterize the potential links between the INP variability observed in the SW and the SSA, and the biogeochemical composition of the seawater. We will first discuss the correlations between the biogeochemical parameters of the seawater and the different INP data sets (SW, SSA), and the impact of the type of watermass on those correlations. Then, we will investigate whether there is a significant link between the generated SSA INP and the SW/SML INPs.

III.3.4.1 Correlations between seawater INPs and the biogeochemical parameters

III.3.4.1.a Over the whole campaign

The correlations between the seawater INPs concentrations and the biogeochemical parameters were computed in the same manner as in the previous

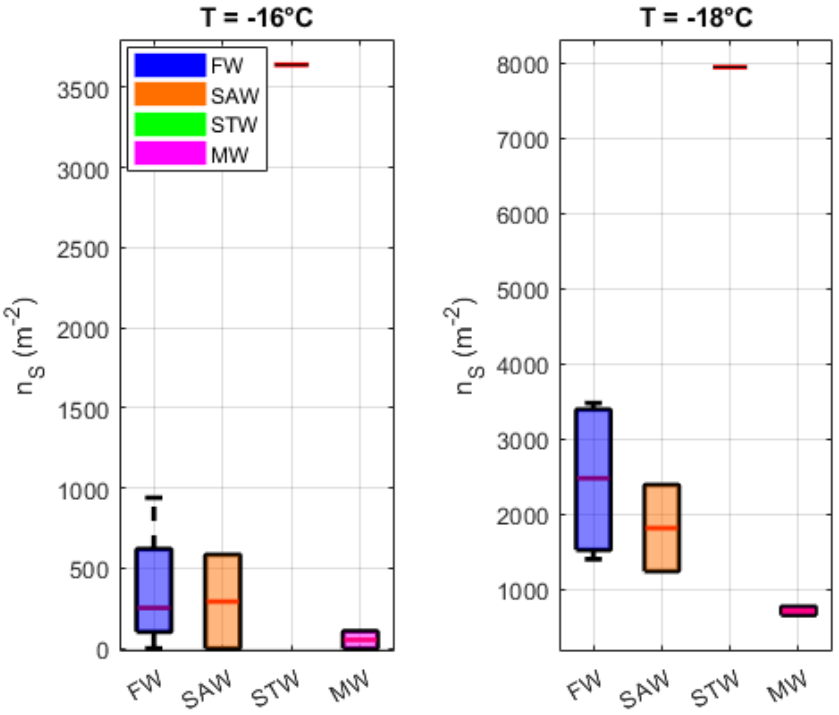

(a) Total SSA.

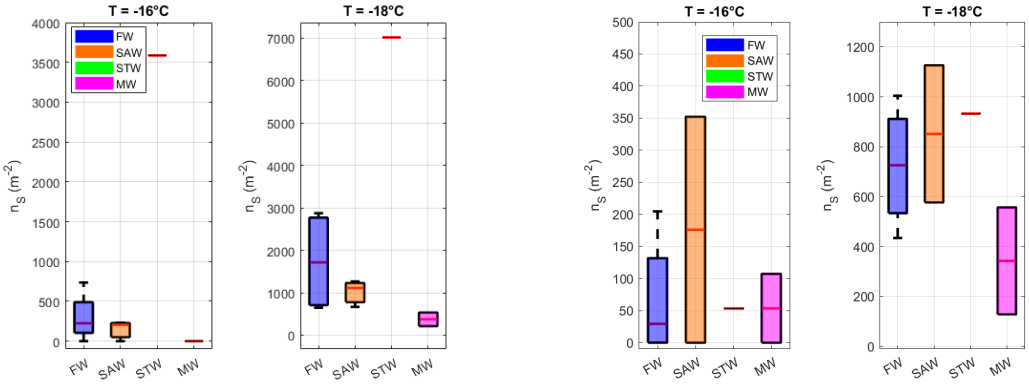

(b) Submicron SSA.

(c) Supermicron SSA.

Figure III.36 – Boxplots of INP concentrations for UH INPs in the SSA for a) Total SSA, b) Submicron SSA, and c) Supermicron at -16 °C and -18 °C for the different watertypes. Blue boxes represent the SW, orange boxes the SAW, green boxes the STW and pink boxes the MW. The edges of the boses represent the 25th and 75th percentile, the red lines represent the median, the whiskers represent the points lower than 3 times the interquartile interval and the red crosses represent the outliers.

section, using the total INPs, heat labile INPs and heat stable INPs at $T_1 = -14$ °C and $T_2 = -16$ °C. The correlations with the unheated and heated T_{10} were also calculated.

The results are presented in table III.6, where only the significant correlations, corresponding to $p < 0.05$, are shown. The carbohydrates (CHO) and amino acids (AA) data were grouped into *dissolved* (DCHO and DAA) and *particulate* (TCHO and TAA) for the sake of brevity. The correlation tables for the detailed CHO and AA are provided in Appendix B.2.4.

Table III.6 – Correlations between INP in the SW at -14 and -16 °C, for total INP, heat stable INP and heat labile INP, and the biogeochemical data measured in the SW during the cruise. Only the significant ($p < 0.05$) correlations are shown.

		S	T_{SW}	Chl-a	Syn	Nano	Pico	Bact	DiFl	DiA	Fl	TOC	TN	DAA	PAA	DCHO	PCHO
INT1	R(P)	0.63(0.01)	0.63(0.02)	—	—	—	—	—	—	—	—	—	—	—	—	—	—
INT1 HL	R(P)	0.70(0.03)	0.73(0.02)	—	—	—	—	—	—	—	—	—	—	—	—	—	—
INT1 HS	R(P)	—	—	—	—	—	—	—	0.82(0.05)	—	—	—	—	0.70(0.03)	—	—	—
INT2	R(P)	—	—	—	—	—	—	—	—	—	—	0.52(0.02)	—	—	—	0.43(0.05)	0.48(0.03)
INT2 HL	R(P)	—	—	—	—	—	—	—	—	—	—	0.46(0.03)	—	—	—	—	0.49(0.03)
INT2 HS	R(P)	—	—	0.42(0.04)	—	—	-0.46(0.03)	—	0.45(0.04)	—	—	—		—	—	—	—
T10	R(P)	—	0.43(0.03)	—	—	—	-0.42(0.05)	—	—	—	—	—	—	—	—	—	—
T10 HS	R(P)	—	—	—	—	—	—	—	—	—	—	0.44(0.005)	—	—	—	—	—

Both the salinity and T_{SW} exhibit a positive correlation with the total and Heat Labile INP concentrations at -14 °C of about $R \approx 0.7$. T_{SW} also correlates with T_{10}. This suggests that in warmer and saltier waters, the INP activity increases with warmer temperatures. This is in line with the previous observations in Section III.3.3.1.c, where higher INP concentrations were observed in the Frontal and Subtropical seawater regions. The positive relationship with salinity is opposite to what was observed during the TONGA campaign, and to observations in previous studies (Irish et al. 2017, Irish et al. 2019b), where a negative relationship between the INP concentration or T_{10} and the salinity was measured. This would confirm that relationships to salinity and temperature are only coincidental and valid only for very specific environments.

The picoplanktons (Pico) exhibit a significant, negative correlation ($R \approx -0.4$) with the heat stable INP concentrations at -16 °C and with T_{10}. A similar result was observed during the PEACETIME campaign in the Mediterranean Sea (Trueblood et al. 2021). Conversely to the TONGA campaign, we do not observe any significant correlation between the INP data and the bacterial abundance. DiFl correlates positively with Heat Stable INPs at both temperatures, although the correlation is best at -14 °C ($R = 0.82$). To summarise, the smaller planktons (Pico) are more negatively correlated to the heat stable INPs, while the bigger planktons (DiFl) are positively correlated to total and heat labile INPs.

TOC correlates with the total and HL INPs at -16 °C and with T_{10}^{HS} ($R \approx 0.5$), which is a similar observation than in the previous section. This is also consistent with other studies (Wilson et al. 2015, Trueblood et al. 2021) that highlighted a strong link between TOC and INP concentrations, thus we confirm the role of TOC as a potential marker of IN activity.

Dissolved Amino Acids are positively correlated to the heat stable INPs at -14 °C ($R = 0.70$), and dissolved and particulate carbohydrates are positively correlated to the total and heat labile INPs at -16 °C ($R \approx 0.5$). Carbohydrates and amino acids are organic macromolecules, and they are one of the major components of the organic carbon present in the ocean (Pakulski et al. 1994). They are part of the nutrition cycle of living organisms and can be present as exudates from microorganisms in the ocean, and can be found in sea spray aerosols (Ogunro et al. 2015, Wolf et al. 2019). Previous studies have reported that such macromolecules were ice active (Pummer et al. 2015; McCluskey et al. 2017). The detailed correlations with the different CHO are presented in tables B.5 and B.6.

III.3.4.1.b Segregating by water types

As previously noted in III.3.3.1.c, we observe distinct properties of the INPs, depending on the types of water during the cruise. These groups are FW+STW INPs and SAW+MW INPs. In order to have a better understanding of the INPs during the cruise and a better comparison with the oligotrophic seawaters characterized in previous studies, we studied the correlations between the INPs in each of these groups with the seawater biochemistry. The correlations in the FW+STW are presented in Table III.7. No correlations were found in the SAW+MW. Some of it is explained by the fact that the INP concentrations were lower in these regions, especially at -14 °C where a large part of the samples had just started to freeze. The behaviour observed in the FW+STW is partly similar to the one of the general INP population. The same, but stronger, correlations are observed with the seawater salinity and temperature ($R \approx 0.8$) at -14 °C. *Syn* and Pico are negatively correlated with the INP concentrations at -16 °C (total, HL and HS), with $0.6 < R < 0.8$. However, we observed different relationships to other tracers than those observed for all water types together.

Table III.7 – Correlations in the FW + STW for SW INPs.

		Salinity	T_{SW}	Chl-a	Syn	Nano	Pico	Bacteria	TOC	TN	DAA	PAA	DCHO	PCHO
INT1	R(P)	0.79(0.02)	0.85(0.01)	—	—	—	—	-0.78(0.04)	-0.81(0.01)	—	—	—	—	—
INT1 HL	R(P)	—	—	—	—	—	—	—	—	—	-0.82(0.05)	—	—	—
INT1 HS	R(P)	—	—	—	—	—	—	—	—	—	—	—	—	—
INT2	R(P)	—	—	—	-0.81(<0.005)	—	-0.82(<0.005)	—	—	—	—	—	—	—
INT2 HL	R(P)	—	—	—	+0.64(0.03)	—	-0.60(0.05)	—	—	—	—	—	—	—
INT2 HS	R(P)	—	—	—	—	—	-0.64(0.03)	—	—	—	—	-0.79(0.01)	—	—
T10	R(P)	—	0.63(0.03)	—	—	—	—	—	—	—	—	—	—	—
T10 HS	R(P)	—	—	—	—	—	—	—	—	—	—	—	—	—

The PAA are also negatively correlated with the HS INPs at -16 °C ($R \approx 0.8$). Bacteria, TOC and DAA are negatively correlated ($R \approx -0.8$) with the total and HL INPs at -14 °C. The correlation observed previously between the dinoflagellates and the HS INPs is also not present in either seawater masses. Thus, in the richer and warmer waters of the subtropical region, there seem to be a negative effect of some microorganisms in the FW on the INP activity.

TOC is higher in the FW than in the SAW/MW, which leads to higher concentrations of INP in the FW compared to the SAW and explains the positive

correlation between TOC and INP when merging all water types together. However, within these higher concentrations of INP in FW, there is an additional variability resulting in a negative correlation between TOC and INP, likely due to the presence of some bacteria and/or picophytoplancton that have an inhibiting INP effect on the IN activity. This indicates that there are at least two types of INP, and that microorganisms act differently on these INP populations, via its impact on the quality of the organic carbon.

Fewer INP measurements are available at the warmer temperatures in the SAW+MW, making it impossible to derive the correlations for HS INPs at -14 °C. We report very strong negative correlations between the the total INPs at -14 °C, the HS INPs at -16 °C and T_{10}^{HS} with TOC ($R \approx 0.9$). TN was also negatively correlated with HS INPs at -16 °C, with $R = 0.72$. It has been observed in the subantarctic region that there were less ice clouds, suggesting that a local phenomena was inhibiting the INP activity: Kanitz et al. (2011) and Vergara-Temprado et al. (2018) hypothesize that supercooled clouds in the Southern Ocean are starved for INPs due to local effects. It was hypothesized on the basis of limited observations, mainly from satellites, that global climate models (GCMs) might be glaciating what are in reality persistent supercooled liquid clouds. Indeed, GCMs simulations in which convective parameterizations have been forced to produce greater amounts of supercooled liquid water have reduced short wavelength radiative biases (Kay et al. 2016). The negative link between TOC and INPs we observe here may be consistent with the hypothesis that local effects inhibit ice nucleation and the formation of ice clouds.

Thus, the INPs in the SW type in this study follow two distinct behaviours depending on the region and the seawater type. In the next section, we will analyse the link between SW/SML INPs and SSA INPs. However, we will not analyse the correlations between SSA INPs and the biogeochemical parameters of the seawater directly, as these comprise successive transfer functions (from SW to SML, and then from SML to SSA), and little statistics given the limited amount of data points in the SSA.

III.3.4.2 Discussion: Link between seawater INPs and SSA INPs

The goal of this section is to investigate if the SSA INP have any relationship with (either or both) the INPs in the bulk SW and the INPs in the SML.

We present in Table III.8 the correlations between the SSA INPs (total, submicron and supermicron) versus the other INP data sets (SW, SML, ambient) at the fixed temperatures defined previously. The SML INPs exhibit consistently good correlations at both temperatures, with R in the range of 0.9 to 1.0, with almost all the SSA INPs data sets. Only the supermicron and total SSA INPs at -16 °C do not correlate with the SML INPs at -14 °C. The SW INPs correlate significantly less ($|R| \approx 0.7$) with submicron and supermicron SSA INPs at -16 °C, and total SSA INPs at -18 °C. The ambient INPs do not show any significant link with the generated SSA dataset.

These differences are also visible in Figure III.37, where we show the scatter

Table III.8 – Correlations between INPs in the generated SSA (SUBM, SUPM and TOT) and INPs in the SML, SW and ambient air (AMB). Only the significant ($p < 0.05$) correlation coefficients are shown. The strongest correlations ($p < 0.005$) are indicated in bold. Only the data with more than 5 available points were computed.

		SML T1	SML T2	SW T1	SW T2	AMB T1	AMB T2
SUBM T1	R(P)	0,88(0.05)	**0,98(<0.005)**	—	—	—	—
SUBM T2	R(P)	0,92(0.03)	**1,00(<0.005)**	—	0,66(0.04)	—	—
SUPM T1	R(P)	—	0,89(0.04)	-0,69(0.04)	—	—	—
SUPM T2	R(P)	0,90(0.04)	0,88(0.005)	—	—	—	—
TOT T1	R(P)	—	0,97(0.01)	—	—	—	—
TOT T2	R(P)	0,94(0.02)	**1,00(<0.005)**	—	0,68(0.03)	—	—

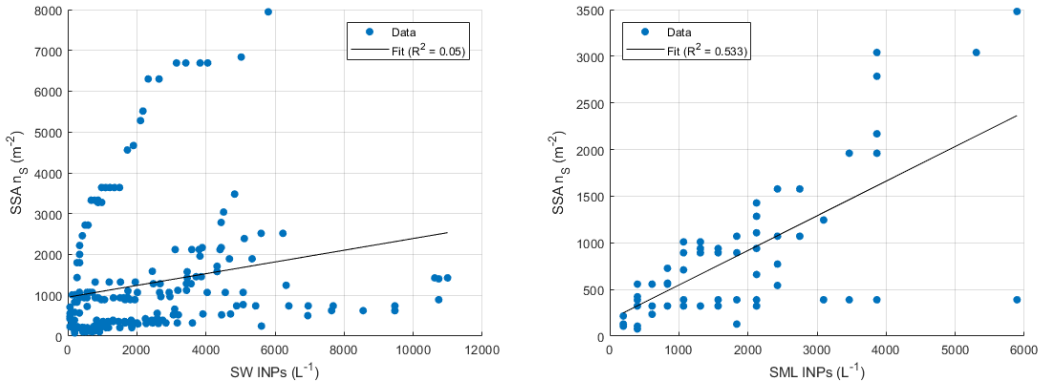

(a) Total SSA INPs vs bulk SW INPs. (b) Total SSA INPs vs SML INPs.

Figure III.37 – Scatter plot of total SSA INPs vs bulk SW INPs (a) and SML INPs (b). A linear regression fit line is also shown on both figures with the R^2 coefficient.

plots over all temperatures of total SSA INPs versus the SW and SML INPs with a linear regression fit over the dataset. We observe a much better agreement between the SSA and SML INPs, confirming our previous observations that SSA INPs are more linked to SML INPs, and the hypothesis that the SSA INPs are more related to the SML than to the bulk SW, even though caution must be taken given the low number of samples in the SML.

To our knowledge, only one study has investigated the IN activity of artificially generated SSA in comparison to SW INP (Trueblood et al. 2021), making our observations difficult to evaluate. Trueblood et al. (2021) observed two classes of INPs, one at -18 °C and one at -22 °C that were correlated to different parameters in the SML. It was however not specified in their study whether direct correlations existed between the INP_{SSA} and the INP_{SW} or the INP_{SML} data sets, apart from the remark that INP_{SSA} at -18 °C were correlated to INP_{SW} at -16 °C, which is similar to what we observe here (see Table III.8). However, the concern with their observations was that further validation was required

considering the small sample size ($N = 4$).

We also have $N = 4$ in our case, which does not yield satisfactory validation. Even though Trueblood et al. (2021) did not specify whether INP_{SSA} and INP_{SML} were correlated, they showed that INP_{SSA} at -15 °C were correlated to several parameters from the SML like organics, phytoplankton and bacteria counts. We were able to investigate the correlation between the INP_{SSA} in our study with the parameter measured in the SML (nitrogen, TOC, bacteria, Syn, Nano and Pico abundances). With a maximum sample size of $N = 4$ the only significant correlations are those of INP_{SSA} at -18 °C with dissolved Nitrogen ($R = 0.93$), and with nanoplanktons ($R = 0.96$). We also note that a correlation of $R = 0.93$, although insignificant with $p = 0.07$, exists between INP_{SSA} and bacterial abundance in the SML. Our observations are close to what Trueblood et al. (2021) observed, although both studies only have a sample size of $N = 4$ and thus require more validation. It is however surprising that the SSA INP do not shown any link with TOC_{SML}, as several other studies have noted a statistically significant link between organic matter in the SML and INP concentrations in the SSA. However, this may be explained by the lack of data in both INP and SML parameters.

Nonetheless, we can still conclude that the generated SSA INPs are mostly submicron in size, and that they are more related to SML INPs than to bulk SW INPs. We have a sufficient number of samples only in the SW to study the relationships with biogeochemical parameters. Based on the observation that INP_{SML} are correlated to INP_{SW}, and INP_{SSA} is strongly correlated to INP_{SSA}, we propose to (1) predict INP in the SW based on a predictor from the SW, (2) calculate a relationship between INP_{SML} and INP_{SW}, and (3) express the n_S as a function of INPs in the SML. These calculations will be treated in the next section on parameterizations.

III.3.5 Conclusions of the S2C campaign

The Sea2Cloud cruise took place on board of the research vessel *Tangaroa* in the Southern Ocean leaving from Wellington, New Zealand on 15th March and returned on 27th March 2020. The general objectives of this cruise were to link the ocean and atmosphere processes in order to reduce the uncertainties in our understanding of the climatic system in the Southern hemisphere. In particular, the objectives within this thesis were to measure and characterize the IN properties of the seawater (SW), of the surface microlayer (SML) and of the sea spray aerosols (SSA), and to understand the link between the ocean and atmospheric ice nucleation processes in various seawater types.

Most of the sampling took place in the underway system of the ship, where bulk seawater was run continuously, allowing for SW INP samples to be collected three times per day. In addition, artificial sea spray aerosols were generated using a bubbling system. These generated SSA INPs were collected once a day on size segregated filters, allowing for the characterisation of submicron and supermicron INPs. Several other biogeochemichal parameters were also

measured in the SW and generated SSA, including, but not limited to, organic carbon, planktons and bacterial abundances. SML samples were also taken from a pneumatic workboat 1 km away from the ship. Although less frequent ($N = 7$) than the bulk SW samples, they were also analysed for IN activity and for biological and chemical characterization. In addition to the above samples, ambient air was collected on total particle filters for INP analysis.

All INP analysis was performed using the offline immersion freezing instrument LINDA. In order to discriminate between heat labile and heat stable INPs, the samples were subjected to a heating treatment.

The cruise was divided in four different areas corresponding to four types of oceanic waters, defined by their salinity. In general, the frontal (FW) and subtropical (STW) waters were characterized with higher biomass and plankton blooms, while the subantarctic (SAW) and mixed (MW) waters were poorer. However, smaller phytoplanktons exhibited lower values in the FW and STW.

Starting with the bulk SW INP samples, the majority of samples started freezing around -13 to -14 °C, both for untreated and heated samples, suggesting that the heat labile material did not influence the onset freezing temperatures. However, at the end of the analysis at -18 °C, the heated samples exhibited freezing fractions 30% lower than the unheated samples. The measured INP concentrations were lower than values observed in the Atlantic and Artic (Wilson et al. 2015; Irish et al. 2017; Irish et al. 2019b), and the heat treatment resulted in a notable decrease, showing that heat labile material represented more than 65% of the total INPs.

The bulk SW INPs exhibited higher concentrations in the FW and STW, which are regions of generally higher biomass. In particular, peaks were observed on both sampling days in the STW, suggesting an effect of elevated biomass and plankton blooms on the IN activity of the SW. On the other hand, higher ratios of heat stable INPs ratios were observed in the poorer SAW.

Moving up to the SML, similar observations in terms of freezing temperatures and concentrations are made. However, the contribution of heat labile INPs ratios was greater, with values ranging between 80 and 100%. This difference is especially visible at the colder temperatures. This confirms that the SML is enriched in biological material compared to the SW. INP in the SML showed similar temporal correlations to those in the SW, but were enriched by a factor of 2.

However, after heat treatment we observe that this enrichment was a result of biological material as the heat stable INPs did not show any enrichment. This observation is consistent with other studies that noted an enrichment in biological INPs in other regions.

We derived the correlations between the bulk SW INP dataset at -14 °C and -16 °C with the parameters measured in the SW. We observe generally positive correlations between the total INPs and heat labile INPs with the organic matter (TOC, carbohydrates). The picoplanktons were however negatively correlated

with the heat stable INPs and the freezing temperature, while the dinoflagellates were positively correlated with the heat stable INPs. Separating the INPs between those sampled in the FW/STW and those sampled in the SAW/MW showed different behaviours, and no correlations were found for the INPs in the SAW/MW. In the FW/STW, we observe stronger negative correlations between the picoplanktons and the INPs at -16 °C, which is consistent with Trueblood et al. (2021). *Synechococcus* is also negatively correlated with total INPs at -16 °C, but is positively correlated with the heat labile INPs. Contrary to correlations on the full cruise period, we do not observe positive correlations between TOC and the INP concentrations when reducing the data set to the FW/STW water types, instead the organic matter was negatively correlated to the INP concentrations in these regions, which highlights that marine INPs have varying properties depending on the type of water (amount of biomass, organic matter...). The anti-correlation to TOC is in line with recent observations that ice clouds were rarer in regions of increased TOC in the Southern Ocean, suggesting an inhibiting effect in these regions.

The INPs in the generated SSA were active at temperatures between -12 and -18 °C. Heating the samples did not shift the onset freezing temperatures, but resulted in a decrease in measured concentrations and in a decrease in the activation fraction at the lower temperatures (-16 to -18 °C). Submicron INPs froze on average at 1 °C warmer temperatures than supermicron INPs, and they constituted about two thirds of the total SSA INPs. The heat labile fractions were comparable at -16 °C for both size ranges, but at -18 °C submicron INPs were dominated by heat labile material, which was not the case for supermicron INPs. The total SSA concentrations were lower than what was measured in other studies and than of a general parameterization for pristine marine SSA (McCluskey et al. 2018c).

Ambient INPs concentrations (normalized to the total aerosol surface) were in general even lower than those in the artificial SSA. Recent observations in the Southern Ocean by McCluskey et al. (2018a) also showed lower atmospheric INP concentrations in this region than in the other marine regions of the globe. No relationship between ambient INP and SSA INP indicate that either the mixing of aerosols from different sources or transport and aging in the atmosphere have en effect on the IN properties of sea spray aerosols.

Submicron SSA INPs exhibited peak values in the STW and also had higher concentrations in the FW, which resembles the trends for SW INPs. Supermicron INPs did not follow those trends, as the highest concentrations were observed more in the SAW and FW. According to McCluskey et al. (2018b), we surmise that the majority of SSA INPs during the campaign were of the DOC type rather than the POC type, that is, smaller than 1 µm and resistant to heating.

The fraction of INP concentration in SSA (n_S) was correlated with INP in the SML ($R \approx 0.9$), and slightly less to INP in the SW ($R \approx 0.6$). Therefore it is possible to predict the n_S fraction in sea spray as a function of INP in the SML

based on a relationship linking both measures.

III.4 Development of parameterizations for INPs in the Southern Ocean

As previously discussed, there is a need for finding predictors and working parameterizations and models for estimating INPs in marine regions. Previous studies have attempted to use diverse kinds of parameters linked to carbon, such as TOC (Wilson et al. 2015) or POC (Trueblood et al. 2021). Other studies have hypothesised that the ratio of INPs to NaCl was conserved from the seawater to the SSA (Irish et al. 2019a; Gong et al. 2020) but those still need a good prediction of the INP variability in the seawater.

The goal of this section is to use the observations from the TONGA and S2C campaign to derive empirical parameterizations in order to predict the INP concentrations in the different mediums (SW and SSA).

We first show three parameterizations for INPs in the SW during the TONGA campaign utilizing the three best predictors we observed for this campaign: TOC, bacterial abundance and bacteriocholorophyll-a concentrations. Then, we do the same for INP in the the S2C SW, which are significantly different from the oligotrophic seawaters analyzed during TONGA (and also influenced by the presence of hydrothermal sources) and derive a parameterization for SSA INP using the S2C data and linking the SW, SML and SSA INPs.

III.4.1 Predicting seawater INPs during the TONGA cruise

Section III.2.3.3 allowed us to determine that POC, bacteria concentrations (C_{Bact}) and bacteriocholorophyll-a concentrations ($C_{\mathrm{BactChloro}}$) were the best candidates as parameters for deriving a parameterization for INP in the seawater, as they exhibit the strongest correlations across the whole temperature spectrum.

The best fit at each temperature was determined for each parameter P_i. We tested fits of exponential, linear and power law form. For all three parameters P_i, the best fit at a fixed temperature was of the form $IN_{\mathrm{SW,pred}} = \alpha P + \beta$, with α and β the fit coefficients.

We then determined the best fit at all temperatures for each $\log(IN/P_i)$ (Fig. III.38a,c and e), in the form:

$$\log(IN/P_i) = a_i \cdot T + b_i, \tag{III.4}$$

where P_i are either POC, C_{Bact} and $C_{\mathrm{BactChloro}}$, and a_i and b_i are the corresponding fit coefficients. The coefficients found for each parameter were then used as starting points in a Montecarlo simulation, with instructions of minimizing the number of points predicted by the model within a factor of 5 of the observed data. This allowed us to determine the final values of the set of coefficients for each of the three parameters considered. The results are shown in figures III.38b (bact), III.38d (bactchloro) and III.38f (POC), where the INP concentrations predicted by the model are plotted against the measured values. The final

equation for each parameterization is:

$$IN_{SW} = C_{\text{Bact}} \cdot \exp\big(-0.5725 \cdot T - 14.5750\big), \tag{III.5a}$$

$$IN_{SW} = C_{\text{BactChloro}} \cdot \exp\big(-0.5659 \cdot T + 5.8445\big), \tag{III.5b}$$

$$IN_{SW} = \text{POC} \cdot \exp\big(-0.6015 \cdot T + 5.3098\big). \tag{III.5c}$$

Table III.9 – Fit statistics for predicting SW INP during the TNG cruise. RG_f are the ratio of points predicted within a factor f of the observations, N is the number of points used.

Parameter	RG_2 (%)	RG_5 (%)	RG_{10} (%)	R^2	N
Bact.	71.9	98.4	100	0.711	373
BactChloro	69.9	97.4	99.4	0.658	153
POC	82.3	95.0	100	0.728	141

The statistics for each parameterization are given in Table III.9. We indicate the ratios of points predicted within a factor 2 (RG2), factor 5 (RG5) and factor 10 (RG10) of the measured values, the R^2 and the number of data points used N. Each of the three models considered seem to perform similarly at factors of 5 and 10 of the observed values, with RG5 and RG10 above 95%. However, their performances vary more within a factor 2, with Bact and BactChloro near 70% of well predicted points, and POC at 82.3%. Each model has a tendency to slightly overpredict warm INPs (T>-12 °C), while underpredicting cold INP (T<-16 °C). In general, points at warmer temperatures were also predicted predicted with less accuracy, with a bigger spread overall than at the medium and cold temperatures. This is explained by the fact that the variability in INP concentrations is a lot higher at warmer temperatures than at the lower temperatures.

We compare those results to the prediction of Wilson et al. (2015) (W15) model where INPs are predicted as a function of TOC and temperature:

$$IN = \text{TOC} \cdot \exp\left(-0.4459 \cdot T + 11.2189\right), \tag{III.6}$$

This model overpredicts consistently the INP concentrations in our study. However, one caveat of this comparison is that this model was developed for predicting INP concentrations in the Arctic SML, and used the TOC concentration in the SML, while here we are aiming to predict the INPs in the bulk SW. It is thus expected that this model overpredicts the INPs from our study, if the SML is enriched in INP but not in TOC in the SML compared to the bulk SW. The differences could also be explained by differing marine environments, and by the temperature ranges (-5 to -30 °C in Wilson et al. (2015), -5 to -16 °C in our study).

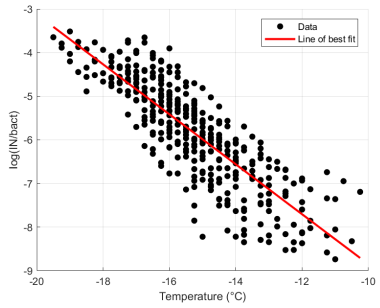

(a) $\log(IN_{SW}/C_{\text{Bact}})$ as a function of temperature and line of best fit ($y = ax + b$).

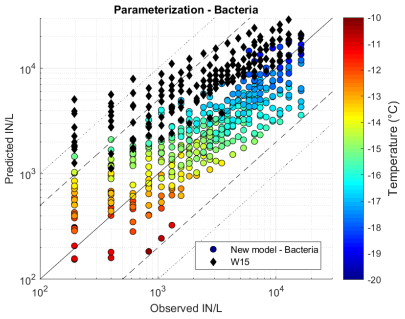

(b) Comparison of predicted values and observed values of IN_{SW} using C_{Bact} as a predictor (Eq. III.5a).

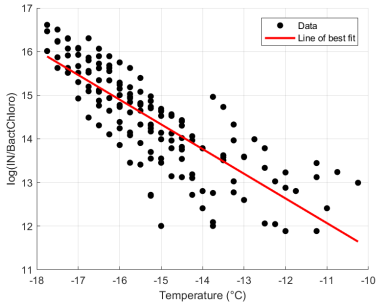

(c) $\log(IN_{SW}/C_{\text{BactChloro}})$ as a function of temperature and line of best fit ($y = ax + b$).

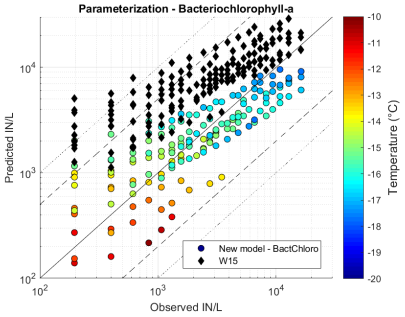

(d) Comparison of predicted values and observed values of IN_{SW} using $C_{\text{BactChloro}}$ as a predictor (Eq. III.5b).

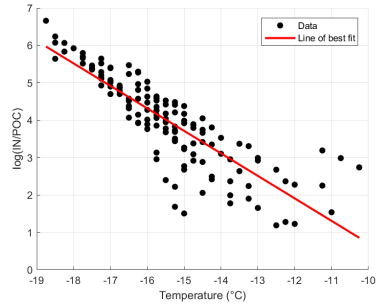

(e) $\log(IN_{SW}/POC)$ as a function of temperature and line of best fit ($y = ax + b$).

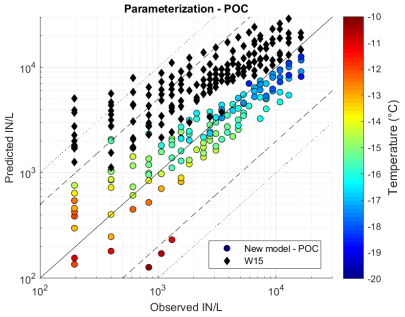

(f) Comparison of predicted values and observed values of IN_{SW} using POC as a predictor (Eq. III.5c).

Figure III.38 – Left: Best fits for predicting SW INPs as a function of temperature using a) bacterial abundance (C_{Bact}), c) bacteriocholorphyll-a concentrations ($C_{\text{BactChloro}}$), e) POC concentration. Right: Comparison of predicted and observed values using temperature and b) bacterial abundance, d) bacteriocholorphyll-a concentrations, f) POC concentration as a parameter, corresponding to Equations III.5. The solid, dashed and dotted line shown are the 1:1, 1:5 and 1:10 lines. The results of W15 for IN_{SML} as a function of temperature and TOC are shown as black diamonds.

In summary, these three parameterizations are able to predict INP concentrations in the seawater more accurately than W15, using other types of tracers than organic carbon, and we show that tose tracers perform relatively the same. As we also found that INP in the seawater would be in majority heat stable, small INP linked to DOC, our hypothesis is that only the variability of INP is driven by POC and larger INP, and this variability would "add" to a constant pool of the DOC type INP always present and more constant. Models in the previous studies were mostly focused on using organic matter in various forms (POC, DOC, TOC...), but it is likely that the relation to POC is dependant on the type of marine environment considered in each study, as they generally exhibit radically different properties depending on the region. This will be further discussed below, were we develop a parameterization for SSA INP using organic carbon in the SW and compare it to the TNG results.

III.4.2 A new parameterization of SSA INPs using the S2C cruise data

Here, we present the derivation of a parameterization for predicting SSA INPs that uses TOC_{SW} as a predicting parameter. The general strategy for this derivation was to link the SW INPs to a parameter measured in the SW using the correlations calculated in Section III.3.4, as SW data are more available in our study, and they are easier to measure in general. Then, we calculated a fit representing the transfer from the SW INPs to the SML INPs, and one representing the transfer from the SML INPs to the SSA INPs. Those three fits were then combined into one equation.

The first step for extracting a parameterization of INP in the seawater from the S2C data was to derive a fit for SW INPs as a function of temperature. As INP in the seawater was correlated to TOC, like Wilson et al. (2015), we used INP per gram TOC_{SW}. This parameter is widely available both in our study and in other studies. This is presented in Fig. III.39a. The equation of the fit is:

$$\mathrm{INP}_{\mathrm{gTOC,SW}} = \exp\left(1.0447 \cdot T - 0.9581\right), \tag{III.7}$$

with $\mathrm{INP}_{\mathrm{gTOC,SW}}$ the INP concentrations in the SW per gram TOC, and T the temperature in °C. Our measured values are low compared to the values calculated by W15, with about two orders of magnitude of difference. It is important to again note that the W15 parameterization used INP concentrations from the SML, while the values we use here are for the bulk SW. Considering our values span about one order of magnitude at all temperatures, this fit performs well ($R^2 = 0.47$). The fit determined in Eq. III.5c using the TNG data with POC concentrations in the SW is also shown, and its evaluation is close to W15. One caveat is that POC values during S2C were not directly measured, but were evaluated under the premise that the DOC/TOC ratio was conserved in a given water mass, which can lead to errors in the calculations. We showed in Sec. III.3.3 that SW INPs in TNG were slightly more abundant than in S2C, but not

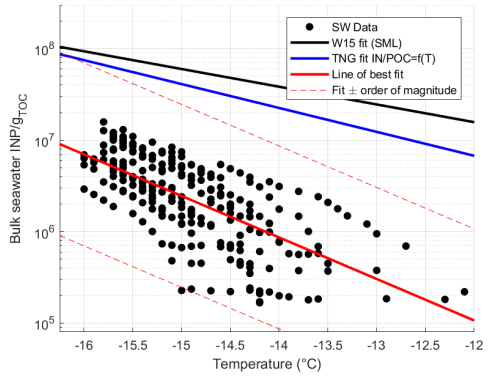

(a) Scatter plot and line of best fit for bulk SW INPs per gram TOC as a function of temperature. The blue and red line correspond respectively to the fit determined in Eq. III.5c and W15.

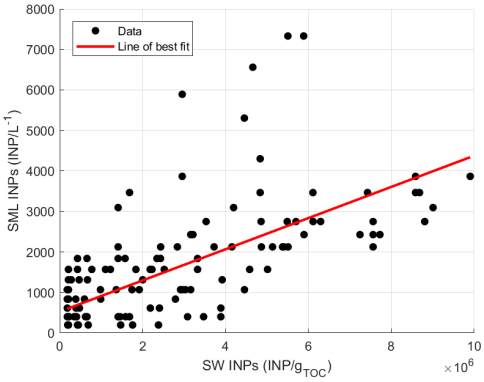

(b) Scatter plot of SML INPs versus SW INPs per gram TOC, with the line of best fit.

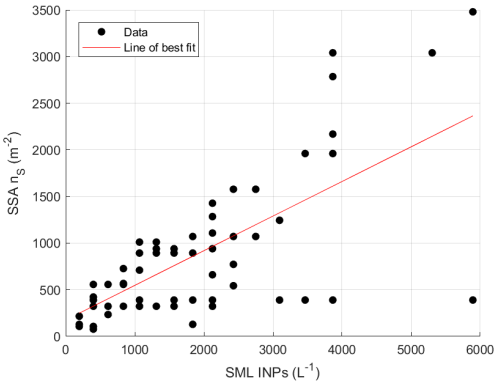

(c) Scatter plot of total SSA n_S versus SML INPs, with the line of best fit.

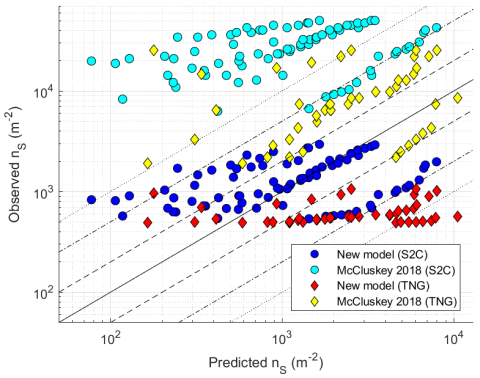

(d) Comparison of predicted SSA n_S versus observed n_S. The pristine marine INPs fit from McCluskey et al. (2018c) is included for reference. Both S2C and TNG data are used.

Figure III.39 – Steps for deriving the parameterization for SSA INPs during S2C (Eq. III.10).

Table III.10 – Fits information from Figure III.39.

x data	y data	Equation	Coeff. Values	R^2
T	INP_{SW}/g_{TOC}	$y = \exp(a_1 x + b_1)$	$a_1 = 1.0447$ $b_1 = -0.9581$	0.474
INP_{SW}/g_{TOC}	INP_{SML}/L	$y = a_2 x + b_2$	$a_2 = 3.8513 \times 10^{-4}$ $b_2 = 525.42$	0.472
INP_{SML}/L	n_S	$y = a_3 x + b_3$	$a_3 = 0.3713$ $b_3 = 175.81$	0.533

with differences as high as we observe here (1 to 2 orders of magnitude), so the difference in predictions between the TNG SW fit and the S2C SW fit can not be explained only by differences in INP/POC, highlighting different behaviours depending on the location and type of water.

Next, we derived a fit representing the transfer from the SW INPs to the SML INPs. This is shown in Fig. III.39b. The equation for this fit is:

$$\mathrm{INP}_{\mathrm{SML}} = 3.8513 \times 10^{-4} \cdot \mathrm{INP}_{\mathrm{gTOC,SW}} + 525.42, \tag{III.8}$$

with $\mathrm{INP}_{\mathrm{SML}}$ the concentration of INPs per liter of water in the SML.

Then, we represented the transfer from the SML INPs to the SSA INPs (Fig. III.39c). The linear fit has $R^2 = 0.53$ and its equation is:

$$n_S = 0.3713 \cdot \mathrm{INP}_{\mathrm{SML}} + 175.81, \tag{III.9}$$

with n_S the surface site density of INPs in the SSA.

Finally, we combined all the fits together, yielding the following equation:

$$n_S(T, \mathrm{TOC}_{SW}) = \alpha \cdot \exp\left(\beta T + \gamma\right) \cdot \mathrm{TOC}_{SW} + \delta, \tag{III.10}$$

with $\alpha = 5.3049 \times 10^{-14}$, $\beta = -1.0051$, $\gamma = -0.5266$ and $\delta = 488.51$, T the temperature in °C and TOC_{SW} the concentration of Total Organic Carbon in the SW in grams per liter of water. This equation allows to predict the SSA INP concentrations in the form of n_S, as a function of a parameter of the SW. Seawater TOC is indeed more readily available than parameters from the SSA or the SML, such as particulate carbon, which should make this parameterization usable more easily in atmospheric models.

We show in Figure III.39d the results of these calculations by comparing the predicted n_S and the observed n_S. We also compare the results of the calculations using McCluskey et al. (2018c)'s fit (MC18) and TONGA data. The blue and cyan points indicate the S2C data, and the red and yellow points indicate the TNG data. We see that MC18 generally over predicts the values, especially in the case of the S2C data which are overpredicted by about an order of magnitude. However, most of TNG data predicted by MC18 are within an order of magnitude of the observed values. The new model performs well with the S2C, with about 95% of the points within an order of magnitude of the observations. On the other hand, it tends to underpredicts the values from the TNG campaign.

Interestingly, a series of data points in the S2C data set are also underpredicted and shows a similar behaviour than the TNG dataset. These points correspond to the data of 24/03, where remarkably higher INP concentrations were observed. These data were sampled in the subtropical waters, and TNG data were also sampled in tropical waters. This shows that the higher abundance of INPs in tropical waters can not be explained by an increase in TOC. Since INP in the TONGA seawater was however correlated to TOC, we conclude that TOC has different relationships to INP in different types of seawaters. This highlights

the need for a more specific biological tracers than TOC in order to universally predict INPs in the ocean. We only have one day of measurements in the STW during S2C, and can not test if a specific relation to TOC in the subtropical seawaters of the S2C data set would be similar to the TONGA relationship between INP_{SW} and TOC in these specific seawaters.

III.5 General conclusion and perspectives on marine INPs in the Southern Ocean

As part of the Sea2Cloud project[3], two cruise campaigns took place in the Southern Ocean, with the objectives of investigating how emissions from microorganisms in the ocean affect the properties of clouds in the atmosphere. The TNG cruise took place in tropical waters near the Tonga volcanic arc from 01/11/2019 to 03/12/2019, and the S2C took place south of New-Zealand from 15/03/2020 to 27/03/2020. During both cruises, we sampled INPs directly from the bulk seawater and from artificial sea spray aerosols (SSA) generated from seawater. Additionally, surface microlayer (SML) and ambient atmosphere samples were collected during the S2C cruise. Several other biogeochemical parameters, which characterise the state of the ocean, were also measured, including organic carbon, microorganisms abundance and other biological markers.

INP concentrations during the S2C were lower than during the TNG cruise, with the measured concentrations being in the range of 10^3-10^4 IN/L in the SW between -15 and -18 °C; and surface site densities n_S in the range of 10^3-10^4 m^{-2} in the SSA. Both cruises exhibit lower concentrations than other studies in different oceans (e.g. Wilson et al. 2015; Irish et al. 2017), and similar concentrations than those in Southern Ocean waters (McCluskey et al. 2018a). For both campaigns, heat labile INPs were dominant in the SW and in the SSA, showing a strong influence of biogenic INPs in the SO. The SML INPs abundances during the S2C cruise were generally enriched compared to SW INPs, roughly by a factor of 2 but with a high variability among samples, and exhibited higher heat labile fractions. This would confirm that marine aerosols in the southern hemisphere are worse INPs than those in the northern hemisphere, even for the biologically richest waters.

In both campaigns, measurements could be split into separate water masses, that allowed further analysis of the properties of the INPs in either the SW or SSA. The TNG SW INPs were marked by higher abundances in the water influenced by volcanic activity, which are richer waters in terms of nutrient and biomass. The impact of subwater volcanic activity could be one reason why the overall TONGA INP concentrations are above those of the S2C ones. The S2C INPs were also higher in the richer frontal and subtropical waters, but did not show a direct link to biomass, as frontal waters clearly show the highest contents in Chl-a, POC, and most biological content, but not the highest INP content compared to STW. However, the concentrations of INPs in the subtropical waters during the S2C cruise were closer to the average INP concentrations during the TNG cruise, showing that INPs were low in tropical and subtropical seawaters, but even lower in the subantarctic seawater.

Linear correlation were computed for both datasets with the collocated bio-

[3] https://sea2cloud.wordpress.com/

geochemical parameters of each campaign. We showed that INPs during the TNG cruise were strongly correlated with pigment concentrations (particularly bacteriochlorophyll-a), bacterial abundances and POC. We surmise that INPs during the TNG cruise are more linked to the POC-type INPS, as defined by McCluskey et al. (2018b). Dissolved organic matter was also linked with the heat stable INP concentrations, highlighting the presence of an INP population closer to the DOC-type as well. SSA INP concentrations did not exhibit significant links with either the SW INPs or the SW parameters, but the data set of INP in SSA during TONGA might be too reduced.

INP concentrations during the S2C cruise were generally positively linked with the organic matter TOC, but negatively linked with picophytoplanktons, suggesting that picophytoplanktons may have an inhibiting effect on the ice nucleating activity, which is consistent with an other study in the Mediterranean sea (Trueblood et al. 2021). SSA INPs during the S2C cruise were more strongly linked to SML INPs than to SW INPs, which is also consistent with Trueblood et al. (2021). SW INPs were also strongly linked with SML INPs.

Using the relationships found between the INP datasets and the collocated measurements, we derived several empirical parameterizations for predicting INPs in the different mediums. In the SW, using the TNG dataset, we showed that it was possible to predict INP concentrations as a function of either the bacterial abundance, the concentration of bacteriochlorohyll-a or the concentration of POC. We show that all three parameterization have better results than a previous fit that used TOC (Wilson et al. 2015). We thus show that biological tracers could be used as predictors for INP concentrations in marine regions.

With the S2C dataset, we used the links we observed between SW, SML and SSA INPs to derive a parameterization for SSA INPs. This parameterization is a two step parameterization that uses the concentration of TOC in the SW for determining INP in the seawater, and then a relationship to link INP in the SW to INP in the SSA (via an enrichment factor in the SML that could be approximated to a factor 2). We show that this parameterization has better predictions than the fit for pristine marine SSA proposed by McCluskey et al. (2018c). Furthermore, we show that concentrations of INPs in the subtropical waters are generally underpredicted by the S2C model, and that it is also the case for the TNG data. Thus, we show that in tropical waters INPs are generally more abundant , and that they have a different behaviour than INPs found at higher latitudes (in the frontal or subantarctic seawaters) at T<-20 °C.

With both campaigns, we have improved our understanding of the sources of marine INPs. We see that their IN properties in the seawater, in the SSA and in the ambient atmosphere are significantly different, either because of the mixing of aerosols from different sources or because their IN properties are modified during transport in the atmosphere. One follow-up question are the IN properties of aerosols in an atmosphere far from the immediate aerosol sources. To answer this question, we will use the instrumented Puy de Dôme observatory to investigate the IN properties of ambient aerosols at a mountain site that

is influenced by a variety of air masses.

IV

Seasonal variations, origin and parameterization of ice-nucleating particles at a mountain station in central France

Outline of the current chapter

IV.1 Abstract

Understanding how aerosol particles interact with atmospheric water is critical to understanding their impact on climate and precipitations. Ice Nucleating Particles (INPs) trigger the formation of atmospheric ice crystals. They are challenging to characterize because of their scarceness in the atmosphere and their variability. This variability depends partly on the different INP sources but also on the temperature at which they are activated. Considerably more variability is observed at warm temperatures (>-20°C). At these temperatures the aerosol particles of biological origin can contribute significantly to INP number concentration, but their properties and variability are still poorly understood, making it difficult to predict their concentrations. This study incorporates a series of offline, long-term, size-segregated measurements of INPs, collected at the Puy de Dôme station (PUY, 1465 m a.s.l.). PUY is an ideal place to study INPs concentrations as it is advected by a variety of airmasses, with about 20% of them being free tropospheric airmasses.

This study presents offline size segregated ambient INP measurement at the PUY site collected over a period of 6 months from October 2018 to May 2019. We measured concentrations of INPs between -5 and -18 °C, with concentrations of about 0.001 INP/L_{air} at the warmest temperatures, and between 0.01 and 0.1 INP/L_{air} at the coldest temperatures. We observe that the majority of INP measured at temperatures warmer than -15 °C are heat labile, in line with other studies. We observe higher contribution of heat labile INPs during the winter, and lower ratios in spring. Given that a range of air mass sources were encountered during this study period we were able to provide classifications of INP properties based on air mass source. This analysis was complemented by a comparison with collocated sampling instrumentation at the site. Using this combination of measurements, we propose a new parameterization using the total number of aerosols. This parameterization is easy to implement and unlike existing parameterizations it is optimised for warmer temperature INP analysis. The parameterization showed good performance when tested on independent datasets collected from different European sites.

IV.2 Introduction

Atmospheric aerosol particles have a wide range of physical and chemical properties. Understanding how these aerosol particles interact with atmospheric water vapor is essential to evaluate their impact on the energy budget of the Earth and on the atmospheric water cycle (Hartmann et al. 1992; Lohmann et al. 2005; Boucher et al. 2013).

In clouds at temperatures above -38 °C, aerosol particles can induce heterogeneous freezing and lead to the formation of atmospheric ice crystals (Pruppacher 2010) by reducing the energy barrier required by the ice nucleation process. These aerosols are referred to as Ice Nucleating Particles (INPs). INPs are

very scarce in the atmosphere, with concentrations ranging from 0.1 to 10 L^{-1} (while the total concentration of aerosols is ranging from 10^5 L^{-1} to 10^7 L^{-1}), thus making them difficult to detect and quantify, and therefore to understand. Furthermore, depending on their nature, INPs are active at different ranges of temperatures between 0 and -38 °C. Some specific aerosol particles were identified as having good ice nucleating abilities include mineral dust, soil dust, and primary biological aerosol particles (Kanji et al. 2017), either of terrestrial origin (Schneider et al. 2021) or of marine origin (Wilson et al. 2015; McCluskey et al. 2017). Dust-derived particles have been identified as the dominant INP type at temperatures below -20 °C, whereas biological INPs such as bacteria or fungal spores are the dominant types identified active at temperatures above -15 °C (Kanji et al. 2017; Huang et al. 2021), as high as -2 °C (Maki et al. 1974). It was also recently shown that biogenically derived secondary organic aerosols could also have ice nucleating properties (Wolf et al. 2020a).

Another element of uncertainty in our current understanding of ice nucleation in the atmosphere are the different pathways by which an ice crystal may form. These pathways, or activation modes, are described in detail by Kanji et al. (2017). There are generally four different modes considered in the literature (deposition ice nucleation, contact freezing, immersion freezing and condensation freezing ; see Kanji et al. (2017) for a thorough description of each mode). The different INP sampling instruments can often operate over only one or two ice nucleation modes, which is another obstacle to understanding and comparing INP measurements.

To date there is not one instrumental method that can characterize INPs across the full temperature range between 0 and -38 °C. Different sampling and analytical procedures, both online and offline, have been widely used in the past and therefore reproductibility of instrumental methods in both controlled (DeMott et al. 2018) and ambient conditions (Lacher et al., in prep) is essential (DeMott et al. 2011). Online methods allow the measurement of INP concentrations with high time resolution (seconds to minutes), making it possible to follow the high temporal variability of ambient INP concentrations. Current online instruments operate at temperatures colder than -15 °C and provide much needed information on the temporal variability of INP particles. However, due to low INP concentrations, they often need to be operated downstream of a particle concentrator (Gute et al. 2019). Offline methods are low cost, and generally easier to deploy in different sampling sites. Since samples are accumulated over longer time periods, they allow examining low concentrations of INPs. This makes them more efficient for studying biological INPs than online measurements.

In the last decade, significant technological advances have been made in the development of new measurement methods for atmospheric INP, leading to a substantial increase in the number of field campaigns aimed at answering scientific questions on the sources and variability of INPs in different atmospheric environments. However, only a few studies focused on analysing INP seasonal trends and variability (e.g. Pouzet et al. 2017; Wex et al. 2019; Hartmann et al.

2019; Schrod et al. 2020; Schneider et al. 2021). These studies have shown an increased number of INP in the spring and summer, but seasonal data is still lacking in different types of environments.

Having these long term INP data sets are essential if we are to derive accurate parameterizations that will allow the prediction of INP from the aerosol properties under different atmospheric conditions and environments. This would allow them to be integrated into global models to study and predict climate and precipitation more accurately. Historically, the most commonly used INP parameterizations are those based on temperature since it is easier to implement into numerical models without needing additional measurements (Fletcher et al. 1962; Meyers 1992). With the increase in collocated measurements of ambient aerosols and INP properties, a number of parameterizations have been developed using a wide range of parameters. Some parameterizations use aerosol number concentration (DeMott et al. 2010a, Tobo et al. 2013, DeMott et al. 2015), others use aerosol surface concentration (Ullrich et al. 2017), or aerosol chemical properties (Niemand et al. (2012) for dusts, Atkinson et al. (2013) for feldspar, Wex et al. (2015) and Patade et al. (2021) for biological material). However, a major drawback from the majority of these parameterizations is that they have been optimized for temperatures below -20 °C and therefore do not accurately predict INP concentrations at warmer temperatures (Schneider et al. 2021; Huang et al. 2021).

Due to the huge variability in INP types and properties between the different regions of the globe, there is a strong motivation to increase the number of field studies (Murray et al. 2012; Kanji et al. 2017; Huang et al. 2021), especially at warm temperatures, in order to increase data availability and to better understand ice nucleation by biological aerosols. In this context, measurements were performed during the Puy de Dôme Ice Nucleation Intercomparison Campaign (PICNIC) at the summit of the Puy de Dôme Mountain (PUY, 1465m a.s.l.) in Central France in October 2018. In addition to characterising INP concentrations and variability at a high altitude remote station, this field campaign had a second objectives to compare a range of both offline and online ice nucleation measurement techniques in ambient environments (Lacher et al., in prep). After PICNIC, weekly size resolved filters were collected for analysis of INP concentrations until May 2019.

In this work, an overview is provided for INP measurements at PUY, including their concentrations, seasonal variability, and relation with aerosol physical and chemical properties. Using a combination of these measurements, we propose a parameterization optimised for warm temperature (>-20 °C) INP activity. We then test this parameterization on two independent data sets.

IV.3 Methods

IV.3.1 Site description and instrumental set-up

The Puy de Dôme station (PUY) is located at the top of the Puy de Dôme mountain (45°46' N, 2°57' E, 1465 m a.s.l.) in central France. The site is influenced by long range air masses from both the continental and oceanic sectors (Farah et al. 2018, Baray et al. 2020). Given both its altitude and surrounding geography this site can be situated occasionally in the lower free troposphere, making it an interesting site to study the properties of different atmospheric layers (e.g. Freney et al. 2016; Farah et al. 2018). The PUY site is identified as a global atmospheric monitoring station (GAW) as well as being an ACTRIS (Aerosol, Clouds and Trace Gases Research Infrastructure) facility. A detailed description of the station is available in Baray et al. (2020). In addition to the measurement of continuous meteorological parameters (temperature, humidity pressure), the station is equipped with a wide range of both online and offline measurement methods, to study in-situ gas and aerosol properties.

For this work we use measurements of aerosol size and number concentration using a custom made Scanning Mobility Particle Sizer (SMPS) coupled with a condensation particle counter (CPC, TSI) measuring particle diameters from 10 nm up to 600 nm. An optical particle counter (OPC, Grimm model 1.108) was measuring supermicronic aerosol number concentration from sizes 0.3 to 20 µm. However, due to poor data coverage (Fig. C.1) only measurements from the SMPS will be used. The lack of OPC measurements represents a 1% decrease on the total aerosol number concentrations, and up to 10% in total aerosol surface area. Only total aerosol number concentrations ($N_{aer,tot}$, representing sizes from 10 nm up to 600 nm), number concentrations of aerosols with diameters greater than 500 nm ($N_{aer,500}$) and the aerosols surface area ($S_{aer,tot}$) and surface measured by the SMPS will be used in this study. The Magee Scientific Aethalometer© AE33 was used for black carbon measurement. Filter based aerosol chemistry measurements were obtained from a high volume (500 L/min) sampler located on the rooftop of the station.

Concentrations of INPs were measured during two consecutive periods with different sampling procedures. During the PICNIC campaign (starting from 09/10/2018 to 24/10/2018), high-volume filter samples (500L/min, total volume sampled: ≈ 550 m^3) were taken on 147 mm diameter quartz filters every day (from 10:00 to 18:00) and night (from 22:00 to 06:00). Prior to analysis, the filters were conserved at -10 °C in the laboratory for 2 to 3 months. After the PICNIC campaign, a period of Weekly Ice Nuclei Samples (WINS) were collected from 07/11/2018 to 25/05/2019. A 4-stage Dekati© impactor and 25 mm diameter quartz filters were used for size segregated INP measurements, with size bins of 0.1 µm - 1 µm, 1 µm - 2.5 µm, 2.5 µm - 10 µm and >10 µm. Contrary to PICNIC, the sampling was done from inside the observatory behind a whole air aerosol inlet (WAI) with a 50% cut-size diameter of 30 µm and a flow rate of 10 L/min. The chemical properties of the aerosols during the

sampling periods were analysed using the same filters as those used for the INP analysis. Chemical analysis of the filters was performed using ion chromatography using the method described by Bourcier et al. (2012), thus providing mass concentrations of anions (Cl^- NO_3^-, SO_4^{2-}, Oxalate) and cations (Na^+,NH_4^+, K^+, Mg^{2+},Ca^{2+}).

In parallel to the PICNIC campaign, a number of other European sites collected filter samples for INP analysis. In this study, we used quartz filter measurements from the ACTRIS station Montsec d'Ares (MSA; 42°3 N, 0°44 E, 1570 m a.s.l.). Those filters were collected by the Institute of Environmental Assessment and Water Research (IDAEA), Barcelona, Spain. Similarly to PUY, MSA is a continental background altitude site. The atmospheric conditions at MSA are characteristic of Mediterranean climate with local and regional atmospheric air masses and Saharan dust inclusions (Ripoll et al. 2014a; Ripoll et al. 2014b; Ealo et al. 2016). These datasets were to validate/evaluate the newly developped parameterization (Section IV.6).

IV.3.2 Ice nucleating particles analysis

INP analysis of offline filters were made with the LINDA (LED-based Ice Nucleation Detection Apparatus) technique, (Stopelli et al. 2014), an offline method used to analyse samples of INP and their properties in the immersion freezing mode (Pouzet et al. 2017; Hiranuma et al. 2019). This instrument allows the analysis of large volumes of samples, at warm temperatures (>-20 °C).

LINDA consists of a LED array underneath an array of 52 Eppendorf© tubes filled with a 0.9% NaCl solution containing INPs. The array of tubes is placed in a cooling bath, with a P_{-800} temperature probe at each corner. An USB CMOS Monochrome Camera placed above the array allows detecting the freezing of the tubes by the variation of the intensity of the light transmitted through the tubes. The temperature in the cooling bath was decreased at a rate of -0.33/min.

For the analysis with LINDA, punches of the filters (4.5 cm^2 for PICNIC, 4.3 cm^2 for WINS) were washed in a 25 mL solution of 0.9% NaCl during 20 minutes by agitation, then half of the tubes (26) were filled using the resulting solution (200 µL in each tube). The remaining solution was then heated for 30 minutes in boiling water at 100 °C, and was used to fill the remaining half of the tubes of LINDA. This heat treatment allows the removal of the biological INPs, and it has been used widely as a method for identifying biological INPs (e.g. Christner et al. 2008a; Wilson et al. 2015; O'Sullivan et al. 2018). This is supported by the fact that most biological INPs active at such high temperatures are composed of proteinaceous material, such as bacteria (Huang et al. 2021), and are thus heat-labile. In the following discussion we refer to the INPs from heated samples as "Heat Stable" (HS) INPs and the difference between untreated and heated samples as "heat-labile" (HL) INP concentrations.

The cumulative INP concentration n_{INP} were calculated using Vali (1971) formula:

$$n_{INP} = \frac{\ln N_0 - \ln N(T)}{V}, \tag{IV.1}$$

where N_0 is the total number of droplets (here the number of Ependorf tubes, 26), $N(T)$ is the number of droplets frozen at temperature T and V is the volume of a droplet (here, $V = 200$ µL).

Blank filters were analysed through the same procedure in order to estimate background errors. On average, blank samples started freezing at around -10 °C, but remained below the filter samples until about -18 °C (Figure C.2). PICNIC blanks were generally higher than WINS blanks, and they were frozen at -16 °C, instead of about -19 °C for WINS blanks. However, heated blank samples showed increased IN activity at all temperatures compared to unheated blanks, which hints that the heat treatment slightly contaminated the samples. However, the effect of this pollution is rather small (less than 10% of a standard deviation), and only significant at the end of the temperature spectrum.

IV.4 General observations and time series

IV.4.1 General features of the INP concentrations

The cumulative INP temperature spectra for both campaigns are shown in Figure IV.1 for all samples, and represented as boxplots in Figure C.4. Heat stable (HS) INPs are defined as the heated samples, while heat labile (HL) INP concentrations were calculated as the difference between the unheated and heated samples samples. In both field campaigns, the total INP concentrations (unheated samples) vary between 10^{-4} INP/stdL to 10^{-1} INP/stdL at the highest temperatures, and around 10^{-1} INP/stdL at the coldest temperatures. Both datasets show similar freezing onset, around -6 ± 1 °C, but all samples are activated for PICNIC at -13 °C, while it is at -18 °C for WINS. This difference is probably explained by the difference in INP concentrations of the samples from the two campaigns. These values are comparable with global INP data (Kanji et al. 2017), and with other studies in similar temperature ranges using droplet freezing techniques for studying immersion freezing (e.g. DeMott et al. 2018; Ladino et al. 2019; Tobo et al. 2019; Conen et al. 2022).

A clear decrease in INP numbers is visible after the heating treatment, indicating a large fraction of INP of heat-labile INPs (Fig. IV.1), which is indicative of particles of biological origin containing proteinaceous ice-active material (Christner et al. 2008a, Hill et al. 2016; Huang et al. 2021), with concentrations ranging from 10^{-4} INP/stdL to 10^{-2} INP/stdL at the higher temperatures (> -10 °C), and between 10^{-2} and 10^{-1} INP/stdL at the lowest temperatures (< -10 °C). For both datasets, the heat treatment decreases the freezing onset of the samples by about 3 to 4 °C. At temperatures above -10 °C, about 80-90% of the observed IN activity can be attributed to biological origins, which is in line with other studies at the same temperatures at mountain sites in cloud water (Joly et al. 2014), snow (Hill et al. 2014) or rain water (Lu et al. 2016). A much larger variability is observed at the warmer temperatures (> -10 °C), represented by the outliers in Figure C.4. At -12 °C, an average of 45% of INPs are heat labile for PICNIC, and 31% for WINS while at -18 °C less than 10% of all INPs are HL.

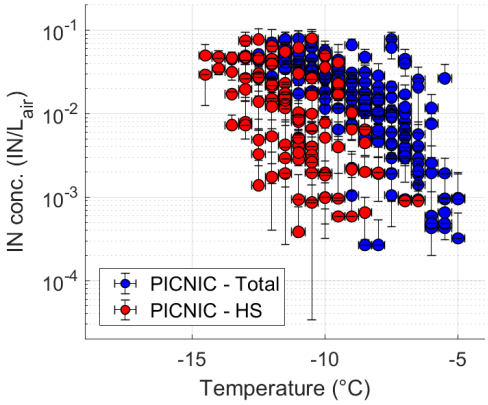

(a) Cumulative INP concentrations during the PICNIC campaign

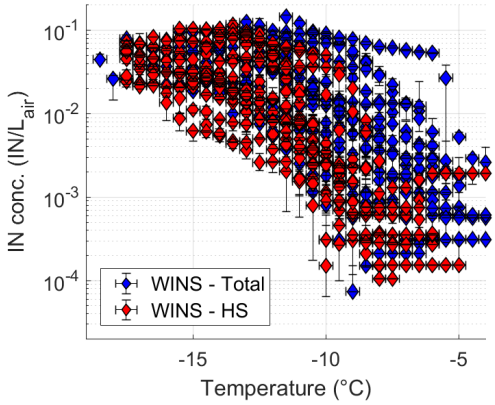

(b) Cumulative INP concentrations during the WINS campaign

Figure IV.1 – Mean cumulative INP concentrations at PUY during the a) PICNIC campaign, b) WINS campaign for INP_{tot} (blue), INP_{HS} (red).

This is consistent with other studies that used heat treatment for differentiating heat labile biological INPs in different types of environments (e.g. Joly et al. 2014; Hill et al. 2016; McCluskey et al. 2018c; O'Sullivan et al. 2018; Schneider et al. 2021; Conen et al. 2022).

IV.4.2 Day-night contrast during PICNIC

The average diurnal concentrations of total and HS INP concentrations measured during the PICNIC experiment are shown in Figure IV.2. The median concentrations of heat labile INPs (Fig. IV.2c-d) are generally the same at night than during the day, but the interquartile range (25 to 75%, materialized by the boxes in Fig. IV.2) is a lot higher at night than during the day, showing that the variability of INP concentrations at night is very high. The concentrations of heat stable INPs (Fig. IV.2c-d) are consistently higher during day time than night time. This is particularly the case at colder temperatures (<-12 °C), where the difference is about 0.03 INP/stdL. Thus, the contribution of HL INPs to the total INPs is higher at night than during the day.

This trend is surprising as most biological activity is emitted in the planetary boundary layer that is transported to the site more efficiently during the day. This is potentially linked to the increased abundance of particles of biological origin during the night previously observed at PUY by Gabey et al. (2013). The day-night difference of other aerosol parameters were also computed to investigate their impact on INPs (Figure IV.2).

The day-night difference of other aerosol parameters were also computed to investigate their relationship with the INP trends (Figure IV.3). $N_{aer,tot}$ shows a 22% increase on average from night to day, which is in line with the trends of HS INPs. The variation in total aerosol is similar, although a bit lower, than the observations from Venzac et al. (2009), where autumn diurnal aerosol concen-

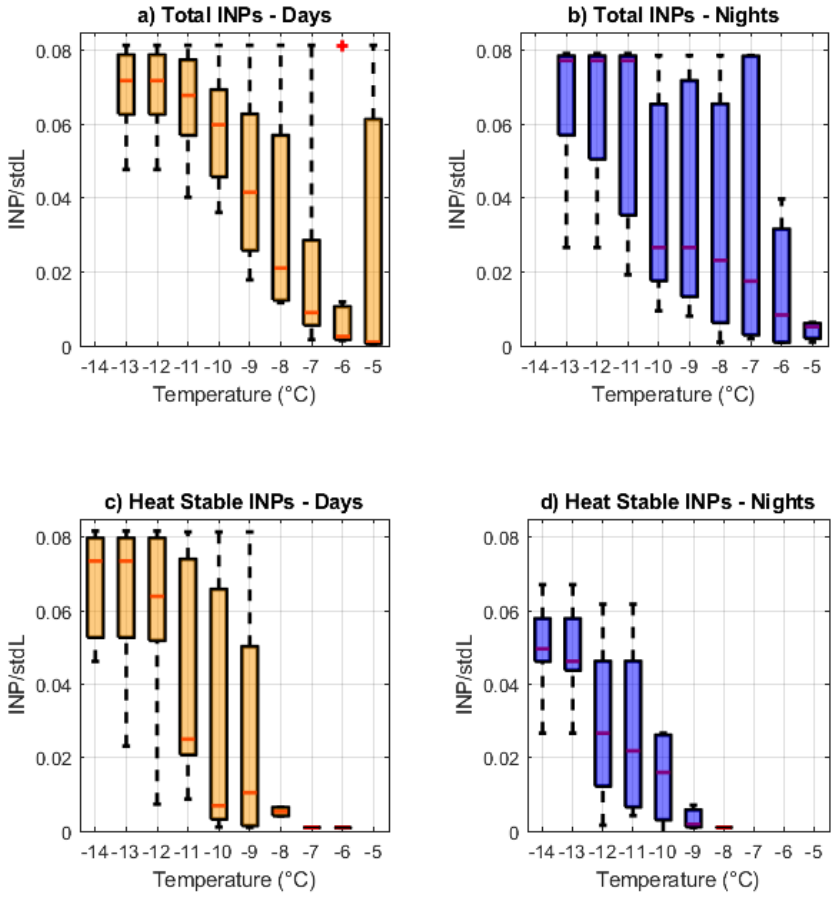

Figure IV.2 – Diurnal variation of Total and Heat Stable INP concentrations during PICNIC. Night and day values corresponds respectively to the periods 22:00 to 06:00 and 10:00 to 18:00.

tration varied from 1100 to 2800 cm^{-3}. During the day the increasing boundary layer height means that smaller particles from nearby sources are transported to the site.

On the contrary, $N_{aer,500}$ increases on average by 19% at night, which is in line with the increase of HL INPs at night. At night the PUY is sampling at the top of the mixing layer or in the residual layer where aerosol concentrations are more often long range transported. S_{aer} does not show a significant variation during the period. For the chemical parameters, Na^+ increases by 44% on average during the day compared with Cl^-, NO_3^- and Ca^{2+} that increase from 10 to 15%. For SO_4^{2-}, concentrations decreases by 10% during daytime. The other chemical parameters do not show any significant variation (below 5%).

IV.4.3 Seasonal variations

We show in Figure IV.4 the weekly time series of INP data (HS and HL) at -8 °C, -12 °C and -15 °C and of the collocated measurements.

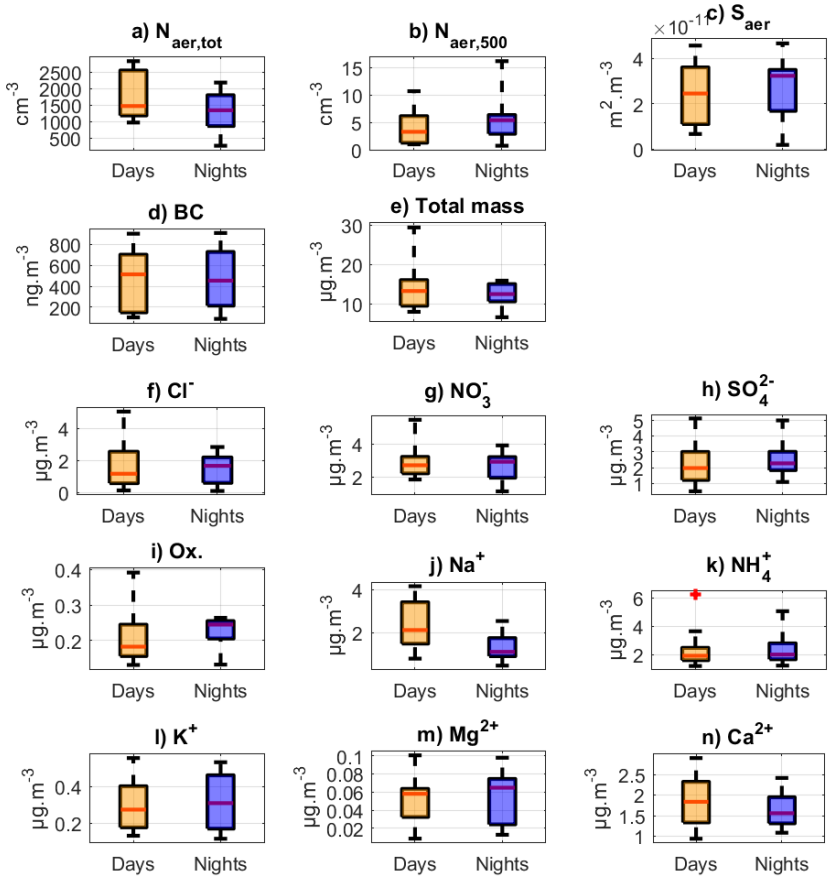

Figure IV.3 – Diurnal variations of physical and chemical parameters at PUY. Night and day values corresponds respectively to the periods 22:00 to 06:00 and 10:00 to 18:00.

As observed in Figure IV.1, these temperatures correspond respectively to the temperature at which a majority of HL INPs is activated, the temperature where both HL and HS INP are present at roughly the same concentrations, and to the temperature at which the majority of all INPs have been activated, and where INP are in majority heat stable. PICNIC concentrations are not shown at -15 °C, as all INP were activated above -14 °C.

A clear seasonal variation can be seen on the INP concentrations measured at PUY, at all freezing temperatures selected, and for both heat labile and heat stable INP, with higher concentrations during spring and autumn and minima during winter (Fig. IV.4a to c). This same trend has been reported in precipitation water (Pouzet et al. 2017) and in a boreal forest in Finland (Schneider et al. 2021). We observe similar seasonal variations of aerosol numbers ($N_{aer,tot}$, $N_{aer,500}$, Fig. IV.4d), surface area (S_{aer}, Fig. IV.4e) and composition (Fig. IV.4f-g). The link with $N_{aer,500}$) is consistent with the observations by DeMott et al. (2010a), who illustrated that dust INP concentrations were strongly related to

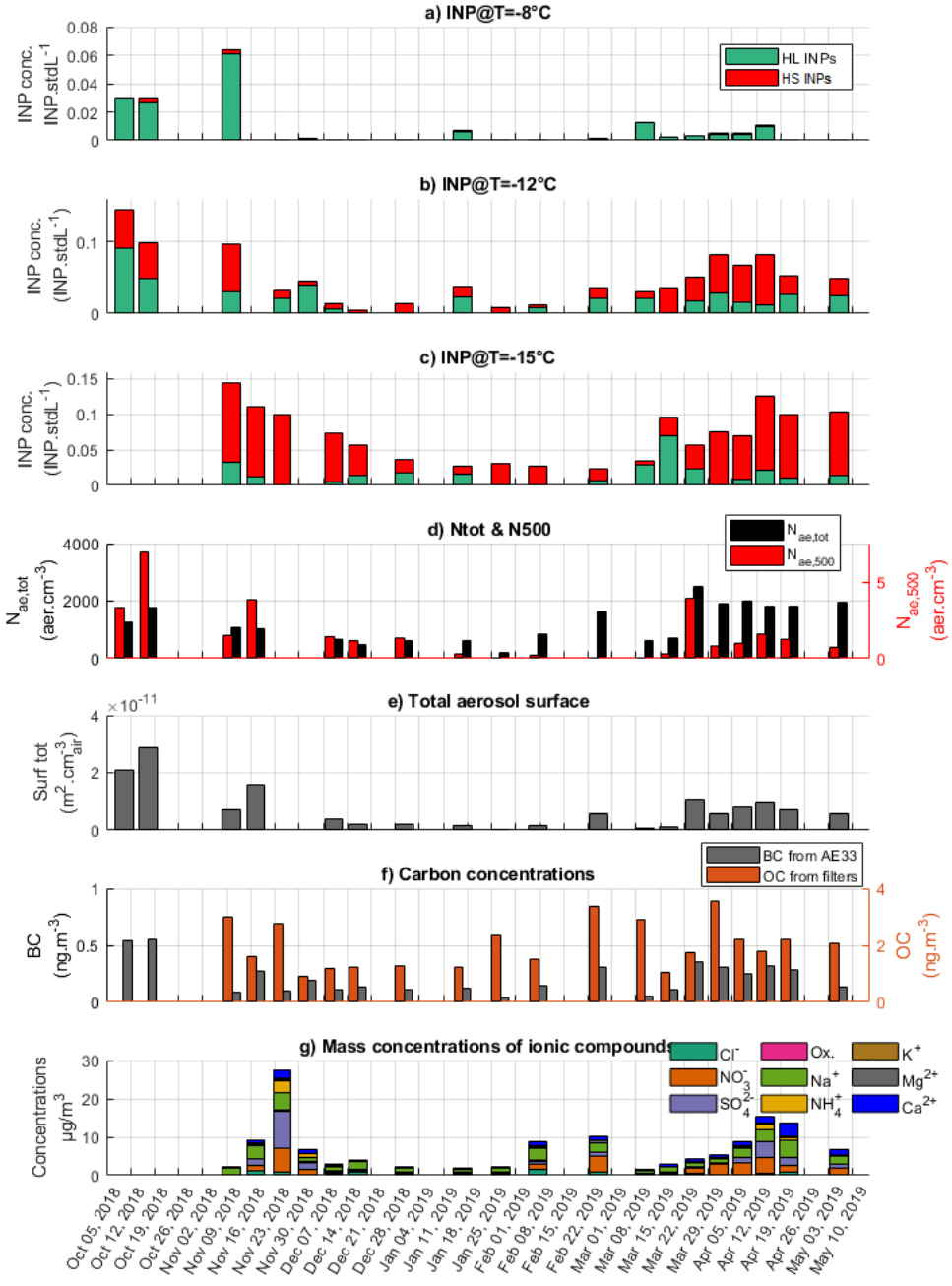

Figure IV.4 – Time series at PUY of weekly averaged data for the PICNIC and WINS sampling period : (a) INP data at -8 °C, (b) INP data at -12 °C, (c) INP data at -15 °C, (d) $N_{aer,tot}$ and $N_{aer,500}$ number concentrations (cm^{-3}), (e) Total surface of aerosols (m^2/m^3_{air}), (f) Carbon concentrations (BC,OC) ($\mu g/m^3$), (g) Masses of cations and anions from filters ($\mu g/m^3$).

the number of aerosols larger than 500 nm.

Furthermore, the seasonal trend in aerosol properties at PUY has previously been reported for aerosol concentrations by Farah et al. (2021), Bourcier et al. (2012) and Venzac et al. (2009). At PUY, this seasonal variation is strongly influenced by the variability in the boundary layer height that does not reach the site as often during winter compared to summer, as observed by different studies (Venzac et al. 2009; Farah et al. 2018). Additionally, the lower aerosol concentrations (and hence INP) during winter can be partially explained by a decrease of biological particles due to to a decrease in vegetation cover.

IV.4.4 Size segregation

During the WINS experiment, size segregated filters were collected, allowing the examination of INP variability for both submicron and supermicron aerosol particles (Figures IV.5 and C.3). At all temperatures, both submicron and supermicron INPs show similar seasonal variation with a wintertime minimum. However, INPs are consistently more abundant in the supermicron range than in the submicron range, contributing $64 \pm 32\%$, $61 \pm 21\%$ and $65 \pm 19\%$ to the total INPs at -8 °C, -12 °C, and -15 °C respectively. This is in line with previous studies showing that INPs are abundant in the supermicron range at temperatures warmer than -20 °C, with 80% and 55% of INPs, respectively at -15 °C and -20 °C, being supermicronic (Huffman et al. 2013; Mason et al. 2016; Creamean et al. 2018).

The ratio of HL (and hence thought to be of biogenic origin) INPs at -8 °C and -12 °C is higher by 10% for submicron INPs than for supermicron INPs: the fraction of HL to total INP are $97 \pm 7\%$; $57 \pm 39\%$ and $44 \pm 8\%$ at -8 °C, -12 °C and -18 °C respectively in the submicron mode, while they are $88 \pm 22\%$, $47 \pm 26\%$ and $32 \pm 27\%$ at -8 °C, -12 °C and -18 °C respectively for the supermicron mode. This contradicts previous literature findings, stating that biological aerosols are generally observed in supermicron aerosol particles (Després et al. 2012; Huang et al. 2021). However, the number of size segregated measurements on INPs is very low, and even less so over long periods of time.

IV.5 Correlations with atmospheric parameters

In the following section, we compare the long term WINS data set with collocated atmospheric measurements to determine which aerosol properties can be used to explain INP variability. Correlations between total INPs concentrations (INPtot), heat-labile INPs concentrations (INP HL) and heat stable INPs (INP HS) and various aerosol physical ($N_{aer,tot}$, $N_{aer,500}$ and S_{aer}) and chemical (Black Carbon BC, Ion concentrations Cl^-, NO_3^-, SO_4^{2-}, Oxalate, Na^+ NH_4^+, K^+, Mg^{2+}, Ca^{2+}) properties were investigated for WINS data (Tables IV.1 and IV.2).

The correlations were computed at three temperatures (-8 °C, -12 °C and -15 °C), to better understand the dominant relationships in each of the temperature regimes and to better distinguish between the influencing factors of “cold” and

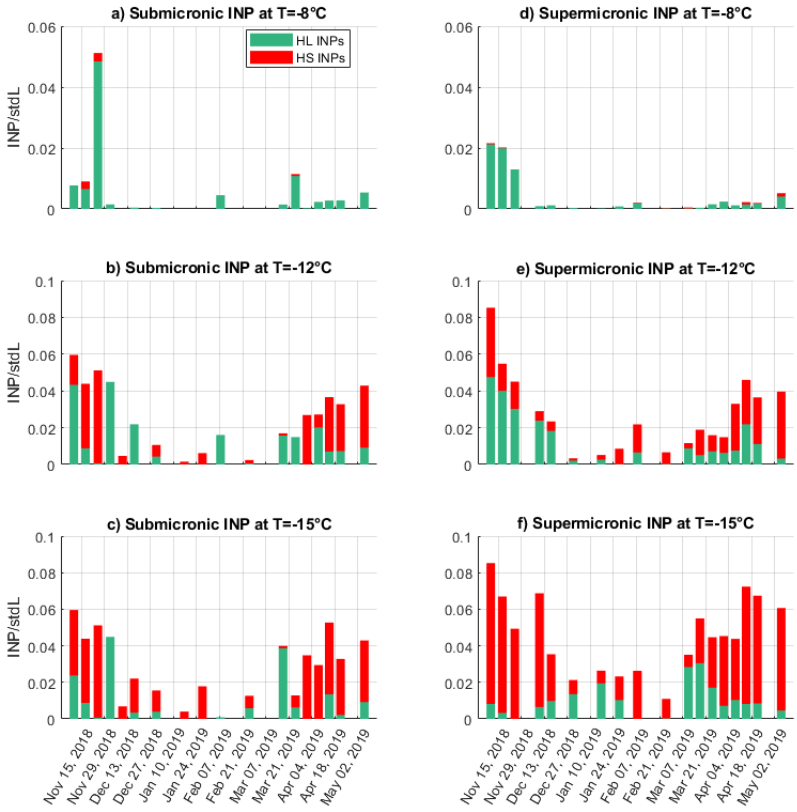

Figure IV.5 – Time series of submicronic (a-c) and supermicronic (d-f) INP concentrations during WINS at -8 °C, -12 °C and -15 °C.

"warm" INPs. HS and HL INPs at -8 °C are not included in the following tables because we showed previously that HS INPs represent less than 10% of the total INPs at this temperature.

IV.5.1 Grouped INP data

For physical parameters $N_{aer,tot}$ and S_{aer}, good relationships ($R^2 > 0.7$) were measured with INPtot at -8 °C (Table IV.1). However, relatively lower correlations are observed for $N_{aer,500}$ ($R^2 \approx 0.35$) with INPs at -8 °C. At -12 °C and -15 °C, only HS INPs have significant correlated to $N_{aer,tot}$, which is not surprising, considering that concentrations of heat labile biological INPs are low at these temperatures.

Overall, INP concentrations at warmer temperatures (>-12 °C), have best correlations with anthropogenic species SO_4^{2-}, Oxalate and NH_4^+ ($R^2 > 0.6$). INP concentrations have lower correlations ($R^2 \approx 0.25$) with Na^+ and K^+, tracers of marine origin and NO_3^-, a compound that may be the result of the reaction of HNO3 with NaCl. At intermediate temperatures, INP_{-12} correlates ($R^2 \approx 0.2$) with Na^+ and NH_4^+. For HS INPs at -12 °C, the correlations with Na^+ and Ca^{2+} (respectively marine and dust tracers), are similar as those with the anthro-

Table IV.1 – Linear regression correlations coefficients and p-values (Pearson's test) between INP concentrations at -8 °C, -12 °C and -15 °C (IN_{-8}, IN_{-12}, IN_{-15}) and aerosol parameters. Only significant ($P < 0.05$) correlations are indicated. Values with no significant correlations are indicated as double dashes. Values with $P < 0.005$ are indicated in bold.

		$N_{aer,tot}$	$N_{aer,500}$	S_{aer}	BC	Cl^-	NO_3^-	SO_4^{2-}
IN_{-8}	R^2(P)	**0.70(<0.005)**	0.39(0.01)	**0.74(<0.005)**	—	—	0.25(0.03)	**0.61(<0.005)**
IN_{-12}	R^2(P)	—	—	—	—	—	—	—
IN_{-12} HS	R^2(P)	0.40(0.01)	—	—	—	—	0.24(0.03)	0.35(0.01)
IN_{-12} HL	R^2(P)	—	—	—	—	—	—	—
IN_{-15}	R^2(P)	—	—	—	—	—	—	—
IN_{-15} HS	R^2(P)	0.28(0.04)	—	—	—	—	—	0.24(0.04)
IN_{-15} HL	R^2(P)	—	—	—	—	—	—	—

		Ox.	Na^+	NH_4^+	K^+	Mg^{2+}	Ca^{2+}
IN_{-8}	R^2(P)	**0.73(<0.005)**	0.24(0.03)	**0.60(<0.005)**	0.25(0.03)	—	—
IN_{-12}	R^2(P)	—	0.24(0.03)	0.21(0.05)	—	—	—
IN_{-12} HS	R^2(P)	—	0.38(0.01)	0.37(0.01)	—	—	0.33(0.01)
IN_{-12} HL	R^2(P)	—	—	—	—	—	—
IN_{-15}	R^2(P)	—	—	—	—	—	—
IN_{-15} HS	R^2(P)	—	0.31(0.02)	0.27(0.03)	—	—	0.22(0.05)
IN_{-15} HL	R^2(P)	—	—	—	—	—	—

pogenic tracers, while HL INPs do not show any significant correlation with the classical chemical tracers measured here. At lower temperatures, INPtot do not correlate with any of the chemical compound, however, HS INPs show low correlations with SO_4^{2-}, Na^+, NH_4^+ and Ca^{2+} ($R^2 \approx 0.3$).

Hence, total and HL INPs in our study are linked with terrestrial and anthropological tracers (SO_4^{2-}, Oxalate, NH_4^+) above -12 °C. Those tracers are also linked, albeit less strongly, with HS INPs. Additionnally, HS INPs are linked to dust tracers (Ca^{2+}). These results indicate a strong influence from local terrestrial sources. Furthermore, both HL INP (at all temperatures) and HS INP (at colder temperature) at the PUY are weakly linked to marine tracers (NaCl). This indicates an influence from distant marine sources. INPs of marine origin are suspected to play an important role in cloud formation in the remote ocean environment (Wilson et al. 2015; DeMott et al. 2016; McCluskey et al. 2018c), but have never been shown to be important in continental areas where terrestrial sources are considered a major contribution (Burrows et al. 2013; Huang et al. 2021). Atlantic air masses represent about 40-50% of the air masses during the autumn and winter at PUY (Farah et al. 2018; Farah et al. 2021).

In order to determine whether these relationships are driven by submicron and supermicron aerosols we examined correlations with size segregated INP measurements.

IV.5.2 Size segregation

Correlations between the aerosol data (aerosol concentrations and surface) and respectively the submicronic INP dataset (INPsub) and the supermicronic INP dataset (INPsup) are shown in Tables IV.2 and C.1. The aim of this section is to compare the correlations observed for the total INP dataset (INPtot) and the size-segregated datasets in order to provide more insights on the sources of INPs at PUY.

Table IV.2 – Linear regression correlations coefficients and p-values (Pearson's test) between submicron INP concentrations at -8 °C, -12 °C and -15 °C (IN_{-8}, IN_{-12}, IN_{-15}) and aerosol parameters. Only significant ($P < 0.05$) correlations are indicated. Values with no significant correlations are indicated as double dashes. Values with $P < 0.005$ are indicated in bold.

		$N_{aer,tot}$	$N_{aer,500}$	S_{aer}	BC	Cl^-	NO_3^-	SO_4^{2-}
IN_{-8}	R^2(P)	0.30(0.03)	**0.57(<0.005)**	—	—	—	—	**0.48(<0.005)**
IN_{-12}	R^2(P)	0.38(0.01)	—	—	—	—	—	0.27(0.02)
IN_{-12} HS	R^2(P)	—	—	—	—	—	—	**0.59(<0.005)**
IN_{-12} HL	R^2(P)	—	—	—	—	—	—	—
IN_{-15}	R^2(P)	0.30(0.03)	—	—	—	—	—	0.22(0.04)
IN_{-15} HS	R^2(P)	—	—	—	—	—	—	**0.46(<0.005)**
IN_{-15} HL	R^2(P)	—	—	—	—	—	—	—

		Ox.	Na^+	NH_4^+	K^+	Mg^{2+}	Ca^{2+}
IN_{-8}	R^2(P)	**0.76(<0.005)**	—	**0.47(<0.005)**	**0.38(<0.005)**	0.28(0.02)	0.21(0.05)
IN_{-12}	R^2(P)	—	0.28(0.02)	0.28(0.02)	—	0.29(0.02)	0.31(0.01)
IN_{-12} HS	R^2(P)	0.30(0.02)	0.22(0.04)	**0.63(<0.005)**	**0.45(<0.005)**	**0.40(<0.005)**	**0.40(<0.005)**
IN_{-12} HL	R^2(P)	—	—	—	—	—	—
IN_{-15}	R^2(P)	—	—	0.24(0.03)	—	—	0.23(0.04)
IN_{-15} HS	R^2(P)	—	0.28(0.02)	**0.48(<0.005)**	**0.49(<0.005)**	0.24(0.03)	0.34(0.01)
IN_{-15} HL	R^2(P)	—	—	—	—	—	—

For HL INPsup at -15 °C (Table C.1) no correlation is observed with $N_{aer,tot}$, $N_{aer,500}$, or with S_{aer}. This is surprising in the case of $N_{aer,500}$ as it represents the large aerosols. However, the absence of significant correlations could be explained by the lack of supermicron aerosol number concentrations data over the period, as only half the data points were available.

At -8 °C, INPsub (Table IV.2) do not correlate as well with $N_{aer,tot}$ as INPtot ($R^2 = 0.21$ instead of $R^2 = 0.70$), but they show a better correlation to $N_{aer,500}$ ($R^2 = 0.47$ instead of 0.39). This would indicate that most submicron warm INP are measured when the high fractions of submicron aerosols larger than 500 nm are present in the sampled airmass.

Table IV.2 shows that INPsub correlate across the whole temperature spectrum with a different range of chemical parameters than the full INP data set. Among the marine tracers of supermicronic origin (Cl^-, NO_3^- and Na^+) only Na^+ correlate with total and HS INPs at -12 and -15 °C ($R^2 < 0.3$). Tracers of anthropogenic activities (NO_3^-, SO_4^{2-}) correlate with all INP classes and temper-

atures, except for HL INPs at -12 and -15 °C. Tracers of dust-based aerosols (K^+, Mg^{2+} and Ca^{2+}) show correlations in the range of 0.2 to 0.4 all over the data set, with higher values for HS INPs, which is consistent with dust-based INPs being non-biological.

However, despite contributing higher number concentrations, supermicronic INP (Table C.1), only show low correlations between the heat stable fraction at -15 °C and NO_3^-, Na^+ and Mg^{2+}.

These results show that INPs at PUY have diverse origins, with influences from various anthropogenic, terrestrial, marine and dust sources. The lack of correlation observed with aerosol surface area confirms that even if there are some chemical relationships, the main correlations are driven by aerosol number concentrations. The best correlations were found with anthropogenic and terrestrial tracers, especially at temperatures >-12 °C. Marine tracers exhibit weak correlations (R^2=0.2–0.3) with a large part of the INP data set, hinting at an influence from distant marine sources. This is consistent with other observations that have shown that marine INPs were a lot less important than dust INPs over continental areas (DeMott et al. 2010a; Burrows et al. 2013; Gong et al. 2020).

More physical, chemical or biological data coupled with intensive INP measurements would be needed in order to have a better understanding of the influence of the chemical and physical composition of INPs at PUY. In particular, being able to better differentiate the potential sources with reduced sampling periods would be of great help.

IV.6 Parameterization

IV.6.1 Overview of past works

Studies focusing on the impact of INPs on climate and precipitations relied either on very simplified parameterizations, or by theorizing relations between particle type and IN properties (DeMott et al. 2010a). Kanji et al. (2017), provide an in depth description of the different types of parameterizations that have been developed in the past.

Specifically, parameterizations are divided in two types: a time-dependent approach (stochastic effects), such as the time-dependent freezing rate model (Vali et al. 2015b); and a time-independent approach, which supposes that ice nucleation activity depends only on temperature or aerosol properties such as number concentration (deterministic effects). It has been suggested that the time dependence effects are less important than temperature or aerosol properties dependence (Langham et al. 1958; Vali 2014). The parameterizations we will consider here are of time-independent nature, such as Meyers (1992), which depends only on temperature, or DeMott et al. (2010a) and DeMott et al. (2015) which depend on temperature and particle concentrations.

Meyers (1992) (henceforth M92) proposed a simple parameterization of the

form:

$$n_{INP} = \exp\Big(a + b[273.15 - T_C]\Big), \tag{IV.2}$$

where n_{INP} is the predicted number of INPs and T_C the temperature of the cloud in °C.

Based on a global observational data set from CFDC measurements, DeMott et al. (2010a) showed that, at temperatures colder than -20 °C and for dust INPs, the number of INP was also a function of a power law of the number of aerosols with diameters greater than 500 nm ($N_{aer,500}$)). They proposed a parameterization (henceforth D10) of the form:

$$n_{INP} = a(273.15 - gT_K)^b \cdot N_{aer,500}^{c(273.15-T_K)+d}, \tag{IV.3}$$

with a = 0.0000594, b = 3.33, c = 0.0264, d = 0.0033 and T_K the cloud temperature in K.

Tobo et al. (2013) also proposed a parameterization based on $N_{aer,500}$, but taking into account the number of fluorescent biological aerosol particles. This parameterization has been further modified in DeMott et al. (2015) (henceforth D15) as:

$$n_{INP} = (\mathrm{cf})N_{aer,500} \cdot \alpha^{(273.15-T_K)+\beta} \cdot \exp\Big(\gamma[273.15 - T_K] + \delta\Big), \tag{IV.4}$$

with cf = 1, α= 0, β= 1.25, γ= 0.46, δ= -11.6.

Niemand et al. (2012) developed a parameterization (henceforth N12) for immersion freezing of desert dust particles based on the surface site density of INP (n_S, in INP/m^2) formulated as:

$$n_S = \exp\Big(0.517[T_K - 273.15] + 8.934\Big). \tag{IV.5}$$

Wex et al. (2015) developed a parameterization (henceforth W15) aimed for predicting biological INPs, using Snomax© as a reference, and calculating surface site density n_S. Snomax© is an artificially-made aerosol based on the proteins of natural bacteria that act as ice nucleation initiators. The n_S predicted by W15 is as follows:

$$n_S = \frac{(1.4 \times 10^{12})\Big[1 - \exp(-2.00 \times 10^{-10})\exp(-2.34 \times T)\Big]}{\text{geometric SSA}_{\text{Snowmax}}}, \tag{IV.6}$$

with a value of 7.99 m^2.g^{-1} for geometric SSA of Snomax©, which is taken from AIDA measurements in Hiranuma et al. (2019).

In Figure IV.6, the five parameterizations described above (M92, W15, , D10 and D15) are used to predict INP concentrations from aerosol properties measured during the campaign, and plotted against INP concentrations measured at the corresponding time, for temperatures between -4 and -18 °C.

Figure IV.6 illustrates a large spread in predictions across all parameterizations, spanning over 6 orders of magnitude for a given range of INP concen-

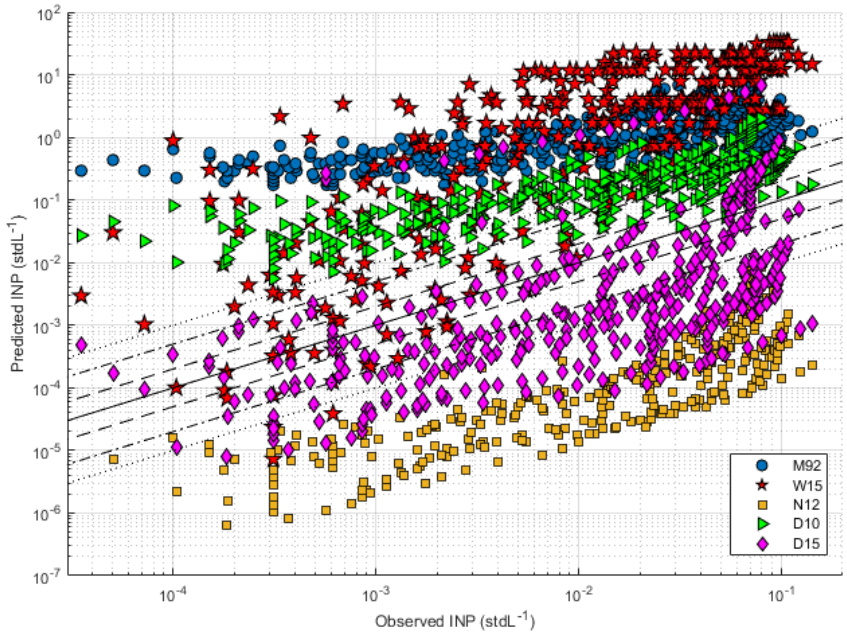

Figure IV.6 – A set of parameterizations applied to the WINS data : M92 - blue circles ; W15 - red stars ; N12 - orange squares ; D10 - green triangles ; D15 - pink diamonds. The solid line, dashed lines, dash-dotted lines and dotted lines represent respectively the 1:1 ratio line, the 1:2 ratio lines, the 1:5 ratio lines and the 1:10 ratio lines.

trations. We calculate that only 0% to 7% of the measurements are predicted within a factor of 2, 0% to 21% are predicted within a factor of 5, and 3% to 38% are predicted within a factor of 10. The best agreement is observed for D10 and D15, and the worst for M92 and W15. These results can be explained by 1) D10 and D15 were calculated through global INP data combined from several field studies in various environments, and, even though these parameterizations are oriented towards temperatures below -20 °C and dust INPs, this results in a better estimation in INP concentrations; 2) M92 only depends on temperature, and does not take into account the number of aerosols, which leads to an underestimating of INP concentrations; 3) W15 is calculated from Snomax©, which is derived from *P. syringae* bacteria: even though our data shows a high number of biological INP, this bacteria might only be one of the many biogenic INPs in our study. This could also suggest that pure bacteria species may have very high INP properties, but when exposed to atmospheric aging and evolution, (and hence mixed with other aerosol species), these INP properties are decreased.

One drawback of the D15 and the D10 is that they are optimized from measurements with a continuous flow diffusion chamber with operating temperatures lower than -20 °C. Therefore, they are weakly constrained for temperatures warmer than -20 °C. Furthermore, because they consider only larger aerosols at lower temperatures, the D10 and D15 parameterizations implicitly tend to consider only mineral dust. As a result of the simplicity of this parameterizations, and of the widespread availability of aerosol number concentra-

tions, a number of studies have optimised this parameterizations for their data, corresponding to specific environments. For example, Schneider et al. (2021) worked from D15 in order to derive parameterizations coefficients predicting INPs in a boreal forest, an environment rich in biological aerosols. They reported an agreement of about 90 to 99% (80 to 95% and 41 to 57%) within a factor of 10 (5 and 2) was reported between the observations and predictions, depending on the season.

In the following section, we use the INP measurements presented in this work to optimise the previous parameterizations (D15), for temperatures higher than -20 °C . This new parameterizations was evaluated against two independent datasets.

IV.6.2 Development of a new parameterizations

The WINS data set was chosen for deriving the parameters as it contains the highest number of data points available (754 points, reduced to 377 points when averaging the INP data over 0.5 °C), and covers 6 months of continuous measurements with INP activation temperatures varying from -5 °C to -18 °C. In addition, size segregated INP filters were collected during this measurement period, which allows further analysis of the INP size distribution. We then chose the PICNIC dataset as well as the data set from MSA as independent data sets to test the newly derived parameterizations (660 points, reduced to 330 points when averaging over 0.5 °C).

The starting point for the development of this new parameterizations was D15, despite better agreement between measured and predicted data for D10 than for D15 (Fig. IV.6), it was easier to work from D15 to achieve better INP prediction. Rather than using aerosol number concentration $N_{aer,500}$) as the aerosol variable, we instead used $N_{aer,tot}$, as we showed previously that it had better significant (Pearson test p-value <0.05) correlations across the whole INP spectra than all other parameters investigated in this study.

Further investigations on the relationship between $N_{aer,tot}$ and the INP concentrations at each temperature are shown in Figure IV.7, more specifically with $\log(N_{aer,tot})$. We found the best fit is linear at a given temperature. For this reason, we chose to replace the $N_{aer,500}$ power law from D15, that is also dependent on temperature, with a linear function only dependent on $\log(N_{aer,tot})$. The final set of parameters was calculated using a Markov chain Monte Carlo algorithm. Thus the equation of the new parameterizations is :

$$n_{INP}(T, N_{aer,tot}) = a \cdot (\log N_{aer,tot} + b) \exp(c[d - T_C]), \tag{IV.7}$$

where a = 0.0489; b = -0.2349; c = 0.4293; d = -6.6477; T_C the cloud temperature in Celsius and n_{INP} the number of INP per liter of air.

In Figure IV.8, we plot the predicted data against the observed data, for our parameterizations (referred to as B22) and for D10 and D15. Up to 57.3% of points predicted by our model falls within a factor of 2 of the observed data (RG2), versus 8.3% for D15 and 3.3% for D10. A total of 87.7% of points were

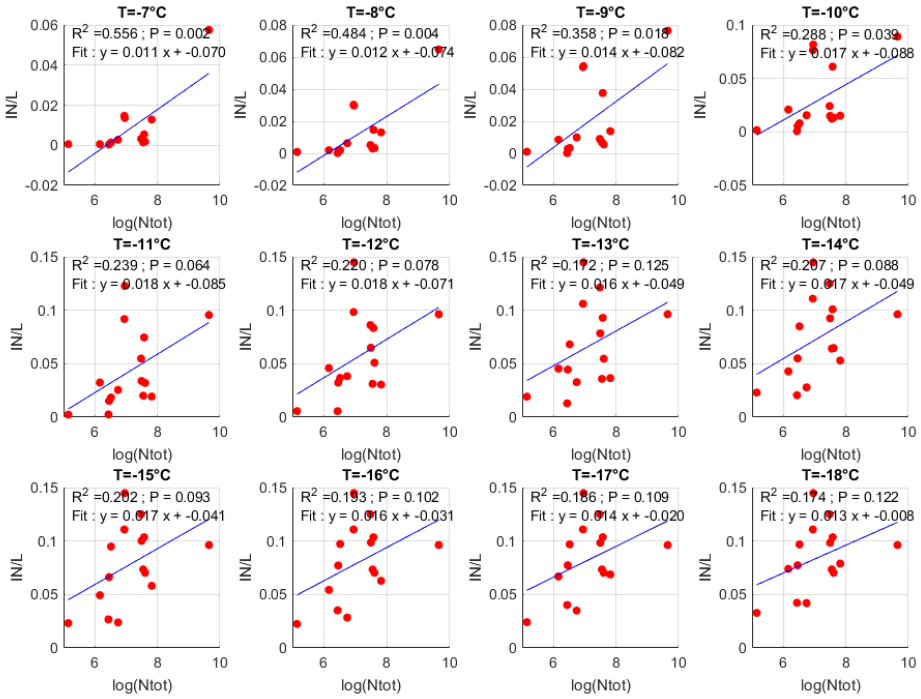

Figure IV.7 – Scatter plots and linear regression fits for INP concentrations against $\log(N_{aer,tot})$. The INP data are averaged over 1°C.

predicted within a factor of 5 (RG5), versus 24.2% for D15 and D10, and 98.0% of points were predicted within a factor of 10 (RG10), versus 39.7% for D15 and 50.3% for D10. Highest discrepancies were observed for highest INP concentrations, with an average underestimated by the parameterization for high to intermediate temperatures (-6 °C to -12 °C) and overestimated for low temperatures (below -15 °C), this is opposite to what we observe for the D10 and D15 parameterization.

This indicates that in some circumstances, factors other than the aerosol number concentration can play an important role for predicting INP concentrations, such as the nature of the particles acting as INP, as shown by the link between aerosol chemistry and INP concentrations discussed Section IV.5. It is important to consider that a large variability is associated with measurements made at temperatures above -12 °C. However, we did not manage to reach better agreements between predicted and observed values using any of the chemical parameters. These results show that taking into account the total aerosol number concentration yields better predictions than when only larger particles like D10 and D15.

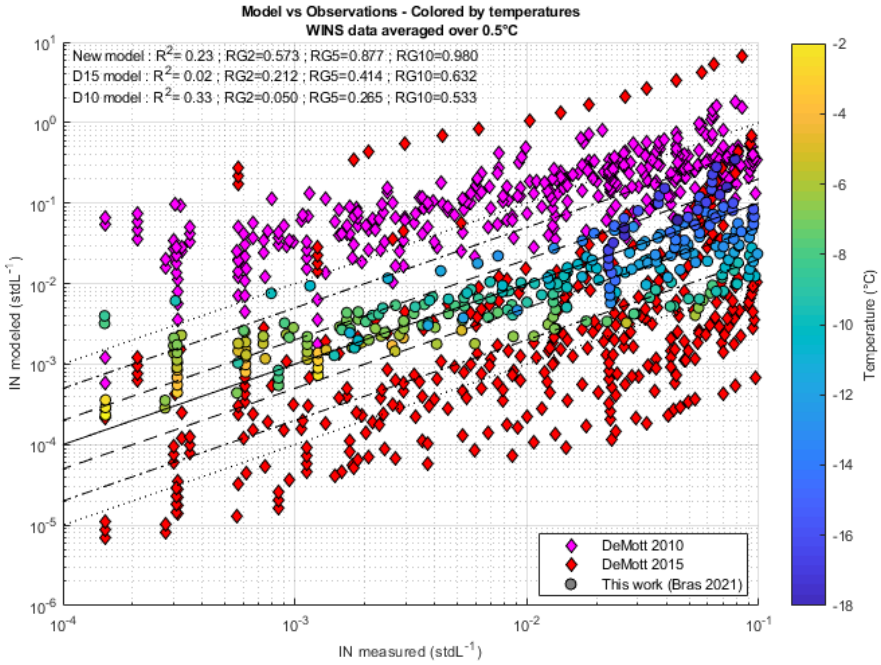

Figure IV.8 – New parameterization from this work (B22) compared to D10 (pink diamonds) and D15 (red diamonds) using the data from WINS. The solid line, dashed lines, dash-dotted lines and dotted lines represent respectively the 1:1 ratio line, the 1:2 ratio lines, the 1:5 ratio lines and the 1:10 ratio lines.

IV.6.3 Application on other sites

Two independent data sets were combined and used together to test the B22 parameterizations: the data from the PICNIC campaign at the PUY station, and the data from the MSA site from the Pan-European IN sampling campaign. MSA is a similar site to PUY in terms of altitude, and the availability of the aerosol data during the sampling period allowed us to test the B22 parameterization. MSA INP freezing spectra are similar to that of the PUY measurements, with similar freezing onsets between -4 °C and -6 °C, and concentrations ranging between 10^{-4} and 10^{-1} INP/stdL (Figure C.5). The lower freezing temperatures observed are between -14 °C and -16 °C. MSA is continental background altitude site, and as such is similar to PUY. Results show the good ability of the B22 parameterizations to predict INP concentrations, with 38.7% of the INP concentrations predicted within a factor 2, 86.4% within a factor 5 and 92.8% within a factor 10.

Predicted data for PICNIC are more often underestimated, especially at higher measured concentrations (10^{-2} to 10^{-1} INP/stdL), while for MSA they are more often overestimated at lower concentrations (about 10^{-3} INP/stdL). It is unsure of why there are such differences, as both sites exhibit roughly the same INP concentrations (10^{-3} to 10^{-1} INP/stdL), freezing temperatures (-5 to -15 °C) and aerosol concentrations (300 to 3000 cm^{-3}).

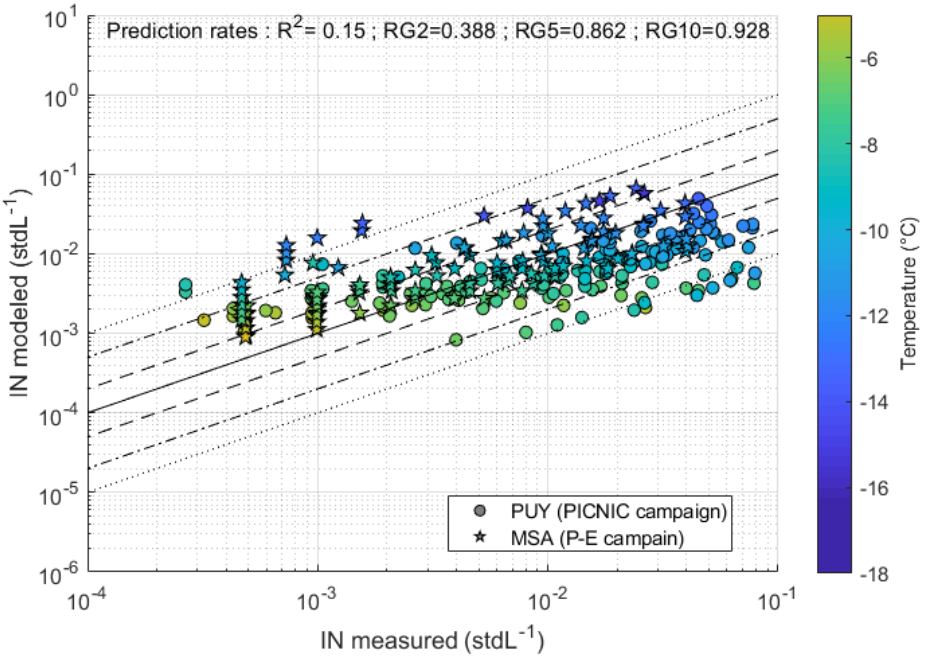

Figure IV.9 – Verification of the new parameterization using the PICNIC and MSA data sets

IV.7 Conclusions

Diurnal INP measurements were taken during the PICNIC measurement campaign at the observation station at Puy de Dôme in Central France during October 2018. This was followed by the collection of weekly size-segregated INP samples from November 2018 to May 2019 (WINS). These filter samples were extracted into 0.9% NaCl water and were then analyzed using the immersion freezing apparatus LINDA to determine the concentration of INP as a function of temperature. For each filter sample extracted a fraction of the solution underwent heat treatment to obtain information on the contribution of biological material to INP concentration.

We report INP concentrations between -5 °C and -18 °C and a freezing onset of -4 to -6 °C, which are relatively high temperatures in the case of ice nucleation, and have rarely been reported. The observed concentrations are in the range of other measurements from the literature at similar sites and temperatures (Mason et al. 2016; Kanji et al. 2017). Above -10 °C, we observe that more than 80% of the INPs are heat-labile, and thus potentially of biological origin. But at colder temperatures, the ratio of heat labile INPs to total INPs is still high, with biological INPs representing from 40% at -14 °C to 20% at -16 °C to -18 °C of the total INP concentration. Two other studies on INPs of biological origin in cloud water and precipitations that took place at PUY (Joly et al. 2014; Pouzet et al. 2017) have reported ratios of about 100% of biological INP at -8 °C, to 77% at -12 °C, which is much higher than in the aerosol phase in our study. Similar biological fractions are also reported at other mountain sites

in snow (Hill et al. 2014) or rain water (Lu et al. 2016), and in other studies in rural (Garcia et al. 2012) or forest sites (Schneider et al. 2021).

Size-segregated data (submicronic and supermicronic INPs) were also analysed, and in agreement with previous studies we show that supermicronic INPs roughly constituted two thirds of the total INP number. Biological INPs were also slightly less abundant in the supermicron mode than in the submicron mode. Similar to the seasonal variations in aerosol concentrations, INP concentrations (both heat labile and heat stable), and sub and supermicronic) had lowest concentrations in winter and highest in autumn and spring. The seasonal variation of aerosol concentrations were reported to be significantly influenced by the seasonal variation of the boundary layer height, reaching the site more often during the warmer seasons than during winter. The INP concentrations seem to also follow this trend. In addition, snow cover and a decrease in vegetation coverage near the site likely contributed to the higher ratio of non-biological INPs to total INPs observed in winter.

In order to characterize the origin of INPs in our study and to determine the best parameters for deriving a predictive parameterization based on our data set, correlations were calculated between INP data (all INPs, heat labile INPs and heat stable INPs) at three temperatures, roughly representative of the different regimes (biological, mixed and non-biological) of our data set, and different physical (aerosol numbers and surface concentration) and chemical parameters. In general, significant correlations were measured for INPs at temperatures >-15 °C. We most notably observed that INPs across all temperatures showed consistently significant correlations with $N_{aer,tot}$. We highlight strong links with anthropological and terrestrial tracers (SO_4^{2-}, NH_4^+, Oxalate). Tracers of marine aerosols (Cl^-, Na^+, NO_3^-) showed weak correlations with INP concentrations, which hints at a potential influence of marine aerosols on the IN activity at PUY.

Correlations with the size-segregated data were also computed. Supermicronic INP did not show significant correlations with any of the studied parameters, while submicronic INPs showed similar significant correlations with the physical variables than the whole data set. Showing that these relationships are driven principally by aerosol number concentration. Intermediate correlations were also found with marine, dust and anthropogenic tracers for submicronic INPs, which further hints at various possible sources of INPs at PUY.

On the basis of the relationship between INP and the variable $N_{aer,tot}$, the WINS data set was used to develop a new parameterization. The total number concentration of aerosols is a widely available parameter in most studies and observation stations, making it easy to use it as a parameter for predicting INP concentrations. This parameterization is optimized for warmer temperatures above -20°C, which are in general dominated by biological activity. This parameterization has been successfully tested on two other similar data sets, one from the PICNIC campaign, and one from Montsec d'Ares (MSA) during the Pan-European INP measurement campaign in 2018. Our parameterization is optimised for warmer temperatures and subsequently is better adapted

for offline measurements than existing parameterizations D15 or D10 that use aerosol number concentrations or surface.

This study provides INP data and analysis from a remote altitude site which is influenced by long range air masses, and shows that biological INP are of primary importance in such sites. In understanding the interactions between aerosols and clouds, it is critical to correctly assess and predict the concentrations of INPs around the globe. Future research activities should focus on performing both long term and size-segregated INP measurements. This information would provide a better link to the INP seasonal variability to local atmospheric properties, and to better characterize dominant sources to INP activity. Additionally, parallel measurements of biological aerosols would assist in better characterizing the link between aerosol biological content and its INP activity. In particular, being able to better differentiate the potential sources of INPs, and thus sampling INPs with higher time resolutions could assist in understanding those links.

IV.8 Acknowledgements

This research received funding from the European Commission under the Horizon 2020 –Research and Innovation Framework Program via the ACTRIS-2 Trans-National Access, and from the ANR-CHAIN (ANR 14-CE01-0003 -01). The authors gratefully acknowledge CNRS-INSU for supporting measurements performed at the SI-COPDD, and those within the long-term monitoring aerosol program SNO-CLAP, both of which are components of the ACTRIS French Research Infrastructure, and whose data is hosted at the AERIS data center (https://www.aeris-data.fr/).

V

General conclusion

Outline of the current chapter

Atmospheric ice nucleation has been observed and studied since the beginning of the 20th century, with the observations of Alfred Wegener, Tor Bergeron and Walter Findeisen, but it has gained more attention in the last decade (DeMott et al. 2011). A focus has been placed on identifying the major INP activation processes, their sources and the different atmospheric variables influencing their concentrations and activity. Several predictors have been identified to calculate INP abundances for incorporation into global models, a process that in light of the latest IPCC report (Masson-Delmotte et al. 2021), has become increasingly important in order to enhance our understanding of climate processes and climate change.

This renewed interest in INP studies has prompted the evolution of sampling techniques, allowing both online and offline characterization of ice nucleating particles from -2 to -38 °C and therefore identifying the dependence of IN formation on different aerosol types. The number of field campaigns all over the globe has also seen a steady increase, allowing the retrieval of INP concentrations in various environments, especially in remote locations. This includes mountainous and marine regions, where field campaigns are in general harder to organize due the inaccessibility of such sites.

Biogenic particles have been identified as a key contributor at mixed-phase clouds conditions ($T > -20$ °C). This is especially the case in marine regions, where the impact of ocean activity on the atmosphere is still largely unknown. The influence of atmospheric transport and aging on the IN properties of the ambient aerosols is another uncertainty in ice nucleation research. In order to answer these questions, the work presented in this manuscript includes measurements collected during two cruise campaigns in the Southern Ocean and on two high-altitude mountain sites, with a long term dataset collected at the Puy de Dôme site, a mountainous observation station, during a ACTRIS TNA field campaign organised in 2018.

This final chapter aims to present the summary of the main results obtained and the perspectives of this work.

V.1 Ice nucleating particles in the seawater and sea spray in the Southern Hemisphere

The first half of this thesis focused on characterizing INP populations in the Southern Hemisphere waters sampled during two cruise campaigns: One in tropical waters near the Tonga volcanic arc (TNG cruise), and the other in poor oligotrophic waters south of New Zealand (S2C cruise). Samples of seawater and sea spray aerosols were collected daily during both campaigns and analyzed for INPs in immersion freezing conditions.

In both seawater and sea spray, INPs were measured between -5 and -18 °C. The concentrations of SSA and SW INPs measured in both campaigns were lower than in other studies in different marine environments, and of the same order of magnitude than an other study in the Southern Ocean. In both cam-

paigns, we observed differences in INP concentrations in contrasted ocean conditions, with notably higher concentrations in tropical and subtropical waters compared to subantarctic waters. It is possible that there is a latitudinal gradient in INP concentrations in the seawater that should be investigated by merging data sets that have been acquired from different ship campaigns.

Heat labile INPs were dominant at most temperatures for both campaigns, highlighting a strong influence from biogenic material on the IN properties in the seawater and in the sea spray. The best correlations between INP in the seawater and biological tracers were observed in general with organic matter, bacteria and photosynthetic pigments.

Utilizing the strong link observed between SML and SSA INPs, we developed a parameterization with the S2C dataset that aims to represent 1) the link between SW INPs and a SW TOC, 2) the transfer of SW INPs to SML INPs and 3) the transfer of SML INPs to SSA INPs. The resulting equation allows to predict SSA INPs as a function of SW TOC. This parameterization performs better than another parameterization of SSA INPs (McCluskey et al. 2018c), and we show that tropical SSA INPs were in general underpredicted in comparison to the other types of water, thus further suggesting different behaviors for INPs in function of watermasses. Hence we suggest that INP should be predicted first in seawater, with parameterizations specific for given seawater types. The transfer from INP concentrations in the seawater to SSA can be calculated based on the relationship we calculated from the S2C data, which are among the first to gather at the same time INP concentrations in the SW, in the SML, and in the SSA. Our parameterization aims to be implemented in a meso-scale study in the Southern Ocean, with the goal of comparing model predictions of ice content in clouds with the radar observations from the S2C cruise campaign.

Although we succeeded in providing parameterizations that should help providing better predictions of INP concentrations emitted in the marine atmosphere of the oceans of the southern hemisphere, our work confirms that there are several types of INP that necessarily have different biological sources in the seawater and/or a different transfer mechanism from seawater to SSA. It is likely that at least two populations of INP coexist in the seawater: one linked to the particulate carbon, which is a "fresh" form of organic matter; and one linked to the dissolved organic carbon, known to be more processed. Also, the submicron INPs have different features than the supermicron INP that could be linked to the emission of SSA as film drops or jet drops. In order to further separate the different marine INP sources and their specific links to biogenic variables, a few recommendations can be provided for future marine studies:

- More collocated SW/SML/SSA samples, with enough sample points to conduct a thorough statistical analysis, would be a great asset in the future. Indeed, both campaigns showed that small datasets limits our understanding of those links.

- McCluskey et al. (2018b) hypothesized that 0.2 µm was a cut-off size for differentiating marine INP types (DOC or POC type). We were not able

to provide INP concentrations at these sizes for our studies, which would have been helpful for characterizing the INP populations. Thus, we recommend taking into account this size of 0.2 µm when sampling INPs in marine environments, for example by filtering.

- An additional segregation tool for INPs could also be used for future studies: hydrogen peroxyde (H_2O_2) treatment would be a great addition to the heat treatment for the analysis of INP samples with LINDA. This would allow the retrieval of the concentrations of organic INPs. This procedure has been used in other studies (e.g. McCluskey et al. 2018b) and is an other tool for assessing the nature of the INPs in a given sample or environment. Although this would greatly increase the analysis times, we recommend adding this treatment to future INP studies. This is especially the case for marine INPs, but this could also be used in continental INPs studies.

- One caveat of ship-based experiments is a lack of hindsight and reproducibility, due to the nature of the measurements. Thus, it can be difficult to make conclusions based on individual studies. Over the last 5 years, a number of field and cruise campaigns have taken place, in the Arctic (Nicosia 2018), in the Mediterranean (Trueblood et al. 2021), and in the Southern Ocean. This represents a consequent dataset spanning the extreme regions of the globe and merits a dedicated analysis of all measurements combined, which would thus reduce the uncertainty from individual studies, and allow us to paint a broader picture of the links between the ocean properties and the ice nucleating activity in the atmosphere.

V.2 Continental ice nucleating particles in ambient air at a mountainous site

In order to understand the effect of atmospheric transport and aging on the IN properties of the aerosols, we measured INP concentrations at a continental site that is influenced by different air masses types. Two consecutive field campaigns took place at the Puy de Dôme observatory (PUY, 1465 m a.s.l.) in Central France (Baray et al. 2020). As part of the PICNIC campaign which took place in October 2018, we collected high volume filter samples twice a day. After PICNIC, we collected weekly size-segregated filter samples at PUY over a six months period.

We observed INP activation between -5 and -18 °C, with concentrations of about 0.001 INP/L_{air} at the warmest temperatures, and between 0.01 and 0.1 INP/L_{air} at the coldest temperatures. This is consistent with other studies at similar temperatures (Huang et al. 2021). We also observed a majority of heat labile, potentially biogenic INPs at temperatures > −12 °C, and a ratio of heat labile INPs above 80% at temperatures > −10 °C. Size segregation revealed that supermicron INPs consisted of about two thirds of the total INP concentrations.

INP concentrations at all temperatures were at a minimum in winter and at a maximum in autumn and spring. Lower ratios of biogenic INPs were observed in the winter, explained by a decrease in vegetation cover and biogenic aerosols emissions. Statistical analysis revealed strong links with local terrestrial sources (SO_4^{2-}, NH_4^+), but also with distant marine (Na^+) and desert (K^+, Ca^{2+}) sources, showing that INPs at PUY are originating from various backgrounds.

INP concentrations are also strongly correlated to the total number of aerosols. We used this relationship to develop a new parameterization for predicting INPs at temperatures relevant for mixed-phase clouds and dominated by biological INPs. The total number of aerosols is a common measurement in most studies and observation sites, making it simple to employ as a predictor of INP concentrations in the remote continental atmosphere where a large variety of sources are mixed and aerosol are known to be aged since their emission. We show that this parameterization is more efficient than other past works for the environment of Puy de Dôme. This parameterization has also been evaluated on two separate data sets from continental high altitude sites with similar features to Puy de Dôme.

The PUY station is an interesting location to study the atmosphere, and it has been recognized as so since about 150 years, receiving the label as world observatory site from the GAW network (Baray et al. 2020). However, ice nucleation experimentations are quite recent in this location, with a study in low altitude clouds (Joly et al. 2014), a long-term study in cloud water and precipitations (Pouzet et al. 2017), and more recently the larger scale PICNIC experiment, which intended to intercompare INP measurement techniques. Thus, we have only scratched the surface on INP studies at PUY. We propose here a list of recommendations and perspectives on this subject:

- Since 2004, weekly high-volume filter samples (similar to those used for PICNIC) have been collected and stored at LaMP[1]. These filters are used for the analysis of several parameters, but the remainder of the filters are stored and are available for analysis by new and evolving techniques. Combined with the instrumental array at PUY, these filters provide a powerful opportunity to have an insight on long-term INP variations at the PUY station. The measured INP concentrations can be compared to the collocated measurements at the Puy de Dome (Baray et al. 2020) to provide a consequent dataset of INP properties and their variability with different atmospheric parameters.

- In addition to those offline, long term measurements, a new CFDC is being built at the laboratory. This online instrument will eventually be deployed at PUY for studying INP activity at colder temperatures, thus expanding the temperature spectrum at which the LINDA operates. Again, coupled with the extensive instrumentation of the station, this would provide an valuable insight into ice nucleation at PUY. This work will be accompanied by similar objectives in the framework of the ANR EQUIPEX

[1] Laboratoire de Météorologie Physique, Aubière, France

Obs4Clim project where the Puy de Dôme site can potentially become a reference site for atmospheric ice nucleation measurements in France.

- More generally, including regular or online measurements of the biological fraction of the aerosol in parallel to regular INP measurements would help to constrain the contribution of biological aerosol to IN activity. For example, a Wideband Integrated Bioaerosol Sensor (WIBS) has been deployed the past 2 years at PUY. This instrument is able to monitor in real-time the concentrations of bioaerosols. This instrument could be a great asset in investigating the ice nucleating activity of bioaerosols, coupled with on-line INP measurement techniques, like CFDCs.

V.3 General discussion and perspectives

As a closure on this thesis, we show in Figure V.1 a comparison of the surface site densities n_S of the INPs measured in Chapters III and IV, and observations data and two fits from past studies. Our observations include the ambient atmospheric n_S measured at PUY during PICNIC and WINS, the generated SSA n_S measured during TNG and S2C and the ambient SSA n_S measured during the S2C. Literature data include ambient SSA n_S measured at Mace Head Research Station (McCluskey et al. 2018c), desert dust dominated aerosol n_S measured in the Tropical Atlantic (Price et al. 2018) and desert dust n_S measured during controlled experiments at the AIDA in Karlsruhe (Ullrich et al. 2017). The fits used in Fig. V.1 are both of the form $n_S(T) = \exp a \cdot T + b$, and are respectively derived for desert dust aerosols (Niemand et al. 2012) and pristine North Atlantic SSA (Mace Head Station,McCluskey et al. 2018c). The choice to use n_S data, which are normalized data instead of absolute INP concentrations, results from the need to be able to compare ambient air concentrations with artificially generated aerosol concentrations. This choice limits the number of available data we can use as comparison from the literature, but gives an other general view than the one published by Kanji et al. (2017).

This comparison shows that, like INP concentrations per volume of air (Kanji et al. 2017), surface site densities can span several orders of magnitude at a given temperature in the atmosphere. Marine n_S are about 4 orders of magnitude lower than terrestrial or dust-based n_S at all temperatures, but we also observe that Southern Hemisphere marine n_S are lower than Northern Hemisphere n_S (McCluskey et al. 2018c in the North Atlantic). Furthermore, we note that in the Southern Ocean ambient SSA n_S are even lower than generated SSA n_S, hinting at atmospheric processes during aging that further reduce the INA of SSA.

Our measurements of continental n_S are lower than those of dust aerosol in a controlled environment (Ullrich et al. 2017). They were also closer, although lower, than those measured in a dust dominated natural atmosphere (Price et al. 2018). These observations illustrate the effect of mixing and transport on the

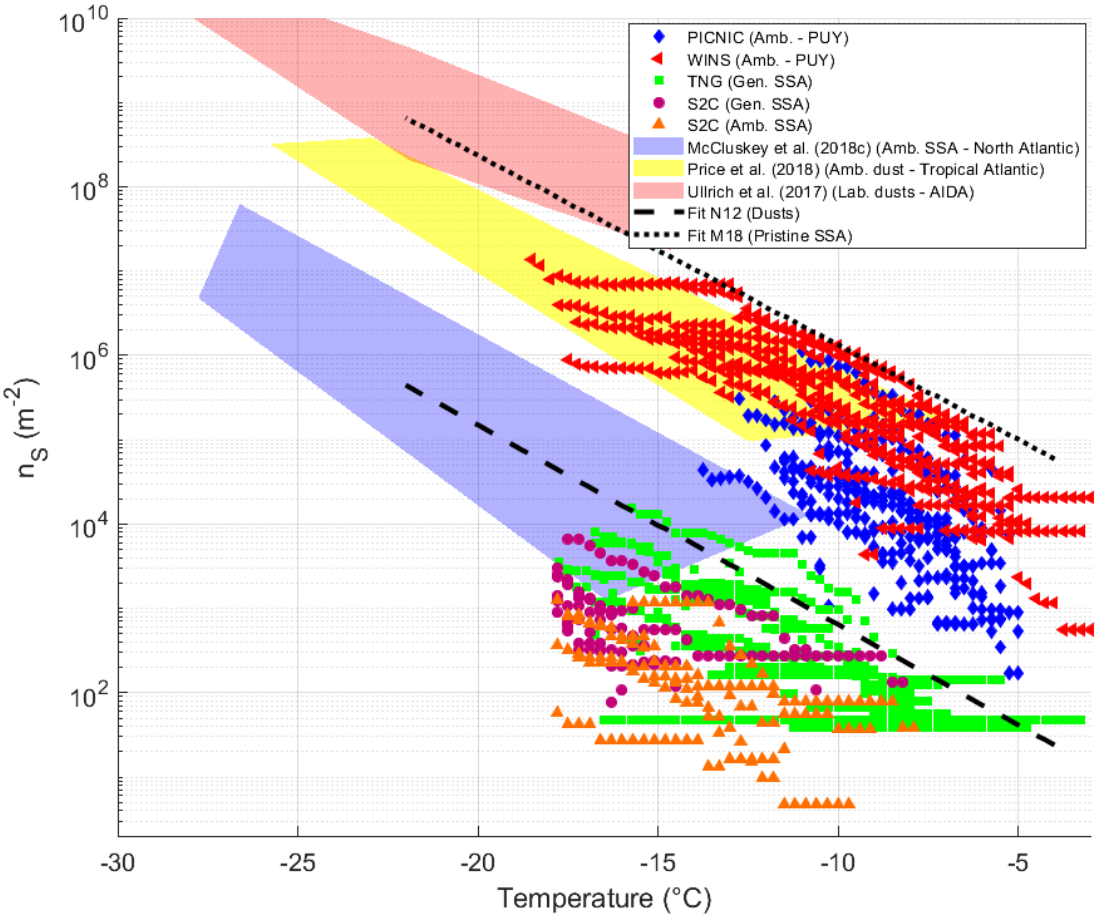

Figure V.1 – Comparison of observations of ambient and SSA n_S in this thesis (colored markers) with past works: Colored areas represent observations in other studies (blue: McCluskey et al. (2018c); yellow: Price et al. (2018); red: Ullrich et al. (2017)), lines represent two fits (dashed line: Niemand et al. (2012) - N12; dotted line: McCluskey et al. (2018c) - M18).

IN properties at a site influenced by a variety of air masses, resulting in "averaged" n_S properties.

During this thesis, we showed the potential influence of marine INPs even over land, but it was not possible to separate marine aerosols from other types of aerosols in order to study how their IN properties are modified during transport over land. We list here ideas on how to investigate the effect of transport and mixing on the properties of INPs, specifically the impact of aged SSA in the remote ocean at warm temperatures ($T > -20$ °C):

- Study aging effects in controlled conditions in the laboratory, e.g. with controlled atmospheric chambers or by treating sample filters before droplet freezing analysis.
- Aircraft studies in the remote oceans, using high-volume filters in order to have high enough concentrations at warm temperatures for offline analysis. This could be coupled with a particle concentrator (Gute et al. 2019).

- In a similar manner than the PUY site, using an mountainous site for FT measurements in an ocean dominated region would allow us to limit the influence of terrestrial aerosols on the INP population, and thus to only measure ambient aged marine aerosols. One such station could be the Maïdo Observatory, located 2200 m a.s.l in La Réunion Island in the Indian Ocean (Baray et al. 2013). Like PUY, this monitoring station is equipped with a wide array of instruments for atmospheric sampling and aerosol characterization. Long term measurements at such station would offer a strong insight on the influence of aged marine SSA INPs in the atmosphere in a region that is less affected by terrestrial aerosols than PUY.

A

Suplementary: TNG cruise

Outline of the current chapter

A.1 Seawater parameters

A.1.1 Explanation on the biological measured during TNG and S2C

Various microorganisms were measured during the campaign, and their names and nature may be confusing, thus were give her a brief description of each of them, using Castellani et al. (2017).

- *Heterotrophic bacteria* are unicellular microorganisms that feed on other bacteria or dissolved carbon (hence the qualification "heterotrophic", literally "which feeds on others"). While feeding, they participate in breaking of cells and releasing primary carbon in the seawater.
- *Cyanobacteria* are unicellular microorganisms that feed on light using photosynthesic pigments such as chlorophyll-a. They are thus phototrophic organisms. Examples of cyanobacteria measured in S2C and TNG include *Synechococcus* and *Prochlorococcus*, which are both smaller than 2 µm. Both of them are very widespread in marine environments, and They are responsible for a significant part of photosynthesis and oxygen generation in the oceans and across the earth. Other types of cyanobacteria include *diazotrophs*, bacteria that also consume nitrogen, such as UCYN-A, UCYN-B and UCYN-C that were measured during the TNG cruise.
- Phytoplanktons are microscopic photosynthetic algae. Like cyanobacteria, they play a huge role in the production of oxygen on Earth. The most prominent examples of phytoplanktons from both campaigns are *nanophytoplanktons* (2-20 µm) and picophytoplanktons (<2 µm). Flagellates, dinoflafellates and diatoms are also phytoplanktons.

A.1.2 Figures and statistics

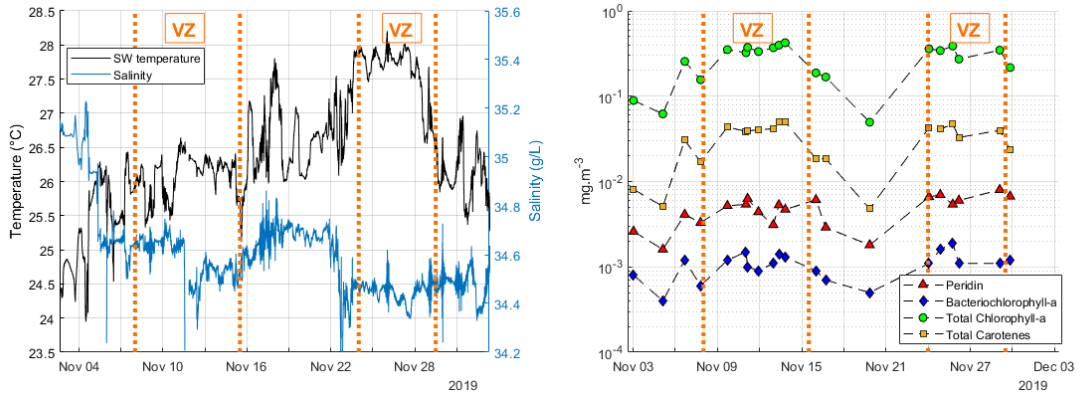

(a) Water temperature and Salinity

(b) Pigments

Figure A.1 – Time series of parameters from Table III.3 - Part 1 : Other parameters. a) Water temperature and salinity; b) Pigments concentrations (Peridinin, Bacteriochlorophyll-a, Chlorophyll-a, sum of carotenes). Orange dotted lines and VZ labels mark the limits of the Volcanic Zone.

Table A.1 – Summary of statistics of the parameters from Table III.3 from the whole cruise (black text), the Volcano Zone (orange text) and the Oligotrophic Zone (blue text). Statistics include the mean, the standard deviation (written as mean ± stddev), the maximum and the minimum of each parameter.

	All cruise			**Volcano Zone**			**Oligotrophic Zone**		
	Mean ± stddev	Max	Min	Mean ± stddev	Max	Min	Mean ± stddev	Max	Min
σ_{21C}	**74,19 ± 0.67**	**75,67**	**73,07**	**74,20 ± 0.62**	**75,47**	**73,41**	**74,18 ± 0.72**	**75,67**	**73,07**
T_{SW}	**26,39 ± 0.92**	**27,94**	**24,34**	**26,77 ± 0.82**	**27,94**	**25,68**	**26,10 ± 0.84**	**27,32**	**24,34**
S	**34,61 ± 0.20**	**35,13**	**34,37**	**34,51 ± 0.11**	**34,69**	**34,37**	**34,67 ± 0.21**	**35,13**	**34,40**
BChl-a	$(1,04 \pm 0.39) \times 10^{-3}$	$1,90 \times 10^{-3}$	$4,00 \times 10^{-4}$	$1,29 \pm 0.27 \times 10^{-3}$	$1,90 \times 10^{-3}$	$1,10 \times 10^{-3}$	$(7,79 \pm 3.08) \times 10^{-4}$	$1,20 \times 10^{-3}$	$4,00 \times 10^{-4}$
Chl-a	**0,25 ± 0.13**	**0,41**	**0,05**	**0,35 ± 0.05**	**0,41**	**0,27**	**0,15 ± 0.09**	**0,28**	**0,05**
Per	$(4,44 \pm 1.77) \times 10^{-3}$	$7,35 \times 10^{-3}$	$1,60 \times 10^{-3}$	$(5,53 \pm 1.28) \times 10^{-3}$	$7,35 \times 10^{-3}$	$3,10 \times 10^{-3}$	$(3,61 \pm 1.98) \times 10^{-3}$	$7,35 \times 10^{-3}$	$1,60 \times 10^{-3}$
Car	$(2,94 \pm 1.59) \times 10^{-2}$	$5,00 \times 10^{-2}$	$4,80 \times 10^{-3}$	$(4,10 \pm 0.64) \times 10^{-2}$	$5,00 \times 10^{-2}$	$3,16 \times 10^{-2}$	$(1,65 \pm 1.13) \times 10^{-2}$	$3,16 \times 10^{-2}$	$4,80 \times 10^{-3}$
F_0	$(1,32 \pm 0.69) \times 10^{-1}$	$3,35 \times 10^{-1}$	$2,05 \times 10^{-2}$	$(1,67 \pm 0.68) \times 10^{-1}$	$3,35 \times 10^{-1}$	$1,07 \times 10^{-1}$	$(1,08 \pm 0.52) \times 10^{-1}$	$1,76 \times 10^{-1}$	$2,05 \times 10^{-2}$
σ_{PSII}	**3,42 ± 1.12**	**5,07**	**1,51**	**2,99 ± 1.01**	**4,41**	**1,58**	**3,74 ± 1.17**	**5,07**	**1,51**
PicoPhyto	**432,93 ± 172.81**	**781,05**	**214,95**	**480,01 ± 167.53**	**771,43**	**233,64**	**391,87 ± 157.18**	**781,05**	**214,95**
NanoPhyto	**1200,00 ± 384.34**	**2087,38**	**578,43**	**1427,58 ± 355.96**	**2087,38**	**899,68**	**1091,86 ± 344.45**	**1775,64**	**578,43**
Proc	**1820,10 ± 454.51**	**2915,86**	**1107,84**	**2113,25 ± 421.68**	**2915,86**	**1459,55**	**1644,68± 353.147**	**2410,26**	**1107,84**
Syn	$(7,671 \pm 1.77) \times 10^5$	$1,22 \times 10^6$	$5,04 \times 10^5$	$(8,58 \pm 1.88) \times 10^5$	$1,22 \times 10^6$	$6,28 \times 10^5$	$(7,34 \pm 1.54) \times 10^5$	$1,04 \times 10^6$	$5,04 \times 10^5$
TotEuks	$(3,74 \pm 4.63) \times 10^4$	$2,01 \times 10^5$	$6,57 \times 10^2$	$(6,69 \pm 5.45) \times 10^4$	$2,01 \times 10^5$	$1,67 \times 10^4$	$(2,18 \pm 2.73) \times 10^4$	$1,14 \times 10^5$	$6,57 \times 10^2$
TotBact	$(9,56 \pm 1.66) \times 10^3$	$8,98 \times 10^4$	$7,89 \times 10^2$	$(1,53 \pm 2.19) \times 10^4$	$8,98 \times 10^4$	$3,45 \times 10^3$	$(4,85 \pm 7.02) \times 10^3$	$2,70 \times 10^4$	$7,89 \times 10^2$
UCYN-A	$(7,63 \pm 7.41) \times 10^5$	$1,70 \times 10^6$	$8,08 \times 10^2$	$(1,34 \pm 0.55) \times 10^6$	$1,70 \times 10^6$	$2,26 \times 10^5$	$(5,29 \pm 6.36) \times 10^5$	$1,70 \times 10^6$	$8,08 \times 10^2$
UCYN-B	$(1,01 \pm 1.04) \times 10^6$	$2,77 \times 10^6$	$2,36 \times 10^3$	$(3,01 \pm 4.54) \times 10^5$	$1,10 \times 10^6$	$9,26 \times 10^3$	$(1,24 \pm 1.03) \times 10^6$	$2,77 \times 10^6$	$2,36 \times 10^3$
UCYN-C	**158,46 ± 85.76**	**390,00**	**75,10**	**96,83 ± 39.70**	**167,79**	**75,10**	**179,30 ± 83.69**	**390,00**	**75,10**
POC	**40,40 ± 14.05**	**59,80**	**20,14**	**51,17 ± 8.71**	**59,80**	**37,54**	**33,75 ± 11.67**	**54,61**	**20,14**
DOC	**71,86 ± 4.06**	**77,65**	**63,27**	**71,42 ± 4.07**	**77,00**	**63,27**	**70,55 ± 5.00**	**77,65**	**63,27**
O_2	**193,86 ± 8.46**	**201,52**	**179,72**	**192,06 ± 9.10**	**200,16**	**179,72**	**197,49 ± 5.13**	**201,52**	**187,39**

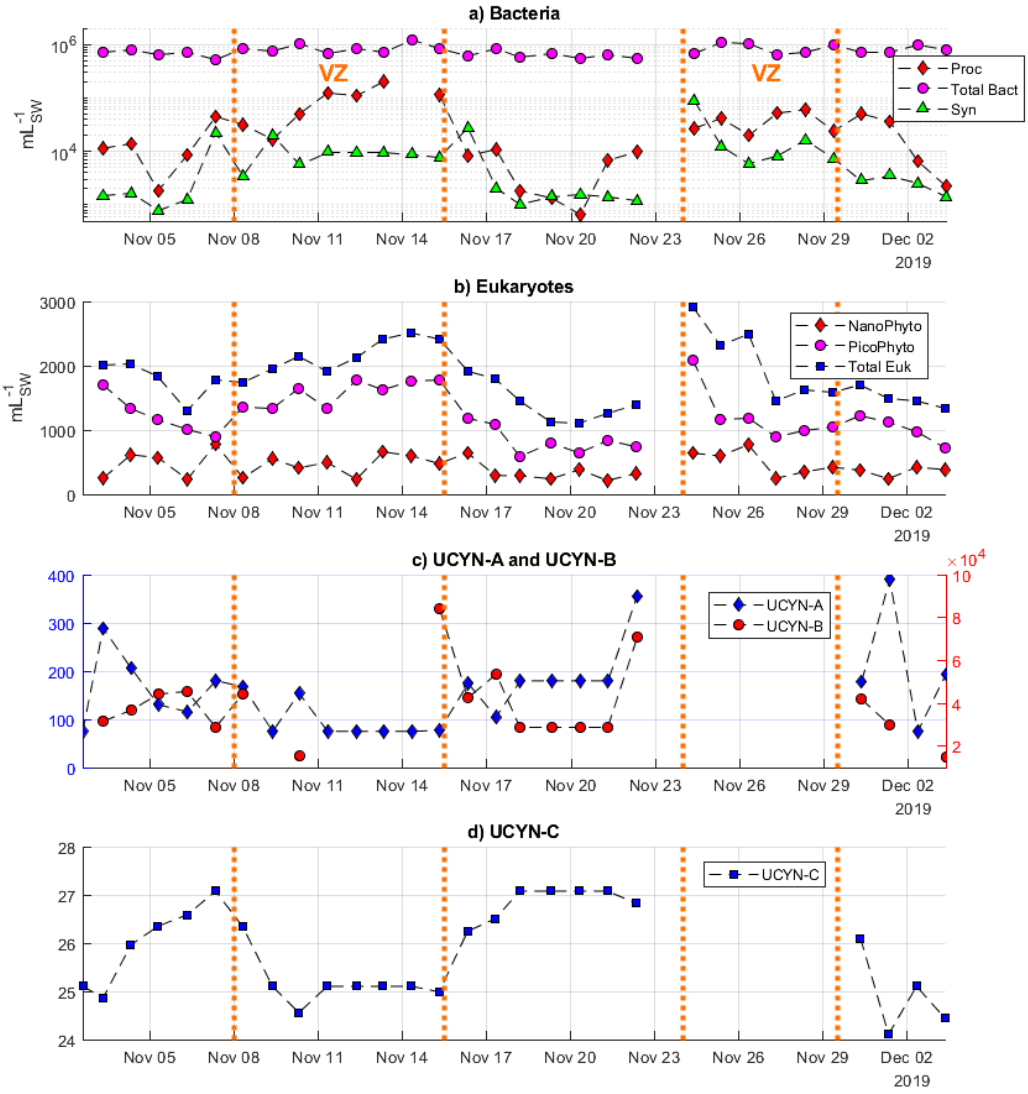

Figure A.2 – Time series of parameters from Table III.3 - Part 2 : Microbiological parameters in the sea water. a) Bacteria (*Prochlorococcus*, *Synechococcus*, total bacterial abundance) measured by FCM; b) Eukaryotes (Nanophytoplanktons, picophytoplanktons, total eukaryotes abundance) measured by FCM; c) Abundances of UCYN-A and UCYN-B; d) Abundances of UCYN-C. Orange dotted lines and VZ labels mark the limits of the Volcanic Zone.

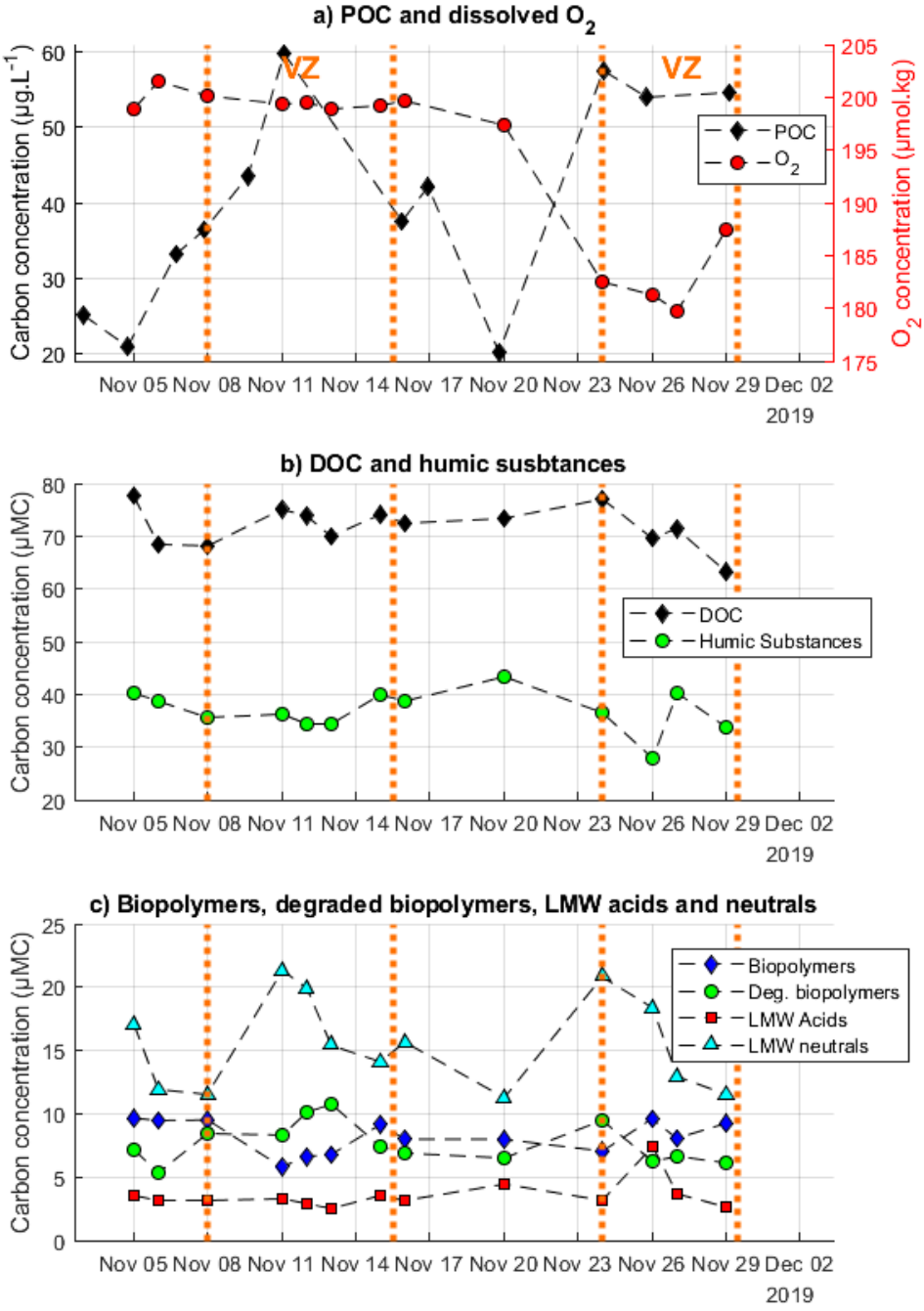

Figure A.3 – Time series of parameters from Table III.3 - Part 3: Organic Matter. a) POC and dissolved oxygen; b) DOC and humic substances; c) Biopolymers, degraded biopolymers, Low Molecular Weight acids and Low Molecular Weight neutrals. Orange dotted lines and VZ labels mark the limits of the Volcanic Zone.

A.2 Seawater INPs

A.2.1 Additional figures on INP spectra and time series

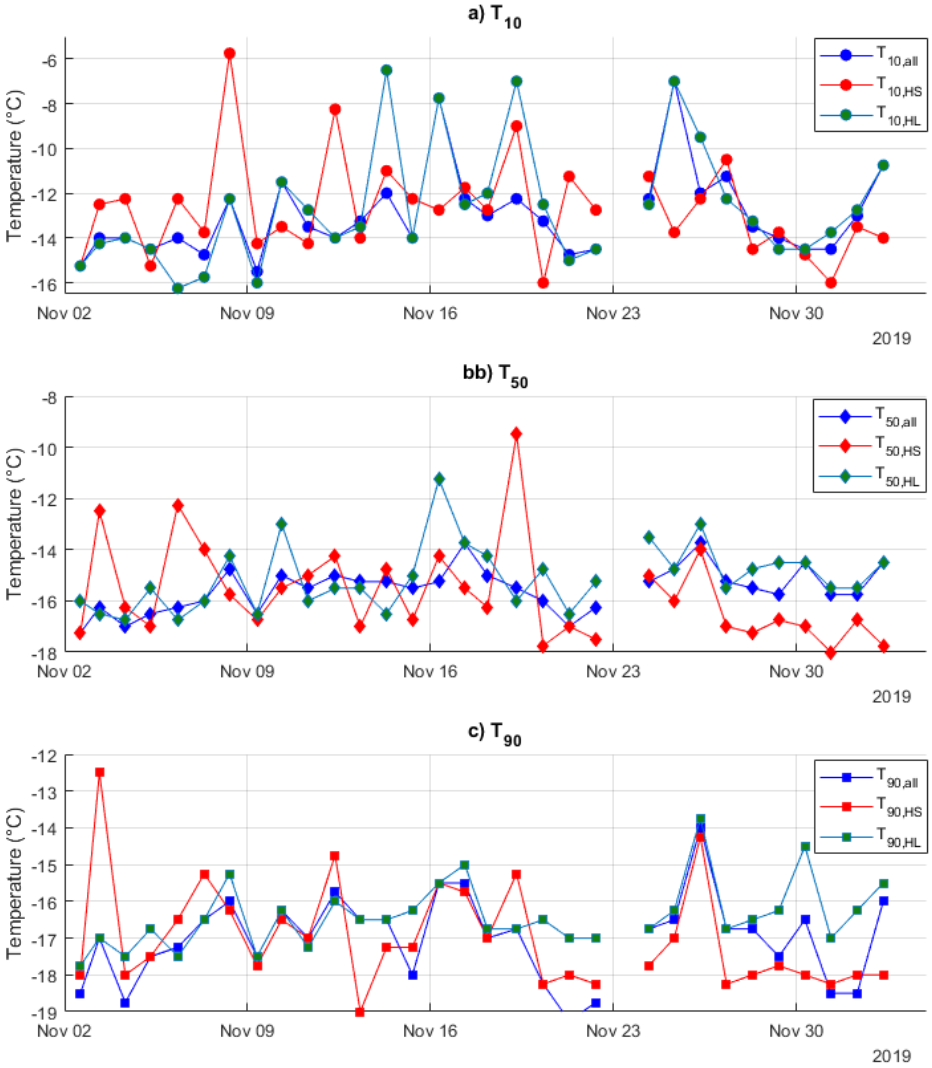

Figure A.4 – Time series of T_{10}, T_{50} and T_{90} in the SW.

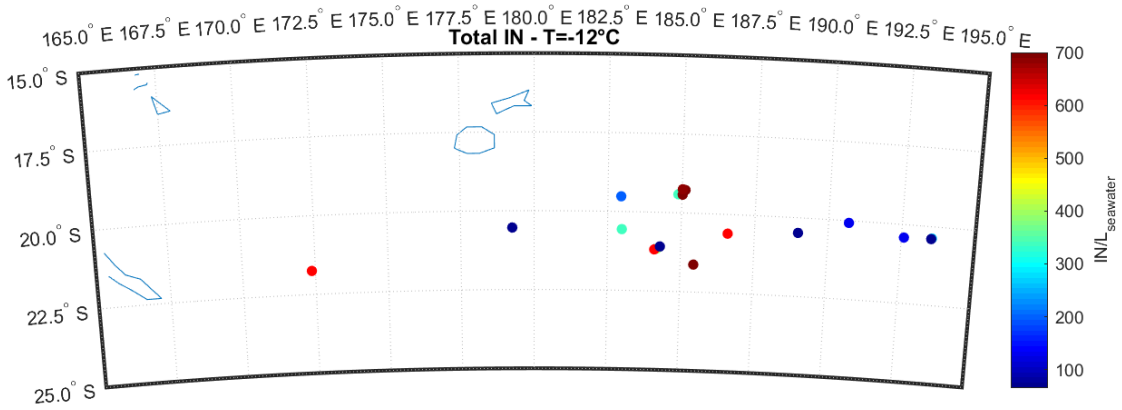

(a) Total IN - T_1 = -12 °C

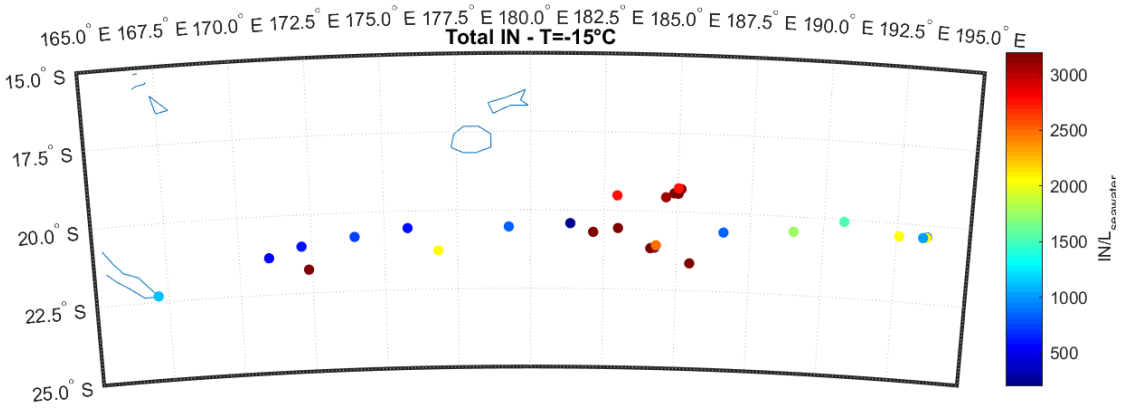

(b) Total IN - T_2 = -15 °C

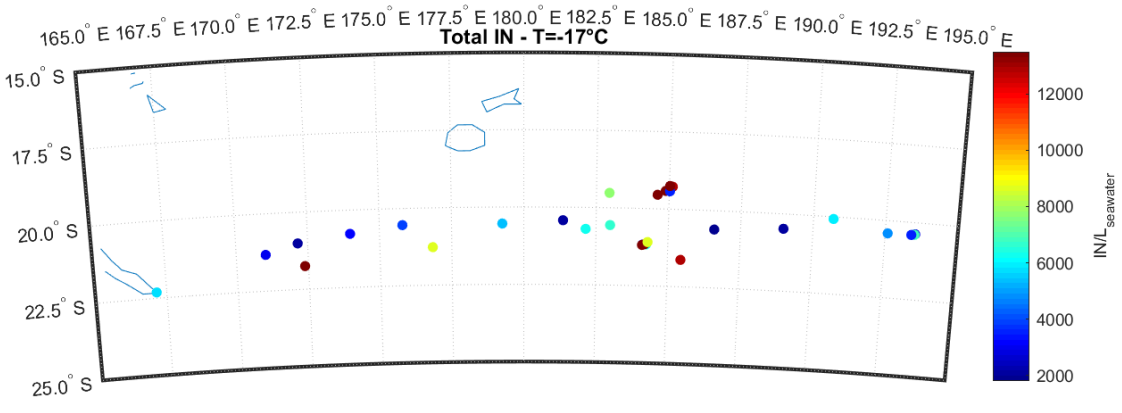

(c) Total IN - T_3 = -17 °C

Figure A.5 – INP concentrations at a) T = -12 °C ; b) T = -15 °C c) T = -17 °C showed along the trajectory of the ship. Coastlines are showed as the blue lines.

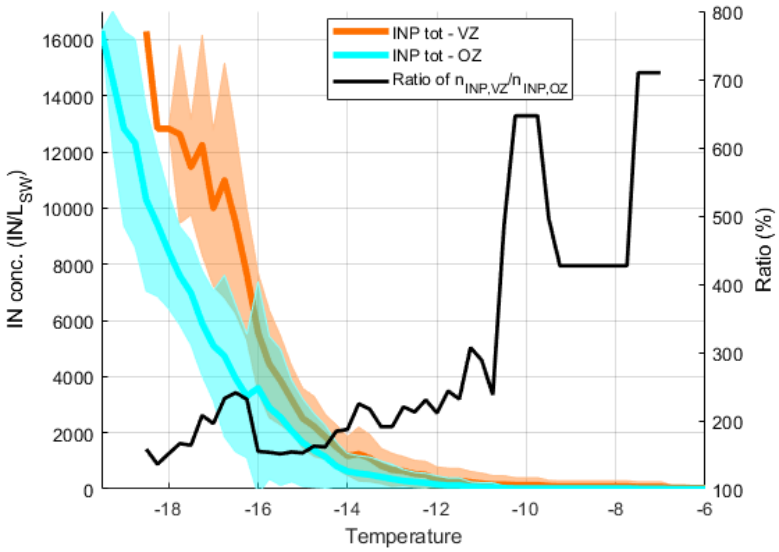

Figure A.6 – Comparison between the mean INP concentrations in the volcanic zone (orange) and oligotrophic zone (cyan). The shaded areas represent the standard deviation at a given temperature and the lines represent the mean values.

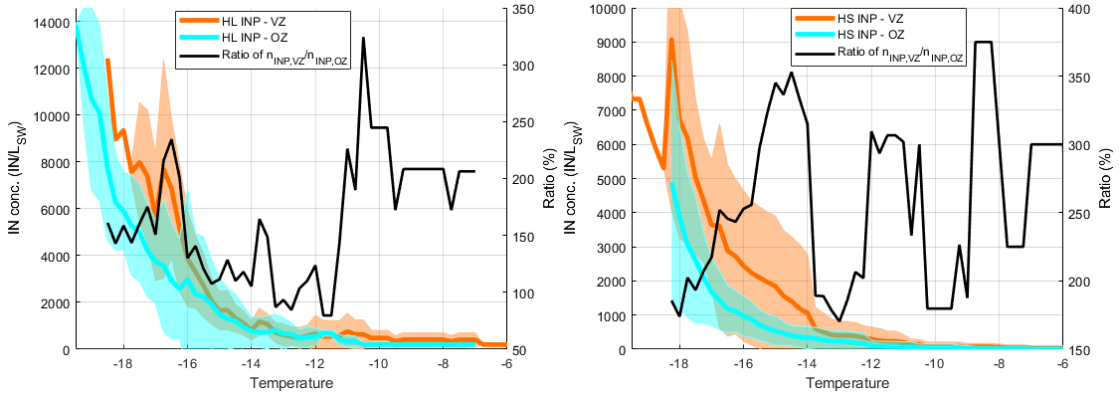

(a) HL INP mean temperature spectra (b) HS INP mean temperature spectra

Figure A.7 – INP concentrations separated between the volcano (orange) and the oligotrophic (cyan) zones. The shaded areas represent the standard deviation at a given temperature and the lines represent the mean values.

A.2.2 Additional correlation tables: VZ and OZ segregation

Table A.2 – Correlations between INP concentrations (total INPs, heat stable INPs and heat labile INPs) at T_1, T_2 and T_3 and the selected paramaters, in the Volcano Zone. Only significant ($p < 0.05$) correlation coefficients ($-1 < R < 1$) are shown. Non significant coefficients are shown as "—". Bold values indicate the significant correlations with $P < 0.005$.

		T_{SW}	Sal.	BChl-a	Chl-a	Per.	Car.	Pico	Nano
INT1	R(P)	—	—	0.86(0.01)	—	—	—	—	—
INT1 HS	R(P)	—	—	—	—	—	—	—	—
INT1 HL	R(P)	—	—	—	—	—	—	—	—
INT2	R(P)	—	-0,39(0,03)	—	—	—	—	—	—
INT2 HS	R(P)	—	-0.35(0.05)	—	—	—	—	0.69(0.01)	
INT2 HL	R(P)	—	—	0,81(0,05)	—	—	—	—	—
INT3	R(P)	—	0,35(0,05)	—	—	—	—	—	—
INT3 HS	R(P)	—	0,41(0,02)	—	—	—	—	0.61(0.02)	—
INT3 HL	R(P)	—	0,40(0,03)	—	—	—	—	—	—

		TotEuk	TotBact	Proc	Syn	UCYN-A	UCYN-B	UCYN-C
INT1	R(P)	—	0.59(0.03)	—	—	—	—	—
INT1 HS	R(P)	—	—	—	—	—	—	—
INT1 HL	R(P)	—	0.77(0.04)	—	—	—	—	—
INT2	R(P)	—	—	—	—	—	—	—
INT2 HS	R(P)	0.53(0.05)	—	—	—	—	—	—
INT2 HL	R(P)	—	—	—	—	—	—	—
INT3	R(P)	—	—	—	—	—	—	—
INT3 HS	R(P)	—	0.53(0.05)	—	—	—	—	—
INT3 HL	R(P)	—	—	—		—	—	—

		POC	DOC	O_2	BP	HuS	dBP	LMW acids	LMW neutrals
INT1	R(P)	—	—	-0.73(0.03)	—	—	—	—	—
INT1 HS	R(P)	—	—	-0.75(0.02)	—	—	—	—	—
INT1 HL	R(P)	—	—	—	—	—	—	—	—
INT2	R(P)	—	—	—	—	—	—	—	—
INT2 HS	R(P)	—	—	—	0.72(0.03)		-0.78(0.01)	0.89(<0.005)	—
INT2 HL	R(P)	—	—	—	—	—	—	—	-0.75(0.03)
INT3	R(P)	—	—	—	—	—	0.71(0.03)	—	—
INT3 HS	R(P)	—	—	-0.67(0.05)	—	—	—	0.66(0.05)	—
INT3 HL	R(P)	—	—	—	—	—	0.75(0.03)	—	—

Table A.3 – Correlations between INP concentrations (total INPs, heat stable INPs and heat labile INPs) at T_1, T_2 and T_3 and the selected paramaters, in the Oligotrophic Zone. Only significant ($p < 0.05$) correlation coefficients ($-1 < R < 1$) are shown. Non significant coefficients are shown as "—". Bold values indicate the significant correlations with $P < 0.005$.

		T_{SW}	Sal.	BChl-a	Chl-a	Per.	Car.	Pico	Nano
INT1	R(P)	—	—	—	—	—	—	—	—
INT1 HS	R(P)	—	—	—	—	—	—	—	—
INT1 HL	R(P)	—	—	—	—	—	—	—	0.80(0.03)
INT2	R(P)	—	—	—	—	0.82(0.02)	—	—	—
INT2 HS	R(P)	—	—	0.82(0.02)	0.85(0.02)	—	—	—	—
INT2 HL	R(P)	—	—	0.90(0.04)	**0.99(<0.005)**	**0.99(<0.005)**	**0.99(<0.005)**	—	—
INT3	R(P)	—	—	—	—	—	—	—	—
INT3 HS	R(P)	—	—	—	—	—	—	—	—
INT3 HL	R(P)	—	—	—	—	—	—	—	—

		TotEuk	TotBact	Proc	Syn	UCYN-A	UCYN-B	UCYN-C
INT1	R(P)	—	—	—	—	—	—	—
INT1 HS	R(P)	—	—	—	—	—	—	—
INT1 HL	R(P)	0.80(0.03)	0.86(0.01)	—	—	0.86(0.01)	-0.85(0.01)	—
INT2	R(P)	—	0.51(0.02)	—	—	—	—	—
INT2 HS	R(P)	—	—	—	—	—	—	—
INT2 HL	R(P)	—	—	—	—	—	—	—
INT3	R(P)	—	0.55(0.01)	—	—	0.44(0.05)	-0.44(0.05)	—
INT3 HS	R(P)	—	—	—	—	—	—	-0.55(0.01)
INT3 HL	R(P)	—	0.46(0.04)	—		—	—	—

		POC	DOC	O_2	BP	HuS	dBP	LMW acids	LMW neutrals
INT1	R(P)	—	—	—	—	—	—	—	—
INT1 HS	R(P)	—	—	—	—	—	—	—	—
INT1 HL	R(P)	—	—	—	—	—	—	—	—
INT2	R(P)	—	—	—	—	—	—	—	—
INT2 HS	R(P)	—	-0.81(0.05)	—	—	—	—	—	—
INT2 HL	R(P)	—	—	—	—	—	—	—	—
INT3	R(P)	—	—	—	—	—	—	—	—
INT3 HS	R(P)	—	—	—	—	—	—	-0.87(0.03)	—
INT3 HL	R(P)	—	—	—	-0.83(0.04)	—	—	—	—

A.3 SSA INPs

A.3.1 Additional figures on INP spectra and time series

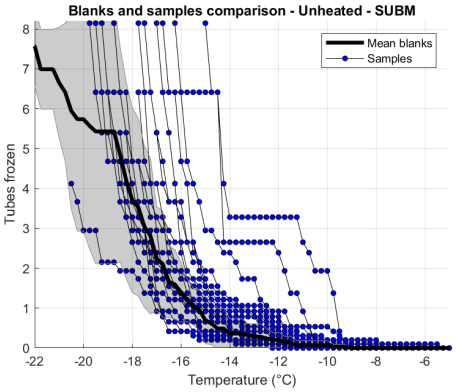

(a) Unheated submicronic samples

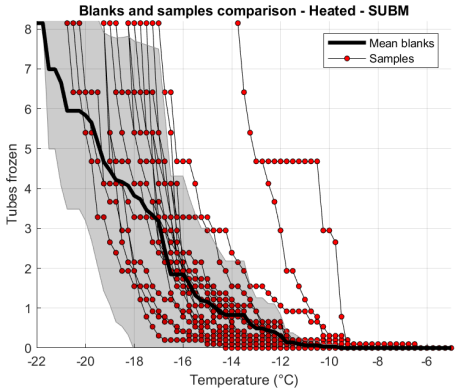

(b) Heated submicronic samples

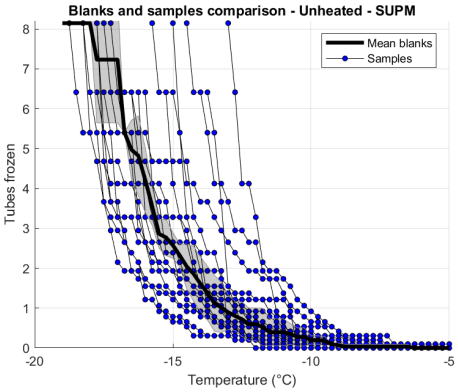

(c) Unheated supermicronic samples

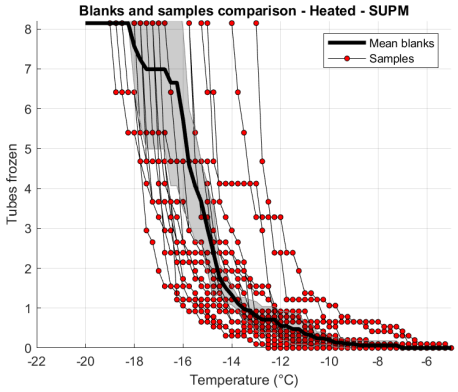

(d) Heated supermicronic samples

Figure A.8 – Comparison of blank filters and sampled filters in the SSA. Sampled filters are represented as blue dots. Different blank filters are represented as red dotted lines, and the average value of blank samples is represented as the black line, with the grey area representing one standard deviation.

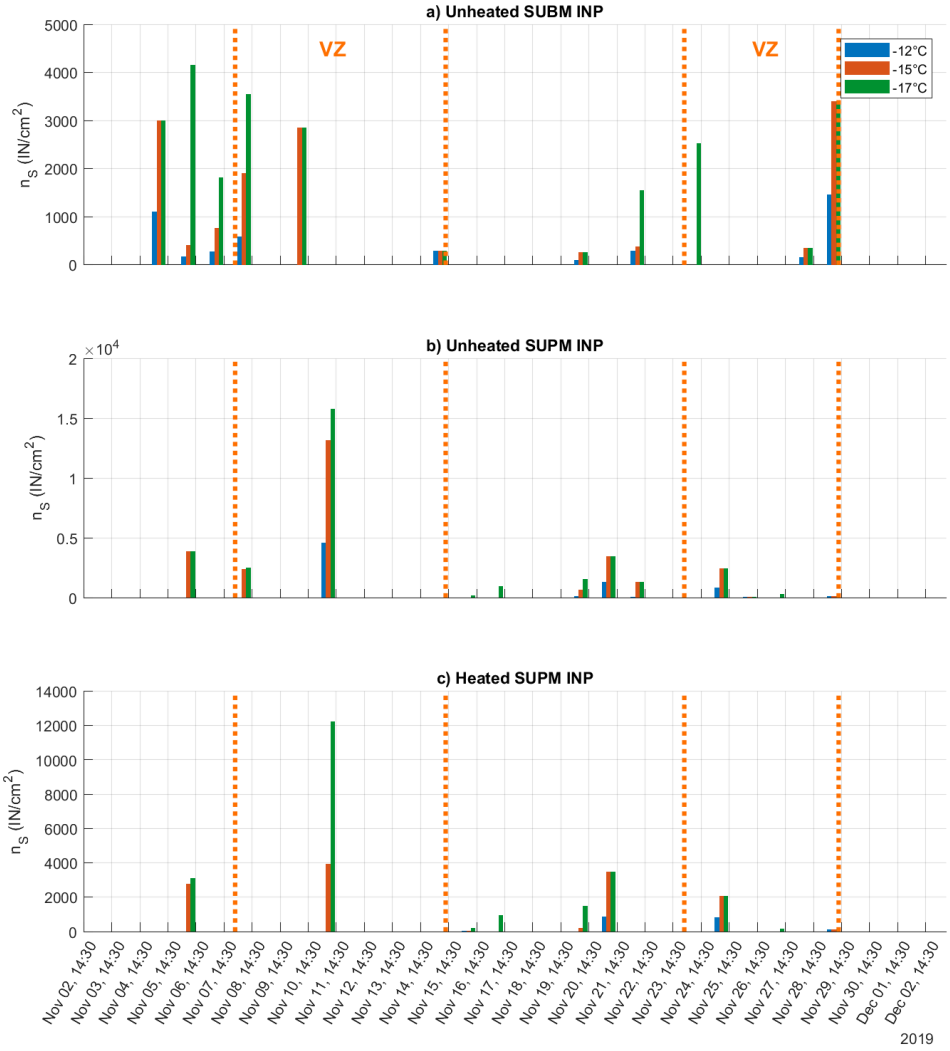

Figure A.9 – Time series of submicronic and super micronic INPs in the SSA studied at $T_1 = -12$ °C (blue), $T_2 = -15$ °C (orange) and $T_3 = -17$ °C (green): a) Unheated submicronic INPs; b) Unheated supermicronic INPs; c) Heated supermicronic INPs.

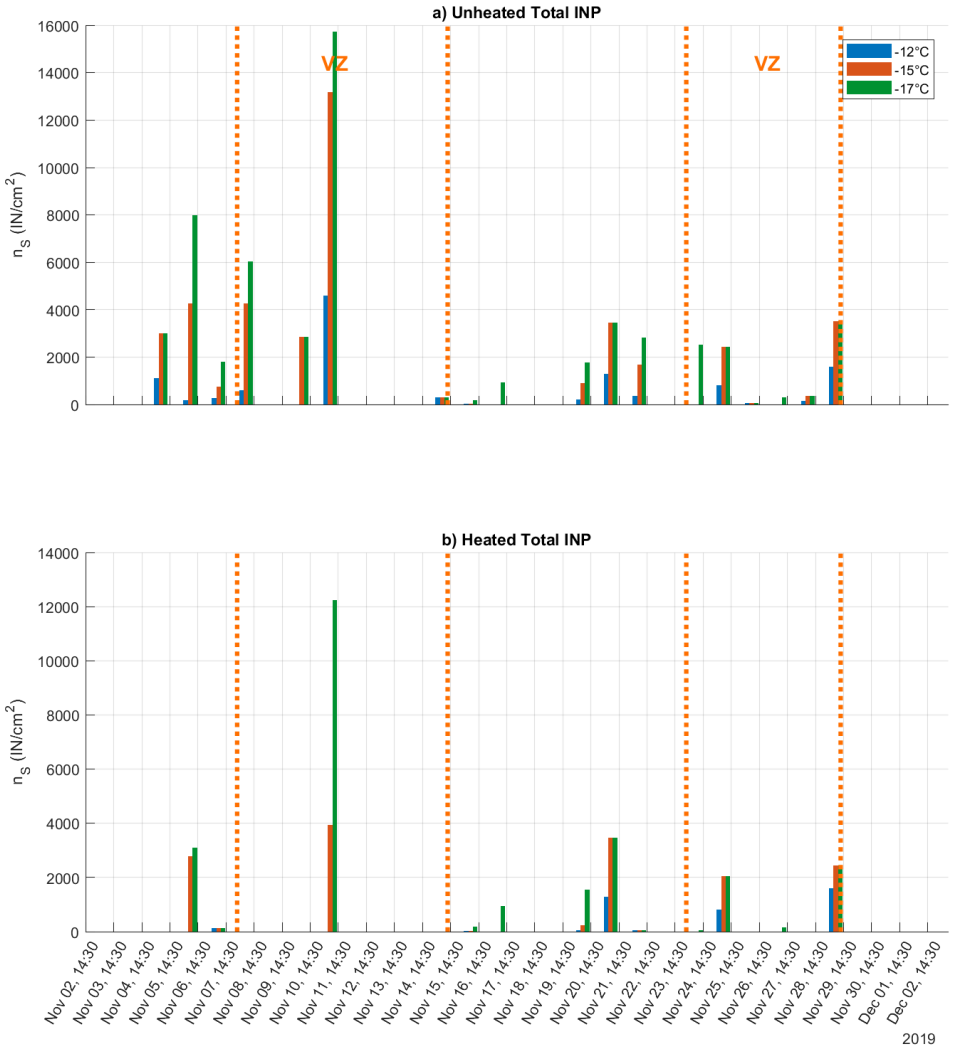

Figure A.10 – Time series of total n_S in the SSA studied at $T_1 = -12$ °C (blue), $T_2 = -15$ °C (orange) and $T_3 = -17$ °C (green): a) Unheated total n_S; b) Unheated total n_S.

B

Suplementary: S2C cruise

Outline of the current chapter

B.1 Supplementary figures on INP concentrations

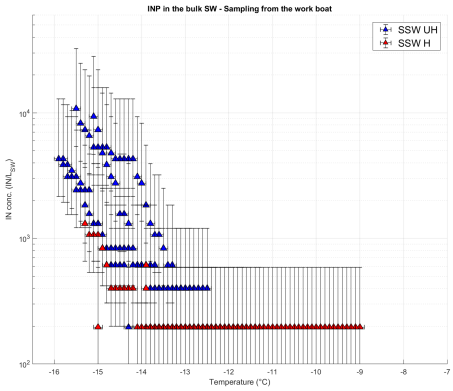

(a) INP concentrations in the SW measured from the WBOAT.

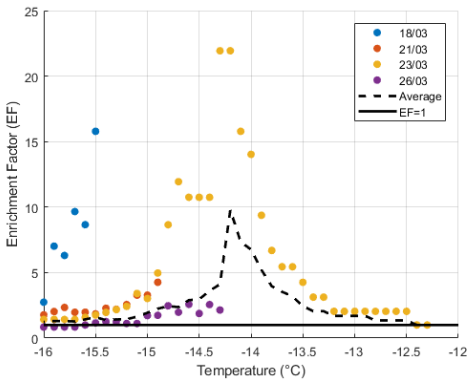

(b) Enrichment factor.

Figure B.1 – INP concentrations in the SW measured with the WBOAT, compared to the INP concentrations in the SW measured with the UWAY.

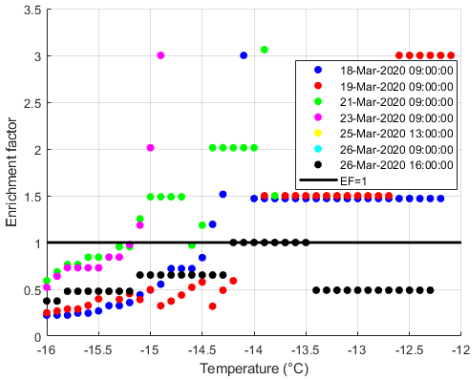

Figure B.2 – Enrichment factor for Heat Stable INPs.

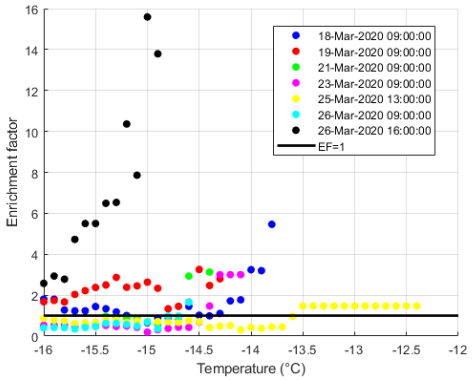

Figure B.3 – Enrichment factor for Heat Labile INPs.

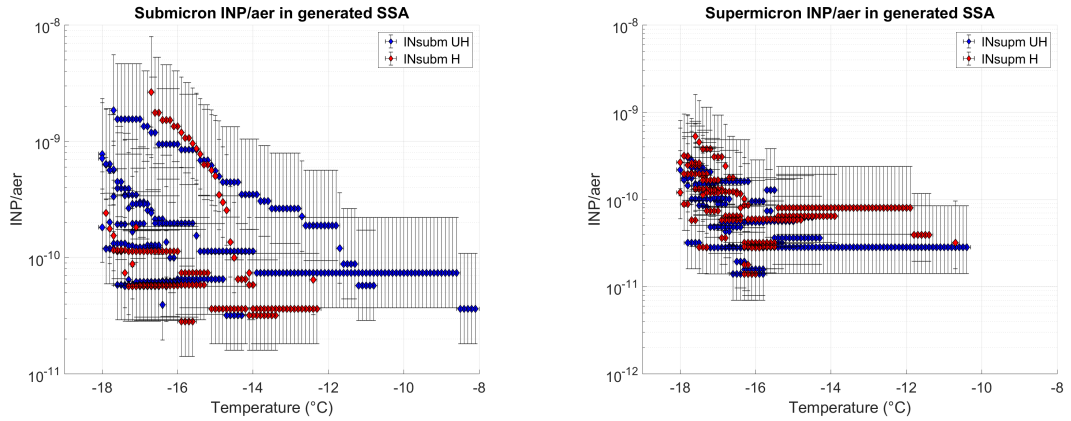

(a) Submicron INP. (b) Submicron INP.

Figure B.4 – INP/aer temperature spectra for the generated SSA (bubbler): a) Submicron INP, b) Supermicron INP. The unheated and heated samples are represented as blue and red respectively.

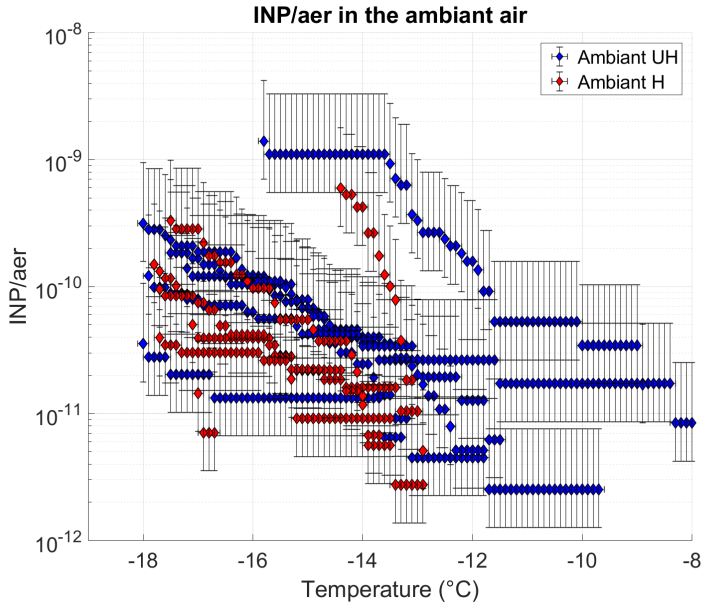

Figure B.5 – INP/aer temperature spectra for the ambiant SSA. The unheated and heated samples are represented as blue and red respectively.

B.2 Supplementary data and figures on variations and correlations

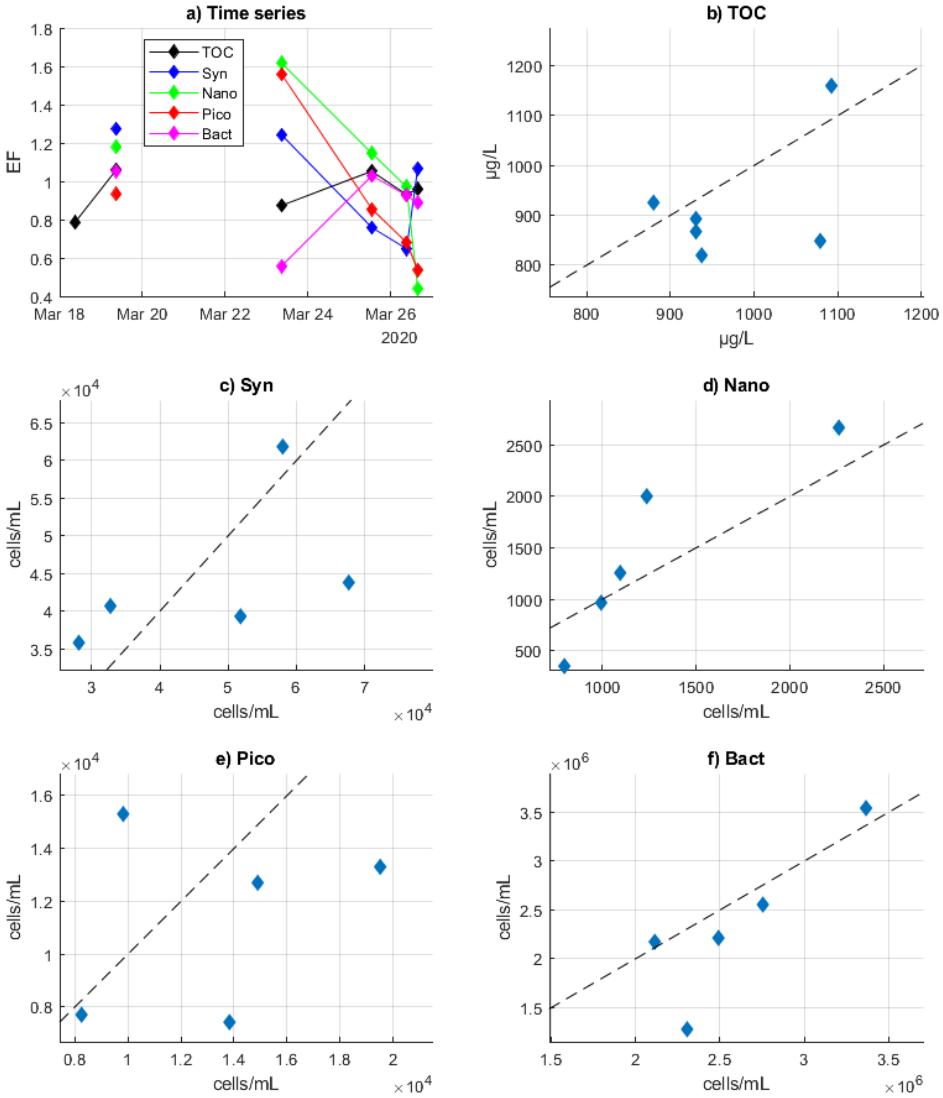

Figure B.6 – Timeseries and values of enrichment factors between the SW and the SML for TOC, Syn, Nano, Pico and Bact.

B.2.1 Variations of INP concentrations between the different water types

B.2.1.1 Seawater INPs

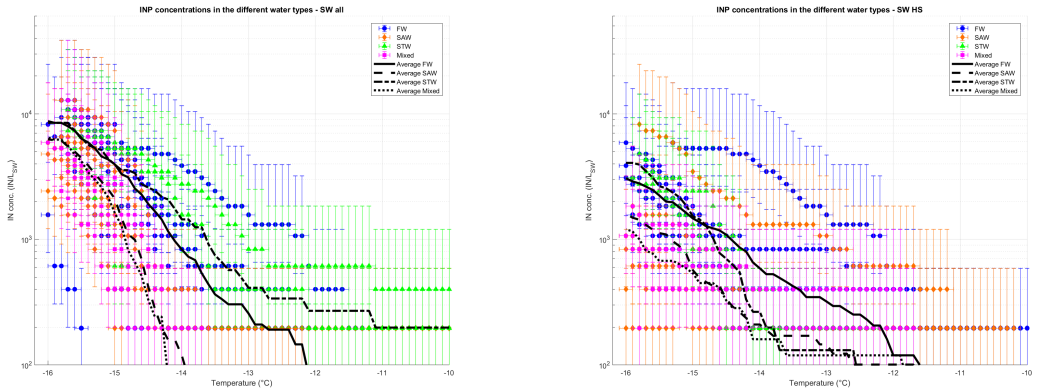

(a) Unheated SW INPs.

(b) Heat stable SW INPs

Figure B.7 – INP temperature spectra in the bulk SW for a) unheated INPs and b) heat stable INPs. The INP sampled in the different water types are represented as blue dots (FW), orange diamonds (SAW), green triangles (STW) and pink squares (Mixed). The averages in each water types are also represented as a plain line (FW), dashed line (SAW), dash-dotted line (STW) and dotted line (Mixed).

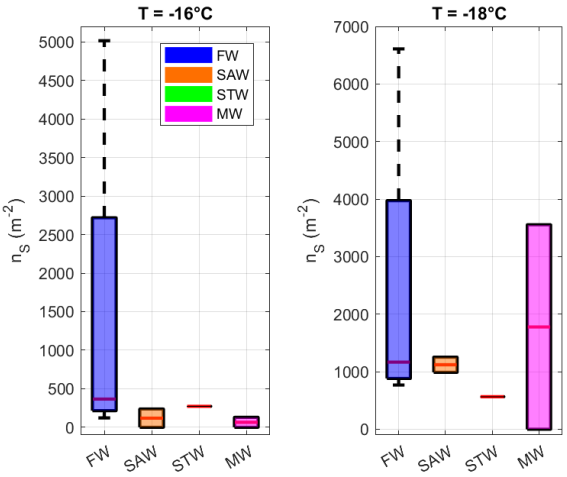

Figure B.8 – Box plots of heat stable INP concentrations at -14 °C and -16 °C in the different water types (blue: FW, orange: SAW, green: STW, pink: MW).

B.2.1.2 SSA INPs

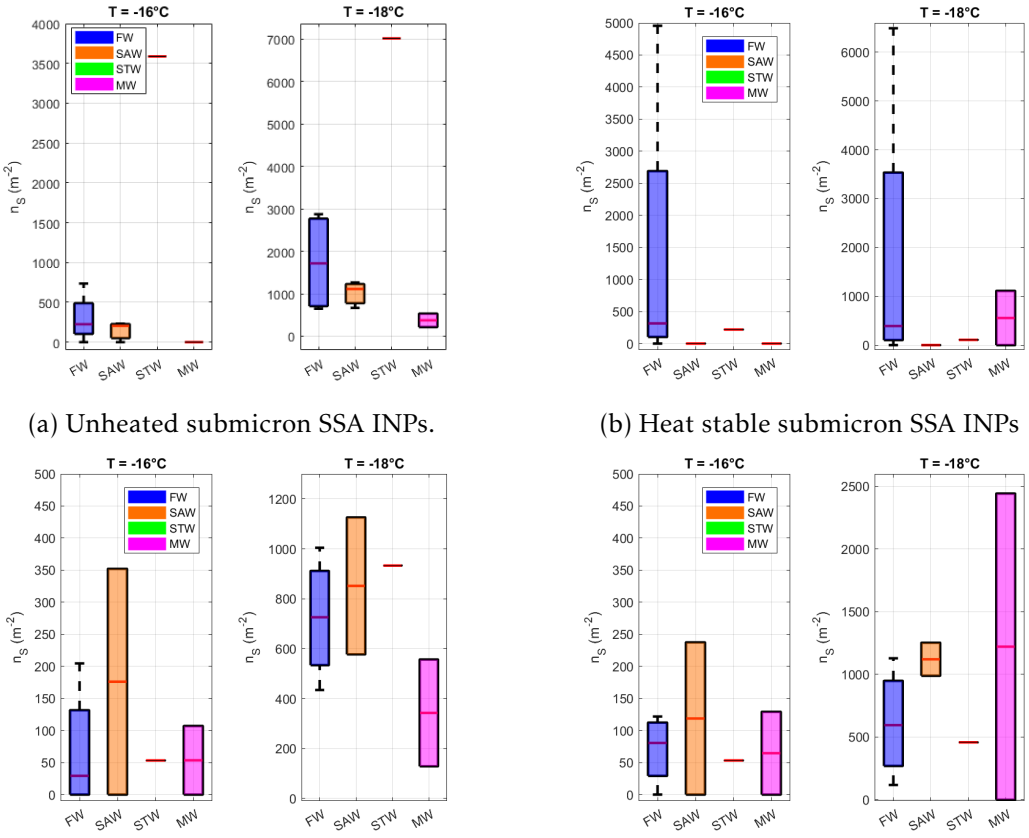

(a) Unheated submicron SSA INPs.

(b) Heat stable submicron SSA INPs

(c) Unheated supermicron SSA INPs.

(d) Heat stable supermicron SSA INPs

Figure B.9 – Boxplots of INP concentrations in the SSA at -16 °C and -18 °C in the different water types.

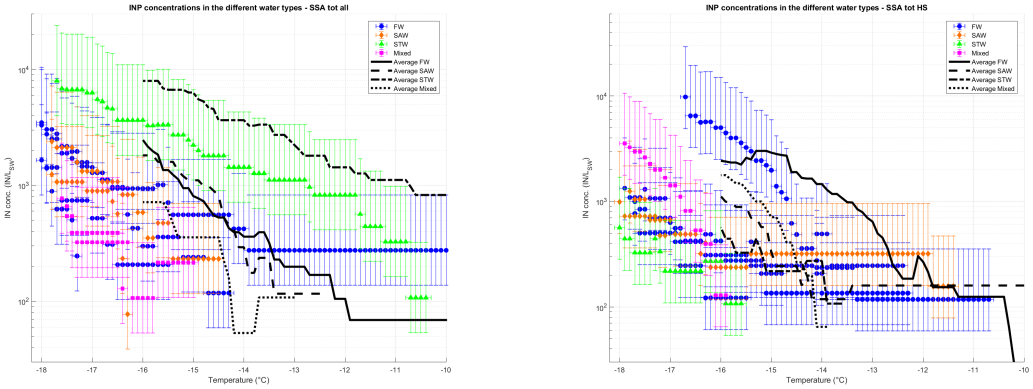

(a) Unheated total SSA INPs.

(b) Heat stable total SSA INPs

Figure B.10 – INP temperature spectra in the total SSA for a) unheated INPs and b) heat stable INPs. The INP sampled in the different water types are represented as blue dots (FW), orange diamonds (SAW), green triangles (STW) and pink squares (Mixed). The averages in each water types are also represented as a plain line (FW), dashed line (SAW), dash-dotted line (STW) and dotted line (Mixed).

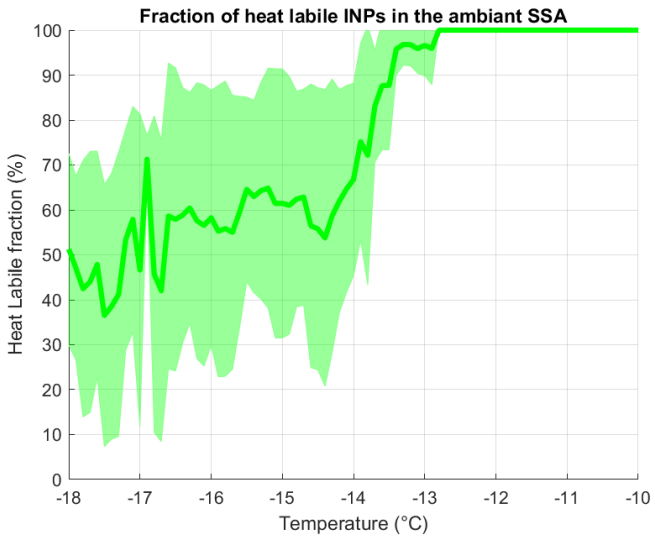

Figure B.11 – Fraction of Heat Labile INPs in the ambiant SSA. The plain lines corresponds to the average and the shaded area to the standard deviation of the data set.

B.2.2 Variations of the parameters between the seawater types

Table B.1 – Summary of mean and standard deviation of the parameters from the S2C campaign, during the full cruise and segregated by watertypes.

	Full cruise	FW	SAW	STW	MW
TOC SSA	$(2.21 \pm 0.80) \times 10^{-9}$	$(2.78 \pm 0.58) \times 10^{-9}$	$(1.88 \pm 0.38) \times 10^{-9}$	0.92×10^{-9}	—
NaCl SSA	$(8.72 \pm 7.18) \times 10^{-9}$	$(12.75 \pm 0.83) \times 10^{-9}$	$(5.38 \pm 0.95) \times 10^{-9}$	2.62×10^{-9}	—
Salinity	34.597 ± 0.309	34.470 ± 0.035	34.378 ± 0.093	35.322 ± 0.018	34.824 ± 0.059
T SW	14.66 ± 1.35	13.88 ± 0.46	13.92 ± 0.35	17.44 ± 0.87	15.90 ± 0.26
Syn	$(5.90 \pm 4.84) \times 10^4$	$(5.28 \pm 4.23) \times 10^4$	$(4.68 \pm 1.07) \times 10^4$	$(6.19 \pm 1.96) \times 10^4$	$(8.82 \pm 4.16) \times 10^4$
Nano	1578 ± 725	2384 ± 570	1381 ± 542	867 ± 48	808 ± 329
Pico	$(1.37 \pm 0.64) \times 10^4$	$(1.16 \pm 0.50) \times 10^4$	$(1.35 \pm 0.42) \times 10^4$	$(1.26 \pm 0.40) \times 10^4$	$(1.58 \pm 0.46) \times 10^4$
Bact	$(2.50 \pm 0.90) \times 10^6$	$(3.32 \pm 0.81) \times 10^6$	$(1.99 \pm 0.34) \times 10^6$	$(1.71 \pm 3.4) \times 10^6$	$(3.00 \pm 0.85) \times 10^6$
DiFl	12.5 ± 7.6	20.3 ± 10.3	12.6 ± 5.2	12.9 ± 5.2	8.8 ± 4.5
DiA	8.3 ± 10.8	20.0 ± 15.0	2.1 ± 1.5	1.1 ± 1.1	6.1 ± 6.4
Fl	2.2 ± 1.2	2.2 ± 1.2	1.7 ± 0.7	2.8 ± 1.0	2.5 ± 0.9
TOC	940 ± 150	1097 ± 51	825 ± 147	897 ± 14	900 ± 31
TN	131 ± 36	144 ± 33	145 ± 39	96 ± 4.8	108 ± 5.8
DAA	413 ± 135	499 ± 133	355 ± 103	290 ± 21	508 ± 90
PAA	380 ± 288	736 ± 237	210 ± 74	176 ± 20	212 ± 28
DCHO	708 ± 248	1002 ± 81	539 ± 72	607 ± 181	507 ± 17
PCHO	324 ± 438	812 ± 486	94 ± 58	124 ± 74	116 ± 116

B.2.3 Correlations in the SW

Table B.2 – Correlations between SW INPs and ocean parameters - Full cruise.

		Salinity	T_{SW}	Syn	Nano	Pico	Bacteria	TOC	TN	DAA	PAA	DCHO	PCHO
INT1	R(P)	0.63(0.01)	0.63(0.02)	—	—	—	—		—	—	—	—	—
INT1 HL	R(P)	0.70(0.03)	—	—	—	—	—	—	—	—	—	—	—
INT1 HS	R(P)	—	—	—	—	—	—	—	—	0.70(0.03)	—	—	—
INT2	R(P)	—	—	—	—	—	—	—	—	—	—	0.43(0.05)	0.48(0.03)
INT2 HL	R(P)	—	—	—	—	—	—	0.46(0.03)	—	—	—	—	0.49(0.03)
INT2 HS	R(P)	—	—	—	—	-0.46(0.03)	—			—	—	—	—
T10	R(P)	—	0.43(0.03)	—	—	-0.42(0.05)	—	—	—	—	—	—	—
T10 HS	R(P)	—	—	—	—	—	—		—	—	—	—	—

Table B.3 – Correlations between SW INPs and ocean parameters - SAW+MW.

		Salinity	T_{SW}	Syn	Nano	Pico	Bacteria	TOC	TN	DAA	PAA	DCHO	PCHO
INT1	R(P)	—	—	—	—	—	—	-0.98(<0.005)	—	—	—	—	—
INT1 HL	R(P)	—	—	—	—	—	—	—	—	—	—	—	—
INT1 HS	R(P)	—	—	—	—	—	—	—	—	—	—	—	—
INT2	R(P)	—	—	—	—	—	—	—	—	—	—	—	—
INT2 HL	R(P)	—	—	—	—	—	—	—	—	—	—	—	—
INT2 HS	R(P)	—	—	—	—	—	—	-0.94(<0.005)	-0.72(0.01)	—	—	—	—
T10	R(P)	—	—	—	—	—	—	—	—	—	—	—	—
T10 HS	R(P)	—	—	—	—	—	—	-0.87(<0.005)	—	—	—	—	—

B.2.4 Carbohydrates and amino acids in the SW

Table B.4 – Summary of Carbohydrates (CHO) and Amino Acids (AA) measured in this study. Courtesy of Anja Engel and Theresea Barthelmeß, associated to GEOMAR Helmholtz Center for Ocean Research Kiel.

Name	Symbol	Type
Fucose	Fuc	CHO
Rhamnose	Rha	CHO
Galactosamine	GalN	CHO
Arabinose	Ara	CHO
Glucosamine	GlcN	CHO
Galactose	Gal	CHO
Glucose	Glc	CHO
Mannose/Xylose	ManXyl	CHO
Galacturonic acid	GalX	CHO
Glucuronic acid	GlcX	CHO
Aspartic acid	AsX	AA
Glutamic acid	GlX	AA
Serine	Ser	AA
Glycine	Gly	AA
Threonine	Thr	AA
Arginine	Arg	AA
Alanine	Ala	AA
Gamma-aminobutyric acid	GABA	AA
Tyrosine	Tyr	AA
Valine	Val	AA
Isoleucine	Iso	AA
Phenylalanine	Phe	AA
Leucine	Leu	AA

Table B.5 – Correlations between SW INPs and PCHO data.

		Fuc	Rha	GalN	Ara	GlcN	Gal	Glc	ManXyl	GalX	GlcX
INT1	R(P)	—	—	0.78(<0.005)	—	0.70(<0.005)	0.48(0.02)	—	—	—	0.71(<0.005)
INT1 HL	R(P)	—	—	0.76(<0.005)	—	0.60(<0.005)	—	—	—	—	0.68(<0.005)
INT1 HS	R(P)	—	—	—	—	0.52(0.01)	0.65(<0.005)	—	—	—	—
INT2	R(P)	0.42(0.05)	0.51(0.01)	—	—	—	—	0.44(0.04)	—	—	—
INT2 HL	R(P)	—	0.53(0.01)	—	—	—	—	—	—	—	—
INT2 HS	R(P)	—	—	—	—	—	—	—	—	—	—
T10 UH	R(P)	—	—	0.68(<0.005)	—	0.68(<0.005)	0.57(0.01)	—	—	—	0.65(<0.005)
T10 H	R(P)	—	—	—	—	—	0.47(0.03)	—	—	—	—

Table B.6 – Correlations between SW INPs and DCHO data.

		Fuc	Rha	GalN	Ara	GlcN	Gal	Glc	ManXyl	GalX	GlcX
INT1	R(P)	—	—	—	—	—	—	—	—	—	0.53(0.01)
INT1 HL	R(P)	—	—	—	—	—	—	—	—	—	0.45(0.03)
INT1 HS	R(P)	—	—	—	—	0,86(0.01)	—	—	—	—	—
INT2	R(P)	0.54(0.01)	—	—	—	—	—	0.44(0.04)	—	—	—
INT2 HL	R(P)	0.44(0.04)	—	—	—	—	—	—	—	—	—
INT2 HS	R(P)	—	—	—	—	—	—	—	—	—	—
T10 UH	R(P)	—	—	—	—	—	—	—	—	—	0.53(0.01)
T10 H	R(P)	—	—	—	—	—	—	—	—	—	—

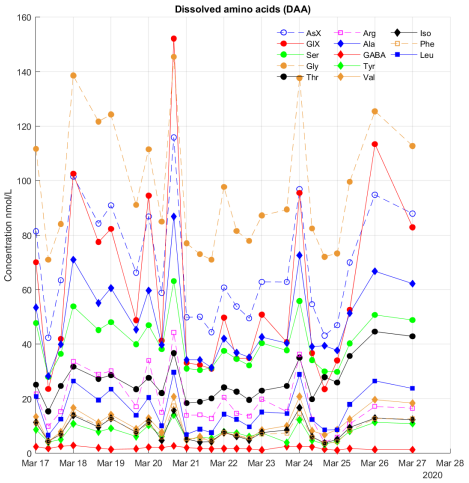

(a) Dissolved Amino Acids (DAA)

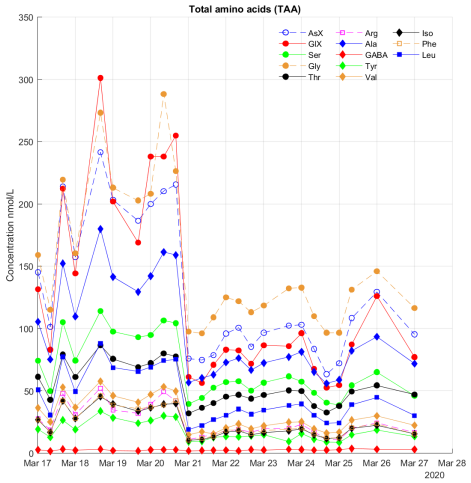

(b) Total Amino Acids (TAA)

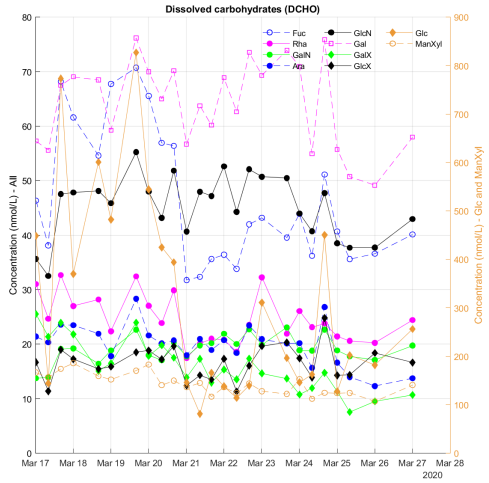

(c) Dissolved Carbohydrates (DCHO)

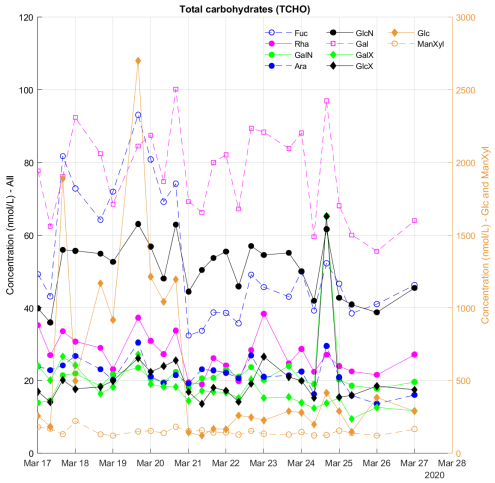

(d) Total Carbohydrates (TCHO)

Figure B.12 – Time series of a) Dissolved Amino Acids, b) Total Amino Acids, c) Dissolved Carbohydrates, d) Total Carbohydrates. For c) and d), Glc and ManXyl are plotted on the right axis for visibility.

B.2.5 Correlations in the SSA

B.2.5.1 Total SSA INP

Table B.7 – Correlations between total SSA INPs and ocean parameters - Whole cruise.

		TOC	NaCl	Salinity	T_{SW}	Syn	Nano	Pico	Bacteria	TOC	TN	DAA	PAA	DCHO	PCHO
INT1	R(P)	—	—	—	—	—	—	—	—	—	—	—	—	—	—
INT1 HL	R(P)	—	—	—	—	—	—	-0.96(0.04)	—	—	—	—	—	—	—
INT1 HS	R(P)	—	—	—	—	—	—	—	—	—	—	—	—	—	—
INT2	R(P)	—	—	—	—	—	—	—	—	—	—	—	—	—	—
INT2 HL	R(P)	—	—	—	—	—	—	—	—	—	—	—	—	—	—
INT2 HS	R(P)	—	—	—	—	0.80(0.02)	—	0.74(0.04)	—	—	—	—	—	—	—

Table B.8 – Correlations between total SSA INPs and ocean parameters - Frontal and subtropical waters.

		TOC	NaCl	Salinity	T_{SW}	Syn	Nano	Pico	Bacteria	TOC	TN	DAA	PAA	DCHO	PCHO
INT1	R(P)	—	—	—	—	—	—	—	—	—	—	—	—	—	—
INT1 HL	R(P)	—	—	—	—	—	—	—	—	—	—	—	—	—	—
INT1 HS	R(P)	—	—	—	—	—	—	—	—	—	—	—	—	—	—
INT2	R(P)	—	—	0.92(0.03)	—	—	—	—	—	-0.97(0.01)	—	—	-0.97(0.01)	-0.89(0.04)	—
INT2 HL	R(P)	—	—	0.95(0.05)	—	—	—	—	—	-0.98(0.02)	—	—	-0.98(0.02)	—	—
INT2 HS	R(P)	—	—	—	—	0.91(0.03)	—	0.91(0.03)	—	—	—	—	—	—	—

B.2.5.2 Submicron SSA INP

Table B.9 – Correlations between submicron SSA INPs and ocean parameters - Full cruise.

		TOC	NaCl	Salinity	T_{SW}	Syn	Nano	Pico	Bacteria	TOC	TN	DAA	PAA	DCHO	PCHO
INT1	R(P)	—	0.88(0.02)	—	—	—	—	—	—	—	—	—	—	—	—
INT1 HL	R(P)	—	0.99(0.01)	0.97(0.03)	0.97(0.03)	—	—	—	—	—	—	—	—	—	—
INT1 HS	R(P)	—	—	—	—	—	—	—	—	—	—	—	—	—	—
INT2	R(P)	—	—	—	—	—	—	—	—		—	—	—	—	—
INT2 HL	R(P)	—	—	—	—	—	—	—	—		—	—	—	—	—
INT2 HS	R(P)	—	—	—	—	0.95(0.01)	—	0.90(0.04)	—	—	—	—	—	—	—
T10	R(P)	—	0.78(0.02)	—	—	—	—	—	—	—	—	—	—	—	—
T10 HS	R(P)	0.97(0.04)	—	—	—	—	—	—	—	—	—	—	—	—	—

Table B.10 – Correlations between submicron SSA INPs and ocean parameters - Frontal and subtropical waters.

		TOC	NaCl	Salinity	T_{SW}	Syn	Nano	Pico	Bacteria	TOC	TN	DAA	PAA	DCHO	PCHO
INT1	R(P)	—	—	—	—	—	—	—	—	—	—	—	—	-0.95(0.05)	—
INT1 HL	R(P)	—	—	—	—	—	—	—	—	—	—	—	—	—	—
INT1 HS	R(P)	—	—	—	—	—	—	—	—	—	—	—	—	—	—
INT2	R(P)	—	—	0.94(0.02)	—	—	—	—	—	-0.97(0.01)	—	—	-0.97(<0.005)	-0.87(0.05)	—
INT2 HL	R(P)	—	—	0.97(0.03)	—	—	-0.95(0.05)	—	—	-0.99(0.01)	—	—	-0.99(0.01)	—	—
INT2 HS	R(P)	—	—	—	—	0.98(0.02)	—	0.96(0.04)	—	—	—	—	—	—	—
T10	R(P)	—	—	—	—	—	—	—	—	—	—	—	—	—	—
T10 HS	R(P)	0.97(0.03)	—	—	—	0.99(0.01)	—	0.99(0.01)	—	—	—	—	—	—	—

B.2.5.3 Supermicron INP

Table B.11 – Correlations between submicron SSA INPs and ocean parameters - Full cruise.

		TOC	NaCl	Salinity	T_{SW}	Syn	Nano	Pico	Bacteria	TOC	TN	DAA	PAA	DCHO	PCHO
INT1	R(P)	—	—	—	—	—	—	—	—	—	—	—	—	—	—
INT1 HL	R(P)	—	—	—	—	—	—	—	—	—	—	—	—	—	—
INT1 HS	R(P)	—	—	—	—	—	—	—	—	—	—	—	—	—	—
INT2	R(P)	—	—	—	—	—	—	—	—	—	—	—	—	—	—
INT2 HL	R(P)	—	—	—	—	—	—	—	—	—	—	—	—	—	—
INT2 HS	R(P)	—	-0.77(0.05)	—	—	—	—	—	—	—	—	—	—	—	—
T10	R(P)	—	—	—	—	—	—	—	—	—	—	—	—	—	—
T10 HS	R(P)	—	—	—	—	—	—	0.90(0.01)	—	—	—	—	—	—	—

Table B.12 – Correlations between supermicron SSA INPs and ocean parameters - Frontal and subtropical waters.

		TOC	NaCl	Salinity	T_{SW}	Syn	Nano	Pico	Bacteria	TOC	TN	DAA	PAA	DCHO	PCHO
INT1	R(P)	—	—	—	—	—	—	—	—	—	—	—	—	—	—
INT1 HL	R(P)	—	—	—	—	—	—	—	—	—	—	—	—	—	—
INT1 HS	R(P)	—	—	—	—	—	—	—	—	—	—	—	—	—	—
INT2	R(P)	-0.88(0.05)	—	—	—	—	—	—	—	—	—	—	—	—	—
INT2 HL	R(P)	—	—	—	—	—	—	—	—	—	—	—	—	—	—
INT2 HS	R(P)	—		—	—	—	—	—	—	—	—	—	—	—	—
T10	R(P)	—	—	—	—	—	—	—	—	—	—	—	—	—	—
T10 HS	R(P)	—	—	—	—	—	—		—	—	—	0.99(0.01)	—	—	—

C

Suplementary: PICNIC and WINS at PUY

Outline of the current chapter

C.1 Methods

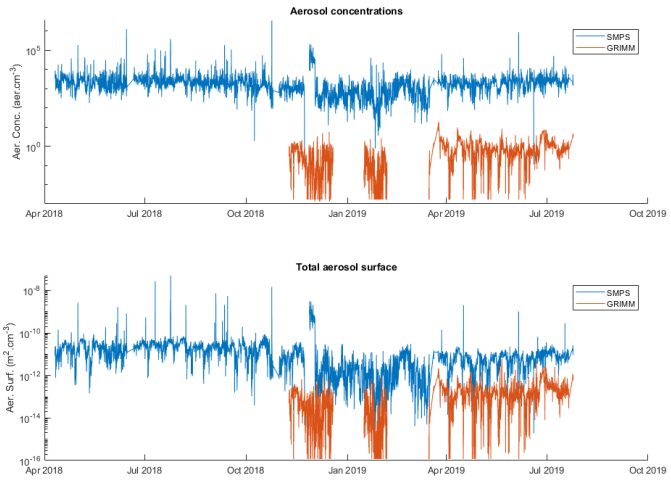

Figure C.1 – Comparison of the time series of SMPS and GRIMM data over a period of 1.5 year. When counting the total number of aerosols or the total surface of aerosols, the GRIMM values represent less than 1% of the total variability over the period.

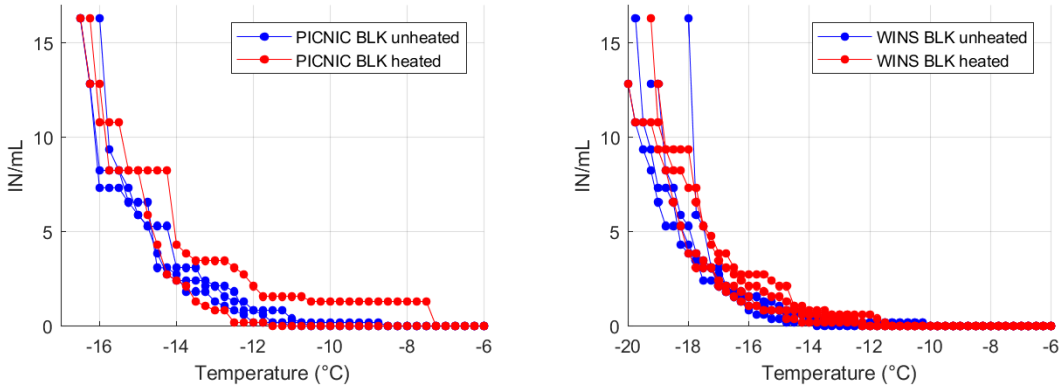

(a) PICNIC blanks.

(b) WINS blanks.

Figure C.2 – INP concentrations on blank filters during the PICNIC and WINS campaign, for unheated (blue) and heated (red) samples. The concentrations are given in INP per mL of 0.9% NaCl solution used for the analysis. The LOD corresponding to the experiment settings is 16.29 INP/mL.

C.2 INP spectra

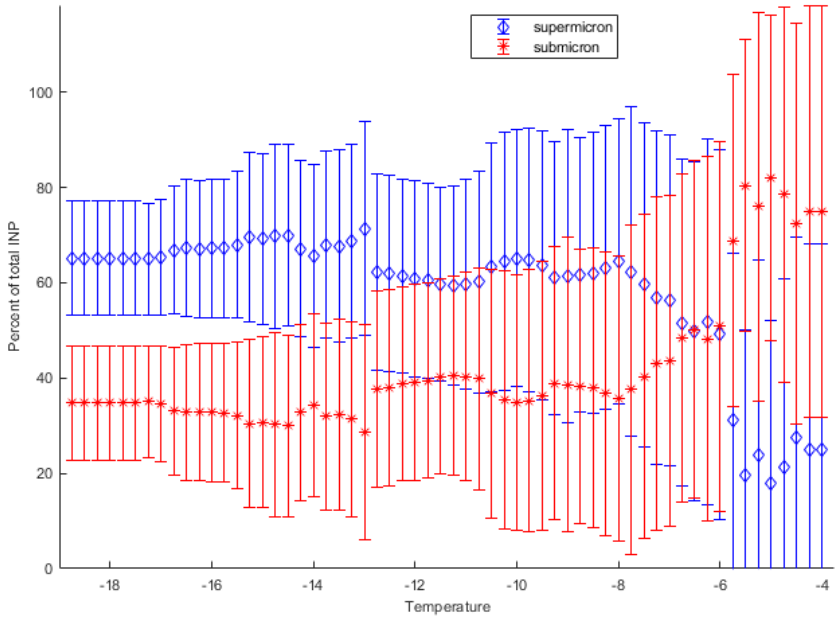

Figure C.3 – Spectra of submicronic and supermicronic fractions of INP from the WINS data. Error bars correspond to one standard deviation.

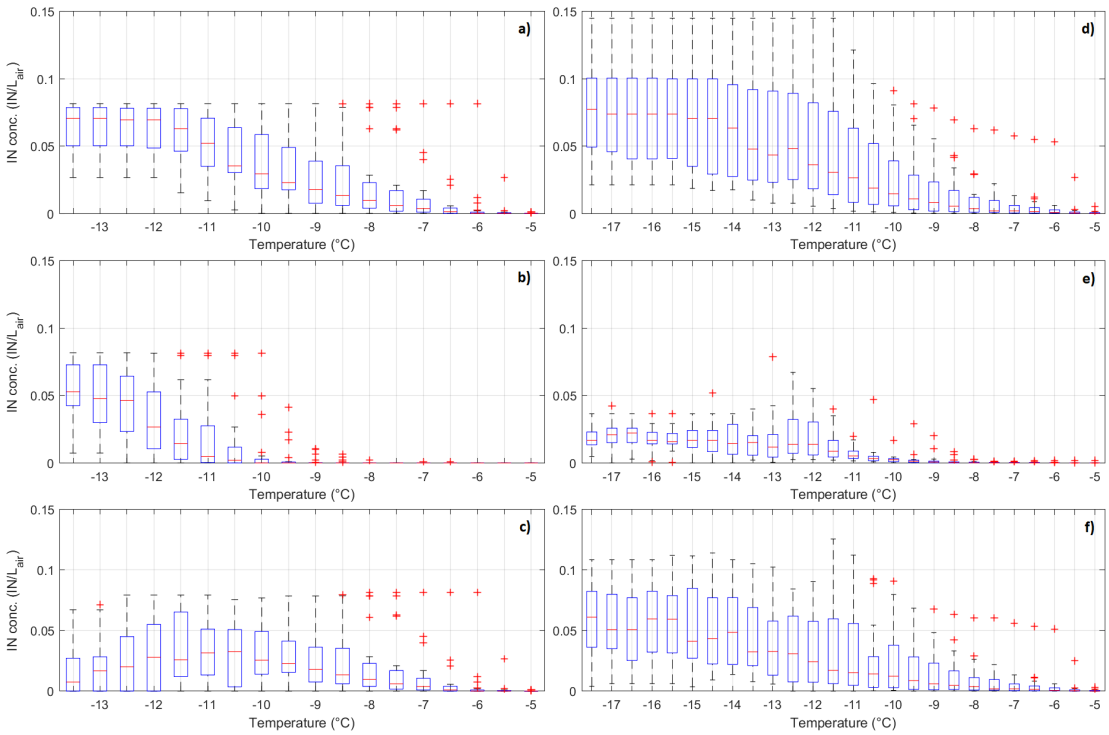

Figure C.4 – Boxplots of mean cumulative concentrations of INPs from PICNIC (a) All INPs, b) Heat Stable INPs, c) Heat labile INPs) and WINS (d) All INPs, e) Heat Stable INPs, f) Heat labile INPs) are plotted against temperature every 0.5°C. The red line represents the median value and the extremities of the boxes the 25% and 75% percentiles. The whiskers show the most extreme points that are not outliers. Outliers are represented by the red crosses

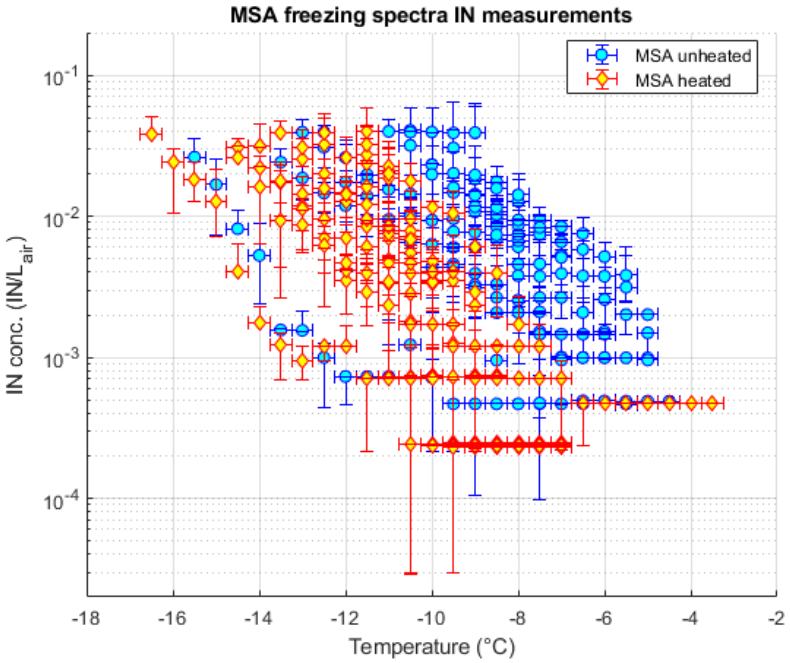

Figure C.5 – INP concentrations measured at MSA.

C.3 Statistical analysis

Table C.1 – Linear regression correlations coefficients and p-values (Pearson's test) between supermicron INP concentrations and aerosol parameters. Only significant ($P < 0.05$) correlations are indicated. Values with no significant correlations are indicated as double dashes. Values with $P < 0.005$ are indicated in bold.

		$N_{aer,tot}$	$N_{aer,500}$	S_{aer}	BC	Cl^-	NO_3^-	SO_4^{2-}
INT1	R^2(P)	—	—	—	—	—	—	—
INT2	R^2(P)	—	—	—	—	—	—	—
INT2 HS	R^2(P)	—	—	—	—	—	—	—
INT2 HL	R^2(P)	—	—	—	—	—	—	—
INT3	R^2(P)	—	—	—	—	—	—	—
INT3 HS	R^2(P)	—	—	—	—	—	—	—
INT3 HL	R^2(P)	—	—	0.26(0.04)	—	—	—	—

		Ox.	Na^+	NH_4^+	K^+	Mg^{2+}	Ca^{2+}
INT1	R^2(P)	—	—	—	—	—	—
INT2	R^2(P)	—	—	—	—	—	—
INT2 HS	R^2(P)	—	—	—	—	—	—
INT2 HL	R^2(P)	—	—	—	—	—	—
INT3	R^2(P)	—	—	—	—	—	—
INT3 HS	R^2(P)	—	—	—	—	—	—
INT3 HL	R^2(P)	—	0.29(0.03)	—	—	0.32(0.02)	—

D

Paper: The Puy de Dôme ICe Nucleation Intercomparison Campaign (PICNIC): Comparison between online and offline freezing techniques in ambient air

The Puy de Dôme ICe Nucleation Intercomparison Campaign (PICNIC): Comparison between online and offline freezing techniques in ambient air

L. Lacher[1], M. Adams[2], K. Barry[3], B. Bertozzi[1], H. Bingemer[4], C. Boffo[5], Y. Bras[6], N. Büttner[1], D. Castarede[7], D. J. Cziczo[8,9], P. J. DeMott[3], R. Fösig[1], M. Goodell[8], K. Höhler[1], T. C. J. Hill[3], C. Jentzsch[10], L. A. Ladino[11], E. J. T. Levin[3], S. Mertes[10], O. Möhler[1], K. A. Moore[3], B. J. Murray[2], J. Nadolny[1], T. Pfeuffer[5], D Picard[6], Carolina Ramírez-Romero[11], M. Ribeiro[6], S. Richter[4], J. Schrod[4], K. Sellegri[6], F. Stratmann[10], E. Thomson[7], H. Wex[10], M. Wolf[8], and E. Freney[6]

[1]Institute of Meteorology and Climate Research, Karlsruhe Institute of Technology, Karlsruhe, 76021, Germany
[2]School of Earth and Environment, University of Leeds, Leeds LS2 9JT, United Kingdom
[3]Department of Atmospheric Science, Colorado State University, Fort Collins, 80523, Colorado, United States
[4]Institute for Atmospheric and Environmental Sciences, Goethe University Frankfurt, Frankfurt, 60438, Germany
[5]Bilfinger Noell GmbH, Würzburg, 97080, Germany
[6]Laboratoire de Météorologie Physique, Université Blaise Pascal, 63178 Clermont-Ferrand, France
[7]Department of Chemistry and Molecular Biology, University of Gothenburg, Gothenburg, 40530, Sweden
[8]Department of Earth, Atmospheric and Planetary Sciences, Massachusetts Institute of Technology, Cambridge, 02139, Massachusetts, United States
[9]Department of Earth, Atmospheric, and Planetary Sciences, Purdue University, West Lafayette, 47907, Indiana, United States
[10]Leibniz Institute for Tropospheric Research, Leipzig, 04318, Germany
[11]Center of Atmospheric Science, Universidad Nacional Autónoma de México, Mexico City, 04510, Mexico

Correspondence to: Larissa Lacher (larissa.lacher@kit.edu), Evelyn Freney (evelyn.freney@uca.fr)

Abstract.

Aerosol particles which induce ice formation in clouds (i.e., ice-nucleating particles; INPs) impact cloud properties, their lifetime, and precipitation formation. Only a tiny fraction of all aerosol particles are INPs, and while their concentration increases exponentially with decreasing temperature, ambient INP concentrations can be below 0.1 L^{-1}. The accurate detection of such low numbers is technically challenging, which is why no single-best method exists. INP concentrations can be detected online with high-time resolutions of minutes, or offline, where filters are collected for several hours to days. Several such methods exist in the field of ice nucleation research, and need to be validated and tested against each other in order to accurately quantify INPs. Here we present ambient INP measurements from a total of ten freezing techniques. This ensures that the freezing methods are compared using a naturally dispersed aerosol, and tests their sensitivity and agreement also at low INP concentrations. Measurements were performed for two weeks in October 2018 at the Puy de Dôme observatory. INP concentrations were detected at mixed-phase cloud conditions. Two continuous flow diffusion chambers (CFDC; Colorado State University-Continuous Flow Diffusion Chamber, CSU-CFDC; Spectrometer for Ice Nuclei, SPIN) and two expansion chambers (Portable Ice Nucleation Experiments, PINEs) measured the INP concentration with a high-time resolution of minutes and below -20°C. Seven filter-based offline techniques determined the temperature-dependent INP concentration above ~-30°C for sampling times of ~ 8 hours (FRankfurt Ice Nuclei Deposition FreezinG Experiment, FRIDGE; Ice Nucleation Droplet Array INDA; Ice Nucleation Spectrometer of the Karlsruhe Institute of Technology, INSEKT; Ice Spectrometer, IS; Leipzig Ice Nucleation Array, LINA; LED based Ice Nucleation Detection Apparatus LINDA; Micro-Orifice Uniform Deposit Impactor–Droplet Freezing Technique, MOUDI-DFT). A special focus in this intercomparison campaign was placed on having the same sampling times for the methods: INP concentrations measured with the online instruments were compared within 10 minutes and at the same temperature (± 1 °C), while the filter collection for the offline methods were started and stopped simultaneously and compared at 1 °C steps. The INP concentration measured with the PINEs agrees well to CSU-CFDC, as the majority of the data fall within a factor of 2. While SPIN compares still quite well to CSU-CFDC (80% of the data fall within a factor of 5), there is a consistent trend for underestimating the INP concentration. This might be caused by a non-complete exposure of all aerosol particles to supersaturated conditions within the aerosol lamina, which was set to lower values as compared to CSU-CFDC. The offline methods which sampled filters in the laboratory via a whole air inlet also show a quite good agreement over the INP-temperature spectra range (more than 45% of the data fall within a factor of 2). Measurements using different filter materials, namely quartz fiber versus polycarbonate filters, the latter with two different pore sizes), and filter holders (standard filter holder and the HERA (High Volume Aerosol Sampler) revealed no difference in the temperature dependent INP concentration. However, consistently higher INP concentrations from filters collected directly on the rooftop at the Puy de Dôme station, as compared to those filters collected via a whole air inlet system, were observed. This suggests systematic losses of larger particles in inlets and their impact on ice nucleation in cloud-relevant environments, which should be considered, even in otherwise well-characterized aerosol field-measurement stations.

1 Introduction

The first formation of ice in mixed-phase clouds is triggered by specific aerosol particles, so-called ice-nucleating particles (INPs; Vali et al., 2015). INP concentration are important for for the formation and further development of clouds, since they can determine their phase (e.g., by a rapid cloud glaciation and associated dissipation effect; Campbell and Shiobara, 2008; Murray et al., 2012; Paukert and Hoose, 2014; Kalesse et al., 2016; Desai et al., 2019) and related radiative properties (e.g. Vergara-Temprado et al., 2018). In addition, INPs have an impact on precipitation formation (e.g., Mülmenstädt et al., 2015; Field and Heymsfield, 2015; Fan et al., 2017). However, the identification and quantification of ambient INPs remains challenging due to their scarceness (Kanji et al., 2017) and limitations in measurement techniques (DeMott et al., 2017; Cziczo et al., 2017).

Different methods to quantify ambient INP concentrations exist and are categorized into online instruments and filter-based offline freezing techniques. Online instruments measure real-time INP concentration with a high temporal resolution (seconds to minutes). It has been shown that INP concentration can fluctuate considerably within short sampling times (e.g., Prenni et al., 2009; Lacher et al., 2017; Welti et al., 2018; Paramonov et al., 2020). Therefore, online methods are better suited to catch such variability, and relate them to e.g. changes in air mass and aerosol properties. On the other hand, currently available online instruments for ambient measurements typically sample only a few litres per sampling interval. This limits the ability of these methods to detect low INP concentrations, which is very important given the naturally low INP concentration, especially at mixed-phase cloud temperatures below -20°C. Offline methods are based on collecting aerosol particles on a sampling substrate or into liquids, typically over longer time periods of hours to days, and therefore are able to collect a larger volume of air (~ m^3), increasing the likelihood to sample very rare INPs. Filter-based INP analysis can also be performed over shorter time periods, but due to the labor-intensive filter-collection and analysis procedure, online methods are often the preferred method to measure INPs with a hight-time resolution.

In order to accurately quantify INPs, existing methods need to be validated and compared with each other, to address potential systematic biases. A set of different methods were compared in laboratory studies using well-known aerosol particles, e.g. by sharing samples of SNOMAX®, cellulose, or illite-rich samples amongst the community of the Ice Nuclei Research Unit (INUIT; Wex et al., 2015; Hiranuma et al., 2015; Hiranuma et al., 2019), during the Leipzig Ice Nucleation chamber Comparison (LINC; Burkert-Kohn et al., 2017), and during the Fifth International Workshop on Ice Nucleation phase 2 (FIN-02; DeMott et al., 2018). Those experiments revealed a generally good agreement between a large set of freezing methods. Hiranuma et al. (2015) indicated that the aerosol particle generation method (dry versus wet suspension) can lead to changes in detected INP concentrations, which was also found by other laboratory studies (Emersic et al., 2016; Boose et al., 2016b). Moreover, it was shown that the methods' comparability depended on the chosen aerosol particle type and nucleation temperature: SNOMAX®, below a nucleation temperature of -10°C, and natural dust samples resulted in good agreement; SNOMAX® above -10°C, illite NX above -25°C, and potassium feldspar between -20 and -25°C resulted in discrepancies amongst instruments, which is explainable by the fact that INP concentrations for those particle types are increasing strongly as a function of temperature in the respective ranges, and any small variability in the instruments' temperature measurements or principles of operation can lead to considerable deviations.

Other aspects which are crucial for intercomparing ice nucleation techniques is the size range of aerosol particles which are INPs. Typically, online instruments, such as continuous flow diffusion chambers (CFDCs), are limited

to sample aerosol particles below ~ 3 µm, as they aim at measuring freshly formed ice crystals within the chamber, and a size overlap with unactivated larger aerosol particles must be avoided. In contrast, filter-based offline techniques are able to sample a larger fraction of the aerosol particles size range. At the same time, many of those techniques sample aerosol particles on filters, which do not collect all the particles smaller than the pore size (e.g., less than ~70% of particles smaller as 100 nm are collected on 200 nm nuclepore filters (Ogura et al., 2016)), which might also not be released from the filter during analysis. Moreover, particle collection efficiency using filters can also be reduced by a possible bounce from the collection substrate. The role of a dominating size of INPs is thereby an important aspect to assess the suitability of a freezing technique to capture the picture of ambient conditions. Supermicron particles were often found to contribute the majority of INP in different studies in North America and Europe (Mason et al., 2016), the Arctic (Creamean et al., 2018) and Cabo Verde islands (Gong et al., 2020), however, with a varying fraction, potentially depending on the sampling location and nucleation temperature. In contrast, the analysis of ice crystal residuals in the lower free troposphere revealed that the majority of particles were submicron in size (e.g., Mertes et al., 2007; Schmidt et al., 2017). Also ice-active organic particles emitted from the Ocean were found to be submircon in size (Wilson et al., 2015) and might dominate the INP population in such remote marine environments. In laboratory-based intercomparison studies it was suggested that the general good agreement between methods was achieved by controlling the aerosol particle size distribution used for the INP experiments (DeMott et al., 2018). At ambient conditions, however, aerosol particles and INPs can span a wide size range, which can be crucial for determining the real ambient INP concentration, and for intercomparing INP measurement techniques which do not cover the same size range. Especially close to emission sources for mineral dust, which is acknowledged to be a key ice nucleator in the troposphere at temperatures below -15 °C (e.g., Atkinson et al., 2013), the occurrence of supermicron particles is likely higher as compared to locations further away. Moreover, the methods' sensitivity to detect low ambient INP concentrations, and the way measurements close to the detection limits are considered for averaging INP concentration over longer sampling intervals are other important aspects for ambient measurements (e.g., Boose et al., 2016). Ambient INPs show a wide range of concentration (e.g., Kanji et al., 2017), and it is crucial that those concentrations are captured precisely.

By conducting measurements on ambient aerosol, impacts from aerosol generation methods and strong impacts from a single INP type is avoided, and the instruments are compared under realistic conditions regarding the naturally low INP number concentration. DeMott et al. (2017) presented a field-based intercomparison campaign using four offline techniques and an online instrument at different locations in the Western USA, including agricultural areas, mountainous desert regions, and at a coastal site. They generally found a good agreement between instruments, especially when measurements were performed with a perfect time overlap. Moreover, a high bias as compared to the online method was observed when aerosol particles were sampled onto filters or into a bulk liquid (below -20°C). It is unclear if this might have been caused by a breakup of aggregates by partial solvation of aerosols, which contain more than one INP, or if it reflect the role of all mixed-phase temperatures (even lower ones) of larger INPs not captured by the online method used in that studys. In a recent study by Brasseur et al. (ACPD) in the Finnish boreal forest, three online instruments were intercompared during four days and a nucleation temperature below -29°C and generally found a good agreement. Such intercomparison efforts need to be expanded to cover the full range of mixed-phase cloud temperatures, and also need to be conducted in environments in which mixed-phase clouds can occur. INP intercomparison activities are especially relevant due

to ongoing efforts for the establishment of INP monitoring networks. E.g., on a European level, the ACTRIS (Aerosol, Clouds and Trace Gases Research Infrastructure) Topical Centre for Cloud In Situ measurements is currently in an implementation phase to include INP concentration as a parameter to be monitored at specific research stations. For such an effort it is crucial to ensure that INP concentrations are precisely quantified using different online or offline instruments.

Here we present results from the Puy de Dôme ICe Nucleation Intercomparison Campaign (PICNIC). The Puy de Dôme station is a mountain top station situated in central France at an altitude of 1465 m. Given its altitude it is often advected by long range transported airmasses, that represent a large spatial scale. It is also an environment in which clouds occur, thus the aerosol population being present at Puy de Dôme is relevant for aerosol cloud interactions. Therefore, intercomparing measurement techniques using ambient particles which are relevant for cloud formation is of great advantage. During PICNIC, a set of seven offline techniques, as well as three online instruments were compared during 14 days in October 2018. A key aspect here is that the offline and online instruments were each intercompared during the exact same sampling time (offline instruments) or within 10 minutes (online instruments), which excludes an impact of the variation of the aerosol population. Only when intercomparing the online to the offline methods, the time intervals were not perfectly overlapping. Moreover, two main sampling locations inside the laboratory, via a total aerosol inlet, and one location directly outside on the laboratory´s rooftop were used, addressing potential sampling biases by particle losses in the inlet and by a purposeful use of upstream impactors for some online instruments. Advances over past studies are sought herein through use of a larger set of methods and coordination of longer shared sampling times.

2 Methods

2.1 Measurement location and time

The PICNIC campaign took place from the 7th to the 20th October 2018, at the Puy de Dôme (1465 m a.s.l.), which is located in central France. An overview on the measurement campaign will be presented by Freney et al. (in preparation). The site is located on a mountain chain, and under low-wind conditions the site is suited to sample undisturbed atmospheric layers originating in the boundary layer, as well as in the lower free troposphere (Asmi et al., 2012; Farah et al., 2018). The site is operated by the *Observatoire du Physique du Globe de Clermont Ferrand* (OPGC) and run by the *Laboratoire de Météorologique Physique* (LaMP), and is an observational facility of the ACTRIS-2, and Global Atmospheric Watch measurement program. Continuous measurements of meteorological conditions, as well as aerosol physical and chemical properties are provided. The submicron aerosol particle size distribution was measured using a custom made scanning mobility particle sizer coupled with a condensation particles counter (CPC, model 3010, TSI) via a whole air inlet (WAI) with a 50% cut-size diameter of 30 µm. In addition, during the course of the campaign, an optical particle counter (OPC; Welas 2500, Palas GmbH, Germany) measured the aerosol particles above 0.7 µm at the WAI. Since the OPC was most of the time attached to an aerosol particle concentrator which used an 2.5 µm impactor (see next section 2.2), size distribution measurements are limited to below 2.5 µm. Measurements were thereby conducted inside the laboratory, and via two identical WAI, as well as on the rooftop (Fig. 1). Full details on the measurement set up of all online and offline techniques are provided in the following section.

In this study, INP concentrations are compared within a factor of 2 and 5. It was indicated that the representations of INPs in models need to be predictable within a factor of 10 to not change cloud microphysics (Phillips et al.,

2003), and our chosen values of 2 and 5 are thus even more conservative and can be considered to represent a good (factor 2) and agreeable (factor 5) comparison.

2.2 Online measurement techniques

Three different online INP instruments were operated behind the WAI in parallel during several hours per day. INP concentrations were determined for single particles activating at a temperature range between ~ -20°C and -30°C, in the condensation/immersion freezing mode. For the intercomparison of these instruments, INP concentrations are only considered when measured within ± 1°C and within ± 10 minutes. This aims at reducing any potential impact of a change in the sampled INP population at presumably nearly identical sampling conditions. We acknowledge that a ± 1°C range can possibly lead to variations in detected INP concentrations, however, a more restrictive approach would further limit the amount of intercomparison data points.

Online INP measurements were partially conducted downstream of the Portable Fine Particle Concentrator (PFPC; Gute et al., 2019), which is optimized for concentrating aerosol particles >0.1 µm. The instrument was deployed at a separate inlet, and was using an impactor with a 50% size-cut at 2.5 µm. Aerosol particles are concentrated with factors of ~ 20 for particles > 0.5 µm, and with lower values for smaller particles. Since the INP measurements using the online instruments were performed simultaneously on the PFPC, the same concentration factors were applied, which therefore did not have an impact on the instruments' comparability, given that the instruments did not use additional impactors smaller then this size-cut of 2.5 µm. The concentration factor used for the online intercomparison is thereby a campaign average of 11.4, and has a standard deviation of 1.7. This concentration factor was infered by consecutive measurements on and off the concentrator with the Colorado State University Continuous Flow Diffusion Chamber (CSU-CFDC, see section 2.2.1), which performed such measurements most frequently. For the comparison to the filter-based offline INP concentrations, a daily average concentration factor from CSU-CFDC was used to calculate ambient INP concentrations in case they were performed at the PFPC. This daily average concentration factor ranged from values of 8.5 to 16.5, reflecting the size-dependency of INPs.

2.2.1 The Colorado State University Continuous Flow Diffusion Chamber (CSU-CFDC)

CSU-CFDC is the longest-existing instrument for online detection of ambient INPs, with a legacy of versions for ground and aircraft-based measurements starting from the late 1980s (Rogers et al., 2001; DeMott et al., 2018). Its working principle is based on the establishment of supersaturated water and ice conditions in flowing air between two ice-coated walls of cylindrical shape in a vertical orientation. Those walls are held at different temperatures, and while the air temperature in the central lamina region is a linear function between these temperatures, the water vapour pressure is a non-linear function of temperature, resulting in a supersaturated region with respect to ice and water between the walls. Aerosols are guided within a particle-free sheath air through this region and can activate into water droplets and ice crystals. While cloud droplets are evaporated downstream using an evaporation section, the remaining ice crystals are detected by their larger size using an OPC (Climet CI-3100). The size threshold to determine ice crystals was thereby 4 µm. CSU-CFDC uses a pair of single-jet impactors upstream of the chamber, for this study with inserts defining 50% size-cuts at 2.5 µm, such that effectively only aerosol particles smaller than this size enter the system. This allows ice crystals to be clearly differentiated from larger ambient aerosol. The measurement uncertainties with regard to temperature and relative humidity with respect to water are stated as ± 0.5 °C and 2.4%, respectively, at -30°C (DeMott et al., 2015). Residence times of aerosols in the supersaturated region are 5 seconds for the flow rate used (1.5 LPM; liter per minute). For this study, water

supersaturation was controlled to be sufficiently high to promote comparison to the results of immersion freezing methods (DeMott et al., 2017). The mean and median supersaturations employed for this study were both equal to 6.5% (i.e., 106.5% relative humidity with respect to water, RH_{water}), with a standard deviation of 1.4%. At this value, it is likely that maximum INP concentrations are not captured, although underestimations would be expected to be less than the factor of 3 noted for mineral dusts in comparing data collected at 105% versus 109% in DeMott et al. (2015). The data are thereby averaged over a time period of 1 minute, which allows a most-close comparison to the other instruments by integrating the INP measurements with CSU-CFDC on the time grid of the other online methods. CSU-CFDC is typically operated for ~ 4 hours before refreshing the ice surfaces on the walls. Operation times in excess of 4 hours can result in an increase in background ice counts (due to frost) in the chamber and thereby degrade the signal-to-noise ratio. CFDC background corrections are needed to account for INP signal contamination that may come in the form of frost crystals flaking from the ice walls (Rogers et al. 2001). Infrequent, high concentration bursts may occur, typically in the time just following wall icing or after a number of hours of operation. These are accounted for with a data pre-screening method to search for outliers in ice crystal arrival rates at the optical particle counter (Moore, 2020). The more common intermittent, low concentration frost events are corrected for by comparing ambient measurements with measurements of HEPA-filtered air. For PICNIC, these filter periods were 5 minutes long, bookending each 10-minute ambient air sample period. The correction for intermittent frost events has recently been modified to improve the estimates of statistical significance and confidence intervals over previous techniques, following Krishnamoorthy and Lee (2013). The background INP counts from filter periods that bracket each ambient measurement are combined into a single Poisson distribution with a characteristic rate parameter. The difference between the ice crystal arrival rates during the ambient measurement and the combined filter period are used to calculate the background-corrected INP concentrations (Moore, 2020). Statistical significance and confidence intervals for each ambient measurement are determined using the moment-based Z-statistic defined in Krishnamoorthy and Lee (2013).

2.2.2 The Spectrometer for Ice Nuclei (SPIN)

The SPIN is a commercially available CFDC developed by Droplet Measurement Technologies (Garimella et al., 2016). It is based on the design of the laboratory instrument ZINC (Zurich Ice Nucleation Chamber; Stetzer et al., 2008) and its mobile version PINC (Portable Ice Nucleation Chamber; Chou et al., 2011). Briefly, two parallel flat plates are separated by 1 cm and each coated with 1 mm of ice prior to experiments. A temperature gradient between the two plates establishes a supersaturation with respect to ice and potentially liquid water. The supersaturation employed for this study was thereby 2.8 (102.8% RH_{water}) ± 1.9% during this campaigns Aerosols are fed into the chamber at a sampling rate of 1 LPM and constrained to a lamina centerline with 9 LPM of sheath air. An impactor with a 50% size-cut at 2.5 µm (BGI Inc., SCC1.062 Triplex) was installed before the SPIN inlet. Activated INP are detected using a light-depolarization OPC (Garimella et al. 2016; Droplet Measurement Technologies). Due to the sigmoidal shape of the size-cut, OPC counts larger than 5 µm in diameter were considered as activated INPs.

Uncertainties in temperature and RH_{water} at mixed-phase cloud conditions are ~ ± 0.5 ˚C and ± 3%, respectively. The uncertainty in INP concentration represent the standard deviation from a 10-minute measurement. SPIN's limit of detection is dependent on background ice concentrations resulting from ice shed from the walls. Backgrounds were measured for 5 minutes on either side of a 10-minute sampling period. Average backgrounds before and after a sampling period were subtracted from the average measured INP concentration. Only data from

when backgrounds were less than half of measured INP concentrations are reported. The campaign-averaged background concentration was ~ 3 L^{-1}. When sampling off the aerosol concentrator, the SPIN LOD is therefore ~ 6 INP L^{-1}. SPIN can typically be operated for four to six hours before backgrounds are too high to preclude measurement of ambient INP concentrations. Next to the results from SPIN presented in this manuscript, focusing at mixed-phase cloud conditions, SPIN also measured cirrus-relevant INP concentrations, which is discussed elsewhere (Wolf et al., 2020).

2.2.3 The Portable Ice Nucleation Experiment (PINE)

The PINE is a new type of mobile instrument to measure INPs (Möhler et al., 2021). It is based on the AIDA (Aerosol Interaction and Dynamics in the Atmosphere) chamber and mimics cloud formation upon air mass lifting by expansion. The instrument is fully automated and can be operated continuously. During the PICNIC campaign, the PINE versions PINE-1A and PINE-1B were deployed. Those versions consist of a 7-liter cylindrical chamber, which are cooled by an external ethanol cooling chiller (Lauda RP 855 (PINE-1A) and 890 (PINE-1B); Lauda-Königshofen, Germany). PINE operates in a cycled mode of flush, expansion, and refill. During the so-called flush mode, aerosol particles are guided through the chamber at a flow rate of 2 LPM for 5 minutes, in order to exchange the sampled volume. Prior to entering the chamber, the sampled air is dried to a frost point temperature of below ~ -13°C, which avoids accumulation of ice on the chamber wall. An OPC (PINE-1A: welas-2500, PINE-1B: fidas-pine, Palas GmbH, Karlsruhe, Germany) attached to the outlet of PINE thereby counts larger unactivated aerosol particles. The flush mode is followed by the expansion mode, when a valve upstream of the chamber is closed while the volumetric flow out of the chamber is set to a constant value of 3 LPM. A total pressure reduction of~300 mbar is thereby induced over a time of ~50 seconds. During this expansion, the air temperature in the chamber is decreased by expansional cooling. As the wall- and air temperature is below the frost point temperature, the chamber is ice-saturated at the start of the expansion, and gets supersaturated with respect to ice and water during the course of the expansion, such that cloud droplets (upon cloud condensation nuclei) and ice crystals (upon INPs) can form. After reaching the expansion, the chamber is set to the refill mode where the chamber is refilled with filtered sample air to reach ambient pressure conditions. Then another cycle of flush, expansion, and refill is started.

During the expansion, the ice crystals are thereby detected by their larger optical size in the OPC, which makes a distinction to cloud droplets possible. As the OPC has a sideward scattering geometry, aspherical ice crystals are detected with a higher scattering intensity as sperical cloud droplets of same volume and refractive index. No ice-background correction is needed for the INP measurements, since the chamber is operated with frost-free walls, which is controlled by regular background experiments, when the sampled air is guided over a filter for several consecutive expansions.

Here, the INP concentrations are averaged over two consecutive experiments (two cycles of flush, expansion, and refill) to increase the detection limit for INPs. During one expansion, about 2 L of air is analyzed. PINE-1A, equipped with the welas-2500 which has an optical detection volume of 10%, thus has a limit of detection of 2.5 INP per liter. The detection limit of PINE-1B for one expansion is lower (0.25 INP per liter), as the fidas-pine sensor attached to it analyzed the full sample volume. The uncertainty for the INP concentration is thereby 20%,

which is an upper estimate from the uncertainties of the determination of the optical detection volume. The uncertainty in temperature is ± 1°C (see Möhler et al. (2021) for further details about the specifications of PINE).

The majority of aerosol particles with an aerodynamic diameter < 2 µm are sampled with PINE (80%), which decreases to > 50% for particles with an aerodynamic diameter of > 4 µm. No impactors were used with the PINE instruments, only when sampling at the PFPC, which is operated with an impactor with a 50% size-cut at 2.5 µm, the sampled particle size was limited to this size.

2.3 Offline measurement techniques

Aerosol particles were collected in bulk for offline INP analysis simultaneously during 8-hour intervals. Here, we present results from day- and nighttime (10 am to 6 pm and 10 pm to 6 am, respectively) from the 7th to the 20th October 2018 (Tab.1). The particles were collected on filters, either behind the WAI inside the laboratory or directly on rooftop (Fig. 1). The results obtained at the different sampling locations aim at investigating a potential loss of INPs in the inlet system. After collection, the samples were transported to the respective laboratories and particles were resuspended from filters to analyze for their ice nucleation activity in the immersion freezing mode. The comparison of the INP freezing spectra determined with the different methods is done at 1°C intervals. A total of seven methods were deployed during the PICNIC, which are described in the following sections, and their specifications regarding filter collection and freezing analysis is summarized in Tab 1.

The cumulative INP concentration calculation as function of the nucleation temperature $c_{INP}(T)$ for all offline techniques follow the well-established Vali (1971) equation:

$$c_{INP}(T) = \frac{V_{sol}}{V_{air}} \frac{1}{V_{drop}} \left(ln\left(\frac{N_{all}}{N_l(T)}\right) - ln\left(\frac{N_{all,BG}}{N_{l,BG}(T)}\right)\right) \quad (1)$$

Where V_{drop} is the droplet volume, N_l is the number of liquid and thus unfrozen droplets, while N_{all} is the number of the total droplets containing the aerosol suspension. The calculation thereby considers the volume of water used to extract the sample V_{sol} and the volume of air sampled V_{air} (considering the filter collection time and the applied flow rate). The number of total droplets from background measurements ($N_{all,BG}$) and the number of liquid droplets from background measurements $N_{l,BG}(T)$ are infered from the freezing curves of field blank filters, which were handeled the same way as the samples only that no flow was guided over the blank filter. The INP errors are indicated by using 95% confidence intervals.

2.3.1 FRankfurt Ice Nuclei Deposition FreezinG Experiment (FRIDGE)

For the FRIDGE measurements, aerosol particles were collected in the laboratory from the WAI inlet. Aerosol was collected by using a custom-built semi-automated multi-filter sampling device. The unit consists of 8 individual filter holders, the 45.7 cm housing, valves, a pump and electronics. The sampling time of each filter can be programmed separately. The flow rate through the filters was determined to be 4.8 ± 0.4 Std LPM on average. This is more than 50% lower than the flow rate that was originally targeted due to a miscalibration and a leakage in the system. Due to the leak, which was detected after the campaign, a few litres of (particle-free) air were not pumped through the inlet. Accordingly, the flow rate needed to be corrected to the above-mentioned value and carries a rather high uncertainty. Aerosol particles were collected onto 47 mm hydrophobic PTFE Fluoropore Membrane Filter of 0.22 µm pore size (Merck Millipore). Filters were not pre-cleaned in any way. It was decided

to limit the sampling time for FRIDGE to 4 hours during daytime (10 am – 2 pm, i.e. the middle of the other instruments), as we expected higher INP concentrations as during nighttime sampling, and thus to better capture potential variability in INP concentrations. The nighttime sample was the same as for the other groups (8 hours). Moreover, on October 18th, we did not increase the sampling time to 24 hours as other methods did for the same reasons. Filters were stored frozen after collection at the site. After transport, they were stored in a refrigerator until the measurements were performed. Upon measuring, the filters were placed in a sterile Eppendorf Tube, which was filled with 5 mL of ultrapure water (Rotipuran ultra, Carl Roth). Particles were then extracted into the ultrapure water by repeated steady shaking for some minutes. We applied no dilutions. By use of an Eppendorf Reference 2 pipette a total of about 200 (184 – 231) 2.5 µL droplets were manually pipetted onto a 47 mm silanized (Dichlordimethylsilan) silicon wafer substrate placed on a cold stage inside of a 500 cm^3 measurement cell. About 65 droplets of 2.5 µL fit onto the substrate at a time, therefore three individual runs per sample were performed to improve the freezing statistics. Before and after each measurement run, the substrate was thoroughly cleaned with pure non-denatured ethanol (Rotipuran, >99.8 %, Carl Roth). During the experiment, the measurement cell was constantly flushed with dry synthetic air at 1 LPM to prevent condensation and riming. Temperature was decreased at a constant rate of 1 °C min^{-1} until every droplet was frozen using a PID-controlled Peltier element. An ethanol cryostat cooling system supported the Peltier by dissipating the heat. The surface temperature was measured with a Pt100 sensor, which has an accuracy of ± 0.2 °C. A camera saved images every 10 seconds and the change in brightness was detected when a droplet was freezing.

2.3.2 Ice Nucleation Droplet Array (INDA)

For subsequent analysis with INDA and LINA (see section 2.3.5), three different types of filters and two different samplers were deployed, with both samplers operating in parallel. All filters were taken at the WAI. Quartz fiber filters (Munktell, MK 360; 47 mm diameter) were used for sampling, as well as polycarbonate filters (Nuclepore, Whatman, 47 mm diameter) with pore sizes of 200 or 800 nm). One sampler was a simple standard filter holder. The sampling flow was deliberately set to different values for different sampling periods, varying between 12 and 37 LPM, resulting in total collected air volumes between 6 and 18 m^3. The other sampler was HERA (High Volume Aerosol Sampler, Hartmann et al., 2020), which was developed for airborne sampling and enables the subsequent sampling of six filters. For HERA, the sampling flow was varied between 15 and 41 LPM, resulting in collected air volumes between 7 and 20 m^3. All samples and blank filters were stored in separate Petri-dishes right after sampling and stored frozen until analysis was done at TROPOS.

INDA is a measurement techniques which was introduced by Conen et al. (2012) and Hill et al. (2014). A suspensions is obtained from washing particles off a polycarbonate filter. For this, the filters are put in 3 mL of ultra-pure water, followed by shaking for 15 min in a flask shaker. Subsequently, typically 0.1 mL of the suspension are used for a LINA experiment (Sec. 2.3.5). Then 3.1 mL of ultra-pure water are added, and 50 µL droplets of this suspension are placed into 96 wells of a PCR tray. For the quarz filter samples, each well is filled with 50 µL of ultra-pure water together with a 1 mm diameter filter punch from the quartz fiber filter. The PCR tray is then immersed in the cooling bath of a thermostat and is illuminated from below. During the cooling down, typically done at 1°C min^{-1}, a picture is taken every 6 s from above. Changes in the color of a well related to

freezing, and are automatically detected. More information can be found in Gong et al. (2020) for the INP analysis of quartz fiber filters and in Hartmann et al. (2020) for polycarbonate filters.

2.3.3 The Colorado State University Ice Spectrometer (IS)

The Colorado State University (CSU) Ice Spectrometer (IS) analyzes arrays of liquid suspensions from filter samples to quantify immersion freezing INP concentrations (e.g., DeMott et al., 2018). Aerosol filter samples were collected on the roof of the laboratory using precleaned, 0.2-µm pore diameter, 47 mm diameter Nuclepore polycarbonate filter membranes held in open-faced sterile Nalgene sampling heads. Mass flow rates were recorded at 1 Hz intervals to tabulate total volume filtered. Filter samples were placed into sterile petri dishes (Pall), stored frozen, and transported frozen using a liquid nitrogen dry shipper, until analysis at CSU.

For analysis, 10 mL of 0.1 µm-filtered (Whatman Puradisc, PTFE membrane) deionized water was added to each tube and placed in a Roto-Torque rotator (Cole-Parmer) for 20 min to create a suspension. Thirty-two aliquots of 50 µL of each sample were dispensed into PCR trays (OPTIMUM® ULTRA Brand from Life Science Products) in the IS aluminum cold blocks. Suspensions were cooled at a rate of ~ 0.33 °C min-1, during which freezing of wells was detected by a CCD camera, and the corresponding temperature recorded with a LabVIEW interface. The lowest freezing temperature achievable was determined by deionized water purity. Lowest temperatures of significant data were generally between -27 and -30 °C. For PICNIC, sample volumes averaged 6500 L for ~8 hour collections (equalling an average flow of 13.5 LPM), during days and overnight. Two-tailed, 95 % confidence intervals for binomial sampling were calculated for the data based on Agresti and Coull (1998).

2.3.4 The Ice Nucleation Spectrometer of the Karlsruhe Institute of Technology (INSEKT)

The INSEKT is a re-build of the IS freezing method (e.g. Schneider et al., 2021). During PICNIC, aerosol particles were collected in the laboratory via the WAI with a standard filter holder. The aerosol particles were collected with a flow rate of 11.3 (±0.2) Std LPM on 47 mm diameter Nuclepore filters (Whatman) with a pore size of 200 nm. The filters were pre-cleaned (10% H_2O_2 solution) and kept frozen after aerosol particle collection, until analysed in the KIT laboratory. For INSEKT analysis, aerosol particles are washed off the filter using 8 mL filtered nanopure water (0.1 µm pore diameter filter and 18MΩ deionized water), and shaken on a rotator for 20 minutes to ensure the release of all particle from the filter. The resulting suspension is then diluted by factors of 1, 15, and 225, and volumes of 50 µl are placed in wells of a sterile PCR tray, alongside filtered nanopure water samples to determine its freezing behaviour for a background correction. The PCR tray is then placed in an aluminium block thermostated with an ethanol cooling bath (LAUDA RP 890; Lauda-Königshofen, Germany). From a starting temperature of 0°C, the wells are cooled down at a rate of 0.33°C min^{-1}. Four pt100 temperature sensors are placed inside the aluminum blocks for each PCR tray, measuring with an accuracy of ±0.1°C and a deviation to the edges of the wells of ±0.1°C, resulting in an uncertainty in temperature of ±0.2°C. A camera detects brightness changes of the wells that correspond to their freezing.

The handling filter blanks prior to the 8th October 2018 started to freeze at -7°C, which was traced back to using non-powder-free gloves during the filter handling procedure at the Puy de Dôme, which was changed thereafter. Therefore, filters handled with non-powder-free gloves had to be disregarded. Moreover, filters containing parts of real insects, which were sampled due to a leak in the WAI mesh, were excluded from the analysis.

2.3.5 The Leipzig Ice Nucleation Array (LINA)

LINA is based on Budke & Koop (2015). The filters are sampled as described in sec. 2.3.2, while only polycarbonate filters can be analyzed in LINA. Of the resulting suspensions from the filter washing water, 90 droplets with a volume of 1 μL are pipetted onto a hydrophobic glass plate, which is placed on a Peltier element. Each droplet is contained in a separate compartment which is covered by a second glass slide. Droplets are illuminated by a ring of light installed above, together with a camera. During the cooling process, typically done at 1 °C min^{-1}, a picture is taken every 6 s from above. Changes in the reflection of the light by the droplets related to freezing are automatically detected. A more detailed description can be found in Gong et al., 2019.

2.3.6 The LED based Ice Nucleation Detection Apparatus (LINDA)

The LED-based Ice Nucleation Detection Apparatus (LINDA) is described in detail in Stopelli et al. (2014). Quartz filters (15 cm diameter) were used for analysis with LINDA, taken with a high volume sampler at the rooftop with a sample flow of 500 LPM. The filters were stored in the freezer at -20°C until analysis in the laboratory of LaMP.

LINDA is an immersion freezing detection device which allows automatic detection of freezing in closed tubes by light transmission. For analysis, 4 circular samples (1.2 cm diameter) were extracted from each filter, and were washed in a 25 mL solution of 0.9% NaCl during 20 minutes, then 200 μL of the resulting solution was introduced in each of the 52 tubes. The array of tubes is placed in a cooling bath, with a Pt100 temperature probe at each corner of the array. A camera placed above the array detects the freezing of the tubes through the variation of intensity of the transmitted light through the tubes. Errors bars were calculated from freezing events from background filters and the NaCl solution.

2.3.7 The UNAM-Micro-Orifice Uniform Deposit Impactor–Droplet Freezing Technique (UNAM-MOUDI-DFT)

Aerosol particles collections was carried out by an inertial cascade impactor (MOUDI 100R, MSP) which divides the particles according to their aerodynamic diameter in each of its 8 stages (cut sizes: 0.18, 0.32, 0.56, 1.0, 1.8, 3.2, 5.6, and 10.0 μm). Hydrophobic glass coverslips (Hamptom Reserarch) were used as substrates on each of the 8 stages. During PICNIC, the collection of particles was done in the laboratory via the WAI at a flow rate of 30 LPM. After particle collection, the samples were stored in 60 mm Petri dishes and refrigerated at ~ 4°C for subsequent analysis in the droplet freezing technique (DFT) back in Mexico City.

The DFT, built in the Micro and Mesoscale laboratory of the Atmospheric Science Center at the UNAM (Cordoba et al, 2020), is based on the design by Mason et al. (2015) and determines the concentration of INPs as a function of temperature and particle size via immersion freezing. Each substrates is isolated in a temperature-controlled cell. Supersaturated conditions with respect to water are generated to trigger cloud droplet formation on the aerosol particles deposition on the substrate. The typical size of the droplets is around 100 μm, and 30 to 40 droplets are formed in the study area (1.2 mm^2). The experiment is monitored in real-time with an optical microscope (Axiolab Zeiss, Germany) with a 5x/0.12 magnification objective coupled to a video camera (MC500-W, JVLAB). Droplets are cooled down from 0°C to -40°C at a cooling rate of 10 °C min^{-1}. The temperature at which each droplet freezes is determined when the temperatures from the cold cell (monitored with a resistance temperature detector RTD, ±

0.1 °C uncertainty) and the videos are integrated. The INP concentration is derived by the following expression from Mason et al. (2015):

$$[INPs(T)] = -ln\left(\frac{N_u(T)}{N_0}\right).\left(\frac{A_{deposit}}{A_{DFT}V}\right).N_0.f_{ne}.f_{nu,0.25-0.10mm}.f_{nu,1mm} \quad (2)$$

where $[INPs(T)]$ is the INP concentration, $N_u(T)$ is the unfrozen droplets (L^{-1}) at a certain temperature T (°C), N_0 is the total number of droplets analyzed, $A_{deposit}$ is the total area where the aerosol was deposited on the MOUDI hydrophobic glass coverslips (cm^2), A_{DFT} is the area analyzed by the DFT, V is the volume of air sampled by the MOUDI (L), f_{nu} is a correction factor that takes into account changes in particle concentration in each of MOUDI sample, and f_{ne} is a correction factor that takes into account the uncertainty associated with the number of nucleation events in each experiment.

3 Results and discussion

3.1 Intercomparison of online instruments

INP concentrations as measured with CSU-CFDC, SPIN, PINE-1A and PINE-1B were typically intercompared from the morning hours to the late afternoon, at ice nucleation temperatures ($T_{nucleation}$) from -20°C to -30°C and at water supersaturated conditions. As an example, Fig. 2 shows a typical day of intercomparison, the 11th October. In the morning hours, the instruments were set to the start conditions ($T_{nucleation}$ = -21°C), which was changed consecutively for every few hours by 2 to 5 °C. As seen from this intercomparison day, the instruments measure the INP concentration at similar $T_{nucleation}$ in the same range, with SPIN being at the lower end.

To identify potential systematic deviations between the three instruments, the results from all intercomparsion experiments are investigated using the CSU-CFDC as a reference instrument, given its long history of operation and good characterization. However, it should be noted that also the CSU-CFDC might not capture the true INP concentration, due to aerosol lamina properties which will be discussed below in more detail. For the comparison with the SPIN and PINEs, the CSU-CFDC data, which have the lowest time resolution of 1 minute, were integrated on the time grid of the other instruments. Moreover, only measurements within ± 1 °C were considered. INP concentrations as measured with SPIN (Fig. 3, panel a) and PINE-1A (Fig. 3, panel b) and PINE-1B (Fig. 3, panel c) are compared against CSU-CFDC at a large dynamic range of INP concentrations (0.1 – 100 INP $stdL^{-1}$). This comparison reveals that SPIN tends to somewhat undercount INP concentrations, independently of $T_{nucleation}$. 35% of the data are within a factor of 2, but still 80% are within factor 5 (Tab. 2, panel a). It should be noted that only 20 data points are compared here. A possible explanation for this systematic deviation could be related to the aerosol lamina properties (DeMott et al., 2015; Garimella et al., 2017). It was found that the aerosol particles in CFDCs are likely spreading beyond the lamina, such that not 100% of particles are in the lamina and exposed to the targeted supersaturation condition. The issue of lamina spreading is thereby variable and depends on the CFDC geometry, the flow conditions, and the temperature gradients between the walls which is creating the supersaturation. This can cause aerosol particles to not be exposed to the targeted supersaturation, resulting in either a non-activation into cloud droplets and ice crystals (immersion freezing mode), or to an activation into ice crystals which are not growing to sizes within the residence time in the chamber to be detected by the OPC (above the ice threshold). SPIN was operated at a lower supersaturation (2.8 ± 1.9%) as compared to CSU-CFDC (6.5 ±

1.4%). Moreover, SPIN also used a larger ice threshold in the OPC of 5 µm, against 4 µm from CSU-CFDC, which has been found to impact INP concentration measurements (Jones et al., 2011). Thus, it is possible that due to a particle spreading effect in combination with the lower supersaturation, fewer particles in SPIN were encapsulated in the intended conditions, and were less likely to reach the critical size threshold. Please note that for this study, no laboratory-derived calibration factors to account for a possible underestimation were applied, as the aim was to investigate such potential deviations amongst instruments using ambient aerosol particles.

The comparison between CSU-CFDC and the expansion chambers PINE-1A and PINE-1B (Fig. 3, panels b and c) show a good agreement. The majority of the compared data fall within a factor of 2 (71% for PINE-1A, and 50% for PINE-1B) and 5 (100% for PINE-1A, and 71% for PINE-1B; Tab. 2, panel b). As seen in Fig. 3, panels b and c, no trend for under- or overcounting is observed. However, it should be noted that their agreement does not necessarily imply that both instruments are able to quantify the true ambient INP concentration. As stated before, the INP concentration as measured with the CSU-CFDC is typically corrected using a calibration factor to account for an incomplete activation within the supersaturation lamina (e.g. a factor of 3 for CSU-CFDC for dust particles; DeMott et al., 2015). The PINE instruments could underestimate INP concentrations as is possible that not all sampled aerosols are activating into cloud droplets. More laboratory experiments will be performed in future laboratory studies to identify such a possible low bias. It should also be noted that, due to a temperature calibration performed after the PICNIC campaign, the PINEs are having fewer overlapping measurements with CSU-CFDC as initially targeted.

3.2 Intercomparison of offline methods

INP concentrations were determined based on 8-hour day- and nighttime filter samples during the campaign, using seven different freezing methods. The timeseries of INP concentrations from those measurements are presented in Fig. 4 at temperatures where many methods determined INP concentrations. At -10 °C (Fig. 4, panel a), -15 °C (Fig. 4, panel b) and -20 °C (Fig. 4, panel c), INP concentrations vary over ~ three orders of magnitude, and most of the time the measurements with the different methods are within the error bars from each other, with a tendency from the IS to measure elevated INP concentrations. In order to get a more complete picture of the results from the offline methods, the freezing spectra from each method for all day- and nighttime samples are shown in Figs. 5, 6, and 7. The INP concentrations were determined between ~ -5°C and -30°C, and span a range from below 0.001 to above 100 INP $stdL^{-1}$. For most sampling intervals, the methods show a good agreement and the INP concentration and the shape of the freezing spectra show a similar behavior. This is an indication for the suitability of the different analysis procedures to determine INP concentrations (droplet freezing on cold stages, freezing of suspensions), and that the different filter holders (standard filter holders, FRIDGE custom-built semi-automated sampler, open-faced Nalgene sampling headsubstrate, MOUDI impactor, HERA) and the filter materials (PTFE fluoropore membrane filters, quarz filters, hydrophobic glass coverslips, polycarbonate filters (200 nm, 800 nm, see also section 3.2.2) can be used for INP collection. Interestingly, the IS and LINDA tend to measure higher INP concentrations, which could be explained by their filter sampling location on the rooftop, meaning that they did not sample via the WAI inlet. Moreover, the INP concentration determined with the online instruments generally agree to the offline freezing spectra (Figs. 5, 6, and 7), which will be discussed in more detail in section 3.3.

In order to get a better insight into the agreement during the whole campaign, we present the freezing spectra from each method compared against the INSEKT measurements as a reference (Fig. 8). This method was chosen since

filter collection for INSEKT was performed in the laboratory at the WAI inlet, similar to that for most of the other methods, and since it covers a large temperature range of INP measurement. Figure 8 includes only data for INDA and LINA obtained from the standard filterholder, as no influence from the two different samplers (standard and HERA) used by TROPOS were observed. Comparisons to INSEKT results on an instrument-by-instrument basis reveal that the methods sampling filters at the WAI on average agree for > 45% of the data within a factor of 2 with INSEKT, and for > 77% within a factor of 5 (Tab. 2, panel b). The FRIDGE method (Fig. 8, panel a) has a slight tendency (still within factors of 2 and 5) to measure lower INP concentrations over the full temperature range as compared to INSEKT. It should be mentioned that the flows for filter collection are associated with a higher degree of uncertainty due to a miscalibration of the flows and the occurrence of a leak (see section 2.3.1). Moreover, the IS and LINDA, sampling filter on rooftop, tend to measure higher INP concentrations (Fig. 8, panels e, f), and only 27% and 19% are within a factor of 2 from the INSEKT measurements, respectively. This is an indication that filter measurements for offline-INP analysis using standard inlet systems could systematically miss larger aerosol particles which are crucial for INP measurements. If this is only valid for ground-based sampling locations or also for aircraft measurements needs to be investigated in future studies.

3.2.1 Impact of sampling conditions

A wider spread between the methods based on filters collected at the rooftop and in the laboratory via the WAI is observed during some sampling intervals. In order to get a better insight into this systematic deviation, the timeseries of the difference between the INP concentration measurements from the IS (rooftop) and INSEKT (laboratory) is investigated regarding the wind velocity and the presence of larger aerosol particles. Those methods were selected for this comparison as they are based on the same freezing analysis principle, and both span a large range of nucleation temperature. As seen in Fig. 9, the difference between the INP concentration measurements from the IS and the INSEKT at -10 °C, -15°C, and -20 °C, given as the lognormal difference, are often occuring during times when the wind velocity was above a threshold of 7 m s^{-1}, above which the transmission efficiency of aerosol particles in the WAI is decreased. The total particle concentration and aerosol particle size distribution measurements are conducted at the WAI (Fig. 9, panels c – f). While the total particle concentration and the particle concentration < 0.5 µm are do not show lower concentrations during high-wind conditions (Fig. 9, panels c, d), the particle concentration above 0.7 µm decreases during wind velocities above 7 m s^{-1} (Fig. 9, panels e, f). Especially during the sampling time interval of the 13th October (daytime) to the 15th October (daytime), the particle concentration above 0.7 µm is lower as compared to the sampling times before (13th October, nighttime) and after (16th October, daytime). Thus, it might be possible that larger aerosol particles were not measured in the laboratory, and lead to the observed difference between the INP concentration measurements at the rooftop. At the same time, this potential cause of discrepancy depends on the assumption that especially the larger fraction of the aerosol particle population dominated the INP population, which is still insufficiently investigated (e.g., Kanji et al., 2017). It should be noted that the size distribution measurements were conducted at the WAI, thus, the interpretation of the presented timeseries of aerosol particles during those high-windspeed times is limited. In order to precisely identify the impact of presence of larger particles connected to transmission efficiencies at elevated windspeeds, more intensive measurements need to be conducted by, e.g., having aerosol particle size distribution measurements at the rooftop and in the laboratory simultaneously.

3.2.2 Testing of quarz fiber and polycarbonate filters

A subsample of the here introduced datasets was designed to test a possible influence on the results when using different filter materials (quartz fiber versus polycarbonate filters). For this comparison, HERA and the standard sampler from TROPOS were operated in parallel using different filter materials. For the analysis, INDA and LINA, both operated at TROPOS, were used to evaluate the filters. For the comparison shown here, HERA was equipped with the polycarbonate filters (200 nm pore size), and the standard sampler with the quarz filter. Figure 10 shows results from sampling intervals between the 9th (daytime) to the 11th (daytime) October. Polycarbonate filters are washed off so that LINA and INDA measurements could be done, while quartz fiber filters can only be analyzed with INDA. No systematic difference between the INP concentrations using those different filter materials is observed, and as agreement between INDA and LINA had been observed before (e.g., Knackstedt et al., 2018; Hartmann et al., 2019, Gong et al., 2020), this gives confidence that both materials can be used.

Moreover, quarz fibre filters and polycarbonate filters with a different pore size (800 nm) were used simultaneously in the TROPOS standard filter and HERA for the analysis with INDA and LINA during some sampling intervals. Quarz fibre filters were used from the 14th nighttime (Fig. 6 panel h) to the 16th daytime sample (Fig. 7, panels a - c), and 800 nm polycarbonate filters for the sampling intervals from the 16th (nighttime) to the 18th (daytime; Fig. 7, panels d - g). When comparing with the overall INP measurements from the other methods, there was no noticeable influence of using quarz fibre filters, or polycarbonate filters with 800 nm pores. This shows that filters with a pore size of 800 nm still have a sufficiently high collection efficiency for the collection of atmospheric INPs. This is in agreement with Soo et al. (2016), who examined the collection efficiencies of a range of different filter materials and pore sizes for test particles with rather small sizes between 10 and 412 nm. They reported that the collection efficiency for polycarbonate filters with 800 nm pore sizes and the here used flow rates > 11 LPM are above 97% for all particles in the examined size range.

3.3 Comparison online and offline methods

The comparison presented in Figs. 5, 6, and 7 also includes the measurements by CSU-CFDC, SPIN, PINE-1A and PINE-B. The INP concentrations presented here are measured within the same time period of the filter collection, but represent the instruments' specific time resolution, which is ~ 1 minute for CSU-CFDC, and ~ 10 minutes for SPIN and both PINE instruments. The measurements with the PINE-1A thereby covers the full 8-hour filter collection time with a few exceptions.

Generally, the INP concentrations from the online instruments compare well to the offline techniques and are within the range of the offline-determined INP concentrations measured at the WAI. There is a slight tendency to measure lower INP concentrations especially on the 10th October (day- and nighttime; Fig. 5, panels g, h). This low bias might be explained by the limitations of the instruments to measure only particles below 2.5 µm by the use of impactors, or below 4 µm due to the natural loss in the inlets for the PINE instruments. Thus, it might be possible that the filters used for the offline INP analysis sampled a higher fraction of larger aerosol particles which were ice-active.

In general, the measurements from the cloud chambers reveal that INP concentrations at a given temperature vary up to an order of magnitude during the sampling interval of 8 hours, a variability which cannot be detected by the offline methods. A combination of both online and offline techniques is therefore of great advantage to capture both the INP concentration over a wide temperature range and their variability at single temperatures.

4 Summary and conclusion

During the PICNIC campaign in October 2018, a suite of online and offline INP measurement techniques were operated simultaneously to compare the temperature dependent INP concentration relevant for the formation of mixed-phase clouds. Two CFDCs (CSU-CFDC and SPIN) and two expansion chambers (PINE-1A, PINE-1B) measured INP concentrations in the temperature range from -20 °C to -30 °C. INP concentrations were thereby compared within ± 10 minutes and ± 1 °C to ensure close as possible sampling and nucleation conditions. The PINE instruments agree well to CSU-CFDC and most INP concentration measurements are within a factor of 2 (71% and 50% for PINE-1A and PINE-1B, respectively). However, it is possible that both instruments underestimate the ambient INP concentration. During the cloud formation process in PINE it is conceivable that not all aerosol particles are activating into cloud droplets during the expansional cooling process, which can cause a low bias of immersion freezing INPs. Also in CFDCs, it is possible that not all aerosol particles under investigation are exposed to targeted supersaturation conditions due to aerosol spreading beyond the aerosol lamina (DeMott et al., 2015; Garimella et al., 2017). Indeed, the comparison of CSU-CFDC and SPIN reveals that SPIN measures lower INP concentrations (only 35% of the data are within a factor of 2), which could arise from such an effect of aerosol spreading beyond the lamina. The supersaturation was lower in SPIN (2.8 ± 1.9%) as in CSU-CFDC (6.5 ± 1.4%) and the instrument-specific size threshold to identify ice crystals was larger in SPIN (5 µm) as in CSU-CFDC (4 µm). Therefore, it is conceivable that fewer particles in SPIN were activated into cloud droplets and ice crystals, or were not growing to ice crystals large enough to be classified as ice. More specific tests to characterize the effect of aerosol spreading beyond the lamina during field studies, as well as laboratory characterization of the established supersaturation conditions, and hence cloud droplet and ice crystal activation, should be performed in future studies. More such intensive INP intercomparisons, resulting in a larger dataset, should be conducted in the future to better understand discrepancies amongst the online instruments.

INP filter sampling was performed during day- and nighttime for 8 hours and analyzed with FRIDGE, INDA, IS, INSEKT, LINA, LINDA, and MOUDI-DFT. The filters for IS and LINDA were collected directly in ambient air on the rooftop of the laboratory, while the other filters were collected at the WAI in the laboratory. The methods using filters collected in the laboratory generally show a good agreement over the investigated temperature range, and are within a factor of 2 when compared to INSEKT as a reference (> 45 %). This indicates that not only the different freezing procedures (droplet freezing, freezing of suspensions) but also the sampling devices (standard filter holders, FRIDGE custom-built semi-automated sampler, open-faced Nalgene sampling headsubstrate, MOUDI impactor, HERA) and sampling substrates (PTFE fluoropore membrane, quarz filters, hydrophobic glass coverslips, polycarbonate filters (200 nm, 800 nm) are adequate for each method to determine INP concentrations. The INP concentrations determined with IS and LINDA sometimes measured higher INP concentrations. As compared to the INSEKT method, only 27 and 19 % of the data derived with IS and LINDA are within a factor of 2, respectively. Especially during high-wind conditions this discrepancy was observed, which might be explained by losses of supermicron aerosol particles and INPs in the WAI. As generally most of ambient INP measurements nowadays are performed at aerosol inlets, it is possible that systematic losses of INPs causes a low bias in INP concentration measurements. This should be considered and characterized in future studies by e.g. quantifying sampling losses of supermicron aerosol particles during different sampling conditions with regard to the meteorology and the presence of particles in the size range relevant for ice nucleation.

The INP measurements of the online instruments, which were performed within the same sampling intervals of the filter collection times, thereby agree quite well to the results from the offline methods. The online instruments show a slight tendency to measure lower INP concentrations during some sampling intervals, which might be caused by the restriction of the online instruments to sample larger aerosol particles, which is needed to avoid an missclassification of unactivated aerosol particles as ice crystals. Nevertheless, we conclude that the here presented methods are suitable to be combined which is required in order to capture the complete temperature range relevant for heterogeneous nucleation in the mixed-phase cloud regime.

Especially within the light of ongoing efforts for INP monitoring networks, we recommend that such intensive INP intercomparison measurements are repeated frequently, also during different different seasons, and also at different measurement sites.

Data availability

The data used in this study will be available via the KITopen data repository.

Author contribution

LL wrote the manuscript with contributions from YB, PJD, LAL, CRR, JS, HW, MW and EF. CSU-CFDC measurements and analysis were provided by KB, PJD, EJTL and KAM. DHC, MG and MW conducted the SPIN measurements and analysis. PINE measurements were performed by LL, MA and OM, and CB, NB, RF, BJM, JN, TP contributed to the instrument setup and data analysis. HB, DC, SR, JS, and ET performed the FRIDGE filter measurements and data analysis. Filter sampling for INDA and LINA and data analysis were conducted by CJ, SM, FS and HW. KB, PJD, TCJH, EJTL and KAM performed and analyzed the IS measurements. INSEKT measurements were performed and analyzed by BB, LL, KH and OM. YB and EF provided the measurements from LINDA. MOUDI-DFT measurements and analysis was conducted by LAL and CRR. DP, KS, and EF provided the meteorological measurements at the Puy de Dôme station and . EF coordinated the PICNIC campaign.

Acknowledgment

We thank the technical team from the Puy de Dôme / OPGC (l'Observatoire de Physique du Globe) for support and service during the campaign. We acknowledge the KIT technical team with a special thanks to Steffen Vogt.

Competing interests

The authors declare that they have no conflict of interest**.**

Financial support

This research received funding from the European Commission under the Horizon 2020 –Research and Innovation Framework Programme via the ACTRIS-2 Trans-National Access, and from the ANR-CHAIN project number ANR-14-CE01-0003 -01. Larissa Lacher received funding from the KIT Technology Transfer Project N059. Barbara Bertozzi acknowledges funding from the European Union´s Horizon 2020 research and innovation programme under the Marie Skłodowska-Curie grant agreement No 764991. Martin Wolf and Daniel Cziczo acknowledge funding from the US National Science Foundation grant AGS-1838429, a supplement to Collaborative Research: An in situ Closure Study of Mixed Phase Clouds at Storm Peak (AGS-1749851). Colorado State University co-authors received partial funding support from U.S. National Science Foundation Award No. 1660486. Luis Ladino and Carolina Ramirez acknowledge partial funding from Conacyt trough the CB-285023 project.

References

Asmi, E., E. Freney, M. Hervo, D. Picard, C. Rose, A. Colomb, and K. Sellegri. 2012. "Aerosol cloud activation in summer and winter at puy-de-Dôme high altitude site in France." Atmos. Chem. Phys. 12 (23):11589-11607. doi: 10.5194/acp-12-11589-2012.

Atkinson, J. D., Murray, B. J., Woodhouse, M. T., Whale, T. F., Baustian, K. J., Carslaw, K. S., Dobbie, S., O/'Sullivan, D., and Malkin, T. L.: The importance of feldspar for ice nucleation by mineral dust in mixed-phase clouds, Nature, 498, 355-358, 10.1038/nature12278, 2013.

Boose, Y., Zamin A. Kanji, Monika Kohn, Berko Sierau, Assaf Zipori, Ian Crawford, Gary Lloyd, Nicolas Bukowiecki, Erik Herrmann, Piotr Kupiszewski, Martin Steinbacher, and Ulrike Lohmann. 2016. "Ice Nucleating Particle Measurements at 241 K during Winter Months at 3580 m MSL in the Swiss Alps." J. Atmos. Sci. 73 (5):2203-2228. doi: 10.1175/JAS-D-15-0236.1.

Boose, Y., A. Welti, J. Atkinson, F. Ramelli, A. Danielczok, H. G. Bingemer, M. Plötze, B. Sierau, Z. A. Kanji, and U. Lohmann. 2016c. "Heterogeneous ice nucleation on dust particles sourced from nine~deserts worldwide -- Part 1: Immersion freezing." Atmos. Chem. Phys. 16 (23):15075-15095. doi: 10.5194/acp-16-15075-2016.

Burkert-Kohn, M., H. Wex, A. Welti, S. Hartmann, S. Grawe, L. Hellner, P. Herenz, J. D. Atkinson, F. Stratmann, and Z. A. Kanji. 2017. "Leipzig Ice Nucleation chamber Comparison (LINC): intercomparison of four online ice nucleation counters." Atmos. Chem. Phys. 17 (18):11683-11705. doi: 10.5194/acp-17-11683-2017.

Campbell, James R., and Masataka Shiobara. 2008. "Glaciation of a mixed-phase boundary layer cloud at a coastal arctic site as depicted in continuous lidar measurements." Polar Science 2 (2):121-127. doi: https://doi.org/10.1016/j.polar.2008.04.004.

Chou, C., O. Stetzer, E. Weingartner, Z. Juranyi, Z. A. Kanji, and U. Lohmann. 2011. "Ice nuclei properties within a Sahara dust event at the Jungfraujoch in the Swiss Alps." Atmos. Chem. Phys. 11:4725 - 4738. doi: 10.5194/acp-11-4725-2011.

Conen, F., Henne, S., Morris, C. E., and Alewell, C.: Atmospheric ice nucleators active ≥ −12 °C can be quantified on PM10 filters, Atmos. Meas. Tech., 5, 321-327, 10.5194/amt-5-321-2012, 2012.

Creamean, J. M., R. M. Kirpes, K. A. Pratt, N. J. Spada, M. Maahn, G. de Boer, R. C. Schnell, and S. China. 2018. "Marine and terrestrial influences on ice nucleating particles during continuous springtime measurements in an Arctic oilfield location." Atmos. Chem. Phys. 18 (24):18023-18042. doi: 10.5194/acp-18-18023-2018.

DeMott, P. J., T. C. J. Hill, M. D. Petters, A. K. Bertram, Y. Tobo, R. H. Mason, K. J. Suski, C. S. McCluskey, E. J. T. Levin, G. P. Schill, Y. Boose, A. M. Rauker, A. J. Miller, J. Zaragoza, K. Rocci, N. E. Rothfuss, H. P. Taylor, J. D. Hader, C. Chou, J. A. Huffman, U. Pöschl, A. J. Prenni, and S. M. Kreidenweis. 2017. "Comparative measurements of ambient atmospheric concentrations of ice nucleating particles using multiple immersion freezing methods and a continuous flow diffusion chamber." Atmos. Chem. Phys. 17 (18):11227-11245. doi: 10.5194/acp-17-11227-2017.

DeMott, P. J., O. Möhler, D. J. Cziczo, N. Hiranuma, M. D. Petters, S. S. Petters, F. Belosi, H. G. Bingemer, S. D. Brooks, C. Budke, M. Burkert-Kohn, K. N. Collier, A. Danielczok, O. Eppers, L. Felgitsch, S. Garimella, H. Grothe, P. Herenz, T. C. J. Hill, K. Höhler, Z. A. Kanji, A. Kiselev, T. Koop, T. B. Kristensen, K. Krüger, G.

Kulkarni, E. J. T. Levin, B. J. Murray, A. Nicosia, D. O'Sullivan, A. Peckhaus, M. J. Polen, H. C. Price, N. Reicher, D. A. Rothenberg, Y. Rudich, G. Santachiara, T. Schiebel, J. Schrod, T. M. Seifried, F. Stratmann, R. C. Sullivan, K. J. Suski, M. Szakáll, H. P. Taylor, R. Ullrich, J. Vergara-Temprado, R. Wagner, T. F. Whale, D. Weber, A. Welti, T. W. Wilson, M. J. Wolf, and J. Zenker. 2018. "The Fifth International Workshop on Ice Nucleation phase 2 (FIN-02): laboratory intercomparison of ice nucleation measurements." Atmos. Meas. Tech. 11 (11):6231-6257. doi: 10.5194/amt-11-6231-2018.

DeMott, P. J., Hill, T. C. J., Petters, M. D., Bertram, A. K., Tobo, Y., Mason, R. H., Suski, K. J., McCluskey, C. S., Levin, E. J. T., Schill, G. P., Boose, Y., Rauker, A. M., Miller, A. J., Zaragoza, J., Rocci, K., Rothfuss, N. E., Taylor, H. P., Hader, J. D., Chou, C., Huffman, J. A., Pöschl, U., Prenni, A. J., and Kreidenweis, S. M.: Comparative measurements of ambient atmospheric concentrations of ice nucleating particles using multiple immersion freezing methods and a continuous flow diffusion chamber, Atmos. Chem. Phys., 17, 11227-11245, 10.5194/acp-17-11227-2017, 2017.

DeMott, P. J., A. J. Prenni, X. Liu, S. M. Kreidenweis, M. D.and Twohy Petters, C. H., M. S. Richardson, T. Eidhammer, and D. C. Rogers. 2010. "Predicting global atmospheric ice nuclei distributions and their impacts on climate." Proc. Natl. Acad. Sci. doi: 10.1073/pnas.0910818107.

DeMott, P. J., A. J. Prenni, G. R. McMeeking, R. C. Sullivan, M. D. Petters, Y. Tobo, M. Niemand, O. Möhler, J. R. Snider, Z. Wang, and S. M. Kreidenweis. 2015. "Integrating laboratory and field data to quantify the immersion freezing ice nucleation activity of mineral dust particles." Atmos. Chem. Phys. 15 (1):393-409. doi: 10.5194/acp-15-393-2015.

Desai, N., K. K. Chandrakar, G. Kinney, W. Cantrell, and R. A. Shaw. 2019. "Aerosol-Mediated Glaciation of Mixed-Phase Clouds: Steady-State Laboratory Measurements." Geophysical Research Letters 46 (15):9154-9162. doi: 10.1029/2019gl083503.

Dusek, U., G. P. Frank, L. Hildebrandt, J. Curtius, J. Schneider, S. Walter, D. Chand, F. Drewnick, S. Hings, D. Jung, S. Borrmann, and M. O. Andreae. 2006. "Size Matters More Than Chemistry for Cloud-Nucleating Ability of Aerosol Particles." Science 312 (5778):1375-1378. doi: 10.1126/science.1125261.

Emersic, C., P. J. Connolly, S. Boult, M. Campana, and Z. Li. 2015. "Investigating the discrepancy between wet-suspension- and dry-dispersion-derived ice nucleation efficiency of mineral particles." Atmos. Chem. Phys. 15 (19):11311-11326. doi: 10.5194/acp-15-11311-2015.

Fan, J., L. R. Leung, D. Rosenfeld, and P. J. DeMott. 2017. "Effects of cloud condensation nuclei and ice nucleating particles on precipitation processes and supercooled liquid in mixed-phase orographic clouds." Atmos. Chem. Phys. 17 (2):1017-1035. doi: 10.5194/acp-17-1017-2017.

Farah, Antoine, Evelyn Freney, Aurélien Chauvigné, Jean-Luc Baray, Clémence Rose, David Picard, Aurélie Colomb, Dani Hadad, Maher Abboud, Wehbeh Farah, and Karine Sellegri. 2018. "Seasonal Variation of Aerosol Size Distribution Data at the Puy de Dôme Station with Emphasis on the Boundary Layer/Free Troposphere Segregation." Atmosphere 9 (7):244.

Field, P. R., and A. J. Heymsfield. 2015. "Importance of snow to global precipitation." Geophysical Research Letters 42 (21):9512-9520. doi: 10.1002/2015gl065497.

Garimella, S., T. B. Kristensen, K. Ignatius, A. Welti, J. Voigtländer, G. R. Kulkarni, F. Sagan, G. L. Kok, J. Dorsey, L. Nichman, D. A. Rothenberg, M. Rösch, A. C. R. Kirchgäßner, R. Ladkin, H. Wex, T. W. Wilson, L. A. Ladino, J. P. D. Abbatt, O. Stetzer, U. Lohmann, F. Stratmann, and D. J. Cziczo. 2016. "The SPectrometer for Ice Nuclei (SPIN): an instrument to investigate ice nucleation." Atmos. Meas. Tech. 9 (7):2781-2795. doi: 10.5194/amt-9-2781-2016.

Garimella, S., Rothenberg, D. A., Wolf, M. J., David, R. O., Kanji, Z. A., Wang, C., Rösch, M., and Cziczo, D. J.: Uncertainty in counting ice nucleating particles with continuous flow diffusion chambers, Atmos. Chem. Phys., 17, 10855-10864, 10.5194/acp-17-10855-2017, 2017.

Gong, X., Wex, H., van Pinxteren, M., Triesch, N., Fomba, K. W., Lubitz, J., Stolle, C., Robinson, T. B., Müller, T., Herrmann, H., and Stratmann, F.: Characterization of aerosol particles at Cabo Verde close to sea level and at the cloud level – Part 2: Ice-nucleating particles in air, cloud and seawater, Atmos. Chem. Phys., 20, 1451-1468, 10.5194/acp-20-1451-2020, 2020.

Gute, Ellen, Larissa Lacher, Zamin A. Kanji, Rebecca Kohl, Joachim Curtius, Daniel Weber, Heinz Bingemer, Hans-Christian Clemen, Johannes Schneider, Martin Gysel-Beer, Stephen T. Ferguson, and Jonathan P. D. Abbatt. 2019. "Field evaluation of a Portable Fine Particle Concentrator (PFPC) for ice nucleating particle measurements." Aerosol Science and Technology 53 (9):1067-1078. doi: 10.1080/02786826.2019.1626346.

Hartmann, M., Blunier, T., Brügger, S. O., Schmale, J., Schwikowski, M., Vogel, A., Wex, H., and Stratmann, F.: Variation of Ice Nucleating Particles in the European Arctic Over the Last Centuries, Geophysical Research Letters, 46, 4007-4016, https://doi.org/10.1029/2019GL082311, 2019.

Hartmann, M., Adachi, K., Eppers, O., Haas, C., Herber, A., Holzinger, R., Hünerbein, A., Jäkel, E., Jentzsch, C., van Pinxteren, M., Wex, H., Willmes, S., and Stratmann, F.: Wintertime Airborne Measurements of Ice Nucleating Particles in the High Arctic: A Hint to a Marine, Biogenic Source for Ice Nucleating Particles, Geophysical Research Letters, 47, e2020GL087770, https://doi.org/10.1029/2020GL087770, 2020.

Hiranuma, N., S. Augustin-Bauditz, H. Bingemer, C. Budke, J. Curtius, A. Danielczok, K. Diehl, K. Dreischmeier, M. Ebert, F. Frank, N. Hoffmann, K. Kandler, A. Kiselev, T. Koop, T. Leisner, O. Möhler, B. Nillius, A. Peckhaus, D. Rose, S. Weinbruch, H. Wex, Y. Boose, P. J. DeMott, J. D. Hader, T. C. J. Hill, Z. A. Kanji, G. Kulkarni, E. J. T. Levin, C. S. McCluskey, M. Murakami, B. J. Murray, D. Niedermeier, M. D. Petters, D. O'Sullivan, A. Saito, G. P. Schill, T. Tajiri, M. A. Tolbert, A. Welti, T. F. Whale, T. P. Wright, and K. Yamashita. 2015. "A comprehensive laboratory study on the immersion freezing behavior of illite NX particles: a comparison of 17 ice nucleation measurement techniques." Atmos. Chem. Phys. 15 (5):2489-2518. doi: 10.5194/acp-15-2489-2015.

Jones, H. M., Flynn, M. J., DeMott, P. J., and Möhler, O.: Manchester Ice Nucleus Counter (MINC) measurements from the 2007 International workshop on Comparing Ice nucleation Measuring Systems (ICIS-2007), Atmos. Chem. Phys., 11, 53-65, 10.5194/acp-11-53-2011, 2011.

Kalesse, Heike, Gijs de Boer, Amy Solomon, Mariko Oue, Maike Ahlgrimm, Damao Zhang, Matthew D. Shupe, Edward Luke, and Alain Protat. 2016. "Understanding Rapid Changes in Phase Partitioning between Cloud Liquid and Ice in Stratiform Mixed-Phase Clouds: An Arctic Case Study." Mon. Weather Rev. 144 (12):4805-4826. doi: 10.1175/mwr-d-16-0155.1.

Kanji, Z. A., Luis A. Ladino, Heike Wex, Yvonne Boose, Monika Burkert-Kohn, Daniel J. Cziczo, and Martina Krämer. 2017. "Overview of Ice Nucleating Particles." Meteorological Monograophs 58:1.1-1.33. doi: 10.1175/amsmonographs-d-16-0006.1.

Karlsson, L., Krejci, R., Koike, M. Ebell, K., and P. Zieger. 2020 “The role of nanoparticles in Arctic cloud formation.” Atmos. Chem. Phys., doi.org/10.5194/acp-2020-417.

Knackstedt, K. A., Moffett, B. F., Hartmann, S., Wex, H., Hill, T. C. J., Glasgo, E. D., Reitz, L. A., Augustin-Bauditz, S., Beall, B. F. N., Bullerjahn, G. S., Fröhlich-Nowoisky, J., Grawe, S., Lubitz, J., Stratmann, F., and McKay, R. M. L.: Terrestrial Origin for Abundant Riverine Nanoscale Ice-Nucleating Particles, Environmental Science & Technology, 52, 12358-12367, 10.1021/acs.est.8b03881, 2018.

Krishnamoorthy, K. and M. Lee, 2013: New approximate confidence intervals for the difference between two Poisson means and comparison. Journal of Statistical Computation and Simulation, 83 (12), 2232–2243, doi:10.1080/00949655.2012.686616.

Lacher, L., U. Lohmann, Y. Boose, A. Zipori, E. Herrmann, N. Bukowiecki, M. Steinbacher, and Z. A. Kanji. 2017. "The Horizontal Ice Nucleation Chamber (HINC): INP measurements at conditions relevant for mixed-phase clouds at the High Altitude Research Station Jungfraujoch." Atmos. Chem. Phys. 17 (24):15199-15224. doi: 10.5194/acp-17-15199-2017.

Mason, R. H., Chou, C., McCluskey, C. S., Levin, E. J. T., Schiller, C. L., Hill, T. C. J., Huffman, J. A., DeMott, P. J., and Bertram, A. K.: The micro-orifice uniform deposit impactor–droplet freezing technique (MOUDI-DFT) for measuring concentrations of ice nucleating particles as a function of size: improvements and initial validation, Atmos. Meas. Tech., 8, 2449-2462, 10.5194/amt-8-2449-2015, 2015.

Mason, R. H., M. Si, C. Chou, V. E. Irish, R. Dickie, P. Elizondo, R. Wong, M. Brintnell, M. Elsasser, W. M. Lassar, K. M. Pierce, W. R. Leaitch, A. M. MacDonald, A. Platt, D. Toom-Sauntry, R. Sarda-Estève, C. L. Schiller, K. J. Suski, T. C. J. Hill, J. P. D. Abbatt, J. A. Huffman, P. J. DeMott, and A. K. Bertram. 2016. "Size-resolved measurements of ice-nucleating particles at six locations in North America and one in Europe." Atmos. Chem. Phys. 16 (3):1637-1651. doi: 10.5194/acp-16-1637-2016.

Mertes, S., Verheggen, B., Walter, S., Connolly, P., Ebert, M., Schneider, J., Bower, K. N., Cozic, J., Weinbruch, S., Baltensperger, U., and Weingartner, E.: Counterflow Virtual Impactor Based Collection of Small Ice Particles in Mixed-Phase Clouds for the Physico-Chemical Characterization of Tropospheric Ice Nuclei: Sampler Description and First Case Study, Aerosol Sci. Tech., 41, 848-864, 10.1080/02786820701501881, 2007.

Moore, K. A., 2020. “Constraining marine ice nucleating particle parameterizations in atmospheric models using observations from the Southern Ocean.” M.S. Thesis, Colorado State University Libraries, https://hdl.handle.net/10217/208435

Mülmenstädt, Johannes, O. Sourdeval, J. Delanoë, and J. Quaas. 2015. "Frequency of occurrence of rain from liquid-, mixed-, and ice-phase clouds derived from A-Train satellite retrievals." Geophys. Res. Lett. 42 (15):6502-6509. doi: 10.1002/2015GL064604.

Ogura, I., Kotake, M., Sakurai, H., and Honda, K.: Surface-collection efficiency of Nuclepore filters for nanoparticles, Aerosol Science and Technology, 50, 846-856, 10.1080/02786826.2016.1200007, 2016.

Paramonov, M., S. Drossaart van Dusseldorp, E. Gute, J. P. D. Abbatt, P. Heikkilä, J. Keskinen, X. Chen, K. Luoma, L. Heikkinen, L. Hao, T. Petäjä, and Z. A. Kanji. 2020. "Condensation/immersion mode ice-nucleating particles in a boreal environment." Atmos. Chem. Phys. 20 (11):6687-6706. doi: 10.5194/acp-20-6687-2020.

Paukert, M., and C. Hoose. 2014. "Modeling immersion freezing with aerosol-dependent prognostic ice nuclei in Arctic mixed-phase clouds." Journal of Geophysical Research: Atmospheres 119 (14):9073-9092. doi: 10.1002/2014jd021917.

Phillips, V. T. J., T. W. Choularton, A. J. Illingworth, R. J. Hogan, and P. R. Field. 2003. "Simulations of the glaciation of a frontal mixed-phase cloud with the Explicit Microphysics Model." Quart. J. Roy. Meteor. Soc. 129 (590):1351-1371. doi: 10.1256/qj.02.100.

Prenni, A., P. DeMott, D. Rogers, S. M. Kreidenweis, G. M. McFarquhar, G. Zhang, and M. R. Poellot. 2009. "Ice nuclei characteristics from M-PACE and their relation to ice formation in clouds." Tellus Ser. B 61 (2):436-448. doi: 10.1111/j.1600-0889.2009.00415.x.

Rogers, David C., Paul J. DeMott, and Sonia M. Kreidenweis. 2001. "Airborne measurements of tropospheric ice-nucleating aerosol particles in the Arctic spring." J. Geophys. Res. Atmos. 106 (D14):15053-15063. doi: doi:10.1029/2000JD900790.

Schmidt, S., Schneider, J., Klimach, T., Mertes, S., Schenk, L. P., Kupiszewski, P., Curtius, J., and Borrmann, S.: Online single particle analysis of ice particle residuals from mountain-top mixed-phase clouds using laboratory derived particle type assignment, Atmos. Chem. Phys., 17, 575-594, 10.5194/acp-17-575-2017, 2017.

Schneider, J., Höhler, K., Heikkilä, P., Keskinen, J., Bertozzi, B., Bogert, P., Schorr, T., Umo, N. S., Vogel, F., Brasseur, Z., Wu, Y., Hakala, S., Duplissy, J., Moisseev, D., Kulmala, M., Adams, M. P., Murray, B. J., Korhonen, K., Hao, L., Thomson, E. S., Castarède, D., Leisner, T., Petäjä, T., and Möhler, O.: The seasonal cycle of ice-nucleating particles linked to the abundance of biogenic aerosol in boreal forests, Atmos. Chem. Phys., 21, 3899-3918, 10.5194/acp-21-3899-2021, 2021.

Soo, J. C., Monaghan, K., Lee, T., Kashon, M., and Harper, M.: Air sampling filtration media: Collection efficiency for respirable size-selective sampling, Aerosol science and technology : the journal of the American Association for Aerosol Research, 50, 76-87, 10.1080/02786826.2015.1128525, 2016.

Stetzer, Olaf, Björn Baschek, Felix Lüönd, and Ulrike Lohmann. 2008. "The Zurich Ice Nucleation Chamber (ZINC)-A New Instrument to Investigate Atmospheric Ice Formation." Aerosol Sci. Tech. 42 (1):64-74. doi: 10.1080/02786820701787944.

Vali, G., P. J. DeMott, O. Möhler, and T. F. Whale. 2015. "Technical Note: A proposal for ice nucleation terminology." Atmos. Chem. Phys. 15 (18):10263-10270. doi: 10.5194/acp-15-10263-2015.

Vergara-Temprado, Jesús, Annette K. Miltenberger, Kalli Furtado, Daniel P. Grosvenor, Ben J. Shipway, Adrian A. Hill, Jonathan M. Wilkinson, Paul R. Field, Benjamin J. Murray, and Ken S. Carslaw. 2018. "Strong control of Southern Ocean cloud reflectivity by ice-nucleating particles." Proc. Natl. Acad. Sci. 115 (11):2687-2692. doi: 10.1073/pnas.1721627115.

Welti, A., K. Müller, Z. L. Fleming, and F. Stratmann. 2018. "Concentration and variability of ice nuclei in the subtropical maritime boundary layer." Atmos. Chem. Phys. 18 (8):5307-5320. doi: 10.5194/acp-18-5307-2018.

Wolf, M. J., Zhang, Y., Zawadowicz, M. A., Goodell, M., Froyd, K., Freney, E., Sellegri, K., Rösch, M., Cui, T., Winter, M., Lacher, L., Axisa, D., DeMott, P. J., Levin, E. J. T., Gute, E., Abbatt, J., Koss, A., Kroll, J. H., Surratt, J. D., and Cziczo, D. J.: A biogenic secondary organic aerosol source of cirrus ice nucleating particles, Nature Communications, 11, 4834, 10.1038/s41467-020-18424-6, 2020.

5 Figures

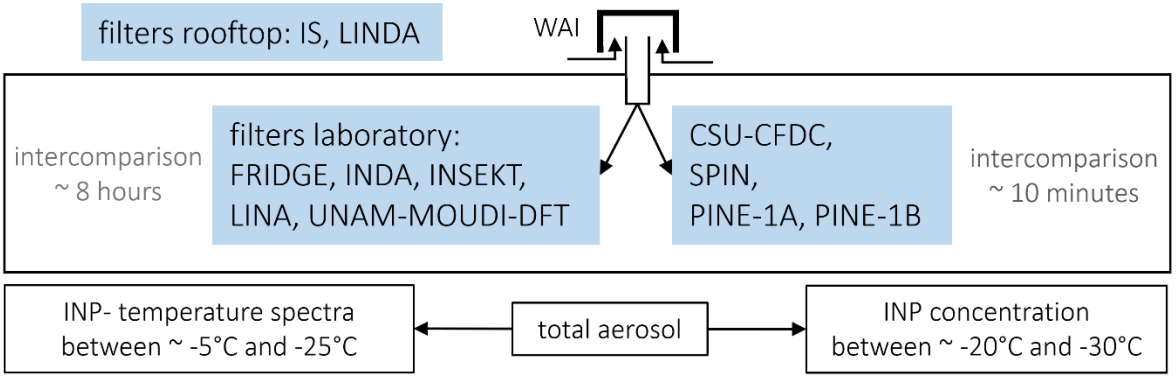

Figure 1: Setup of online (CSU-CFDC, SPIN, PINE) instruments, as well as filter collection for offline freezing analysis; filters were collected and are compared for consecutive 8 hours; online INP measurements are compared within a time resolution of 10 minutes; PINE-1A partly joined the offline intercomparison, measuring at a constant temperature during the 8 hours; online instruments measured partly behind an aerosol concentrator (Gute et al., 2019).

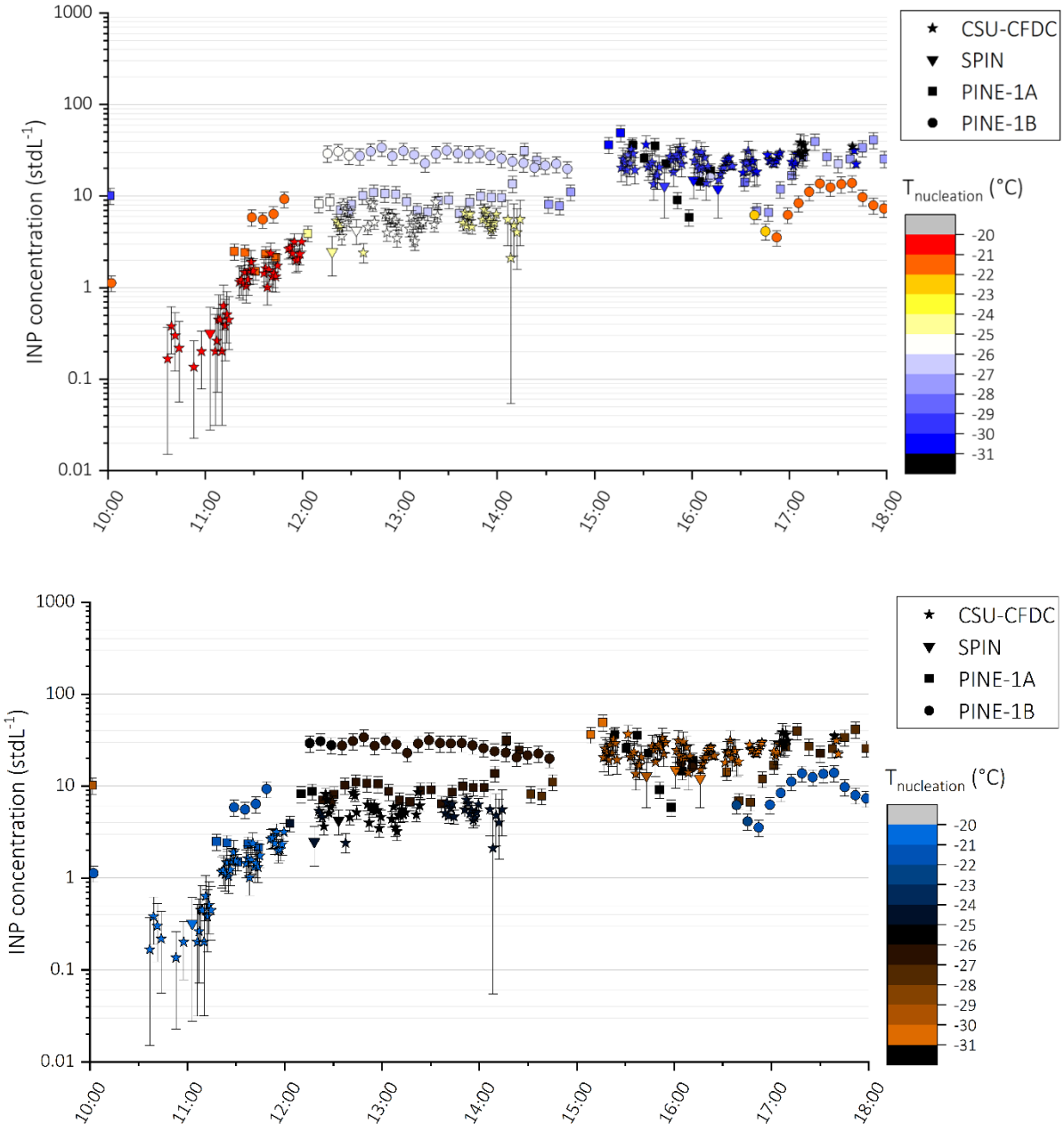

Figure 2: Timeseries of INP concentration above liquid water saturation as measured with CSU-CFDC (star), PINE-1A (square), PINE-1B (circle), and SPIN (triangle) during the 11th October 2018; the color scale represents $T_{nucleation}$; INP concentratinos are measured with a time resolution of ~1 minute (CSU-CFDC) and ~10 minutes (PINE, SPIN).

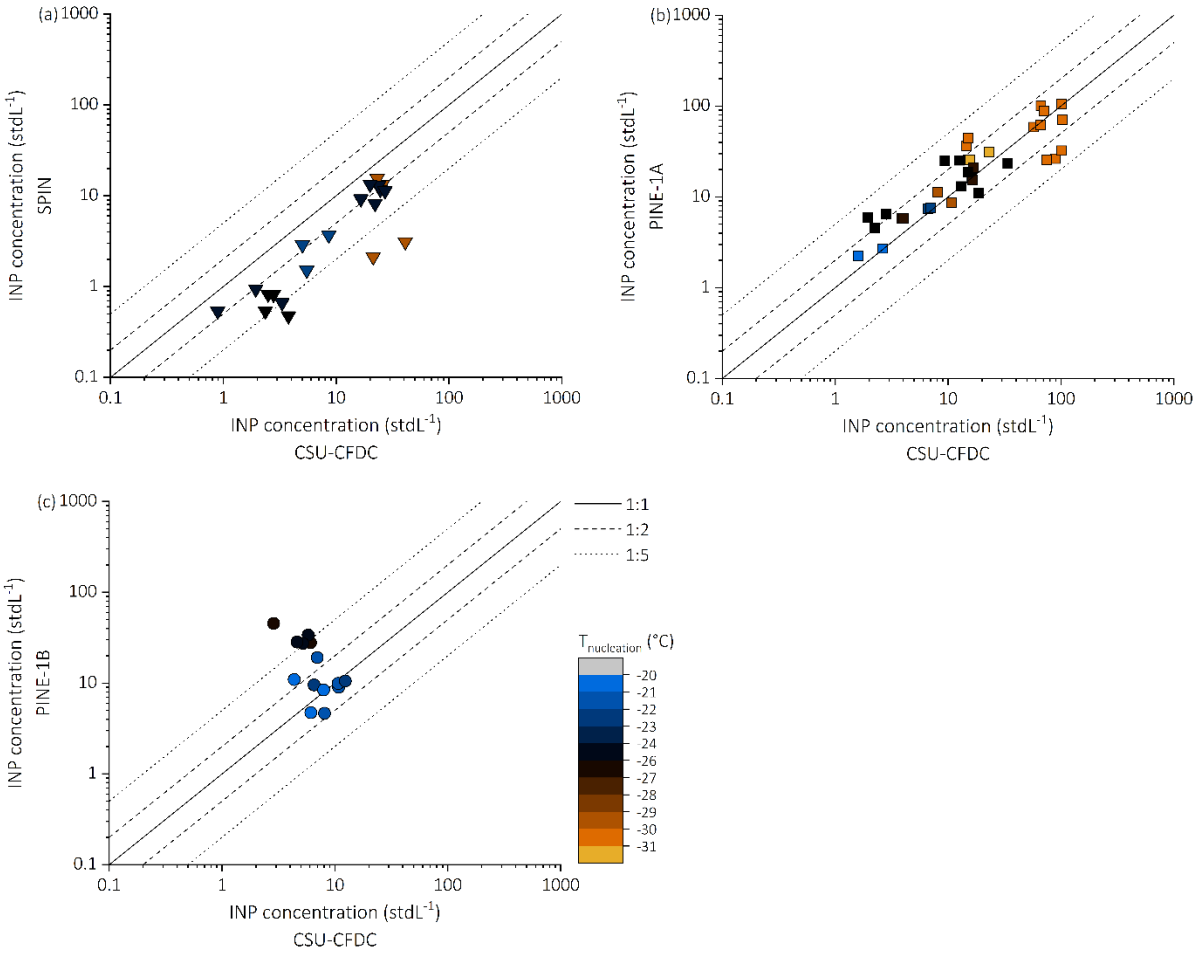

Figure 3: Comparison of INP concentrations measured with the SPIN (panel a), PINE-1A (panel b) and PINE-1b (panel c) against CSU-CFDC; INP measurements are selected for cases that fall within ± 1°C and overlapping sampling time; the measurements are corrected for the use of the aerosol concentrator by applying a correction factor of 11.4, which is the campaign average determined by CSU-CFDC.

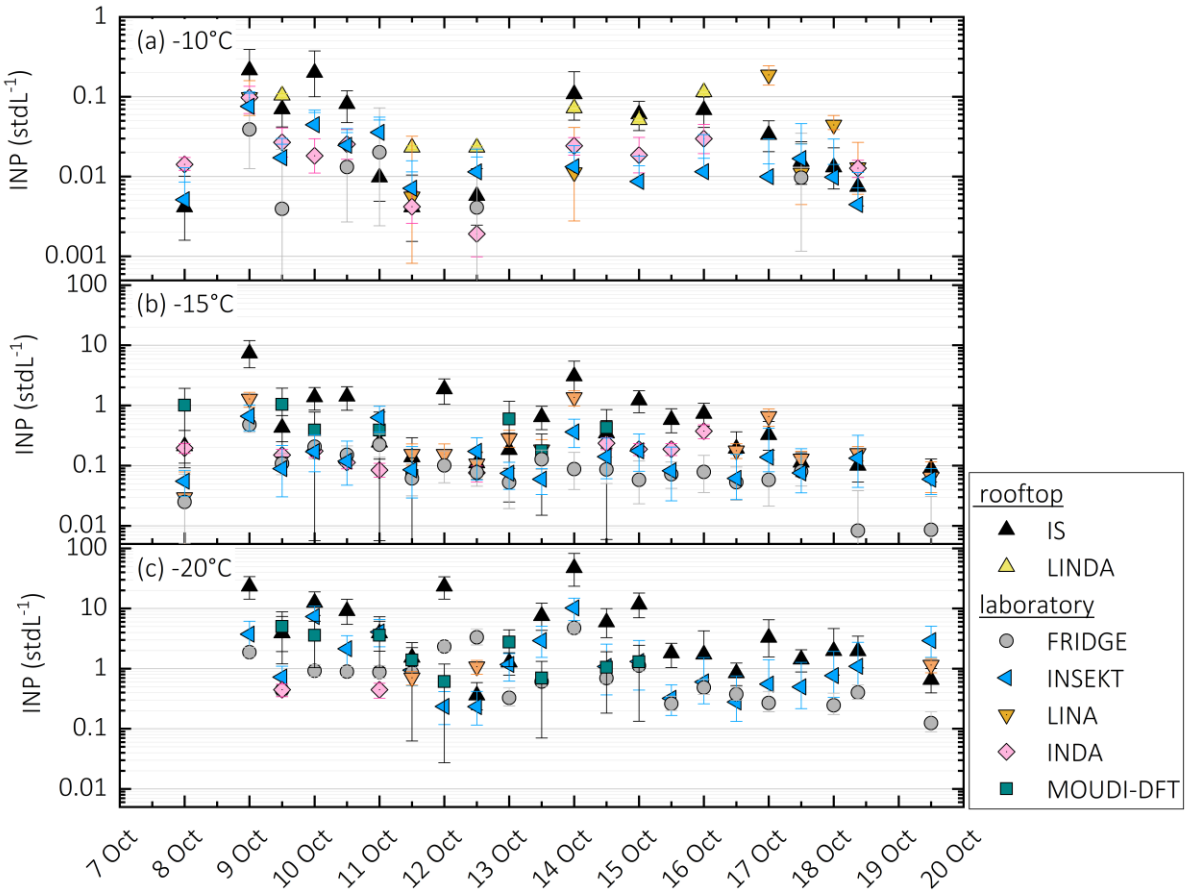

Figure 4: Timeseries of INP concentrations at -10 °C (panel a), -15 °C (panel b), and -20 °C (panel c) as measured with the offline techniques on the rooftop (IS, LINDA) and in the laboratory at the WAI (FRIDGE, INSEKT, LINA, INDA, MOUDI-DFT)

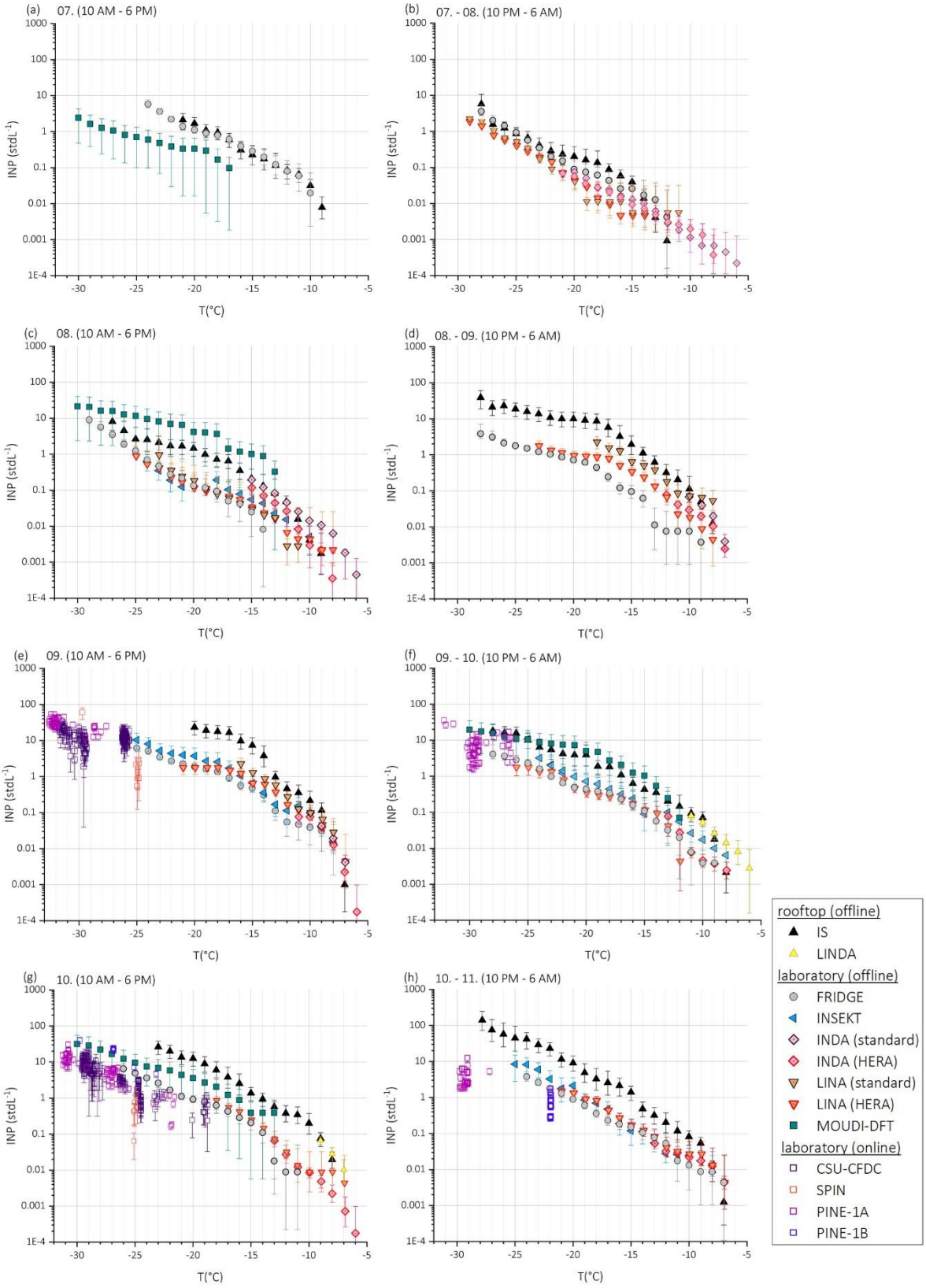

Figure 5: INP freezing spectra of the offline and online methods during the sampling time 7th to the 10th October 2018; the filters for the offline INP analysis were taken during an 8-hour interval, except FRIDGE during the daytime samples (10 am – 2 pm); INP concentrations with the online instruments were determined within the same sampling period, but with a higher time resolution of minutes.

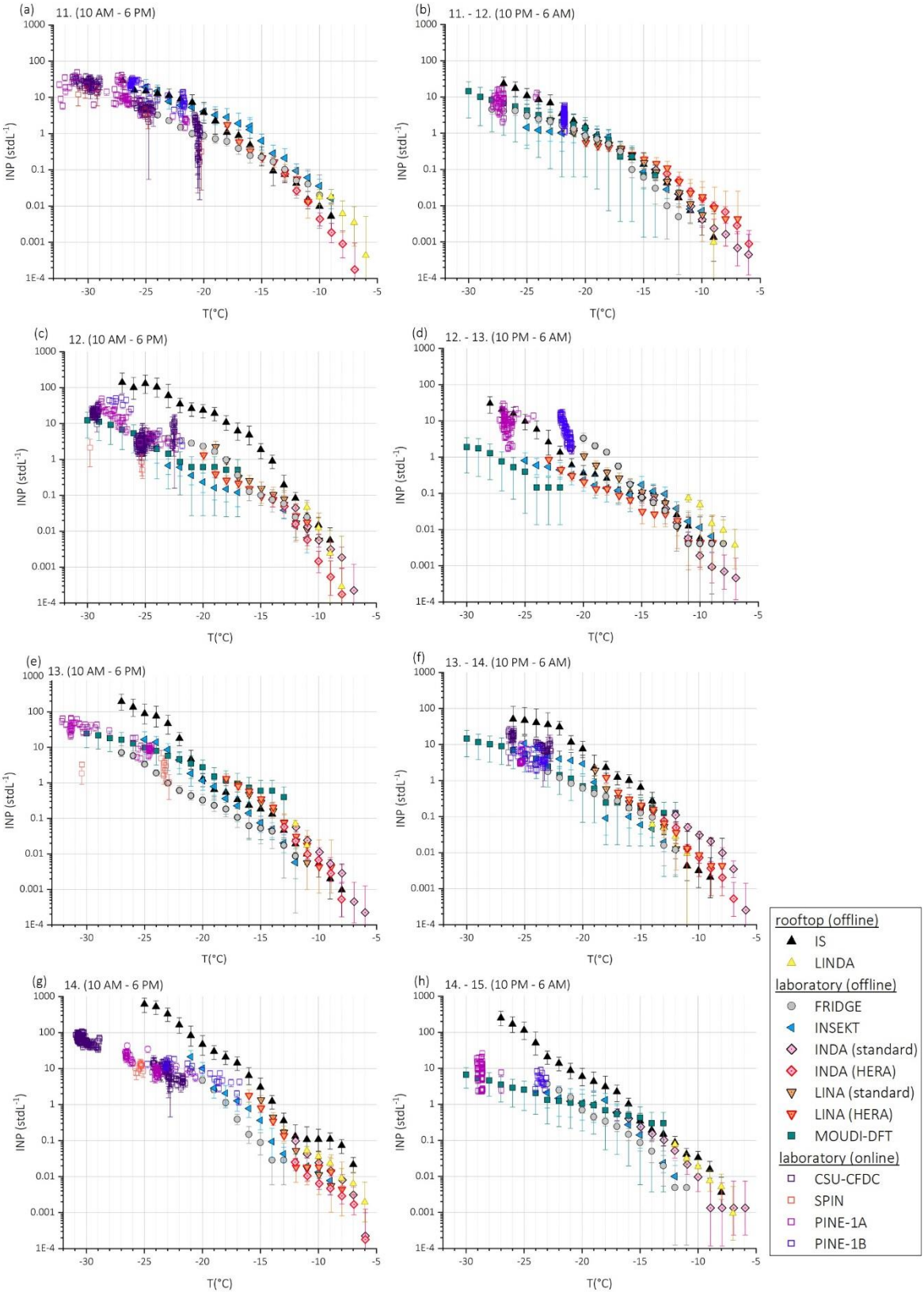

Figure 6: INP freezing spectra of the offline and online methods during the sampling time 11th to the 14th October 2018, see description Fig. 5.

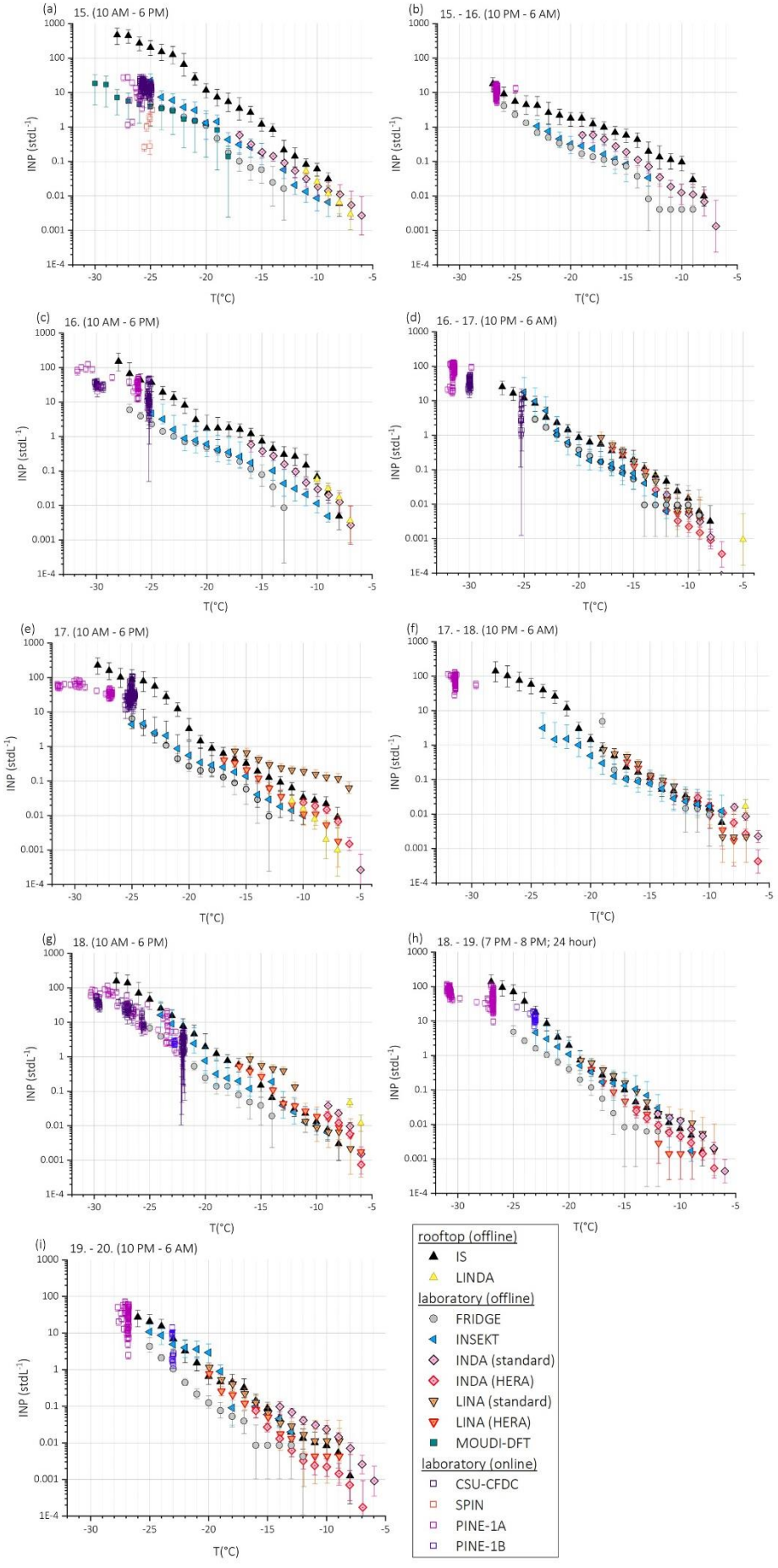
(a) 15. (10 AM - 6 PM)
(b) 15. - 16. (10 PM - 6 AM)
(c) 16. (10 AM - 6 PM)
(d) 16. - 17. (10 PM - 6 AM)
(e) 17. (10 AM - 6 PM)
(f) 17. - 18. (10 PM - 6 AM)
(g) 18. (10 AM - 6 PM)
(h) 18. - 19. (7 PM - 8 PM; 24 hour)
(i) 19. - 20. (10 PM - 6 AM)
INP (stdL^{-1})
T(°C)
rooftop (offline)
IS
LINDA
laboratory (offline)
FRIDGE
INSEKT
INDA (standard)
INDA (HERA)
LINA (standard)
LINA (HERA)
MOUDI-DFT
laboratory (online)
CSU-CFDC
SPIN
PINE-1A
PINE-1B

Figure 7: INP freezing spectra of the offline and online methods during the sampling time 15th to the 19th October 2018, see description Fig. 5.

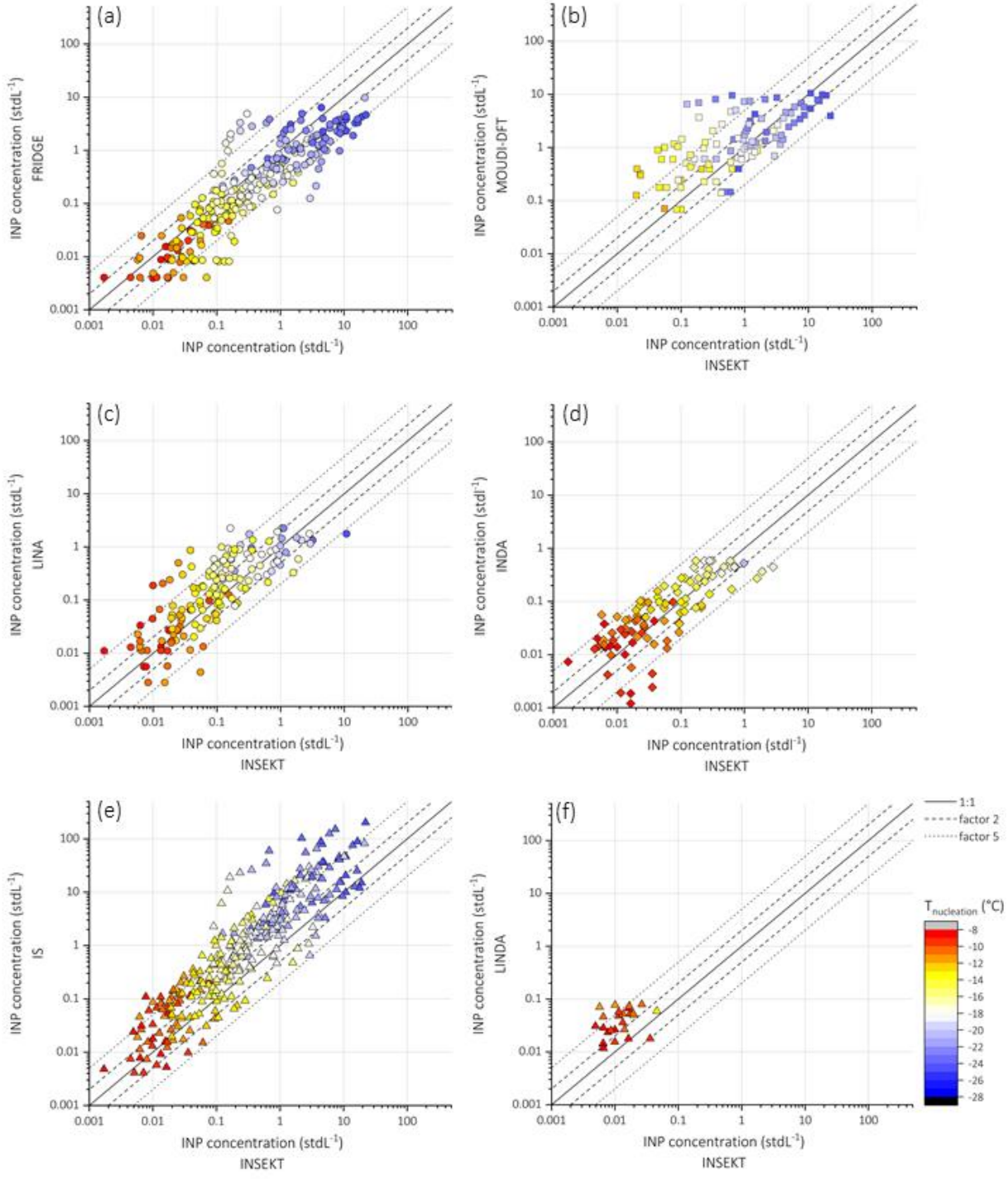

Figure 8: INP concentrations measured with FRIDGE (panel a), UNAM-MOUDI-DFT (panel b), LINA (panel c, filters taken with the standard filter holder), INDA (panel c, filters taken with the standard filter holder), IS (panel e; filter taken on rooftop) and LINDA (panel f; filters taken on rooftop) as function of INP concentrations measured with INSEKT; color-coding represents nucleation temperature.

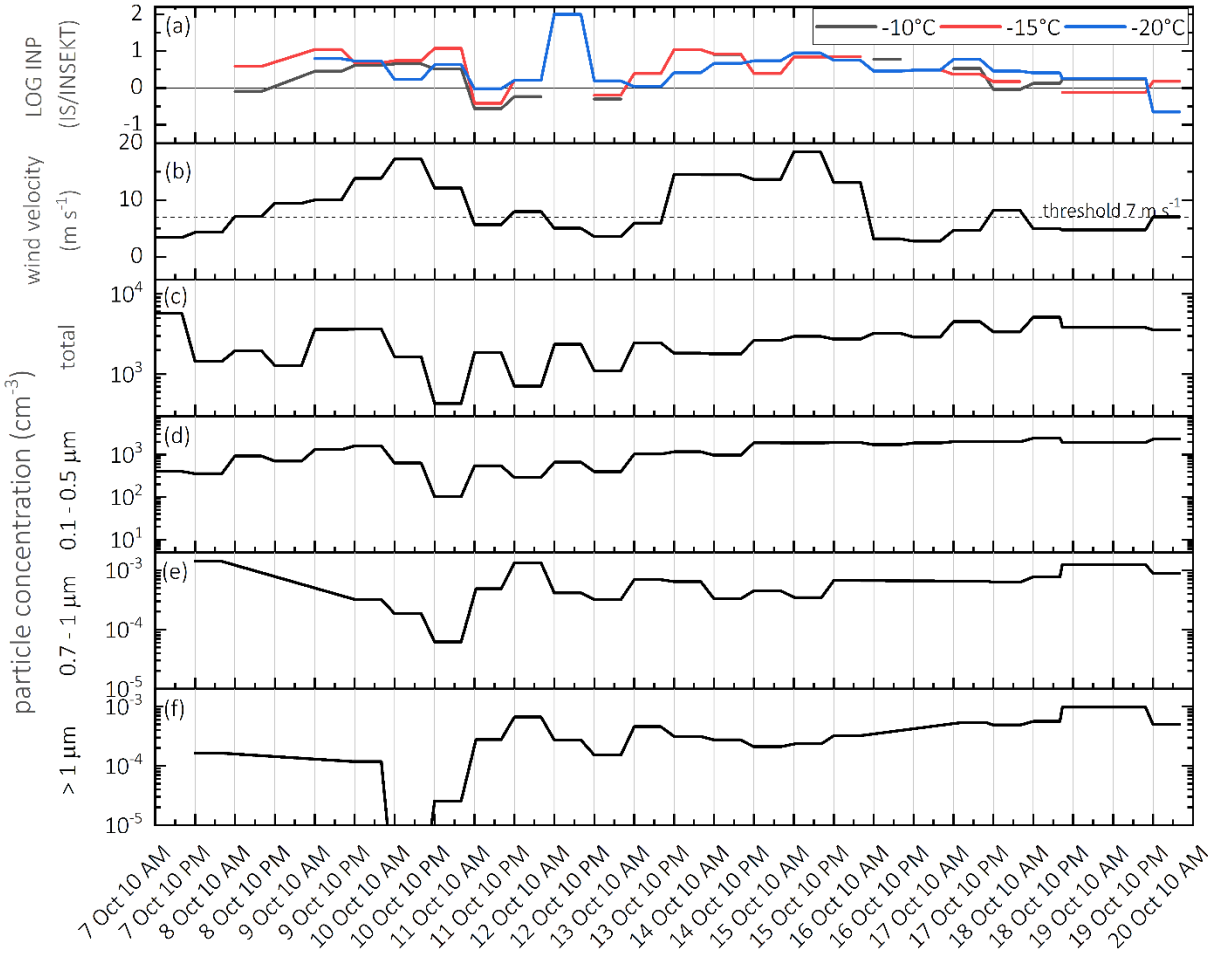

880

Figure 9: Timeseries of INP concentration differences between the IS and INSEKT at a nucleation temperature of -10 °C, -15 °C, and -20 °C °C (panel a), wind velocity (panel b), total particle concentration (panel c), particle concentration in the size range 0.1 – 0.5 µm (panel d), 0.7 – 0.1 µm (panel e), and > 1 µm (panel f).

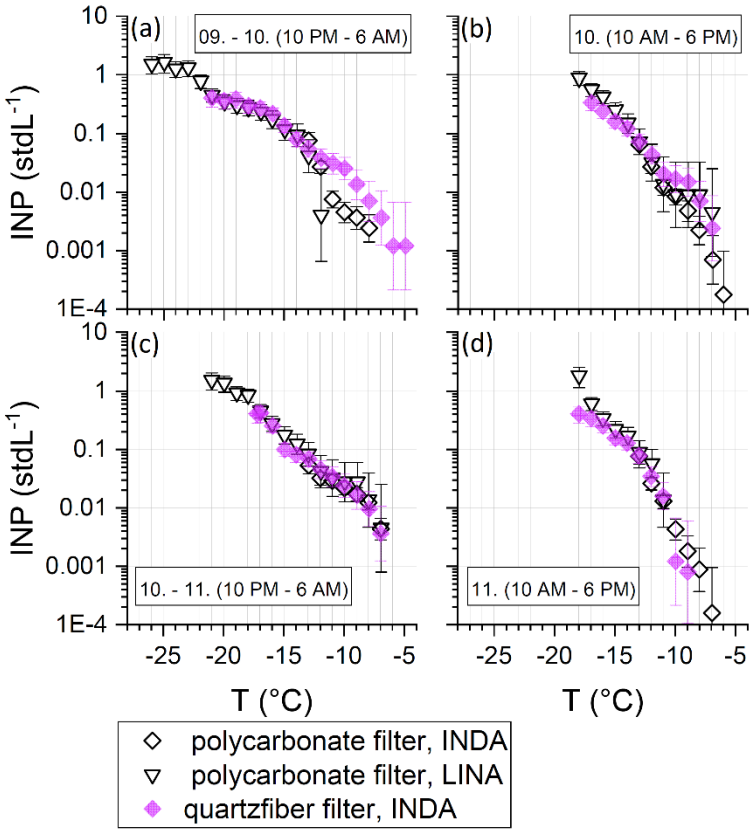

885

Figure 10: Comparison of different filter material for parallel collected filters using INDA and LINA.

6 Tables

Table 1: Specifications of the offline freezing methods.

	Name	FRIDGE	INSEKT	INDA*	IS	LINA*	LINDA	UNAM-MOUDI-DFT
filter collection	location	WAI	WAI	WAI	rooftop	see INDA	rooftop	WAI
	time interval	8 hours (night), 4 hours (day)	8 hours	8 hours	8 hours	*same as INDA*	8 hours	8 hours
	substrate	47 mm PTFE fluoropore membrane filter, 220 nm pore size	47 mm polycarbonate filters, 200 nm pore size	47 mm polycarbonate filters, 200 nm and 800 nm pore size; 47 mm quartz fiber filters	47 mm polycarbonate filters, 200 nm pore size	*same as INDA*	15 cm quarz fiber filters	hydrophobic glass coverslips
	filter holder	custom-built semi-automated multi-filter sampling device	standard	standard, HERA	open-faced sterile Nalgene sampling heads	*same as INDA*	high volume sampler	MOUDI cascade impactor
	flow	4.8 LPM	11 LPM	standard: 12 - 37 L PM HERA: 15-41 LPM	13.5 LPM	*same as INDA*	500 LPM	30 LPM
	filter storage	partly unfrozen	frozen	frozen	frozen	*same as INDA*	frozen	frozen
analysis	liquid volumes	2.5 µl droplets	50 µl suspension	50 µl suspension	50 µl suspension	1 µl droplets	200 µl suspension	100 µm droplets
	freezing rate	1 °C min^{-1}	0.3 °C min^{-1}	1 °C min^{-1}	0.3 °C min^{-1}	1 °C min^{-1}	0.3 °C min^{-1}	10°C min^{-1}

* INDA and LINA use the same collected filter

Table 2: Comparison between the online methods (panel a; reference to CSU-CFDC) and offline methods (panel b, reference to INSEKT).

(a)

method compared to CSU-CFDC	# compared data	within factor 2 (%)	within factor 5 (%)
SPIN	**20**	**35**	**80**
PINE-1A	**34**	**71**	**100**
PINE-1B	**14**	**50**	**71**

(b)

method compared to INSEKT	# compared data	within factor 2 (%)	within factor 5 (%)
FRIDGE	**259**	**46**	**88**
UNAM-MOUDI-DFT	**103**	**45**	**77**
LINA	**147**	**49**	**87**
INDA	**95**	**45**	**91**
IS	**300**	**27**	**65**
LINDA	**26**	**19**	**85**

E

Work during this thesis

Outline of the current chapter

E.1 Personal contribution to the analysis made in this thesis

This section aims to precise what I have personally done as part of the field campaigns, laboratory work and data analysis that were presented in this manuscript.

I actively participated in both field campaigns at Puy de Dôme (PICNIC, WINS). This included retrieving the filter samples and analysing them at the laboratory for INP concentrations. The chemical analysis of the filters was realised by Laetitia Bouvier using the ICCF (Institut de Chimie de Clermont-Ferrand) facilities. I performed all the data and statistical analysis within the PICNIC/WINS campaigns.

I however did not take part in the TNG and S2C cruise campaigns. For TNG, the analysis for INP concentrations at the laboratory was partly done by myself, and partly done by Laetitia Bouvier, whom I trained for this analysis. The S2C INP analysis was performed by Jonathan Trueblood partly on board of the ship and partly at the NIWA laboratory in New Zealand. Chemical analysis of the filters was done by Véronique Pont at the Laboratoire d'Aérologie in Toulouse, France. Biogeochemical parameters were retrieved in both by several laboratories, mentioned in the Acknowledgement sections of each campaign. I performed almost all the data analysis within both cruise campaigns, with the participation of Romain Joseph for the S2C analysis, within his internship at LaMP.

E.2 List of scientific communications

- EAC[1] 2019: Poster *How aerosol size and chemical properties influence ice nuclei number concentrations at a high-altitude site*
- EAC 2021: Poster *Seasonal variations of ice-nucleating particles at mountain station in central France*
- Co-author in Baray et al. (2020)
- Co-author in the overview paper for the PICNIC campaign by L. Lacher (last version in Appendix D).

E.3 Teaching at Université Clermont Auvergne

- 2019-2020: Lab work supervisor in optics (20 hours) and thermodynamics (12 hours)
- 2020-2021: Teaching fellow in optics (18 hours) and lab work supervisor in thermodynamics (12 hours)

E.4 Activities for spreading scientific culture

- Forum Météo-Climat 2019 (Paris)
- Fête de la Science 2019 (Clermont-Ferrand)
- Festival Montagne et Sciences 2020 (Clermont-Ferrand)
- Journées du patrimoine 2020 (Clermont-Ferrand)
- Festival Les Nuées Ardentes 2021 (Orcines)

[1] European Aerosol Conference

Bibliography

[1] J. P. D. Abbatt. "Solid Ammonium Sulfate Aerosols as Ice Nuclei: A Pathway for Cirrus Cloud Formation". In: *Science* 313.5794 (Sept. 22, 2006), pp. 1770–1773. ISSN: 0036-8075, 1095-9203. DOI: 10.1126/science.1129726.

[2] M. Akila et al. "Characterization of bacterial diversity and ice-nucleating ability during different monsoon seasons over a southern tropical Indian region". In: *Atmospheric Environment* 191 (Oct. 2018), pp. 387–394. ISSN: 13522310. DOI: 10.1016/j.atmosenv.2018.08.026.

[3] Josephine Y Aller et al. "Size-resolved characterization of the polysaccharidic and proteinaceous components of sea spray aerosol". In: *Atmospheric Environment* 154 (2017), pp. 331–347.

[4] Josephine Y Aller et al. "The sea surface microlayer as a source of viral and bacterial enrichment in marine aerosols". In: *Journal of aerosol science* 36.5-6 (2005), pp. 801–812.

[5] P. Amato et al. "Survival and ice nucleation activity of bacteria as aerosols in a cloud simulation chamber". In: *Atmospheric Chemistry and Physics* 15.11 (June 12, 2015), pp. 6455–6465. ISSN: 1680-7324. DOI: 10.5194/acp-15-6455-2015.

[6] A. Ansmann et al. "Influence of Saharan dust on cloud glaciation in southern Morocco during the Saharan Mineral Dust Experiment". In: *Journal of Geophysical Research* 113 (D4 Feb. 27, 2008), p. D04210. ISSN: 0148-0227. DOI: 10.1029/2007JD008785.

[7] Gabriel Guarany de Araujo et al. "Survival and ice nucleation activity of Pseudomonas syringae strains exposed to simulated high-altitude atmospheric conditions". In: *Scientific Reports* 9.1 (Dec. 2019), p. 7768. ISSN: 2045-2322. DOI: 10.1038/s41598-019-44283-3.

[8] C. M. Archuleta et al. "Ice nucleation by surrogates for atmospheric mineral dust and mineral dust/sulfate particles at cirrus temperatures". In: *Atmospheric Chemistry and Physics* 5.10 (Oct. 4, 2005), pp. 2617–2634. ISSN: 1680-7324. DOI: 10.5194/acp-5-2617-2005.

[9] K Ardon-Dryer et al. “Ground-based measurements of immersion freezing in the eastern Mediterranean”. In: *Atmospheric chemistry and physics* 14.10 (2014), pp. 5217–5231.

[10] K. Ardon-Dryer et al. “Characteristics of immersion freezing nuclei at the South Pole station in Antarctica”. In: *Atmospheric Chemistry and Physics* 11.8 (Apr. 29, 2011), pp. 4015–4024. ISSN: 1680-7324. DOI: 10.5194/acp-11-4015-2011.

[11] James D. Atkinson et al. “The importance of feldspar for ice nucleation by mineral dust in mixed-phase clouds”. In: *Nature* 498.7454 (June 2013), pp. 355–358. ISSN: 0028-0836, 1476-4687. DOI: 10.1038/nature12278.

[12] HJ Aufm Kampe et al. “The influence of temperature on the shape of ice crystals growing at water saturation”. In: *Journal of Atmospheric Sciences* 8.3 (1951), pp. 168–174.

[13] S. Augustin-Bauditz et al. “The immersion mode ice nucleation behavior of mineral dusts: A comparison of different pure and surface modified dusts”. In: *Geophysical Research Letters* 41.20 (Oct. 28, 2014), pp. 7375–7382. ISSN: 00948276. DOI: 10.1002/2014GL061317.

[14] J-L Baray et al. “Maïdo observatory: a new high-altitude station facility at Reunion Island (21° S, 55° E) for long-term atmospheric remote sensing and in situ measurements”. In: *Atmospheric Measurement Techniques* 6.10 (2013), pp. 2865–2877.

[15] Jean-Luc Baray et al. “Cézeaux-Aulnat-Opme-Puy De Dôme: a multi-site for the long-term survey of the tropospheric composition and climate change”. In: *Atmospheric Measurement Techniques* 13.6 (June 26, 2020), pp. 3413–3445. ISSN: 1867-8548. DOI: 10.5194/amt-13-3413-2020.

[16] Mar Benavides et al. “Fine-scale sampling unveils diazotroph patchiness in the South Pacific Ocean”. In: *ISME Communications* 1.1 (Dec. 2021), p. 3. ISSN: 2730-6151. DOI: 10.1038/s43705-021-00006-2.

[17] Tor Bergeron. “On the physics of clouds and precipitation”. In: *Proc. 5th Assembly UGGI, Lisbon, Portugal, 1935* (1935), pp. 156–180.

[18] Yuanfei Bi et al. “Heterogeneous Ice Nucleation Controlled by the Coupling of Surface Crystallinity and Surface Hydrophilicity”. In: *The Journal of Physical Chemistry C* 120.3 (Jan. 28, 2016), pp. 1507–1514. ISSN: 1932-7447, 1932-7455. DOI: 10.1021/acs.jpcc.5b09740.

[19] Bigg. “Cross Sections of Ice Nucleus Concentrations at Altitude over Long Paths”. In: (1966).

[20] E. K. Bigg. “Ice Nucleus Concentrations in Remote Areas”. In: *Journal of the Atmospheric Sciences* 30.6 (Sept. 1973), pp. 1153–1157. ISSN: 0022-4928, 1520-0469. DOI: 10.1175/1520-0469(1973)030<1153:INCIRA>2.0.CO;2.

[21] E.K. Bigg. "Measurement of concentrations of natural ice nuclei". In: *Atmospheric Research* 25.5 (June 1990), pp. 397–408. ISSN: 01698095. DOI: 10.1016/0169-8095(90)90024-7.

[22] EK Bigg. "A new technique for counting ice-forming nuclei in aerosols". In: *Tellus* 9.3 (1957), pp. 394–400.

[23] EK Bigg et al. "Stratospheric ice nucleus measurements from balloons". In: *Tellus* 15.2 (1963), pp. 162–166.

[24] H. Bingemer et al. "Atmospheric ice nuclei in the Eyjafjallajökull volcanic ash plume". In: *Atmospheric Chemistry and Physics* 12.2 (Jan. 19, 2012), pp. 857–867. ISSN: 1680-7324. DOI: 10.5194/acp-12-857-2012.

[25] G. de Boer et al. "Evidence of liquid dependent ice nucleation in high-latitude stratiform clouds from surface remote sensors: LIQUID INDUCED ICE NUCLEATION". In: *Geophysical Research Letters* 38.1 (Jan. 16, 2011), n/a–n/a. ISSN: 00948276. DOI: 10.1029/2010GL046016.

[26] Yvonne Boose et al. "Heterogeneous ice nucleation on dust particles sourced from nine deserts worldwide – Part 1: Immersion freezing". In: *Atmospheric Chemistry and Physics* 16.23 (Dec. 6, 2016), pp. 15075–15095. ISSN: 1680-7324. DOI: 10.5194/acp-16-15075-2016.

[27] Yvonne Boose et al. "Heterogeneous ice nucleation on dust particles sourced from nine deserts worldwide – Part 2: Deposition nucleation and condensation freezing". In: *Atmospheric Chemistry and Physics* 19.2 (Jan. 28, 2019), pp. 1059–1076. ISSN: 1680-7324. DOI: 10.5194/acp-19-1059-2019.

[28] Yvonne Boose et al. "Ice nucleating particles in the Saharan Air Layer". In: *Atmospheric Chemistry and Physics* 16.14 (July 25, 2016), pp. 9067–9087. ISSN: 1680-7324. DOI: 10.5194/acp-16-9067-2016.

[29] Olivier Boucher et al. "Clouds and Aerosols". In: *Climate Change 2013: The Physical Science Basis. Contribution of Working Group I to the Fifth Assessment Report of the Intergovernmental Panel on Climate Change* (2013).

[30] L. Bourcier et al. "Seasonal variation of water-soluble inorganic components in aerosol size-segregated at the puy de Dôme station (1,465 m a.s.l.), France". In: *Journal of Atmospheric Chemistry* 69.1 (Mar. 2012), pp. 47–66. ISSN: 0167-7764, 1573-0662. DOI: 10.1007/s10874-012-9229-2.

[31] Zoé Brasseur et al. "Measurement report: Introduction to the HyICE-2018 campaign for measurements of ice-nucleating particles and instrument inter-comparison in the Hyytiälä boreal forest". In: *Atmospheric Chemistry and Physics* 22.8 (Apr. 19, 2022), pp. 5117–5145. ISSN: 1680-7324. DOI: 10.5194/acp-22-5117-2022.

[32] S. L. Broadley et al. "Immersion mode heterogeneous ice nucleation by an illite rich powder representative of atmospheric mineral dust". In: *Atmospheric Chemistry and Physics* 12.1 (Jan. 5, 2012), pp. 287–307. ISSN: 1680-7324. DOI: 10.5194/acp-12-287-2012.

[33] Donald A. Bryant et al. "Prokaryotic photosynthesis and phototrophy illuminated". In: *Trends in Microbiology* 14.11 (Nov. 2006), pp. 488–496. ISSN: 0966842X. DOI: 10.1016/j.tim.2006.09.001.

[34] U Bundke et al. "The fast ice nucleus chamber FINCH". In: *Atmospheric Research* 90.2-4 (2008), pp. 180–186.

[35] S. M. Burrows et al. "Ice nuclei in marine air: biogenic particles or dust?" In: *Atmospheric Chemistry and Physics* 13.1 (Jan. 11, 2013), pp. 245–267. ISSN: 1680-7324. DOI: 10.5194/acp-13-245-2013.

[36] Claudia Castellani et al., eds. *Marine Plankton*. Vol. 1. Oxford University Press, Oct. 19, 2017. ISBN: 978-0-19-923326-7. DOI: 10.1093/oso/9780199233267.001.0001.

[37] R. J. Charlson. "ATMOSPHERIC SCIENCE: Reshaping the Theory of Cloud Formation". In: *Science* 292.5524 (June 15, 2001), pp. 2025–2026. ISSN: 00368075, 10959203. DOI: 10.1126/science.1060096.

[38] Stephen M Chiswell et al. "Physical oceanography of the deep seas around New Zealand: a review". In: *New Zealand Journal of Marine and Freshwater Research* 49.2 (2015), pp. 286–317.

[39] C. Chou et al. "Effect of photochemical ageing on the ice nucleation properties of diesel and wood burning particles". In: *Atmospheric Chemistry and Physics* 13.2 (Jan. 22, 2013), pp. 761–772. ISSN: 1680-7324. DOI: 10.5194/acp-13-761-2013.

[40] C. Chou et al. "Ice nuclei properties within a Saharan dust event at the Jungfraujoch in the Swiss Alps". In: *Atmospheric Chemistry and Physics* 11.10 (May 20, 2011), pp. 4725–4738. ISSN: 1680-7324. DOI: 10.5194/acp-11-4725-2011.

[41] B. C. Christner et al. "Geographic, seasonal, and precipitation chemistry influence on the abundance and activity of biological ice nucleators in rain and snow". In: *Proceedings of the National Academy of Sciences* 105.48 (Dec. 2, 2008), pp. 18854–18859. ISSN: 0027-8424, 1091-6490. DOI: 10.1073/pnas.0809816105.

[42] B. C. Christner et al. "Ubiquity of Biological Ice Nucleators in Snowfall". In: *Science* 319.5867 (Feb. 29, 2008), pp. 1214–1214. ISSN: 0036-8075, 1095-9203. DOI: 10.1126/science.1149757.

[43] Brent C. Christner. "Bioprospecting for microbial products that affect ice crystal formation and growth". In: *Applied Microbiology and Biotechnology* 85.3 (Jan. 2010), pp. 481–489. ISSN: 0175-7598, 1432-0614. DOI: 10.1007/s00253-009-2291-2.

[44] Ivan Coluzza et al. “Perspectives on the Future of Ice Nucleation Research: Research Needs and Unanswered Questions Identified from Two International Workshops”. In: *Atmosphere* 8.12 (July 29, 2017), p. 138. ISSN: 2073-4433. DOI: 10.3390/atmos8080138.

[45] F. Conen et al. “Atmospheric ice nucleators active ≥ −12 °C can be quantified on PM₁₀ filters”. In: *Atmospheric Measurement Techniques* 5.2 (Feb. 2, 2012), pp. 321–327. ISSN: 1867-8548. DOI: 10.5194/amt-5-321-2012.

[46] F. Conen et al. “Biological residues define the ice nucleation properties of soil dust”. In: *Atmospheric Chemistry and Physics* 11.18 (Sept. 16, 2011), pp. 9643–9648. ISSN: 1680-7324. DOI: 10.5194/acp-11-9643-2011.

[47] Franz Conen et al. “Atmospheric ice nuclei at the high-altitude observatory Jungfraujoch, Switzerland”. In: *Tellus B: Chemical and Physical Meteorology* 67.1 (Dec. 2015), p. 25014. ISSN: 1600-0889. DOI: 10.3402/tellusb.v67.25014.

[48] Franz Conen et al. “Clues that decaying leaves enrich Arctic air with ice nucleating particles”. In: *Atmospheric environment* 129 (2016), pp. 91–94.

[49] Franz Conen et al. “Measurement report: Ice-nucleating particles active 2265 −15 °C in free tropospheric air over western Europe”. In: *Atmospheric Chemistry and Physics* 22.5 (Mar. 15, 2022), pp. 3433–3444. ISSN: 1680-7324. DOI: 10.5194/acp-22-3433-2022.

[50] P J Connolly et al. “Studies of heterogeneous freezing by three different desert dust samples”. In: *Atmos. Chem. Phys.* (2009), p. 20.

[51] HA Constantinidou et al. “Atmospheric dispersal of ice nucleation-active bacteria: The role of rain.” In: *Phytopathology* 80.10 (1990), pp. 934–937.

[52] Stephen J Cox et al. “Non-hexagonal ice at hexagonal surfaces: The role of lattice mismatch”. In: *Physical Chemistry Chemical Physics* 14.22 (2012), pp. 7944–7949.

[53] J. M. Creamean et al. “Dust and Biological Aerosols from the Sahara and Asia Influence Precipitation in the Western U.S.” In: *Science* 339.6127 (Mar. 29, 2013), pp. 1572–1578. ISSN: 0036-8075, 1095-9203. DOI: 10.1126/science.1227279.

[54] Jessie M Creamean et al. “Marine and terrestrial infb02uences on ice nucleating particles during continuous springtime measurements in an Arctic oilfb01eld location”. In: *Atmos. Chem. Phys.* (2018), p. 20.

[55] Michael Cunliffe et al. “Sampling the sea surface microlayer”. In: *Hydrocarbon and Lipid Microbiology Protocols*. Springer, 2015, pp. 255–261.

[56] Michael Cunliffe et al. “Sea surface microlayers: A unified physicochemical and biological perspective of the air–ocean interface”. In: *Progress in Oceanography* 109 (2013), pp. 104–116.

[57] D. J. Cziczo et al. “Clarifying the Dominant Sources and Mechanisms of Cirrus Cloud Formation”. In: *Science* 340.6138 (June 14, 2013), pp. 1320–1324. ISSN: 0036-8075, 1095-9203. DOI: 10.1126/science.1234145.

[58] Daniel J. Cziczo et al. “Inadvertent climate modification due to anthropogenic lead”. In: *Nature Geoscience* 2.5 (May 2009), pp. 333–336. ISSN: 1752-0894, 1752-0908. DOI: 10.1038/ngeo499.

[59] P. J. DeMott et al. “Ice formation by black carbon particles”. In: *Geophysical Research Letters* 26.16 (Aug. 15, 1999), pp. 2429–2432. ISSN: 00948276. DOI: 10.1029/1999GL900580.

[60] P. J. DeMott et al. “Integrating laboratory and field data to quantify the immersion freezing ice nucleation activity of mineral dust particles”. In: *Atmospheric Chemistry and Physics* 15.1 (Jan. 13, 2015), pp. 393–409. ISSN: 1680-7324. DOI: 10.5194/acp-15-393-2015.

[61] P. J. DeMott et al. “Measurements of the concentration and composition of nuclei for cirrus formation”. In: *Proceedings of the National Academy of Sciences* 100.25 (Dec. 9, 2003), pp. 14655–14660. ISSN: 0027-8424, 1091-6490. DOI: 10.1073/pnas.2532677100.

[62] P. J. DeMott et al. “Predicting global atmospheric ice nuclei distributions and their impacts on climate”. In: *Proceedings of the National Academy of Sciences* 107.25 (June 22, 2010), pp. 11217–11222. ISSN: 0027-8424, 1091-6490. DOI: 10.1073/pnas.0910818107.

[63] P.J. DeMott. “Quantitative descriptions of ice formation mechanisms of silver iodide-type aerosols”. In: *Atmospheric Research* 38.1 (Sept. 1995), pp. 63–99. ISSN: 01698095. DOI: 10.1016/0169-8095(94)00088-U.

[64] PAUL J DeMott. *Laboratory studies of cirrus cloud processes*. Oxford Univ. Press New York, 2002.

[65] Paul J. DeMott et al. “African dust aerosols as atmospheric ice nuclei: AFRICAN DUST AEROSOLS AS ICE NUCLEI”. In: *Geophysical Research Letters* 30.14 (July 2003). ISSN: 00948276. DOI: 10.1029/2003GL017410.

[66] Paul J. DeMott et al. “New Directions: Need for defining the numbers and sources of biological aerosols acting as ice nuclei”. In: *Atmospheric Environment* 44.15 (May 2010), pp. 1944–1945. ISSN: 13522310. DOI: 10.1016/j.atmosenv.2010.02.032.

[67] Paul J. DeMott et al. “Resurgence in Ice Nuclei Measurement Research”. In: *Bulletin of the American Meteorological Society* 92.12 (Dec. 2011), pp. 1623–1635. ISSN: 0003-0007, 1520-0477. DOI: 10.1175/2011BAMS3119.1.

[68] Paul J. DeMott et al. “Sea spray aerosol as a unique source of ice nucleating particles”. In: *Proceedings of the National Academy of Sciences* 113.21 (May 24, 2016), pp. 5797–5803. ISSN: 0027-8424, 1091-6490. DOI: 10.1073/pnas.1514034112.

[69] Paul J. DeMott et al. "The Fifth International Workshop on Ice Nucleation phase 2 (FIN-02): laboratory intercomparison of ice nucleation measurements". In: *Atmospheric Measurement Techniques* 11.11 (Nov. 19, 2018), pp. 6231–6257. ISSN: 1867-8548. DOI: 10.5194/amt-11-6231-2018.

[70] PJ DeMott et al. "The fourth international ice nucleation workshop (ICIS-2007): Objectives and preliminary results". In: *Proceedings of the 15th International Conference on Clouds and Precipitation*. International Commission on Clouds and Precipitation. 2008, Paper–11.

[71] F Dentener et al. "Emissions of primary aerosol and precursor gases in the years 2000 and 1750 prescribed data-sets for AeroCom". In: *Atmos. Chem. Phys.* (2006), p. 24.

[72] VivianeR. Després et al. "Primary biological aerosol particles in the atmosphere: a review". In: *Tellus B: Chemical and Physical Meteorology* 64.1 (Jan. 2012), p. 15598. ISSN: 1600-0889. DOI: 10.3402/tellusb.v64i0.15598.

[73] Brendan T Doherty et al. *Freezing point of seawater*. Sears Foundation for Marine Research, 1974.

[74] A. J. Durant et al. "Ice nucleation and overseeding of ice in volcanic clouds". In: *Journal of Geophysical Research* 113 (D9 May 15, 2008), p. D09206. ISSN: 0148-0227. DOI: 10.1029/2007JD009064.

[75] Adam J. Durant. "Evaporation freezing by contact nucleation inside-out". In: *Geophysical Research Letters* 32.20 (2005), p. L20814. ISSN: 0094-8276. DOI: 10.1029/2005GL024175.

[76] U. Dusek et al. "Size Matters More Than Chemistry for Cloud-Nucleating Ability of Aerosol Particles". In: *Science* 312.5778 (June 2, 2006), pp. 1375–1378. ISSN: 0036-8075, 1095-9203. DOI: 10.1126/science.1125261.

[77] Marina Ealo et al. "Detection of Saharan dust and biomass burning events using near-real-timeintensive aerosol optical properties in the northwestern Mediterranean". In: *Atmospheric Chemistry and Physics* 16.19 (Oct. 10, 2016), pp. 12567–12586. ISSN: 1680-7324. DOI: 10.5194/acp-16-12567-2016.

[78] Sebastian Engelstaedter et al. "North African dust emissions and transport". In: *Earth-Science Reviews* 79.1 (Nov. 2006), pp. 73–100. ISSN: 00128252. DOI: 10.1016/j.earscirev.2006.06.004.

[79] Barbara Ervens et al. "Sensitivities of immersion freezing: Reconciling classical nucleation theory and deterministic expressions". In: *Geophysical Research Letters* 40.12 (2013), pp. 3320–3324.

[80] William D. Fahy et al. "Volcanic ash ice nucleation activity is variably reduced by aging in water and sulfuric acid: the effects of leaching, dissolution, and precipitation". In: *Environmental Science: Atmospheres* 2.1 (2022), pp. 85–99. ISSN: 2634-3606. DOI: 10.1039/D1EA00071C.

[81] A. Farah et al. "Altitude Aerosol Measurements in Central France: Seasonality, Sources and Free-Troposphere/Boundary Layer Segregation". In: *Earth and Space Science* 8.3 (Mar. 2021). ISSN: 2333-5084, 2333-5084. DOI: 10.1029/2019EA001018.

[82] Antoine Farah et al. "Seasonal Variation of Aerosol Size Distribution Data at the Puy de Dôme Station with Emphasis on the Boundary Layer/Free Troposphere Segregation". In: *Atmosphere* 9.7 (June 26, 2018), p. 244. ISSN: 2073-4433. DOI: 10.3390/atmos9070244.

[83] Laura Felgitsch et al. "Birch leaves and branches as a source of ice-nucleating macromolecules". In: *Atmospheric Chemistry and Physics* 18.21 (Nov. 8, 2018), pp. 16063–16079. ISSN: 1680-7324. DOI: 10.5194/acp-18-16063-2018.

[84] W Findeisen. "Kolloid-Meteorologische". In: *American Meteorological Society*, (1938).

[85] Martin Fitzner et al. "Predicting heterogeneous ice nucleation with a data-driven approach". In: *Nature Communications* 11.1 (Dec. 2020), p. 4777. ISSN: 2041-1723. DOI: 10.1038/s41467-020-18605-3.

[86] Neville H Fletcher. "Active sites and ice crystal nucleation". In: *Journal of Atmospheric Sciences* 26.6 (1969), pp. 1266–1271.

[87] Neville H Fletcher et al. *The physics of rainclouds/NH Fletcher; with an introductory chapter by P. Squires and a foreword by EG Bowen*. Cambridge University Press, 1962.

[88] Adam P. Fornea et al. "Heterogeneous freezing of ice on atmospheric aerosols containing ash, soot, and soil". In: *Journal of Geophysical Research* 114 (D13 July 7, 2009), p. D13201. ISSN: 0148-0227. DOI: 10.1029/2009JD011958.

[89] Piers Forster et al. "Changes in Atmospheric Constituents and in Radiative Forcing". In: (2007), p. 106.

[90] Rachel A Foster et al. "Diversity, genomics, and distribution of phytoplankton-cyanobacterium single-cell symbiotic associations". In: *Annual review of microbiology* 73 (2019), pp. 435–456.

[91] Evelyn Freney et al. "Experimental Evidence of the Feeding of the Free Troposphere with Aerosol Particles from the Mixing Layer". In: *Aerosol and Air Quality Research* 16.3 (2016), pp. 702–716. ISSN: 16808584, 20711409. DOI: 10.4209/aaqr.2015.03.0164.

[92] Beth Friedman et al. "Ice nucleation and droplet formation by bare and coated soot particles". In: *Journal of Geophysical Research* 116 (D17 Sept. 13, 2011), p. D17203. ISSN: 0148-0227. DOI: 10.1029/2011JD015999.

[93] Niels-Ulrik Frigaard et al. "Bacteriochlorophyll biosynthesis in green bacteria". In: *Chlorophylls and bacteriochlorophylls*. Springer, 2006, pp. 201–221.

[94] Janine Fröhlich-Nowoisky et al. "Bioaerosols in the Earth system: Climate, health, and ecosystem interactions". In: *Atmospheric Research* 182 (Dec. 2016), pp. 346–376. ISSN: 01698095. DOI: 10.1016/j.atmosres.2016.07.018.

[95] N Fukuta et al. "Ice nucleation by aerosol particles. Theory of condensation-freezing nucleation". In: *Journal of Atmospheric Sciences* 39.3 (1982), pp. 648–655.

[96] A. M. Gabey et al. "Observations of fluorescent and biological aerosol at a high-altitude site in central France". In: *Atmospheric Chemistry and Physics* 13.15 (Aug. 2, 2013), pp. 7415–7428. ISSN: 1680-7324. DOI: 10.5194/acp-13-7415-2013.

[97] Kunfeng Gao et al. "Laboratory studies of ice nucleation onto bare and internally mixed soot–sulfuric acid particles". In: *Atmospheric Chemistry and Physics* 22.8 (Apr. 22, 2022), pp. 5331–5364. ISSN: 1680-7324. DOI: 10.5194/acp-22-5331-2022.

[98] Elvin Garcia et al. "Biogenic ice nuclei in boundary layer air over two U.S. High Plains agricultural regions: BIOGENIC ICE NUCLEI OVER TWO AGRICULTURAL REGIONS". In: *Journal of Geophysical Research: Atmospheres* 117 (D18 Sept. 27, 2012), n/a–n/a. ISSN: 01480227. DOI: 10.1029/2012JD018343.

[99] Sarvesh Garimella et al. "The SPectrometer for Ice Nuclei (SPIN): an instrument to investigate ice nucleation". In: *Atmospheric Measurement Techniques* 9.7 (July 6, 2016), pp. 2781–2795. ISSN: 1867-8548. DOI: 10.5194/amt-9-2781-2016.

[100] Sarvesh Garimella et al. "Uncertainty in counting ice nucleating particles with continuous flow diffusion chambers". In: *Atmospheric Chemistry and Physics* 17.17 (Sept. 14, 2017), pp. 10855–10864. ISSN: 1680-7324. DOI: 10.5194/acp-17-10855-2017.

[101] Klaus Gierens et al. "Ice supersaturation". In: *Atmospheric Physics*. Springer, 2012, pp. 135–150.

[102] Xianda Gong et al. "Characterization of aerosol particles at Cabo Verde close to sea level and at the cloud level – Part 2: Ice-nucleating particles in air, cloud and seawater". In: *Atmospheric Chemistry and Physics* 20.3 (Feb. 6, 2020), pp. 1451–1468. ISSN: 1680-7324. DOI: 10.5194/acp-20-1451-2020.

[103] Lewis O Grant. *The second international workshop on condensation and ice nuclei*. COLORADO State UNIV., Department ATMOSPH. Science MAY, 1971.

[104] Ellen Gute et al. "Field evaluation of a Portable Fine Particle Concentrator (PFPC) for ice nucleating particle measurements". In: *Aerosol Science and Technology* 53.9 (Sept. 2, 2019), pp. 1067–1078. ISSN: 0278-6826, 1521-7388. DOI: 10.1080/02786826.2019.1626346.

[105] Dennis Hartmann et al. "The effect of Cloud Type on Earth's Energy Balance: Global Analysis". In: (1992).

[106] M. Hartmann et al. "Variation of Ice Nucleating Particles in the European Arctic Over the Last Centuries". In: *Geophysical Research Letters* 46.7 (Apr. 16, 2019), pp. 4007–4016. ISSN: 0094-8276, 1944-8007. DOI: 10.1029/2019GL082311.

[107] S Hartmann et al. "Homogeneous and heterogeneous ice nucleation at LACIS: operating principle and theoretical studies". In: *Atmospheric Chemistry and Physics* 11.4 (2011), pp. 1753–1767.

[108] Thomas C. J. Hill et al. "Measurement of Ice Nucleation-Active Bacteria on Plants and in Precipitation by Quantitative PCR". In: *Applied and Environmental Microbiology* 80.4 (Feb. 15, 2014), pp. 1256–1267. ISSN: 0099-2240, 1098-5336. DOI: 10.1128/AEM.02967-13.

[109] Tom C. J. Hill et al. "Sources of organic ice nucleating particles in soils". In: *Atmospheric Chemistry and Physics* 16.11 (June 10, 2016), pp. 7195–7211. ISSN: 1680-7324. DOI: 10.5194/acp-16-7195-2016.

[110] N. Hiranuma et al. "A comprehensive laboratory study on the immersion freezing behavior of illite NX particles: a comparison of 17 ice nucleation measurement techniques". In: *Atmospheric Chemistry and Physics* 15.5 (Mar. 6, 2015), pp. 2489–2518. ISSN: 1680-7324. DOI: 10.5194/acp-15-2489-2015.

[111] Naruki Hiranuma et al. "A comprehensive characterization of ice nucleation by three different types of cellulose particles immersed in water". In: *Atmospheric Chemistry and Physics* 19.7 (Apr. 10, 2019), pp. 4823–4849. ISSN: 1680-7324. DOI: 10.5194/acp-19-4823-2019.

[112] C Hoose et al. "How important is biological ice nucleation in clouds on a global scale?" In: *Environmental Research Letters* 5.2 (Apr. 2010), p. 024009. ISSN: 1748-9326. DOI: 10.1088/1748-9326/5/2/024009.

[113] C. Hoose et al. "Heterogeneous ice nucleation on atmospheric aerosols: a review of results from laboratory experiments". In: *Atmospheric Chemistry and Physics* 12.20 (Oct. 29, 2012), pp. 9817–9854. ISSN: 1680-7324. DOI: 10.5194/acp-12-9817-2012.

[114] C. R. Hoyle et al. "Ice nucleation properties of volcanic ash from Eyjafjallajökull". In: *Atmospheric Chemistry and Physics* 11.18 (Sept. 27, 2011), pp. 9911–9926. ISSN: 1680-7324. DOI: 10.5194/acp-11-9911-2011.

[115] Wei Hu et al. *Biological ice nucleation particles in the urban atmosphere of two megacities Beijing and Tianjin in North China*. other. oral, Mar. 23, 2020. DOI: 10.5194/egusphere-egu2020-7064.

[116] Shu Huang et al. "Overview of biological ice nucleating particles in the atmosphere". In: *Environment International* 146 (Jan. 2021), p. 106197. ISSN: 01604120. DOI: 10.1016/j.envint.2020.106197.

[117] Stefan A. Huber et al. “Characterisation of aquatic humic and non-humic matter with size-exclusion chromatography – organic carbon detection – organic nitrogen detection (LC-OCD-OND)”. In: *Water Research* 45.2 (Jan. 2011), pp. 879–885. ISSN: 00431354. DOI: 10.1016/j.watres.2010.09.023.

[118] J. A. Huffman et al. “High concentrations of biological aerosol particles and ice nuclei during and after rain”. In: *Atmospheric Chemistry and Physics* 13.13 (July 1, 2013), pp. 6151–6164. ISSN: 1680-7324. DOI: 10.5194/acp-13-6151-2013.

[119] K. Hussain et al. “Ice nucleus measurement with a continuous flow chamber”. In: *Quarterly Journal of the Royal Meteorological Society* 110.463 (Jan. 1, 1984), pp. 75–84. ISSN: 1477-870X. DOI: 10.1002/qj.49711046307.

[120] Victoria E. Irish et al. “Ice nucleating particles in the marine boundary layer in the Canadian Arctic during summer 2014”. In: *Atmospheric Chemistry and Physics* 19.2 (Jan. 25, 2019), pp. 1027–1039. ISSN: 1680-7324. DOI: 10.5194/acp-19-1027-2019.

[121] Victoria E. Irish et al. “Ice-nucleating particles in Canadian Arctic sea-surface microlayer and bulk seawater”. In: *Atmospheric Chemistry and Physics* 17.17 (Sept. 8, 2017), pp. 10583–10595. ISSN: 1680-7324. DOI: 10.5194/acp-17-10583-2017.

[122] Victoria E. Irish et al. “Revisiting properties and concentrations of ice-nucleating particles in the sea surface microlayer and bulk seawater in the Canadian Arctic during summer”. In: *Atmospheric Chemistry and Physics* 19.11 (June 12, 2019), pp. 7775–7787. ISSN: 1680-7324. DOI: 10.5194/acp-19-7775-2019.

[123] Ayumi Iwata et al. “Release of Highly Active Ice Nucleating Biological Particles Associated with Rain”. In: *Atmosphere* 10.10 (Oct. 8, 2019), p. 605. ISSN: 2073-4433. DOI: 10.3390/atmos10100605.

[124] Matthew J Jamieson et al. “First study on the effects of interfacial curvature and additive interfacial density on heterogeneous nucleation. Ice crystallization in oil-in-water emulsions and nanoemulsions with added 1-heptacosanol”. In: *Crystal growth & design* 5.2 (2005), pp. 451–459.

[125] M. Joly et al. “Quantification of ice nuclei active at near 0 °C temperatures in low-altitude clouds at the Puy de Dôme atmospheric station”. In: *Atmospheric Chemistry and Physics* 14.15 (Aug. 14, 2014), pp. 8185–8195. ISSN: 1680-7324. DOI: 10.5194/acp-14-8185-2014.

[126] Muriel Joly et al. “Ice nucleation activity of bacteria isolated from cloud water”. In: *Atmospheric Environment* 70 (May 2013), pp. 392–400. ISSN: 13522310. DOI: 10.1016/j.atmosenv.2013.01.027.

[127] Rachel E. Joyce et al. "Biological Ice-Nucleating Particles Deposited Year-Round in Subtropical Precipitation". In: *Applied and Environmental Microbiology* 85.23 (Dec. 2019). Ed. by Alfons J. M. Stams. ISSN: 0099-2240, 1098-5336. DOI: 10.1128/AEM.01567-19.

[128] M. Kamphus et al. "Chemical composition of ambient aerosol, ice residues and cloud droplet residues in mixed-phase clouds: single particle analysis during the Cloud and Aerosol Characterization Experiment (CLACE 6)". In: *Atmospheric Chemistry and Physics* 10.16 (Aug. 30, 2010), pp. 8077–8095. ISSN: 1680-7324. DOI: 10.5194/acp-10-8077-2010.

[129] T. Kanitz et al. "Contrasting the impact of aerosols at northern and southern midlatitudes on heterogeneous ice formation: AEROSOL EFFECT ON ICE FORMATION". In: *Geophysical Research Letters* 38.17 (Sept. 2011), n/a–n/a. ISSN: 00948276. DOI: 10.1029/2011GL048532.

[130] Zamin A. Kanji et al. "Overview of Ice Nucleating Particles". In: *Meteorological Monographs* 58 (Jan. 2017), pp. 1.1–1.33. ISSN: 0065-9401. DOI: 10.1175/AMSMONOGRAPHS-D-16-0006.1.

[131] Bahareh Karimi et al. "A comparative evaluation of freezing criteria and molecular characterization of epiphytic ice-nucleating (Ice+) and non-ice-nucleating (Ice−) Pseudomonas syringae and Pseudomonas fluorescens". In: *Journal of Plant Pathology* 102.1 (Feb. 2020), pp. 169–178. ISSN: 1125-4653, 2239-7264. DOI: 10.1007/s42161-019-00402-7.

[132] Jennifer E. Kay et al. "Global Climate Impacts of Fixing the Southern Ocean Shortwave Radiation Bias in the Community Earth System Model (CESM)". In: *Journal of Climate* 29.12 (June 15, 2016), pp. 4617–4636. ISSN: 0894-8755, 1520-0442. DOI: 10.1175/JCLI-D-15-0358.1.

[133] Alexei Kiselev et al. "Active sites in heterogeneous ice nucleation—the example of K-rich feldspars". In: *Science* 355.6323 (Jan. 27, 2017), pp. 367–371. ISSN: 0036-8075, 1095-9203. DOI: 10.1126/science.aai8034.

[134] Peter Knippertz et al., eds. *Mineral Dust*. Dordrecht: Springer Netherlands, 2014. ISBN: 978-94-017-8977-6 978-94-017-8978-3. DOI: 10.1007/978-94-017-8978-3.

[135] D. A. Knopf et al. "Heterogeneous nucleation of ice on anthropogenic organic particles collected in Mexico City: ICE NUCLEATION ON ANTHROPOGENIC AEROSOL". In: *Geophysical Research Letters* 37.11 (June 2010), n/a–n/a. ISSN: 00948276. DOI: 10.1029/2010GL043362.

[136] DA Knopf et al. "Stimulation of ice nucleation by marine diatoms". In: *Nature Geoscience* 4.2 (2011), pp. 88–90.

[137] Daniel A Knopf et al. "Freezing of water and aqueous NaCl droplets coated by organic monolayers as a function of surfactant properties and water activity". In: *The Journal of Physical Chemistry A* 115.22 (2011), pp. 5579–5591.

[138] Kirsten A. Koehler et al. "Cloud condensation nuclei and ice nucleation activity of hydrophobic and hydrophilic soot particles". In: *Physical Chemistry Chemical Physics* 11.36 (2009), p. 7906. ISSN: 1463-9076, 1463-9084. DOI: 10.1039/b905334b.

[139] Hilding Köhler. "The nucleus in and the growth of hygroscopic droplets". In: *Trans. Faraday Soc.* 32.0 (1936), pp. 1152–1161. ISSN: 0014-7672. DOI: 10.1039/TF9363201152.

[140] Motoi Kumai. "Identification of nuclei and concentrations of chemical species in snow crystals sampled at the South Pole". In: *Journal of Atmospheric Sciences* 33.5 (1976), pp. 833–841.

[141] Anand Kumar et al. "Ice nucleation activity of silicates and aluminosilicates in pure water and aqueous solutions – Part 1: The K-feldspar microcline". In: *Atmospheric Chemistry and Physics* 18.10 (May 23, 2018), pp. 7057–7079. ISSN: 1680-7324. DOI: 10.5194/acp-18-7057-2018.

[142] V. Anil Kumar et al. "Atmospheric ice nuclei concentration measurements over a high altitude-station in the Western Ghats, India". In: *Atmospheric Research* 235 (May 2020), p. 104795. ISSN: 01698095. DOI: 10.1016/j.atmosres.2019.104795.

[143] Anna T. Kunert et al. "Macromolecular fungal ice nuclei in <i>Fusarium</i>: effects of physical and chemical processing". In: *Biogeosciences* 16.23 (Dec. 9, 2019), pp. 4647–4659. ISSN: 1726-4189. DOI: 10.5194/bg-16-4647-2019.

[144] Larissa Lacher et al. "Background Free-Tropospheric Ice Nucleating Particle Concentrations at Mixed-Phase Cloud Conditions". In: *Journal of Geophysical Research: Atmospheres* 123.18 (Sept. 27, 2018), pp. 10, 506–10, 525. ISSN: 2169897X. DOI: 10.1029/2018JD028338.

[145] Larissa Lacher et al. *Sources and nature of ice-nucleating particles in the free troposphere at Jungfraujoch in winter 2017*. preprint. Aerosols/Field Measurements/Troposphere/Chemistry (chemical composition and reactions), June 16, 2021. DOI: 10.5194/acp-2021-415.

[146] Larissa Lacher et al. "The Horizontal Ice Nucleation Chamber (HINC): INP measurements at conditions relevant for mixed-phase clouds at the High Altitude Research Station Jungfraujoch". In: *Atmos. Chem. Phys.* (2017), p. 27.

[147] LA Ladino et al. "Addressing the ice nucleating abilities of marine aerosol: A combination of deposition mode laboratory and field measurements". In: *Atmospheric Environment* 132 (2016), pp. 1–10.

[148] Luis A. Ladino et al. "Ice-nucleating particles in a coastal tropical site". In: *Atmospheric Chemistry and Physics* 19.9 (May 9, 2019), pp. 6147–6165. ISSN: 1680-7324. DOI: 10.5194/acp-19-6147-2019.

[149] EJ Langham et al. "The heterogeneous and homogeneous nucleation of supercooled water". In: *Proceedings of the Royal Society of London. Series A. Mathematical and Physical Sciences* 247.1251 (1958), pp. 493–504.

[150] U Lohmann et al. "Global indirect aerosol effects: a review". In: *Atmos. Chem. Phys.* (2005), p. 24.

[151] U Lohmann et al. "Sensitivity studies of different aerosol indirect effects in mixed-phase clouds". In: *Atmos. Chem. Phys.* (2009), p. 18.

[152] Ulrike Lohmann et al. *An introduction to clouds: from the microscale to climate*. Cambridge: Cambridge University Press, 2016. 391 pp. ISBN: 978-1-107-01822-8.

[153] Zedong Lu et al. "The Diversity and Role of Bacterial Ice Nuclei in Rainwater from Mountain Sites in China". In: *Aerosol and Air Quality Research* 16.3 (2016), pp. 640–652. ISSN: 16808584, 20711409. DOI: 10.4209/aaqr.2015.05.0315.

[154] F. Lüönd et al. "Experimental study on the ice nucleation ability of size-selected kaolinite particles in the immersion mode". In: *Journal of Geophysical Research* 115 (D14 July 17, 2010). ISSN: 0148-0227. DOI: 10.1029/2009JD012959.

[155] Laura Lupi et al. "Does Hydrophilicity of Carbon Particles Improve Their Ice Nucleation Ability?" In: *The Journal of Physical Chemistry A* 118.35 (Sept. 4, 2014), pp. 7330–7337. ISSN: 1089-5639, 1520-5215. DOI: 10.1021/jp4118375.

[156] Leroy R Maki et al. "Ice Nucleation Induced by Pseudomonas syringael". In: 28 (1974), p. 4.

[157] C Marcolli et al. "Effb01ciency of immersion mode ice nucleation on surrogates of mineral dust". In: *Atmos. Chem. Phys.* (2007), p. 11.

[158] C. Marcolli. "Deposition nucleation viewed as homogeneous or immersion freezing in pores and cavities". In: *Atmospheric Chemistry and Physics* 14.4 (Feb. 21, 2014), pp. 2071–2104. ISSN: 1680-7324. DOI: 10.5194/acp-14-2071-2014.

[159] BJ Mason. "The cloud chamber as a tool in cloud physics". In: *Contemporary Physics* 4.1 (1962), pp. 27–48.

[160] R. H. Mason et al. "Ice nucleating particles at a coastal marine boundary layer site: correlations with aerosol type and meteorological conditions". In: *Atmospheric Chemistry and Physics* 15.21 (Nov. 10, 2015), pp. 12547–12566. ISSN: 1680-7324. DOI: 10.5194/acp-15-12547-2015.

[161] R. H. Mason et al. "Size-resolved measurements of ice-nucleating particles at six locations in North America and one in Europe". In: *Atmospheric Chemistry and Physics* 16.3 (Feb. 11, 2016), pp. 1637–1651. ISSN: 1680-7324. DOI: 10.5194/acp-16-1637-2016.

[162] R. H. Mason et al. "The micro-orifice uniform deposit impactor–droplet freezing technique (MOUDI-DFT) for measuring concentrations of ice nucleating particles as a function of size: improvements and initial validation". In: *Atmospheric Measurement Techniques* 8.6 (June 15, 2015), pp. 2449–2462. ISSN: 1867-8548. DOI: 10.5194/amt-8-2449-2015.

[163] V. Masson-Delmotte et al. *IPCC 2021: Climate Change 2021: The Physical Science Basis. Contribution of Working Group I to the Sixth Assessment Report of the Intergovernmental Panel on Climate Change*. 2021.

[164] Masakazu Matsumoto et al. "Molecular dynamics simulation of the ice nucleation and growth process leading to water freezing". In: *Nature* 416.6879 (2002), pp. 409–413.

[165] C. S. McCluskey et al. "Observations of Ice Nucleating Particles Over Southern Ocean Waters". In: *Geophysical Research Letters* 45.21 (Nov. 16, 2018), pp. 11, 989–11, 997. ISSN: 00948276. DOI: 10.1029/2018GL079981.

[166] Christina S. McCluskey et al. "A Dynamic Link between Ice Nucleating Particles Released in Nascent Sea Spray Aerosol and Oceanic Biological Activity during Two Mesocosm Experiments". In: *Journal of the Atmospheric Sciences* 74.1 (Jan. 1, 2017), pp. 151–166. ISSN: 0022-4928, 1520-0469. DOI: 10.1175/JAS-D-16-0087.1.

[167] Christina S. McCluskey et al. "A Mesocosm Double Feature: Insights into the Chemical Makeup of Marine Ice Nucleating Particles". In: *Journal of the Atmospheric Sciences* 75.7 (July 2018), pp. 2405–2423. ISSN: 0022-4928, 1520-0469. DOI: 10.1175/JAS-D-17-0155.1.

[168] Christina S. McCluskey et al. "Characteristics of atmospheric ice nucleating particles associated with biomass burning in the US: Prescribed burns and wildfires: Biomass burning ice nucleating particles". In: *Journal of Geophysical Research: Atmospheres* 119.17 (Sept. 16, 2014), pp. 10458–10470. ISSN: 2169897X. DOI: 10.1002/2014JD021980.

[169] Christina S. McCluskey et al. "Marine and Terrestrial Organic Ice-Nucleating Particles in Pristine Marine to Continentally Influenced Northeast Atlantic Air Masses". In: *Journal of Geophysical Research: Atmospheres* 123.11 (June 16, 2018), pp. 6196–6212. ISSN: 2169-897X, 2169-8996. DOI: 10.1029/2017JD028033.

[170] G McFiggans et al. "The effect of physical and chemical aerosol properties on warm cloud droplet activation". In: *Atmos. Chem. Phys.* (2006), p. 57.

[171] MP Meyers. "New primary ice-nucleation parametrizations in an explicit cloud model". In: (1992). DOI: https://doi.org/10.1175/1520-0450(1992)031%3C0708:NPINPI%3E2.0.CO;2.

[172] O Mohler et al. "Effb01ciency of the deposition mode ice nucleation on mineral dust particles". In: *Atmos. Chem. Phys.* (2006), p. 15.

[173] O Möhler et al. "The effect of organic coating on the heterogeneous ice nucleation efficiency of mineral dust aerosols". In: *Environmental Research Letters* 3.2 (Apr. 2008), p. 025007. ISSN: 1748-9326. DOI: 10.1088/1748-9326/3/2/025007.

[174] Ottmar Möhler et al. "Ice nucleation on flame soot aerosol of different organic carbon content". In: *Meteorologische Zeitschrift* 14.4 (Sept. 15, 2005), pp. 477–484. ISSN: 0941-2948. DOI: 10.1127/0941-2948/2005/0055.

[175] Cindy E Morris et al. "The life history of the plant pathogen Pseudomonas syringae is linked to the water cycle". In: *The ISME Journal* 2.3 (Mar. 2008), pp. 321–334. ISSN: 1751-7362, 1751-7370. DOI: 10.1038/ismej.2007.113.

[176] Cindy E. Morris et al. "Bioprecipitation: a feedback cycle linking Earth history, ecosystem dynamics and land use through biological ice nucleators in the atmosphere". In: *Global Change Biology* 20.2 (Feb. 2014), pp. 341–351. ISSN: 13541013. DOI: 10.1111/gcb.12447.

[177] B. J. Murray et al. "Heterogeneous freezing of water droplets containing kaolinite particles". In: *Atmospheric Chemistry and Physics* 11.9 (May 6, 2011), pp. 4191–4207. ISSN: 1680-7324. DOI: 10.5194/acp-11-4191-2011.

[178] B. J. Murray et al. "Ice nucleation by particles immersed in supercooled cloud droplets". In: *Chemical Society Reviews* 41.19 (2012), p. 6519. ISSN: 0306-0012, 1460-4744. DOI: 10.1039/c2cs35200a.

[179] Benjamin J Murray et al. "Heterogeneous nucleation of ice particles on glassy aerosols under cirrus conditions". In: *Nature Geoscience* 3.4 (2010), pp. 233–237.

[180] Mathieu Nicolet et al. "Single ice crystal measurements during nucleation experiments with the depolarization detector IODE". In: *Atmospheric Chemistry and Physics* 10.2 (2010), pp. 313–325.

[181] Alessia Nicosia. "Experimental investigation of heterogeneous nucleation of ice in remote locations". PhD thesis. 2018.

[182] D Niedermeier et al. "Heterogeneous freezing of droplets with immersed mineral dust particles–measurements and parameterization". In: *Atmospheric Chemistry and Physics* 10.8 (2010), pp. 3601–3614.

[183] D. Niedermeier et al. "Heterogeneous ice nucleation: exploring the transition from stochastic to singular freezing behavior". In: *Atmospheric Chemistry and Physics* 11.16 (Aug. 30, 2011), pp. 8767–8775. ISSN: 1680-7324. DOI: 10.5194/acp-11-8767-2011.

[184] Monika Niemand et al. "A Particle-Surface-Area-Based Parameterization of Immersion Freezing on Desert Dust Particles". In: *Journal of the Atmospheric Sciences* 69.10 (Oct. 2012), pp. 3077–3092. ISSN: 0022-4928, 1520-0469. DOI: 10.1175/JAS-D-11-0249.1.

[185] Tatau Nishinaga, ed. *Handbook of crystal growth. vol. 1, part A part A: Bd. 1. Fundamentals Thermodynamics and kinetics / ed.-in-chief and vol. ed. Tatau Nishinaga*. 2. ed. Vol. 1. Amsterdam Heidelberg: Elsevier, 2015. 594 pp. ISBN: 978-0-444-56369-9 978-0-444-63322-4.

[186] D. O'Sullivan et al. "Ice nucleation by fertile soil dusts: relative importance of mineral and biogenic components". In: *Atmospheric Chemistry and Physics* 14.4 (Feb. 18, 2014), pp. 1853–1867. ISSN: 1680-7324. DOI: 10.5194/acp-14-1853-2014.

[187] D. O'Sullivan et al. "Contributions of biogenic material to the atmospheric ice-nucleating particle population in North Western Europe". In: *Scientific Reports* 8.1 (Dec. 2018). ISSN: 2045-2322. DOI: 10.1038/s41598-018-31981-7.

[188] Oluwaseun O Ogunro et al. "Global distribution and surface activity of macromolecules in offline simulations of marine organic chemistry". In: *Biogeochemistry* 126.1 (2015), pp. 25–56.

[189] J. Dean Pakulski et al. "Abundance and distribution of carbohydrates in the ocean". In: *Limnology and Oceanography* 39.4 (June 1994), pp. 930–940. ISSN: 00243590. DOI: 10.4319/lo.1994.39.4.0930.

[190] Henry P Palmer. *The Wilson Cloud Chamber as a Hygrometer*. 1949.

[191] Suman Pandey et al. "High resolution structures of periplasmic glucose-binding protein of Pseudomonas putida CSV86 reveal structural basis of its substrate specificity". In: *Journal of Biological Chemistry* 291.15 (2016), pp. 7844–7857.

[192] Sachin Patade et al. "Empirical formulation for multiple groups of primary biological ice nucleating particles from field observations over Amazonia". In: *Journal of the Atmospheric Sciences* (Apr. 12, 2021). ISSN: 0022-4928, 1520-0469. DOI: 10.1175/JAS-D-20-0096.1.

[193] Andreas Peckhaus et al. "A comparative study of K-rich and Na/Ca-rich feldspar ice-nucleatingparticles in a nanoliter droplet freezing assay". In: *Atmospheric Chemistry and Physics* 16.18 (Sept. 15, 2016), pp. 11477–11496. ISSN: 1680-7324. DOI: 10.5194/acp-16-11477-2016.

[194] Philipp Pedevilla et al. "Can Ice-Like Structures Form on Non-Ice-Like Substrates? The Example of the K-feldspar Microcline". In: *The Journal of Physical Chemistry C* 120.12 (Mar. 31, 2016), pp. 6704–6713. ISSN: 1932-7447, 1932-7455. DOI: 10.1021/acs.jpcc.6b01155.

[195] Liran Peng et al. "Ice crystal concentrations in wave clouds: Dependencies on temperature, D¿ 0.5 μm aerosol particle concentration, and duration of cloud processing". In: *Atmospheric Chemistry and Physics* 15.11 (2015), pp. 6113–6125.

[196] J. E. Penner et al. "Effects of Aerosol from Biomass Burning on the Global Radiation Budget". In: *Science* 256.5062 (June 5, 1992), pp. 1432–1434. ISSN: 0036-8075, 1095-9203. DOI: 10.1126/science.256.5062.1432.

[197] Donald K. Perovich. "Complex yet translucent: the optical properties of sea ice". In: *Physica B: Condensed Matter* 338.1 (Oct. 2003), pp. 107–114. ISSN: 09214526. DOI: 10.1016/S0921-4526(03)00470-8.

[198] M. D. Petters et al. "Revisiting ice nucleation from precipitation samples: ICE NUCLEATION FROM PRECIPITATION". In: *Geophysical Research Letters* 42.20 (Oct. 28, 2015), pp. 8758–8766. ISSN: 00948276. DOI: 10.1002/2015GL065733.

[199] Glwadys Pouzet et al. "Atmospheric Processing and Variability of Biological Ice Nucleating Particles in Precipitation at Opme, France". In: *Atmosphere* 8.12 (Nov. 21, 2017), p. 229. ISSN: 2073-4433. DOI: 10.3390/atmos8110229.

[200] Kerri A Pratt. "In situ detection of biological particles in cloud ice-crystals". In: *NATURE GEOSCIENCE* 2 (2009), p. 4.

[201] AJ Prenni et al. "The impact of rain on ice nuclei populations at a forested site in Colorado". In: *Geophysical Research Letters* 40.1 (2013), pp. 227–231.

[202] Anthony J Prenni et al. "Biomass burning as a potential source for atmospheric ice nuclei: Western wildfires and prescribed burns". In: *Geophysical Research Letters* 39.11 (2012).

[203] Anthony J. Prenni et al. "Ice nuclei characteristics from M-PACE and their relation to ice formation in clouds". In: *Tellus B* 61.2 (Apr. 2009), pp. 436–448. ISSN: 02806509, 16000889. DOI: 10.1111/j.1600-0889.2009.00415.x.

[204] H. C. Price et al. "Atmospheric Ice-Nucleating Particles in the Dusty Tropical Atlantic". In: *Journal of Geophysical Research: Atmospheres* 123.4 (Feb. 27, 2018), pp. 2175–2193. ISSN: 2169897X. DOI: 10.1002/2017JD027560.

[205] J. M. Prospero. "Long-range transport of mineral dust in the global atmosphere: Impact of African dust on the environment of the southeastern United States". In: *Proceedings of the National Academy of Sciences* 96.7 (Mar. 30, 1999), pp. 3396–3403. ISSN: 0027-8424, 1091-6490. DOI: 10.1073/pnas.96.7.3396.

[206] Joseph M. Prospero. "Environmental characterization of global sources of atmospheric soil dust identified with the NIMBUS 7 Total Ozone Mapping Spectrometer (TOMS) absorbing aerosol product". In: *Reviews of Geophysics* 40.1 (2002), p. 1002. ISSN: 8755-1209. DOI: 10.1029/2000RG000095.

[207] H. R. Pruppacher. *Microphysics of clouds and precipitation*. 2nd. ed. s.l.: Springer, 2010. 976 pp. ISBN: 978-0-7923-4211-3.

[208] Hans R Pruppacher et al. *Microphysics of Clouds and Precipitation: Reprinted 1980*. Springer Science & Business Media, 2012.

[209] B. G. Pummer et al. "Ice nucleation by water-soluble macromolecules". In: *Atmospheric Chemistry and Physics* 15.8 (Apr. 21, 2015), pp. 4077–4091. ISSN: 1680-7324. DOI: 10.5194/acp-15-4077-2015.

[210] J.-P. Putaud et al. "A European aerosol phenomenology – 3: Physical and chemical characteristics of particulate matter from 60 rural, urban, and kerbside sites across Europe". In: *Atmospheric Environment* 44.10 (Mar. 2010), pp. 1308–1320. ISSN: 13522310. DOI: 10.1016/j.atmosenv.2009.12.011.

[211] Goericke Ralf et al. "The pigments of Prochlorococcus marinus: The presence of divinylchlorophyll a and b in a marine procaryote". In: *Limnology and Oceanography* 37.2 (1992), pp. 425–433.

[212] J Ras et al. "Spatial variability of phytoplankton pigment distributions in the Subtropical South Pacifb01c Ocean: comparison between in situ and predicted data". In: (2008), p. 17.

[213] MS Richardson et al. "Measurements of heterogeneous ice nuclei in the western United States in springtime and their relation to aerosol characteristics". In: *J. Geophys. Res* 112 (2007), p. D02209.

[214] A. Ripoll et al. *Long-term real-time chemical characterization of submicron aerosols at Montsec (Southern Pyrenees, 1570 m a.s.l.)* preprint. Aerosols/Field Measurements/Troposphere/Chemistry (chemical composition and reactions), Nov. 19, 2014. DOI: 10.5194/acpd-14-28809-2014.

[215] A. Ripoll et al. "Three years of aerosol mass, black carbon and particle number concentrations at Montsec (southern Pyrenees, 1570 m a.s.l.)" In: *Atmospheric Chemistry and Physics* 14.8 (Apr. 30, 2014), pp. 4279–4295. ISSN: 1680-7324. DOI: 10.5194/acp-14-4279-2014.

[216] David C. Rogers. "Development of a continuous flow thermal gradient diffusion chamber for ice nucleation studies". In: *Atmospheric Research* 22.2 (July 1988), pp. 149–181. ISSN: 01698095. DOI: 10.1016/0169-8095(88)90005-1.

[217] David C. Rogers et al. "A Continuous-Flow Diffusion Chamber for Airborne Measurements of Ice Nuclei". In: *Journal of Atmospheric and Oceanic Technology* 18.5 (May 2001), pp. 725–741. ISSN: 0739-0572, 1520-0426. DOI: 10.1175/1520-0426(2001)018<0725:ACFDCF>2.0.CO;2.

[218] David C. Rogers et al. "Measurements of ice nucleating aerosols during SUCCESS". In: *Geophysical Research Letters* 25.9 (May 1, 1998), pp. 1383–1386. ISSN: 00948276. DOI: 10.1029/97GL03478.

[219] Lynn M Russell et al. "Carbohydrate-like composition of submicron atmospheric particles and their production from ocean bubble bursting". In: *Proceedings of the National Academy of Sciences* 107.15 (2010), pp. 6652–6657.

[220] Silvia Sandrini et al. "Size-resolved aerosol composition at an urban and a rural site in the Po Valley in summertime: implications for secondary aerosol formation". In: *Atmospheric Chemistry and Physics* 16.17 (2016), pp. 10879–10897.

[221] G Santachiara et al. "Atmospheric particles acting as ice forming nuclei in different size ranges". In: *Atmospheric Research* 96.2-3 (2010), pp. 266–272.

[222] E. Sanz et al. "Homogeneous Ice Nucleation at Moderate Supercooling from Molecular Simulation". In: *Journal of the American Chemical Society* 135.40 (Oct. 9, 2013), pp. 15008–15017. ISSN: 0002-7863, 1520-5126. DOI: 10.1021/ja4028814.

[223] Vincent J Schaefer. "The production of ice crystals in a cloud of supercooled water droplets". In: *Science* 104.2707 (1946), pp. 457–459.

[224] Thea Schiebel. "Ice nucleation activity of soil dust aerosols". PhD thesis. KIT-Bibliothek, 2017.

[225] G. P. Schill et al. "Deposition and immersion-mode nucleation of ice by three distinct samples of volcanic ash". In: *Atmospheric Chemistry and Physics* 15.13 (July 10, 2015), pp. 7523–7536. ISSN: 1680-7324. DOI: 10.5194/acp-15-7523-2015.

[226] G. P. Schill et al. "Ice-nucleating particle emissions from photochemically aged diesel and biodiesel exhaust". In: *Geophysical Research Letters* 43.10 (May 28, 2016), pp. 5524–5531. ISSN: 0094-8276, 1944-8007. DOI: 10.1002/2016GL069529.

[227] Ph Schmitt-Kopplin et al. "Dissolved organic matter in sea spray: a transfer study from marine surface water to aerosols". In: *Biogeosciences* 9.4 (2012), pp. 1571–1582.

[228] Julia Schneider et al. "The seasonal cycle of ice-nucleating particles linked to the abundance of biogenic aerosol in boreal forests". In: *Atmospheric Chemistry and Physics* 21.5 (Mar. 16, 2021), pp. 3899–3918. ISSN: 1680-7324. DOI: 10.5194/acp-21-3899-2021.

[229] Jann Schrod et al. "Long-term deposition and condensation ice-nucleating particle measurements from four stations across the globe". In: *Atmospheric Chemistry and Physics* 20.24 (Dec. 22, 2020), pp. 15983–16006. ISSN: 1680-7324. DOI: 10.5194/acp-20-15983-2020.

[230] Jann Schrod et al. "Re-evaluating the Frankfurt isothermal static diffusion chamber for ice nucleation". In: *Atmospheric Measurement Techniques* 9.3 (2016), pp. 1313–1324.

[231] Tim Schulte et al. "Structure and function of native and refolded peridinin-chlorophyll-proteins from dinoflagellates". In: *European Journal of Cell Biology* 89.12 (Dec. 2010), pp. 990–997. ISSN: 01719335. DOI: 10.1016/j.ejcb.2010.08.004.

[232] J. P. Schwarz et al. "Global-scale black carbon profiles observed in the remote atmosphere and compared to models: HIPPO1 BLACK CARBON PROFILES". In: *Geophysical Research Letters* 37.18 (Sept. 2010), n/a–n/a. ISSN: 00948276. DOI: 10.1029/2010GL044372.

[233] AN Schwier et al. "Primary marine aerosol emissions from the Mediterranean Sea during pre-bloom and oligotrophic conditions: correlations to seawater chlorophyll a from a mesocosm study". In: *Atmospheric Chemistry and Physics* 15.14 (2015), pp. 7961–7976.

[234] John H. Seinfeld et al. *Atmospheric chemistry and physics: from air pollution to climate change*. 2. ed. OCLC: 260094879. Hoboken, NJ: Wiley, 2006. 1203 pp. ISBN: 978-0-471-72017-1 978-0-471-72018-8.

[235] K Sellegri et al. "Quantification of coastal new ultra-fine particles formation from in situ and chamber measurements during the BIOFLUX campaign". In: *Environmental Chemistry* 2.4 (2005), pp. 260–270.

[236] Mathias O Senge et al. "Biosynthesis and structures of the bacteriochlorophylls". In: *Anoxygenic photosynthetic bacteria*. Springer, 1995, pp. 137–151.

[237] Rajeshwar P. Sinha et al. "UV-protectants in cyanobacteria". In: *Plant Science* 174.3 (Mar. 2008), pp. 278–289. ISSN: 01689452. DOI: 10.1016/j.plantsci.2007.12.004.

[238] D. V. Spracklen et al. "The contribution of fungal spores and bacteria to regional and global aerosol number and ice nucleation immersion freezing rates". In: *Atmospheric Chemistry and Physics* 14.17 (Sept. 2, 2014), pp. 9051–9059. ISSN: 1680-7324. DOI: 10.5194/acp-14-9051-2014.

[239] I. Steinke et al. "Ice nucleation properties of fine ash particles from the Eyjafjallajökull eruption in April 2010". In: *Atmospheric Chemistry and Physics* 11.24 (Dec. 20, 2011), pp. 12945–12958. ISSN: 1680-7324. DOI: 10.5194/acp-11-12945-2011.

[240] Isabelle Steinke et al. "Complex plant-derived organic aerosol as ice-nucleating particles – more than the sums of their parts?" In: *Atmospheric Chemistry and Physics* 20.19 (Oct. 6, 2020), pp. 11387–11397. ISSN: 1680-7324. DOI: 10.5194/acp-20-11387-2020.

[241] Olaf Stetzer et al. "The Zurich Ice Nucleation Chamber (ZINC)-A New Instrument to Investigate Atmospheric Ice Formation". In: *Aerosol Science and Technology* 42.1 (Jan. 2008), pp. 64–74. ISSN: 0278-6826, 1521-7388. DOI: 10.1080/02786820701787944.

[242] Bjorn Stevens et al. "Water in the atmosphere". In: *Physics Today* 66.6 (June 2013), pp. 29–34. ISSN: 0031-9228, 1945-0699. DOI: 10.1063/PT.3.2009.

[243] E. Stopelli et al. "Freezing nucleation apparatus puts new slant on study of biological ice nucleators in precipitation". In: *Atmospheric Measurement Techniques* 7.1 (Jan. 14, 2014), pp. 129–134. ISSN: 1867-8548. DOI: 10.5194/amt-7-129-2014.

[244] T Storelvmo et al. "Modeling of the Wegener–Bergeron–Findeisen process—implications for aerosol indirect effects". In: *Environmental Research Letters* 3.4 (Oct. 2008), p. 045001. ISSN: 1748-9326. DOI: 10.1088/1748-9326/3/4/045001.

[245] Trude Storelvmo et al. "The Wegener-Bergeron-Findeisen process – Its discovery and vital importance for weather and climate". In: *Meteorologische Zeitschrift* 24.4 (July 21, 2015), pp. 455–461. ISSN: 0941-2948. DOI: 10.1127/metz/2015/0626.

[246] C J Stubenrauch et al. "ASSESSMENT OF GLOBAL CLOUD DATASETS FROM SATELLITES". In: (2013), p. 20.

[247] Ivy Tan et al. "Observational constraints on mixed-phase clouds imply higher climate sensitivity". In: *Science* 352.6282 (2016), pp. 224–227.

[248] Mingjin Tang et al. "Interactions of Water with Mineral Dust Aerosol: Water Adsorption, Hygroscopicity, Cloud Condensation, and Ice Nucleation". In: *Chemical Reviews* 116.7 (Apr. 13, 2016), pp. 4205–4259. ISSN: 0009-2665, 1520-6890. DOI: 10.1021/acs.chemrev.5b00529.

[249] E. S. Thomson et al. "Deposition-mode ice nucleation reexamined at temperatures below 200 K". In: *Atmospheric Chemistry and Physics* 15.4 (Feb. 16, 2015), pp. 1621–1632. ISSN: 1680-7324. DOI: 10.5194/acp-15-1621-2015.

[250] Yu M Timofeyev et al. *Theoretical fundamentals of atmospheric optics*. Cambridge Int Science Publishing, 2008.

[251] Y. Tobo et al. "Organic matter matters for ice nuclei of agricultural soil origin". In: *Atmospheric Chemistry and Physics* 14.16 (Aug. 22, 2014), pp. 8521–8531. ISSN: 1680-7324. DOI: 10.5194/acp-14-8521-2014.

[252] Yutaka Tobo et al. "1 Glacially sourced dust as a potential significant source of ice 2 nucleating particles". In: (2019), p. 27.

[253] Yutaka Tobo et al. "Biological aerosol particles as a key determinant of ice nuclei populations in a forest ecosystem: BIOLOGICAL ICE NUCLEI IN FOREST". In: *Journal of Geophysical Research: Atmospheres* 118.17 (Sept. 16, 2013), pp. 10, 100–10, 110. ISSN: 2169897X. DOI: 10.1002/jgrd.50801.

[254] Kevin E. Trenberth et al. "The Mass of the Atmosphere: A Constraint on Global Analyses". In: *Journal of Climate* 18.6 (Mar. 15, 2005), pp. 864–875. ISSN: 1520-0442, 0894-8755. DOI: 10.1175/JCLI-3299.1.

[255] Jonathan V. Trueblood et al. "A two-component parameterization of marine ice-nucleating particles based on seawater biology and sea spray aerosol measurements in the Mediterranean Sea". In: *Atmospheric Chemistry and Physics* 21.6 (Mar. 25, 2021), pp. 4659–4676. ISSN: 1680-7324. DOI: 10.5194/acp-21-4659-2021.

[256] Romy Ullrich et al. "A New Ice Nucleation Active Site Parameterization for Desert Dust and Soot". In: *Journal of the Atmospheric Sciences* 74.3 (Mar. 2017), pp. 699–717. ISSN: 0022-4928, 1520-0469. DOI: 10.1175/JAS-D-16-0074.1.

[257] G Vali. "1976: The Third International Workshop on Ice Nucleus Measurements". In: *Dept. Atmos. Sei., University of Wyoming, Laramie* (1976).

[258] G. Vali. "Interpretation of freezing nucleation experiments: singular and stochastic; sites and surfaces". In: *Atmospheric Chemistry and Physics* 14.11 (2014), pp. 5271–5294. DOI: 10.5194/acp-14-5271-2014.

[259] G. Vali et al. "Technical Note: A proposal for ice nucleation terminology". In: *Atmospheric Chemistry and Physics* 15.18 (Sept. 16, 2015), pp. 10263–10270. ISSN: 1680-7324. DOI: 10.5194/acp-15-10263-2015.

[260] G. Vali et al. "Time-dependent freezing rate parcel model". In: *Atmospheric Chemistry and Physics* 15.4 (Feb. 25, 2015), pp. 2071–2079. ISSN: 1680-7324. DOI: 10.5194/acp-15-2071-2015.

[261] Gabor Vali. "Nucleation terminology". In: *Bulletin of the American Meteorological Society* 66.11 (1985), pp. 1426–1427.

[262] Gabor Vali. "Quantitative Evaluation of Experimental Results on the Heterogenous Freezing Nucleation of SUpercooled Liquids". In: (1971).

[263] Gabor Vali et al. "TIME-DEPENDENT CHARACTERISTICS OF THE HETEROGENEOUS NUCLEATION OF ICE". In: *Canadian Journal of Physics* 44.3 (Mar. 1, 1966), pp. 477–502. ISSN: 0008-4204, 1208-6045. DOI: 10.1139/p66-044.

[264] H Venzac et al. "Seasonal variation of aerosol size distributions in the free troposphere and residual layer at the puy de Do02c6me station, France". In: *Atmos. Chem. Phys.* (2009), p. 14.

[265] Jesús Vergara-Temprado et al. "Contribution of feldspar and marine organic aerosols to global ice nucleating particle concentrations". In: *Atmospheric Chemistry and Physics* 17.5 (Mar. 15, 2017), pp. 3637–3658. ISSN: 1680-7324. DOI: 10.5194/acp-17-3637-2017.

[266] Jesús Vergara-Temprado et al. "Strong control of Southern Ocean cloud reflectivity by ice-nucleating particles". In: *Proceedings of the National Academy of Sciences* 115.11 (Mar. 13, 2018), pp. 2687–2692. ISSN: 0027-8424, 1091-6490. DOI: 10.1073/pnas.1721627115.

[267] Bernard Vonnegut. "The nucleation of ice formation by silver iodide". In: *Journal of applied physics* 18.7 (1947), pp. 593–595.

[268] J Warner. "An instrument for the measurement of freezing nucleus concentration". In: (1957).

[269] Alfred Wegener. *Thermodynamik der atmosphäre*. JA Barth, 1911.

[270] André Welti et al. “Exploring the Mechanisms of Ice Nucleation on Kaolinite: From Deposition Nucleation to Condensation Freezing”. In: *Journal of the Atmospheric Sciences* 71.1 (Jan. 1, 2014), pp. 16–36. ISSN: 0022-4928, 1520-0469. DOI: 10.1175/JAS-D-12-0252.1.

[271] André Welti et al. “Ship-based measurements of ice nuclei concentrations over the Arctic, Atlantic, Pacific and Southern oceans”. In: *Atmospheric Chemistry and Physics* 20.23 (Dec. 8, 2020), pp. 15191–15206. ISSN: 1680-7324. DOI: 10.5194/acp-20-15191-2020.

[272] André Welti et al. “Time dependence of immersion freezing: an experimental study on size selected kaolinite particles”. In: *Atmospheric Chemistry and Physics* 12.20 (2012), pp. 9893–9907.

[273] H. Wex et al. “Intercomparing different devices for the investigation of ice nucleating particles using Snomax® as test substance”. In: *Atmospheric Chemistry and Physics* 15.3 (Feb. 10, 2015), pp. 1463–1485. ISSN: 1680-7324. DOI: 10.5194/acp-15-1463-2015.

[274] H. Wex et al. “Kaolinite particles as ice nuclei: learning from the use of different kaolinite samples and different coatings”. In: *Atmospheric Chemistry and Physics* 14.11 (June 4, 2014), pp. 5529–5546. ISSN: 1680-7324. DOI: 10.5194/acp-14-5529-2014.

[275] Heike Wex et al. “Annual variability of ice-nucleating particle concentrations at different Arctic locations”. In: *Atmos. Chem. Phys.* (2019), p. 19.

[276] Theodore W. Wilson et al. “A marine biogenic source of atmospheric ice-nucleating particles”. In: *Nature* 525.7568 (Sept. 2015), pp. 234–238. ISSN: 0028-0836, 1476-4687. DOI: 10.1038/nature14986.

[277] Martin J. Wolf et al. “A biogenic secondary organic aerosol source of cirrus ice nucleating particles”. In: *Nature Communications* 11.1 (Dec. 2020), p. 4834. ISSN: 2041-1723. DOI: 10.1038/s41467-020-18424-6.

[278] Martin J. Wolf et al. “A link between the ice nucleation activity and the biogeochemistry of seawater”. In: *Atmospheric Chemistry and Physics* 20.23 (Dec. 11, 2020), pp. 15341–15356. ISSN: 1680-7324. DOI: 10.5194/acp-20-15341-2020.

[279] Martin J. Wolf et al. “Investigating the Heterogeneous Ice Nucleation of Sea Spray Aerosols Using *Prochlorococcus* as a Model Source of Marine Organic Matter”. In: *Environmental Science & Technology* 53.3 (Feb. 5, 2019), pp. 1139–1149. ISSN: 0013-936X, 1520-5851. DOI: 10.1021/acs.est.8b05150.

[280] J. D. Yakobi-Hancock et al. “Feldspar minerals as efficient deposition ice nuclei”. In: *Atmospheric Chemistry and Physics* 13.22 (Nov. 18, 2013), pp. 11175–11185. ISSN: 1680-7324. DOI: 10.5194/acp-13-11175-2013.

[281] J. Y. Yan et al. "Heterogeneous Ice Nucleation Induced by Electric Fields". In: *The Journal of Physical Chemistry Letters* 2.20 (Oct. 20, 2011), pp. 2555–2559. ISSN: 1948-7185. DOI: 10.1021/jz201113m.

[282] Yunbo Zhai et al. "A review on airborne microorganisms in particulate matters: Composition, characteristics and influence factors". In: *Environment International* 113 (Apr. 2018), pp. 74–90. ISSN: 01604120. DOI: 10.1016/j.envint.2018.01.007.

[283] Cuiqi Zhang et al. "The effects of morphology, mobility size, and secondary organic aerosol (SOA) material coating on the ice nucleation activity of black carbon in the cirrus regime". In: *Atmospheric Chemistry and Physics* 20.22 (Nov. 19, 2020), pp. 13957–13984. ISSN: 1680-7324. DOI: 10.5194/acp-20-13957-2020.

[284] B Zobrist et al. "Heterogeneous ice nucleation in aqueous solutions: the role of water activity". In: *The Journal of Physical Chemistry A* 112.17 (2008), pp. 3965–3975.

[285] Tobias Zolles et al. "Identification of Ice Nucleation Active Sites on Feldspar Dust Particles". In: *The Journal of Physical Chemistry A* 119.11 (Mar. 19, 2015), pp. 2692–2700. ISSN: 1089-5639, 1520-5215. DOI: 10.1021/jp509839x.

Characterization of atmospheric ice nucleating particles at remote sites

Abstract

Understanding how aerosol particles interact with atmospheric water is critical to understanding their impact on climate and precipitations. Ice Nuclei Particles (INPs) trigger the formation of atmospheric ice crystals. They are challenging to characterize because of their scarceness in the atmosphere and their variability. This variability depends partly on the different INP sources but also on the temperature at which they are activated. Considerably more variability being observed at warm temperatures (T>-20 °C), where biogenic particles have been identified as a key contributor. This is especially the case in marine regions, where the impact of ocean activity on the atmosphere is still largely unknown. The influence of atmospheric transport and aging on the IN properties of the ambient aerosols is another uncertainty in ice nucleation research. This thesis focused on the measurement and characterization of INPs in mountainous and oceanic regions, at T>-20 °C in the immersion freezing mode. Additional treatment of the samples allowed the retrieval of the concentration of biological INPs.

The first half of this thesis focused on characterizing INP populations in the Southern Hemisphere waters sampled during two cruise campaigns: One in tropical waters near the Tonga volcanic arc, and the other in poor oligotrophic waters south of New Zealand. The concentrations of sea spray (SSA) INPs and seawater (SW) INPs measured in both campaigns were lower than in other marine environments, but similar to other studies in the Southern Oceans. The best correlations were observed between INPs and organic matter, bacteria and photosynthetic pigments, highlighting the strong link between biological activity and INP concentrations. Parameterizations for predicting SW and SSA INPs were developed, showing that the transfer from SW INP to SSA INPs can be calculated based on the relationship between SW INPs and a SW organic carbon.

In order to understand the effect of atmospheric transport and aging on the IN properties of the aerosols, we measured INP concentrations at a continental site that is influenced by different air masses types. Two consecutive field campaigns took place at the Puy de Dôme station in Central France: the intensive, one-month long PICNIC campaign, and the long term WINS campaign. We measured concentrations between 0.001 and 0.1 INP/L_{air}, depending on the temperature. We also observed a majority of heat labile, potentially biogenic INPs at T>-12 °C. INP concentrations were at a minimum in winter and at a maximum in autumn and spring. Lower ratios of biogenic INPs were observed in the winter, explained by a decrease in vegetation cover and biogenic aerosols emissions. A parameterization for predicting warm INPs using the total aerosol concentrations as a predictor was successfully developed and tested.

In summary, this thesis provides new information of ice nuclei particles properties in various remote sites. We were also able to develop empirical parameterizations for predicting INPs for each of these environments.

Keywords: ice nucleating particles, nucleation, clouds, aerosols, remote sites

Laboratoire de Météorologie Physique (LaMP)
– Aubière – France – – –

Résumé

Il est essentiel de comprendre comment les aérosols interagissent avec l'eau atmosphérique pour comprendre leur impact sur le climat et les précipitations. Les noyaux glaciogènes (Ice Nuclei Particles, INPs) déclenchent la formation de cristaux de glace atmosphérique. Ils sont difficiles à caractériser en raison de leur rareté dans l'atmosphère et de leur variabilité. Cette variabilité dépend en partie des différentes sources d'INPs, mais aussi de la température à laquelle ils sont activés. Une variabilité beaucoup plus importante est observée aux températures chaudes (T>-20 °C), où les INPs biogéniques ont été identifiés comme un contributeur clé. C'est notamment le cas dans les régions marines, où l'impact de l'activité océanique sur l'atmosphère est encore largement inconnu. L'influence du transport atmosphérique et du vieillissement sur les propriétés glaciogènes des aérosols ambiants est une autre incertitude dans la recherche sur la nucléation de la glace. Cette thèse s'est concentrée sur la mesure et la caractérisation des INPs dans les régions montagneuses et océaniques, à T>-20 °C en mode de gel par immersion. Un traitement supplémentaire des échantillons a permis de retrouver la concentration des INPs biologiques.

La première moitié de cette thèse s'est concentrée sur la caractérisation des populations d'INPs dans les eaux de l'hémisphère sud échantillonnées lors de deux campagnes par bateau : l'une dans les eaux tropicales près de l'arc volcanique de Tonga, et l'autre dans les eaux oligotrophes pauvres au sud de la Nouvelle-Zélande. Les concentrations en INPs des embruns marins et de l'eau de mer mesurées lors des deux campagnes étaient plus faibles que dans d'autres environnements marins, mais similaires à d'autres études menées dans l'Océan Austral. Les meilleures corrélations ont été observées entre les INPs et la matière organique, les bactéries et les pigments photosynthétiques, mettant en évidence le lien étroit entre l'activité biologique et les concentrations d'INPs. Des paramétrisations pour prédire les INP dans l'eau de mer et les embruns ont été développées, montrant que le transfert des INP dans l'eau de mer aux INPs dans les embruns peut être calculé sur la base de la relation entre les INPs et le carbone organique dans l'eau de mer.

Afin de comprendre l'effet du transport atmosphérique et du vieillissement sur les propriétés INs des aérosols, nous avons mesuré les concentrations d'INP sur un site continental influencé par différents types de masses d'air. Deux campagnes consécutives ont eu lieu à la station du Puy de Dôme : la campagne PICNIC, intensive et d'une durée d'un mois, et la campagne WINS, de longue durée. Nous avons mesuré des concentrations comprises entre 0,001 et 0,1 INP/L_{air}, en fonction de la température. Nous avons également observé une majorité d'INPs biogéniques à T>-12 °C. Les concentrations d'INP étaient minimales en hiver et maximale en automne et au printemps. Des ratios plus faibles d'INPs biogéniques ont été observés en hiver. Une paramétrisation pour prédire les INP à T>-20 °C en utilisant la concentration d'aérosols comme prédicteur a été développée et testée avec succès.

En résumé, cette thèse fournit de nouvelles informations sur les propriétés des particules de noyaux de glace dans divers sites éloignés. Nous avons également été en mesure de développer des paramétrisations empiriques pour prédire les INP pour chacun de ces environnements.

Mots clés : noyaux glaciogènes, nucléation, nuages, aérosols, sites distants